Controlling the morphological and electro-optical properties of polymer dispersed Liquid crystals

Robert L. Folkes

Controlling the Morphological and Electro-Optical Properties of Polymer Dispersed Liquid Crystals

Robert L Folkes

Ph.D

2008

Durham University

Department of Chemistry

Controlling the Morphological and Electro-Optical Properties of Polymer Dispersed Liquid Crystals

Robert Folkes
Department of Chemistry
University of Durham
2007

Abstract

Polymer dispersed liquid crystals have shown potential as the basis for a new display screen technology which can be used to produce flexible displays. The work presented here investigates the properties during the synthesis process of PDLCs, which affect the electro-optical properties of the films produced. An investigation is performed through the use of small angle light scattering, and small angle neutron scattering, into the thermodynamic phase properties of the initial liquid crystal monomer solution from which the PDLCs are formed. Through the use of small angle light scattering and ESEM the phase separation mechanism is determined and the morphological properties of films formed under different thermodynamic conditions are investigated and linked to the electro-optical properties of test films.

It is shown that due to the rod like nature of liquid crystal molecules that the monomer/liquid crystal phase properties cannot be explained by classic polymer solution thermodynamics. Phase separation is shown to occur by one of two mechanisms depending upon whether or not a crosslinking monomer species is present, either a gel phase separation mechanism or a viscoelastic mechanism. Depending upon the initial thermodynamic properties of the system the formation of a polymer network can either act to promote (resulting in a large droplet morphology size) or suppress (resulting in small impure liquid crystal droplets) phase separation. This in turn is linked to the effectiveness of films formed under given conditions as potential display devices.

With thanks to EPSRC and Sony MSL, Stuttgart for funding

Acknowledgements

It would be hard to live three years of your life and there not be many people to whom you are indebted, I take this opportunity to thank as many as possible who have contributed to my time as PhD student both academically and socially.

For their direct help in my work I would like to thank,

Dr Nigel Clarke for direction and advice throughout the project.

Mr Tony Roberts and *Dr Akira Masutani* of Sony's Materials Science Laboratories in Stuttgart for realising the project, and providing support to me when I needed it. In particularly thanks to *Tony* for proving that it is possible to have a good time in Stuttgart, and introducing me to the joys of being drunk on Stuttgart station at 4.30 in the morning.

Drs Ian Henderson, Gavin Buxton and *Richard (Dave) Thompson* for useful conversations on work, and the far more edifying conversations which we had down the pub. Thanks to *Gavin* for many a memorable and on occasions not so memorable drinking experience, I don't believe I will truly ever recover properly from Brugge.

Thanks to *Dr Akio Yasuda, Sony Deutschland* and *EPSRC* for project funding.

Many people have helped me over these three years in teaching me how to us various equipment, these include *Dr Stephen Collins* and *Miss Jude Elder* (Rheometry), *Dr Stephen King* of ISIS (Small angle neutron scattering), *Dr Steven Devine* and *Mr Stuart Eggleston* (ESEM) and *Mr Andy Smith* (PDLC synthesis)

To the memories of the many souls who have passed through this group I'm proud to have been a member of, and the many people who daily travelled the corridors of the Materials Chemistry building and made life here the unique experience it has been.

Thanks to *Mr Tom Crockford, Miss Shruti Kumar, Miss Hanni Lonsdale* and *Mr Alex Dawe* for providing me with an escape in London when life up north proved too much for me, and not calling me a hypocrite when I chose to become an accountant.

Finally to *Dr Ian Henderson, Miss Victoria Whittle, Dr Mathew Gibson, Miss Amy Lawson* (without whose help I would never have discovered the joys of having a drunken undergraduate banging on my door at 11.30 at night demanding tea), *Dr Noppawan (Oat) Motong*, and *Miss Jude Elder* ☺, a better set of friends I could not hope to have had over these three years. It's been fun!

To Jude, thank you for your motivation, your belief and your friendship.

"A child of five could understand this. Fetch me a child of five"

Groucho Marx

I confirm that no part of the material offered has previously been submitted by me for a degree in this or in any other University. If material has been generated through joint work, my independent contribution has been clearly indicated. In all other cases material from the work of others has been acknowledged and quotations and paraphrases suitability indicated.

INTRODUCTION

1 POLYMER DISPERSED LIQUID CRYSTALS 1

2 PDLCS AS DISPLAYS 1

3 LIQUID CRYSTALS 3

3.1 *Advantages of PDLC Screens* 6

3.2 Controlling the Electro-Optical Properties of PDLC screens 7
3.2.1 Contrast Ratio 8
3.2.2 Electronic properties 9

4 PDLC FORMULATION TECHNIQUES 10

5 AIMS OF WORK 11

EXPERIMENTAL

1 MATERIALS 14

1.1 Morphological Work 14

1.2 Phase Property Investigations 15

1.3 Polymer Fluorination Studies 16

2 SMALL ANGLE LIGHT SCATTERING 16

2.1 SALS Concept 16

2.2 Phase Separation Temperature and Time Determination 18

2.3 Determination of Morphology Size 18

2.4 *Elucidation of Phase Separation Mechanism* 19

2.5 Experimental Set-Up 19

2.6 Sample Preparation 20

3 ENVIRONMENTAL SCANNING ELECTRON MICROSCOPY 20

3.1 SEM Concept 20

3.2 Environmental SEM 21

3.3 Sample Preparation and Imaging 21

4 SMALL ANGLE NEUTRON SCATTERING 22

4.1 Small Angle Neutron Scattering to Determine Interaction Parameters 23

4.2 Experimental and Sample Preparation 24

5 RHEOLOGY 25

5.1 Concept 25

5.2 Using Rheology to Determine Phase Separation Mechanics 25

5.3 Experimental Set-Up and Sample Preparation 25

6 ELECTRO-OPTICAL MEASUREMENTS 26

6.1 Experimental Set-Up 27

6.2 Sample Preparation 28

SECTION A – PHASE PROPERTIES OF MONOMER AND POLYMER SOLUTIONS

1 BACKGROUND 30

1.1 Phase Properties and Morphology 30

1.2 Miscibility of Multi-Component Systems 30

1.3 Mixing Thermodynamics 32
1.3.1 Flory-Huggins Theory 32
1.3.2 Limitations of Model 35

1.4 Phase Diagrams 35
1.4.1 Binodal Line 36
1.4.2 Spinodal Line 37

2 AIMS OF WORK 37

3 SMALL ANGLE LIGHT SCATTERING STUDIES 38

3.1 Liquid Crystal/Hydrogenous Monomer Phase Diagrams 38
3.1.1 TL213 with 2-Ethylhexyl Acrylate 38

3.2 Liquid Crystal/Fluorinated Monomer Phase Diagrams 43
3.2.1 TL213 with Heptafluorobutyl Acrylate 43
3.2.2 TL213 with 2-Ethylhexyl Acrylate Doped with Heptafluorobutyl Acrylate 46

3.3 Liquid Crystal/Hydrogenous Polymer Phase Diagrams 46
3.3.1 TL213 with Poly(2-Ethylhexyl Acrylate) 46
3.3.2 TL213 with Poly(n-butyl Acrylate) 50
3.3.3 5CB with Poly(n-butyl Acrylate) 54

3.4 Fluorinated Polymers 55

4 SMALL ANGLE NEUTRON SCATTERING STUDIES 56

4.1 Deuterated 5CB with Poly(n-butyl Acrylate) (3650 $gmol^{-1}$) 56
4.1.1 Results and Discussion 56

5 LIQUID CRYSTAL SOLUTION THERMODYNAMICS 59

5.1 Maier-Saupe Approach 60

5.2 Flory Liquid Crystal Lattice Model 61

6 CONCLUSIONS 65

SECTION B – PHASE SEPARATION MECHANISM AND MORPHOLOGY

1 BACKGROUND 68

1.1 Importance of Morphology Control 68

1.2 Phase Separation of Polymer Solutions and Blends 68
1.2.1 Phase Mixing Energetics 68
1.2.2 Nucleation and Growth 69
1.2.3 Spinodal Decomposition 70
1.2.4 Lever Rule 72

1.3 Phase Separation in Polymer Gels 74
1.3.1 Polymer-Gel Thermodynamics 75

1.4 Phase Separation Mechanism and Morphology Control in Polymer Dispersed Liquid Crystal Systems 78
1.4.1 Control of Morphology in PDLC Formation 78
1.4.2 Spinodal Decomposition and Nucleation & Growth in PDLCs 80
1.4.3 Elastic Contribution and Gel Effects in PDLC Phase Separation 82

2 AIMS OF WORK 83

3 PHASE SEPARATION TIMES OVERVIEW INVESTIGATION 84

3.1 TL213 with 2-Ethylhexyl Acrylate (5% b/v Crosslinker) 84
3.1.1 Results and Discussion 84

4 IN-DEPTH ϕ_{TL213} = 0.70 TO 0.85 MORPHOLOGY STUDY 93

4.1 TL213 with 2-Ethylhexyl Acrylate (15% b/v Crosslinker) 93
4.1.1 Results and Discussion 93

5 PHASE SEPARATION MECHANISM DETERMINATION 96

5.1 Small Angle Light Scattering Study 96
5.1.1 Results and Discussion 96
5.1.2 Viscoelastic Phase Separation 104

5.2 Rheological and Optical Microscopy Studies 105
5.2.1 Rheology Results and Discussion 106
5.2.2 Optical Microscopy Resuilts and Discussion 109

5.3 Conclusions 110

6 MECHANISM AND MORPHOLOGY 111

6.1 TL213 with 2-EthylHexyl Acrylate, Variable Crosslink Density SALS and ESEM Study 111
6.1.1 Results and Discussion 112
6.1.2 Conclusion 127

7 ELECTRO-OPTICAL STUDY 128

7.1 TL213 with 2-Ethylhexyl acrylate Variable Temperature and Composition Study 129
7.1.1 Results and Discussion 129

7.2 Conclusion 142

8 CONCLUSIONS

SECTION C – EFFECT OF FLUORINE DOPING OF THE POLYMER MATRIX ON PDLC MORPHOLOGICAL AND ELECTRO-OPTICAL PROPERTIES

1 BACKGROUND 148

1.1 Concept 148

2 AIMS OF WORK 149

3 SYSTEMS UNDER STUDY 150

4 ELECTRO-OPTICAL STUDIES 151

4.1 Results and Discussion 151

5 CONTACT ANGLE MEASUREMENTS 163

5.1 Aim 163

5.2 Results and Discussion 165

6 CONCLUSION 166

FURTHER WORK

1. MODELLING OF THE FLORY LATTICE THEORY FOR LIQUID CRYSTAL SOLUTIONS 169

2. INVESTIGATION OF POLYMER REACTION KINETICS 169

3. REACTION INDUCED VISCOELASTIC PHASE SEPARATION 170

4. PDLCS FORMED FROM LIQUID CRYSTALLINE MONOMERS 170

Figures and Tables

Introduction

Figure 1 Schematic diagram of Beni and Hackwood's refractive index matching display, diagram taken from[16] 2
Figure 2 Schematic diagram of how a PDLC refractive index matching screen works, diagram from ref[3] 3
Figure 3 Structural formula of 5 cyano-biphenyl 3
Figure 4 Schematic diagram of how the rod like nature of liquid crystals results in birefringence 4
Figure 5 Schematic representation of nematic and smectic phases 4
Figure 6 Schemitic diagram of the domain ordering of liquid crystals in the nematic phase and the effect of applying an electric field across a nematic liquid crystal. 5
Figure 7 Structural formula of 4-Chloro-2',2''-difluoro-4''-pentyl-[1,1':4',1''-terphenyl] 6
Figure 8 Schematic diagram of how reflective displays work using a PDLC film. a) shows the films in the off state and b) the on state. Reproduced from[21] 7
Figure 9 Example of a droplet morphology PDLC film 8

Experimental

Figure 1 2',2'',4''-trifluoro-4-propyl-1,1':4'1''-terphenyl 14
Figure 2 4-Chloro-2',2''-difluoro-4''-pentyl-1,1':4',1''-terphenyl 14
Figure 3 2-ethylhexyl Acryl ate 15
Figure 4 Trimethylol propane triacrylate 15
Figure 5 4-cyano-4'-n-pnetyl-d_{11}-diphenyl 15
Figure 6 Butyl Acrylate 16
Figure 7 2,2,3,3,4,4,4-heptafluorobutyl acrylate 16
Figure 8 2,2,3,3,4,4,5,5,6,6,7,7,7-dodecafluroheptyl acrylate 16
Figure 9 Schematic geometry of a scattering event 17
Figure 10 Schematic representation of Bragg Scattering 17
Figure 11 Small angle light scattering experimental set-up 19
Figure 12 Example transmission applied voltage profile for a PDLC 26

Table 1 Atomic scattering lengths 24
Table 2 Molecular scattering lengths of species under test 24

Section A

Figure 1 Example energy profiles of a, phase mixed system b, phase separated system 30
Figure 2 Schematic diagram of Flory-Huggins lattice 33
Figure 3 Schematic of tangent line linking a pair of equal chemical potential phases ϕ' and ϕ'' 36
Figure 4 Example phase diagram for a symmetric blend ($N_A = N_B$) 37
Figure 5 SALS determined phase diagram for TL213 with 2-ethylhexyl acrylate (in the absence of crosslinker) 39
Figure 6 SALS determined phase diagram for TL213 with 2-ethylhexytl acrylate doped with 15 mol% trimethylol propane triacrylate 39
Figure 7 Phase separation times for TL213 with 2-EthylHexyl Acrylate (5mol% Trimethylol Propane Triacrylate) cured under 2000 mWm^{-2} UV 40
Figure 8 Phase diagram for E7 with uncured NOA-65 as determined by G. W. Smith[12, 13] 41
Figure 9 Phase diagram for TL205 with 2-ethylhexyl acrylate as determined by Amundson et al.[15] 41
Figure 10 Phase diagram for K21 with NOA65 as determined by Nwabunma and Kyu[17] 42
Figure 11 Attempted fit of TL213 with 2-ethylhexyl Acrylate to Flory-Huggins spinodal equation 42
Figure 12 SALS determined phase diagram for TL213 with heptafluorobutyl acrylate 44
Figure 13 The temperature-composition phase diagram for two almost immiscible solids and their completely miscible liquids[18] 44

Figure 14 Attempt to fit TL213 with Heptafluorobutyl Acrylate phase properties to Flory-Huggins spinodal curve 45
Figure 15 Phase diagram showing the effect of fluorine doping of 2-ethylhexyl acrylate when mixed with TL213 46
Figure 16 SALS determined phase diagram for TL213 with poly(2-ethylhexyl acrylate) (92000 gmol^{-1}) 47
Figure 17 Comparison of the phase properties of 2-ethylhexyl acrylate with TL213 in the monomer and polymer forms 47
Figure 18 Attempted fit of TL213 with poly(2-EthylHexyl Acrylate) (Mw 92000) to Flory-Huggins spinodal equation 48
Figure 19 Phase diagram for 7CB with PMMA, A, glass 1 phase state; B, PMMA/solid crystalline 7CB 2 phase; C, PMMA/nematic 7CB 2 phase; D, PMMA/isotropic 7CB 1 phase; E, homogenous 1 phase. Ahn et al.[19] 49
Figure 20 Phase diagram for 7CB with polystyrene; A, glassy 1 phase state; B, PS/solid crystalline 7CB phase 2 phase state; C, PS/nematic 7CB phase 2 phase state; D, PS/isotropic 7CB 2 phase state; E, homogeneous 1 phase state. Ahn et al.[19] 49
Figure 21 Phase diagram of EBBA:PS (Mw 39000) with temperature listed relative to the T_{NI} of the liquid crystal. Work of Lee and Bae[20] 50
Figure 22 SALS determined phase diagram for TL213 with poly(n-Butyl Acrylate) of varying molecular weight 51
Figure 23 Attempted fits of TL213 with samples of poly(n-butyl acrylate) of varying molecular weight (a, 1630 gmol^{-1}, b 3650 gmol^{-1}, 14500 gmol^{-1}) to Flory-Huggins spinodal equation 52
Figure 24 Comparison of fitting derived spinodal curves to original data; a, determined from Mw 14500; b, Mw 3650 53
Figure 25 SALS determined phase diagram for 5CB with poly(n-butyl acrylate) (3650 gmol^{-1}) 54
Figure 26 Attempt to fit phase properties of 5CB with Mw 3650 gmol^{-1} poly(n-butyl acrylate) to Flory-Huggins spinodal curve 55
Figure 27 Fit of SANS data to phenomological interaction parameter equation for d5CB with poly(n-butyl acrylate) (Mw 3650 gmol^{-1}) of composition; a, 85:15; b, 90:10; c, 95:5 57
Figure 28 Spinodal curve generated from the fitting data of 95:5 d5CB:PBA 58
Figure 29 Spinodal curves generated from the fitting data of 85:15 and 90:10 d5CB:PBA 58
Figure 30 Example of a phase diagram fit to the combined Flory-Huggins/Maier-Saupe theory. E44 with NOA65, work of Nwabunma and Kyu[16]. 60
Figure 31 Schematic representation of the way a rod like molecule is treated in Flory Lattice theory[26] 62
Figure 32 Phase diagram of liquid crystal with polymer of increasing molecular weigth (x_d), as derived from Flory lattice theory by Dorgan[30] *(θ is the reduced temperature)* 64

Table 1 Flory-Huggins input fitting parameters for TL213 with 2-ethylhexyl acrylate monomer, refer to footnote 40
Table 2 Output parameters for Flory-Huggins fit of phase diagram of TL213 with 2-EthylHexyl Acrylate 43
Table 3 Flory-Huggins input fitting parameters for TL213 with heptafluorobutyl monomer 45
Table 4 Output parameters for Flory-Huggins fit of phase diagram of TL213 with heptaflurobutyl acrylate 45
Table 5 Flory-Huggins input fitting parameters for TL213 with poly(2-ethylhexyl acrylate) (92000 gmol^{-1}) 48
Table 6 Output parameters for Flory-Huggins fit of phase diagram of TL213 with 92000 gmol^{-1} poly(n-butyl acrylate) 48
Table 7 Flory-Huggins input fitting parameters for TL213 with poly(n-butyl acrylate) 51
*Table 8 Interaction parameter fitting results for TL213 with poly(n-butyl acrylate) of varying molecular weight, *Fit only possible by setting N_p = 70, equivalent of Mw 8962 gmol^{-1}* 53
Table 9 Input parameters for Flory-Huggins fit of phase diagram of 5CB with poly(n-butyl acrylate) (3650 gmol^{-1}) 55
Table 10 Output parameters for Flory-Huggins fit of phase diagram of 5CB with 3650 gmol^{-1} poly(n-butyl acrylate) 55
Table 11 Tabulated values for 'a' and 'b' to SANS data 56

Section B

Figure 1 Energy profile of a meta-stable system capable of undergoing phase separation via nucleation and growth 70
Figure 2 Example of an ESEM image of a PDLC system with a droplet type morphology 70
Figure 3 Schematic representation of spinodal decomposition in terms of domain size. Figure reproduced from Polymers at Surfaces and Interfaces, Jones and Richards[2] 71
Figure 4 Example of spinodal decomposition scattering ring, reproduced from ref[7] 72
Figure 5 Computational simulations of spinodal decomposition morphologies. (a) Co-continuous network, (b) droplet morphology. With thanks to Dr Ian Henderson 72
Figure 6 Schematic diagram showing morphology determination in a system undergoing spinodal decomposition 74
Figure 7 Schematic diagram of the effect of chain elongation of phase mixing in polymer gels 75
Figure 8 SALS determined phase separation times for TL213 with 2-ethylhexyl acrylate (5% b/v Crosslinker) irradiated at 2000 mWm^{-2} 85
Figure 9 Temperature/Composition Phase Curves for TL213 with 2-ethylhexyl acrylate in monomer and Mw 92000 states 86
Figure 10 Schemiatic representation of the relationship between relative reaction rate, monomer concentration, and cure temperature. The curves have been generated based upon a combination of the polymerisation rate equation and the temperature dependent Arrenhius equation for rate constants. Approximate values of the correct proportions have been used for all values except temperature, and monomer concentration (where the values are those as shown on the graph, and initiator concentration which was set at 5% of monomer concentration. 88
Figure 11 Predicted Flory-Huggins spinodal curves at varying degrees of polymerization based upon fit of TL213 with Mw 92000 $gmol^{-1}$ poly(2-ethylhexyl acrylate) 89
Figure 12 ESEM observed morphologies for TL213:2-ethylhexyl acrylate (5% b/v crosslinker) polymerized at 303 K under 2000 mWm^{-2} UV (365 nm); a, 55:45; b, 70:30; c, 75:25; d, 80:20; e, 85:15; f, 90:10. All images 250x magnification, measure bar s 100 μm 90
Figure 13 ESEM observed morphologies for 70:30 TL213:2-ethylhexyl acrylate (5% b/v Crosslinker), polymerized under 2000 mWm^{-2} UV (365 nm); a, 303K; b, 307 K; c, 333 K. All images 250x magnification, measure bar 100 μm 92
Figure 14 ESEM observed morphologies for 85:15 TL213:2-ethylhexyl acrylate (5% b/v crosslinker), polymerized under 2000 mWm^{-2} UV (365 nm); a, 303 K; b, 307 K; c, 333 K 92
Figure 15 ESEM observed morphology images for films formed from TL213:2-ethylhexyl acrylate (15% b/v crosslinker) cured at 303 K, under 2000 mWm^{-2} intensity UV (365 nm) at compositions 70:30 to 85:15 at 1% intervals 95
Figure 16 Example scattering patterns from SALS studies of polymerization induced phase separation of monomer/liquid crystal solutions. 70:30 TL213:2-ethylhexyl acrylate (15% by volume crosslinker) 303 K 5000 mWm^{-2} UV (365 nm) 97
Figure 17 Scattering profile after 72 seconds of polymerization induced phase separation of 70:30 TL213:2-ethylhexyl acrylate (15% by volume crosslinker) polymerized at 303 K under 5000 mWm^{-2} UV (365 nm) 98
Figure 18 Calibration scattering profile of 10 μm diffraction grating 99
Figure 19 Example ESEM observed morphologies for TL213:2-ethylhexyl acrylate cured at 303 K under 2000 mWm^{-2} UV (365 nm) 99
Figure 20 Example scattering patterns from SALS studies of polymerization induced phase separation of monomer/liquid crystal solutions. 70:30 TL213:2-ethylhexyl acrylate (0% crosslinker) 303 K 5000 mWm^{-2} UV (365 nm) 102
Figure 21 Scattering profiles during polymerization induced phase separation of 70:30 TL213:2-ethylhexyl acrylate (0% by volume crosslinker) polymerized at 303 K under 5000 mWm^{-2} UV (365 nm) 103
Figure 22 Schematic diagram of the viscoelastic phase separation mechanism, sourced from review by Tanaka[57] 104
Figure 23 Viscoelastic phase separation mechanism as observed by Tanaka using video phase-contrast microscopy of a polystyrene/poly(vinylmethylether) mixture undergoing a temperature quench[61] 105

Figure 24 Time dependent G" values for varying compositions of TL213:2-ethylhexyl acrylate (15% b/v crosslinker) during polymerization induced phase separation, under 700 mWm^{-2} UV (365 nm) 106
Figure 25 Time dependent G" values for varying compositions of TL213:2-ethylhexyl acrylate (0% crosslinker) during polymerization induced phase separation, under 700 mWm^{-2} 107
Figure 26 SALS determined phase separation times for TL213:2-ethylhexyl acrylate (0% crosslinker) undergoing polymerization induced phase separation at 303 K and under 2000 mWm^{-2} UV (365 nm) 107
Figure 27 Morphology images observed with time by optimcal microscopy (4x magnificantion) of 80:20 TL213:EHA (15% by volume crosslinker) polymerized at 303K under 2000 mWm^{-2} UV intensity 109
Figure 28 Example ESEM observed morphologies from 80:20 TL213:2-ethylhexyl acrylate solutions cured at 303 K under 2000 mWm^{-2} UV (365 nm), with the monomer doped with a, 2 % and b, 15 % by volume crosslinker 110
Figure 29 SALS determined phase separation times for TL213 with 2-ethylhexyl acrylate (2% b/v crosslinker) cured under 2000 mWm^{-2} UV 112
Figure 30 SALS determined phase separation times for TL213 with 2-ethylhexyl acrylate (2% b/v crosslinker) cured under 5000 mWm^{-2} UV 112
Figure 31 SALS determined phase separation times for TL213 with 2-ethylhexyl acrylate (15% b/v crosslinker) cured under 2000 mWm^{-2} UV 113
Figure 32 SALS determined phase separation times for TL213 with 2-ethylhexyl acrylate (15% b/v crosslinker) cured under 5000 mWm^{-2} UV 113
Figure 33 Comparison of morphologies of PDLC films formed from TL213 and 2-ethylhexyl acrylate with 2% b/v crosslinker cured 2000 mWm^{-2} and 5000 mWm^{-2} (303 K). Top row cured at 2000 mWm^{-2} bottom row at 5000 mWm^{-2}, from left to right 70:30, 73:27, 75:25, 77:23 114
Figure 34 Comparison of morphologies of PDLC films formed from TL213 and 2-ethylhexyl acrylate with 15% b/v crosslinker cured 2000 mWm^{-2} and 5000 mWm^{-2} (303 K). Top row cured at 2000 mWm^{-2} bottom row at 5000 mWm^{-2}, from left to right 70:30, 73:27, 75:25, 77:23 115
Figure 35 Comparison of morphologies of PDLC films formed from TL213 and 2-ethylhexyl acrylate with 15% b/v crosslinker cured 2000 mWm^{-2} and 5000 mWm^{-2} (333 K). Top row cured at 2000 mWm^{-2} bottom row at 5000 mWm^{-2}, from left to right 70:30, 73:27, 75:25, 77:23 115
Figure 36 ESEM observed morphologies for 70:30 TL213:2-ethylhexyl acrylate (15% b/v crosslinker) polymerized under 5000 mWm^{-2} UV (365 nm) at varying temperatures. All images 200x magnification, measure bar is 100 μm 117
Figure 37 ESEM observed morphologies for 73:27 TL213:2-ethylhexyl acrylate (15% b/v crosslinker) polymerized under 5000 mWm^{-2} UV (365 nm) at varying temperatures. All images 200x magnification, measure bar is 100 μm 117
Figure 38 ESEM observed morphologies for 75:25 TL213:2-ethylhexyl acrylate (15% b/v crosslinker) polymerized under 5000 mWm^{-2} UV (365 nm) at varying temperatures. All images 200x magnification, measure bar is 100 μm 118
Figure 39 ESEM observed morphologies for 77:23 TL213:2-ethylhexyl acrylate (15% b/v crosslinker) polymerized under 5000 mWm^{-2} UV (365 nm) at varying temperatures. All images 200x magnification, measure bar is 100 μm 119
Figure 40 ESEM observed morphologies for 80:20 TL213:2-ethylhexyl acrylate (15% b/v crosslinker) polymerized under 5000 mWm^{-2} UV (365 nm) at varying temperatures. All images 200x magnification, measure bar is 100 μm 119
Figure 41 Phase diagram for TL213 with unpolymerized 2-ethylhexyl acrylate 120
Figure 42 Predicted Flory-Huggins spinodal curves for TL213 with 2-ethylhexyl acrylate at varying degrees of polymerization based upon fit of TL213 with Mw 92000 $gmol^{-1}$ poly(2-ethylhexyl acrylate) 121
Figure 43 ESEM observed morphologies for 70:30 TL213:2-ethylhexyl acrylate (2% b/v crosslinker) polymerized under 5000 mWm^{-2} UV (365 nm) at varying temperatures. All images 200x magnification, measure bar is 100 μm 124
Figure 44 ESEM observed morphologies for 73:27 TL213:2-ethylhexyl acrylate (2% b/v crosslinker) polymerized under 5000 mWm^{-2} UV (365 nm) at varying temperatures. All images 200x magnification, measure bar is 100 μm 125
Figure 45 ESEM observed morphologies for 75:25 TL213:2-ethylhexyl acrylate (2% b/v crosslinker) polymerized under 5000 mWm^{-2} UV (365 nm) at varying temperatures. All images 200x magnification, measure bar is 100 μm 125

Figure 46 ESEM observed morphologies for 70:30 TL213:2-ethylhexyl acrylate (5% b/v crosslinker) polymerized under 5000 mWm^{-2} UV (365 nm) at varying temperatures. All images 200x magnification, measure bar is 100 μm 126
Figure 47 SALS determined phase separation times for TL213 with 2-ethylhexyl acrylate (0% crosslinker) cured under 2000 mWm^{-2} UV 127
Figure 48 E_{90} switching fields for TL213:2-ethylhexyl acrylate(15% b/v crosslinker) cells of varying composition cured at 303 K under 5000 mWm^{-2} UV (365 nm) 129
Figure 49 ESEM observed morphology images of electro-optical test cells for TL213 with 2-ethylhexyl acrylate (15% b/v crosslinker) cured at 303 K under 5000 mWm^{-2} intensity UV (365 nm), all images 200x magnification, measure bar is 100 μm 131
Figure 50 K values (related to rise switching rate) for TL213:2-ethylhexyl acrylate (15% b/v crosslinker) cells of varying composition cured at 303 K under 5000 mWm^{-2} UV (365 nm) 132
Figure 51 Normalised decay times (τ_{decay}) from 90% switching for TL213:2-ethylhexyl acrylate (15% b/v crosslinker) cells of varying composition cured at 303 K under 5000 mWm^{-2} UV (365 nm) 133
Figure 52 Off and on state %transmissions, and contrast ratios for TL213:2-ethylhexyl acrylate (15% b/v crosslinker) cells of varying composition cured at 303 K under 5000 mWm^{-2} UV (365 nm) 134
Figure 53 E_{90} switching fields for TL213:2-ethylhexyl acrylate (15% b/v crosslinker) cells of varying composition and cure temperature, cured under 5000 mWm^{-2} UV (365 nm) 136
Figure 54 K values (related to rise switching rate) for TL213:2-ethylhexyl acrylate (15% b/v crosslinker) cells of varying composition and cure temperature, cured under 5000 mWm^{-2} UV (365 nm) 136
Figure 55 Normalised τ_{decay} for TL213:2-ethylhexyl acrylate (15% b/v crosslinker) cells of varying composition and cure temperature, cured under 5000 mWm^{-2} UV (365 nm) 136
Figure 57 ESEM observed morphology images of electro-optical test cells for TL213 with 2-ethylhexyl acrylate (15% b/v crosslinker) of composition 70:30 cured under 5000 mWm^{-2} intensity UV (365 nm), all images 200x magnification, measure bar is 100 μm 137
Figure 58 ESEM observed morphology images of electro-optical test cells for TL213 with 2-ethylhexyl acrylate (15% b/v crosslinker) of composition 73:27 cured under 5000 mWm^{-2} intensity UV (365 nm), all images 200x magnification, measure bar is 100 μm 138
Figure 59 ESEM observed morphology images of electro-optical test cells for TL213 with 2-ethylhexyl acrylate (15% b/v crosslinker) of composition 75:25 cured under 5000 mWm^{-2} intensity UV (365 nm), all images 200x magnification, measure bar is 100 μm 139
Figure 60 Schematic of the approximate behaviour of phase separation extent of polymerization with cure temperature for a monomer/liquid crystal system for a fixed composition 141

Section C

Figure 1 E_{90} switching fields for 75:25 TL213:2-ethylhexyl acrylate (15% b/v crosslinker) doped with varying mol% of heptafluorobutyl acrylate, cured at 303 K under 5000 mWm^{-2} UV (365 nm) 151
Figure 2 E_{90} switching fields for 75:25 TL213:2-ethylhexyl acrylate (15% b/v crosslinker) doped with varying mol% of dodecafluoroheptyl acrylate, cured at 303 K under 5000 mWm^{-2} UV (365 nm) 152
Figure 3 K values for 75:25 TL213:2-ethylhexyl acrylate(15% b/v crosslinker) doped with varying mol% of heptafluorobutyl acrylate, cured at 303K under 5000 mWm^{-2} UV (365 nm) 152
Figure 4 K values for 75:25 TL213:2-ethylhexyl acrylate (15% b/v crosslinker) doped with varying mol% of dodecafluoroheptyl acrylate, cured at 303K under 5000 mWm^{-2} UV (365 nm). The results for 14 mol% & 22mol% are much larger than the maximum of the graph 153
Figure 5 ESEM observed images of electro-optical test cells of 75:25 TL213 with 2-ethylhexyl acrylate (15% b/v crosslinker) with varying doping mol% of heptafluorobutyl acrylate, all films cured at 303 K under 5000 mWm^{-2} UV (365 nm), 1000x magnification, measure bar is 20 μm 154
Figure 6 Confocal microscope observed images of electro-optical test cells of 75:25 TL213 with 2-ethylhexyl acrylate (15% b/v crosslinker) with varying doping mol% of heptafluorobutyl acrylate, all films cured at 303 K under 5000 mWm^{-2} UV (365 nm) 154
Figure 7 ESEM observed images of electro-optical test cells of 75:25 TL213 with 2-ethylhexyl acrylate (15% b/v crosslinker) with varying doping mol% of dodecafluoroheptyl acrylate, all films cured at 303 K under 5000 mWm^{-2} UV (365 nm), 1000x magnification, measure bar is 20 μm 155
Figure 8 Confocal microscope observed images of electro-optical test cells of 75:25 TL213 with 2-ethylhexyl acrylate (15% b/v crosslinker) with varying doping mol% of dodecafluoroheptyl

acrylate, all films cured at 303 K under 5000 mWm^{-2} UV (365 nm) 156
Figure 9 Phase mixing curves for TL213 with 2-ethylhexyl acrylate doped with varying amounts of fluorinated monomer units 157
Figure 10 Normalised τ_{decay} for 75:25 TL213:2-ethylhexyl acrylate (15% b/v crosslinker) doped with varying mol% of heptafluorobutyl acrylate, cured at 303 K under 5000 mWm^2 UV (365 nm) 159
Figure 11 Normalised τ_{decay} for 75:25 TL213:2-ethylhexyl acrylate (15% b/v crosslinker) doped with varying mol% of dodecafluoroheptyl acrylate, cured at 303 K under 5000 mWm^2 UV (365 nm). The results for 14 mol% and 22mol% DDFHA acrylate are much larger than the maximum of the graph refer to discussion for an explanation. 159
Figure 12 Off and on state %transmissions, and contrast ratios for 75:25 TL213:2-ethylhexyl acrylate (15% b/v crosslinker) doped with varying mol% of heptaflurobutyl acrylate, cured at 303 K under 5000 mWm^{-2} UV (365 nm) 160
Figure 13 Off and on state %transmissions, and contrast ratios for 75:25 TL213:2-ethylhexyl acrylate (15% b/v crosslinker) doped with varying mol% of dodecafluoroheptyl acrylate, cured at 303 K under 5000 mWm^{-2} UV (365 nm) 161
Figure 14 Comparison of the E_{90} switching fields for equivalent mol% of heptafluorobutyl acrylate and dodecafluoroheptyl acrylate doped PDLC films 162
Figure 15 ESEM observed morphologies of heptafluorobutyl acrylate and dodecafluoroheptyl acrylate PDLC films which give similar switching fields (1000x magnification) 162
Figure 16 Comparison of ESEM observed morphologies of films prepared with approximately the same fraction of fluorinated monomer units, but with different number of fluorine per monomer unit (1000x magnification) 163
Figure 17 Schematic Diagram of Contact Angle Measurement, where θ_c is the contact angle of the droplet on the surface[8] 164
Figure 18 Contact angle measurements for a droplet of TL213 on polymer films with varying degrees of doping with heptafluorobutyl acrylate 165

Table 1 Contact angle measurements for a droplet of TL213 on polymer films with varying degrees of doping with heptafluorobutyl acrylate 165

Appendix A

Figure 1 ESEM observed morphologies for 70:30 TL213:2-EthylHexyl Acrylate (2% b/v Crosslinker) polymerized under 2000 mWm^{-2} UV (365 nm) at varying temperatures. All images 200x magnification, measure bar s 100 μm 172
Figure 2 ESEM observed morphologies for 73:27 TL213:2-EthylHexyl Acrylate (2% b/v Crosslinker) polymerized under 2000 mWm^{-2} UV (365 nm) at varying temperatures. All images 200x magnification, measure bar s 100 μm 172
Figure 3 ESEM observed morphologies for 75:25 TL213:2-EthylHexyl Acrylate (2% b/v Crosslinker) polymerized under 2000 mWm^{-2} UV (365 nm) at varying temperatures. All images 200x magnification, measure bar s 100 μm 173
Figure 4 ESEM observed morphologies for 77:23 TL213:2-EthylHexyl Acrylate (2% b/v Crosslinker) polymerized under 2000 mWm^{-2} UV (365 nm) at varying temperatures. 303 K, 313 K images 200x magnification, measure bar s 100 μm, 323 K image 50x magnification, measure bar 0.5 mm 173
Figure 5 ESEM observed morphologies for 80:20 TL213:2-EthylHexyl Acrylate (2% b/v Crosslinker) polymerized under 2000 mWm^{-2} UV (365 nm) at varying temperatures. 303 K, 313 K images 200x magnification, measure bar s 100 μm, 323 K image 50x magnification, measure bar 0.5 mm 174
Figure 6 ESEM observed morphologies for 70:30 TL213:2-EthylHexyl Acrylate (15% b/v Crosslinker) polymerized under 2000 mWm^{-2} UV (365 nm) at varying temperatures. All images 200x magnification, measure bar is 100 μm 174
Figure 7 ESEM observed morphologies for 73:27 TL213:2-EthylHexyl Acrylate (15% b/v Crosslinker) polymerized under 2000 mWm^{-2} UV (365 nm) at varying temperatures. All images 200x magnification, measure bar is 100 μm 175
Figure 8 ESEM observed morphologies for 75:25 TL213:2-EthylHexyl Acrylate (15% b/v Crosslinker) polymerized under 2000 mWm^{-2} UV (365 nm) at varying temperatures. All images 200x magnification, measure bar is 100 μm 175

Figure 9 ESEM observed morphologies for 77:23 TL213:2-EthylHexyl Acrylate (15% b/v Crosslinker) polymerized under 2000 mWm^{-2} UV (365 nm) at varying temperatures. All images 200x magnification, measure bar is 100 μm 176
Figure 10 ESEM observed morphologies for 80:20 TL213:2-EthylHexyl Acrylate (15% b/v Crosslinker) polymerized under 2000 mWm^{-2} UV (365 nm) at varying temperatures. All images 200x magnification, measure bar is 100 μm 176
Figure 11 ESEM observed morphologies for 70:30 TL213:2-EthylHexyl Acrylate (2% b/v Crosslinker) polymerized under 5000 mWm^{-2} UV (365 nm) at varying temperatures. All images 200x magnification, measure bar is 100 μm 177
Figure 12 ESEM observed morphologies for 73:27 TL213:2-EthylHexyl Acrylate (2% b/v Crosslinker) polymerized under 5000 mWm^{-2} UV (365 nm) at 303, 313, 323 K images 200x magnification, measure bar is 100 μm 333 K image 50x magnification, measure bar 0.5 mm 177
Figure 13 ESEM observed morphologies for 75:25 TL213:2-EthylHexyl Acrylate (2% b/v Crosslinker) polymerized under 5000 mWm^{-2} UV (365 nm) at 303, 313, 323 K images 200x magnification, measure bar is 100 μm. 333 K image 50x magnification, measure bar is 0.5 mm 178
Figure 14 ESEM observed morphologies for 77:23 TL213:2-EthylHexyl Acrylate (2% b/v Crosslinker) polymerized under 5000 mWm^{-2} UV (365 nm) at 303, 313, 323 K images 200x magnification, measure bar is 100 μm. 333 K image 50x magnification, measure bar is 0.5 mm 178
Figure 15 ESEM observed morphologies for 80:20 TL213:2-EthylHexyl Acrylate (2% b/v Crosslinker) polymerized under 5000 mWm^{-2} UV (365 nm) at 303, 313, 323 K images 200x magnification, measure bar is 100 μm. 333 K image 50x magnification, measure bar is 0.5 mm 179
Figure 16 ESEM observed morphologies for 70:30 TL213:2-EthylHexyl Acrylate (5% b/v Crosslinker) polymerized under 5000 mWm^{-2} UV (365 nm) at varying temperatures. All images 200x magnification, measure bar is 100 μm 179
Figure 17 ESEM observed morphologies for 73:27 TL213:2-EthylHexyl Acrylate (5% b/v Crosslinker) polymerized under 5000 mWm^{-2} UV (365 nm) at varying temperatures. All images 200x magnification, measure bar is 100 μm 180
Figure 18 ESEM observed morphologies for 75:25 TL213:2-EthylHexyl Acrylate (5% b/v Crosslinker) polymerized under 5000 mWm^{-2} UV (365 nm) at varying temperatures. 303, 313, 323 K images 200x magnification, measure bar is 100 μm. 333 K image 50x magnification, measure bar is 0.5 mm 180
Figure 19ESEM observed morphologies for 77:23 TL213:2-EthylHexyl Acrylate (5% b/v Crosslinker) polymerized under 5000 mWm^{-2} UV (365 nm) at 303, 313, 323 K images 200x magnification, measure bar is 100 μm. 333 K image 30x magnification, measure bar is 0.5 mm 181
Figure 20 ESEM observed morphologies for 80:20 TL213:2-EthylHexyl Acrylate (5% b/v Crosslinker) polymerized under 5000 mWm^{-2} UV (365 nm) at varying temperatures. 303, 313, 323 K images 200x magnification, measure bar is 100 μm. 333 K image 30x magnification, measure bar is 0.5 mm 181
Figure 21 ESEM observed morphologies for 70:30 TL213:2-EthylHexyl Acrylate (15% b/v Crosslinker) polymerized under 5000 mWm^{-2} UV (365 nm) at varying temperatures. All images 200x magnification, measure bar is 100 μm 182
Figure 22 ESEM observed morphologies for 73:27 TL213:2-EthylHexyl Acrylate (15% b/v Crosslinker) polymerized under 5000 mWm^{-2} UV (365 nm) at varying temperatures. All images 200x magnification, measure bar is 100 μm 182
Figure 23 ESEM observed morphologies for 75:25 TL213:2-EthylHexyl Acrylate (15% b/v Crosslinker) polymerized under 5000 mWm^{-2} UV (365 nm) at varying temperatures. All images 200x magnification, measure bar is 100 μm 183
Figure 24 ESEM observed morphologies for 77:23 TL213:2-EthylHexyl Acrylate (15% b/v Crosslinker) polymerized under 5000 mWm^{-2} UV (365 nm) at varying temperatures. All images 200x magnification, measure bar is 100 μm 183
Figure 25 ESEM observed morphologies for 80:20 TL213:2-EthylHexyl Acrylate (15% b/v Crosslinker) polymerized under 5000 mWm^{-2} UV (365 nm) at varying temperatures. All images 200x magnification, measure bar is 100 μm 184

Introduction

1 Polymer Dispersed Liquid Crystals

Polymer dispersed liquid crystals (PDLCs) are films which consist of liquid crystal droplets encapsulated in a matrix of polymeric species. They are the basis for a new type of display screen technology[1-6], and in particular the basis for flexible displays and electronic books. As such a significant body of work has been performed into understanding the factors which affect their properties as display screens[1, 5, 6], the methods of formulating the PDLC films[2-4, 7] and the properties which effect the mechanisms of formulation and film morphologies formed[8-15]. It is the aim of the work presented in this report to investigate the mechanism by which the films are formed when a polymerization induced phase separation formulation method is utilised; the effect the involvement of a liquid crystalline species has upon this process; the type of morphologies formed and the effect these have upon the electro-optical properties of the films.

2 PDLCs as Displays

Polymer dispersed liquid crystal film based displays work by a concept known as refractive index matching. The idea was first put forward in the work of Beni and Hackwood[16] and first applied to liquid crystals by Craighead et al.[17]. In their paper Beni and Hackwood proposed a display consisting of an array of two components, one which is fixed and has a constant refractive index and a second which has the ability to change its refractive index. Their idea was that if the refractive index of the second species could be controlled, it should be possible to obtain two states; one where the refractive index of the second component matched that of the first and one in which the refractive index differed. In the former case the refractive index matching means that incident light passing through the display would be able to pass across the boundary between the two components without any change to its speed or direction, as such light is not scattered at the interface. In the second case the difference in refractive index between the two components means that incident light does change speed and direction at the interface. If the sizes of the two components of the array are correct (with the width of sections of the array in the range 1-10 μm) then incident light will experience enough interfaces upon hitting the film that the

light will be scattered in all directions. The result of this is that, as long as the matching refractive index is appropriate, in the former state no scattering takes place and the film appears transparent and colourless, and in the latter state the film will appear white due to all the scattering. If then the component which is capable of taking on two different refractive indices can be controlled (refractive index changed upon demand) it should be possible to switch between a scattering (white) and non-scattering (transparent) state. In their original paper, Beni and Hackwood suggested constructing this type of display from a solid matrix, with the second component composed of a liquid with a vapour phase. The liquid is chosen to match the refractive index of the solid, while the vapour differs from it, by the application of electrocapillarity or electro-wetting the liquid can be moved in and out of the solid matrix and therefore the two states can be switched between.

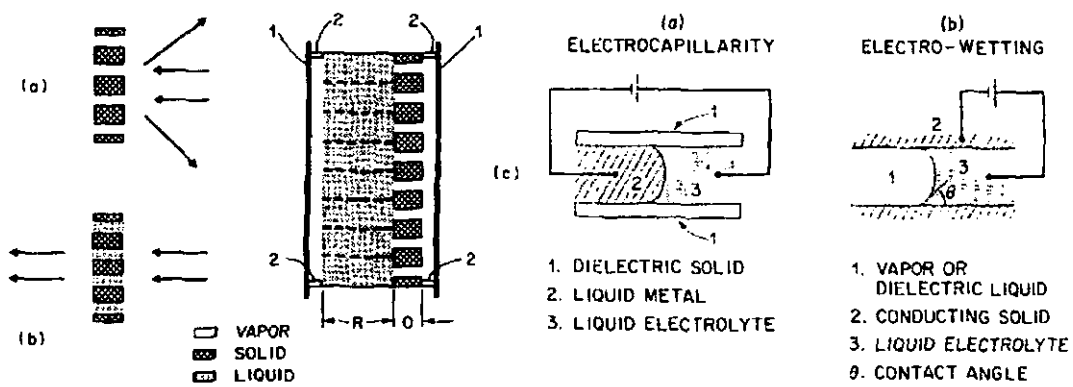

Figure 1 Schematic diagram of Beni and Hackwood's refractive index matching display, diagram taken from[16]

Thermotropic liquid crystal provide the perfect species for use in such displays because, as discussed below, they demonstrate the highly desirable property of possessing two refractive indices and can be switched between them by the application of an electric field. The idea of manufacturing a refractive index matching display from a liquid crystal species encapsulated within a polymeric species one was first proposed by Fergason in his 1984 patent[2] and 1985 paper[2]. Polymers provide the perfect pairing species for liquid crystals in refractive index matching displays for three reasons; firstly many polymers have refractive indices in the required range, both in terms of appearing transparent and in matching that of the liquid crystalline species. Secondly polymers are, when above their glass transition temperature, highly flexible, this makes them perfect for use in flexible displays, and thirdly polymers are very cheap and can be easily manufactured on a large scale.

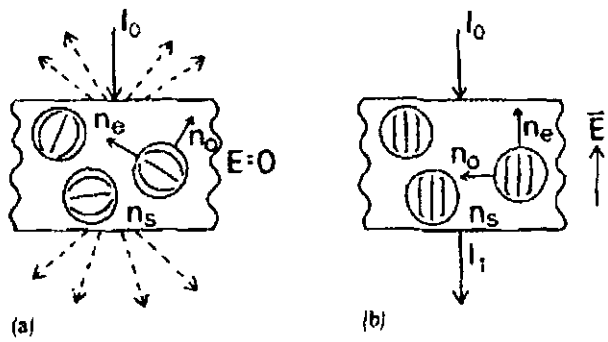

Figure 2 Schematic diagram of how a PDLC refractive index matching screen works, diagram from ref[3]

Figure 2 shows schematically how a PDLC film refractive index matching screen works; while no field is applied to the film, liquid crystal molecules randomly align and the refractive indices of the liquid crystal droplets and the polymer matrix are different, leading to scattering of light and the film appears white (off-state). When an electric field is placed across the film the liquid crystal molecules align and display the same refractive index to incident light as the polymer, so there is no longer scattering and the film appears colourless (the on-state).

3 Liquid Crystals

As the name would suggest liquid crystals are species which demonstrate properties which are a combination of liquid and crystalline phases. There are a number of types of liquid crystal, such as thermotropic, cholesteric, and columnar; the work presented here is only interested in the application of thermotropic liquid crystals, so an explanation of their properties is provided in terms of this type of liquid crystal.

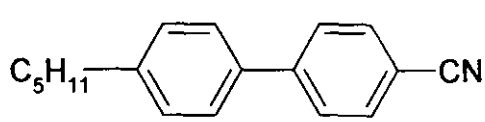

Figure 3 Structural formula of 5 cyano-biphenyl

The distinctive properties of thermotropic liquid crystals result from their molecular structure and electronic properties. Thermotropic liquid crystals are generally of a structure which can be described as rod like, with one axis significantly longer than the other. For example 5-cyano biphenyl (Figure 3), has a backbone consisting of two phenyl groups which are inflexible and as such is much longer than it is wide. This structural asymmetry means that thermotropic liquid crystals demonstrate a phenomenon known as birefringence, whereby, for a single molecule of the liquid crystal, a photon of light hitting it from one structural axis experiences a markedly

different refractive index to a photon of light hitting the other structural axis (Figure 4).

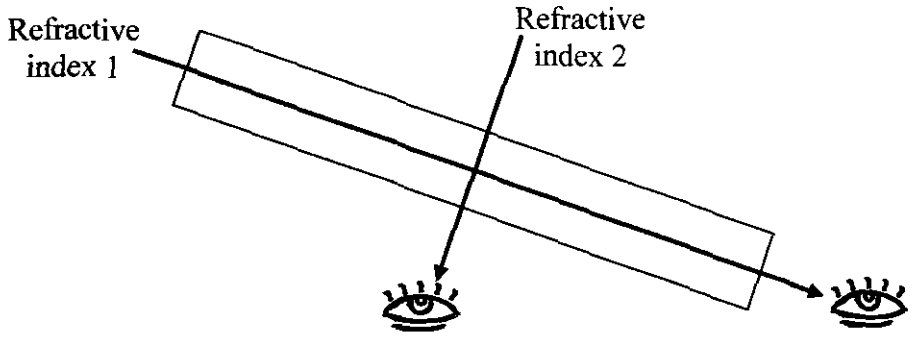

Figure 4 Schematic diagram of how the rod like nature of liquid crystals results in birefringence

This alone is not significant as in a liquid the molecules will be randomly aligned and the effect will be lost as an averaged out refractive index is observed. The second significant property of thermotropic liquid crystals, which again result from their rod like structure, is that in between their isotropic liquid and crystalline solid phases they demonstrate liquid crystalline phases. In these liquid crystalline phases the molecules demonstrate the free diffusion of a liquid, whilst also demonstrating localised ordering more characteristic of a solid.

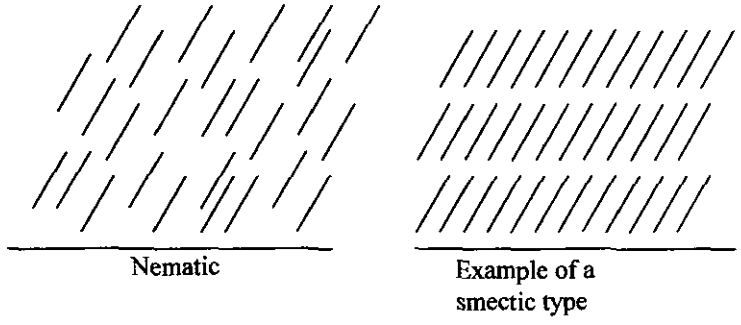

Figure 5 Schematic representation of nematic and smectic phases

There are two main liquid crystalline phases, nematic and smectic; in the nematic phase the molecules demonstrate orientational ordering, but not positional ordering. In a localised area all the liquid crystal molecules will be facing in approximately the same orientation, this orientation being defined by a director, which can either be an external force, such as the application of an electric field, or as the result of dipole interactions between individual molecules. In the latter case the orientation is defined by thermodynamics[18, 19]. In the smectic phase the molecules not only show orientational order but also positional order with molecules arranging themselves into layers. Figure 5 shows schematically the ordering in the nematic and smectic

phases. Most work performed on PDLCs and other liquid crystal based displays, and all the work presented in this report, is performed using liquid crystals which have only a nematic phase, so further consideration of the smectic phase is not presented here.

It is this ordering which allows the effect of the refractive index asymmetry of individual liquid crystal molecules to be used for display purposes; an area (domain) where the molecules are orientated in the same direction will exhibit the same refractive index properties as an individual molecule orientated in that way. So a light photon incident from a given angle will experience the same refractive index regardless of where is enters the liquid crystal.

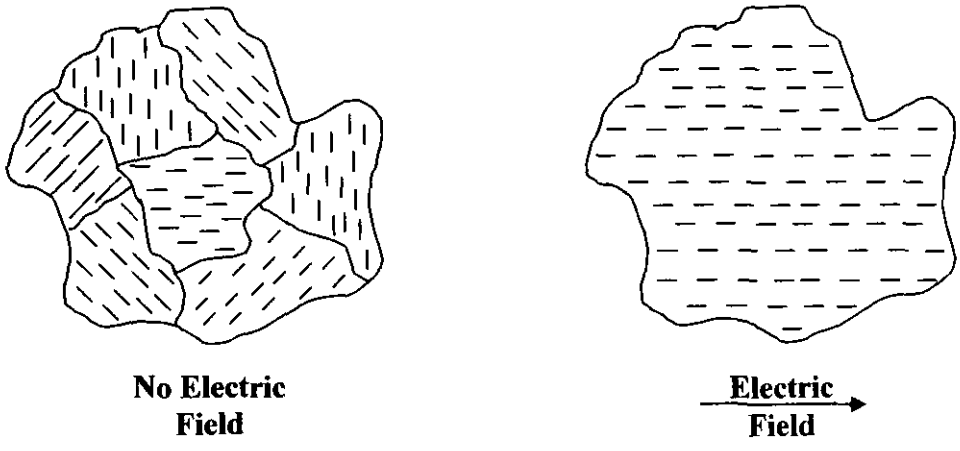

Figure 6 Schemitic diagram of the domain ordering of liquid crystals in the nematic phase and the effect of applying an electric field across a nematic liquid crystal.

As previously stated, the orientation of the director is dependent upon thermodynamics, unless an external force is applied, as such it is possible for different regions of a sample of thermotropic liquid crystal to exhibit different directors (Figure 6). Different refractive indices will therefore be presented to light incident from the same angle depending upon which domain it hits; interfaces between the different domains with different refractive indices are formed, at which light will be scattered. It is for this reason that liquid crystals when in their nematic phase have the appearance of a milky white liquid. The application of an electric field changes this as it causes the liquid crystal molecules to orientate in one single direction for the entire sample. The interfaces between domains of different refractive index are lost, light is no longer scattered and the liquid crystal has the appearance of a colourless liquid.

Electric fields can cause the alignment of liquid crystal molecules for one of two reasons, depending upon the electronic properties of the molecules. If the molecule has no dipole moment (the charge across the molecule is balanced), the application of an electric field results in the creation of a temporary dipole within the molecule, which, due to its structural asymmetry, means the molecules all align to gain the most energetically favourable orientation for the newly induced dipole moment. Most liquid crystals which are used for display screen purposes have a permanent dipole moment resulting from their chemistry. In the case of the bi- and ter-phenyl groups which make up the backbones of most display screen liquid crystals such as 5 cyano-biphenyl (Figure 3) and 4-Chloro-2',2''-difluoro-4''-pentyl-[1,1':4',1''-terphenyl] (Figure 7) the dipole moment is created by attaching groups on either end of the molecules which have different electronegativities, in the case of the former a nitrile group and a hydrocarbon group and the latter a halogenated species and a hydrocarbon. These species will therefore align in an electric field so that the δ+ve end will align towards the negative side of the applied field and δ-ve end towards the positive side of the field.

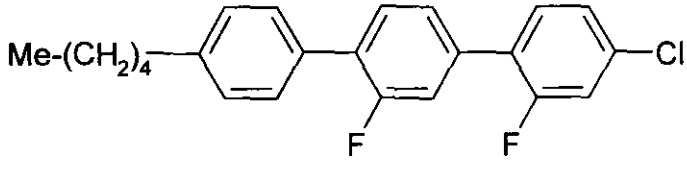

Figure 7 *Structural formula* of 4-Chloro-2',2''-difluoro-4''-pentyl-[1,1':4',1''-terphenyl]

3.1 Advantages of PDLC Screens

As a basis for a display screen technology PDLCs have a number of advantages; firstly by using indium tin oxide for the electronics they can be made from entirely flexible materials. The PDLC layer is flexible, and the indium tin oxide can be printed onto a flexible polymer outer layer which can also act as a water and oxygen barrier. Unlike current liquid crystal displays PDLC based screens can be used to make flexible displays which are perfect for portable devices and e-paper (a thin paper like display which can be read like a book[20, 21]). The reason this is possible while it is not for current liquid crystal based display technologies is twofold; firstly PDLC based screens, unlike current displays, are reflective rather than transmissive[20, 21]. This means, rather than as for current screens which require a back illumination unit to shine light through the liquid crystal layer into the viewers eye, the screen works by external light incident to the screen being either reflected back

and into the eye of the viewer or not depending whether it is in the off or on state respectively (Figure 8).

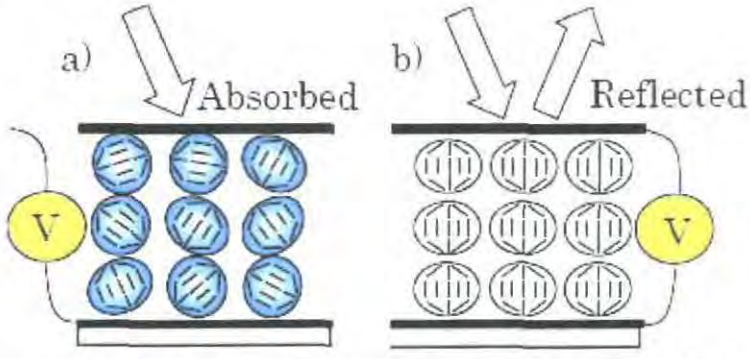

Figure 8 Schematic diagram of how reflective displays work using a PDLC film. a) shows the films in the off state and b) the on state. Reproduced from[21]

Secondly current displays are based upon a concept known as a twisted nematic, whereby the alignment of liquid crystals is used to twist polarised light, in the on state the light is twisted enough so that it is at a 90° angle to its original orientation and so can pass through a second polarizer at 90° to the first. In the off state the light is not twisted as the liquid crystals are randomly aligned and the light cannot pass through the second polarizer. To work this requires high quality polarizers and as yet it has not been possible to develop a polymer based polarizer of the required quality, so glass has to be used. Therefore it is not possible to make a flexible twisted nematic display.

The second advantage of PDLC based screen is the aforementioned reflective nature of the screens; current transmissive devices are considered to be painful and tiring on the eye when viewed for long periods of time making them unsuitable for use as electronic books. PDLCs being based upon a reflective concept act more like paper with the light from an external source being reflected off, are much more suitable and less painful for the eye.

3.2 Controlling the Electro-Optical Properties of PDLC screens

To be of use as display devices screens made from PDLCs need to exhibit three main properties[1, 5, 6]; firstly to be of use for portable devices they need to be able to achieve a high degree of switching (in practice 90% of maximum possible transmission) at a relatively low electric field strength (the ideal for a portable device[21] is a field produced by a voltage of below 10V) so that large batteries aren't required. The second property is a fast switching time, both from the off-state to the on-state by the

application of an electric field and from the on-state to the off-state upon removal of the field. This is required so that the refresh rate of the screen is fast enough to make the displaying of moving images possible (the refresh rates on modern TN-TFT LCD screens is generally of the timescale once every 2-10 ms, although the eye only requires a refresh rate of 24 images per second to view a moving image). The final property is a high contrast ratio, between the on-state light transmission and the off-state transmission; this is a measure of the resolution of the screen, the lower the off-state transmission the whiter the screen will appear and the higher the on-state transmission the clearer the screen will appear.

It has been shown that all of these properties are to a large degree dependent upon the morphological properties of the PDLC films. The best morphology for PDLCs as displays is considered to be a droplet morphology[1, 5, 6, 8, 9, 22, 23] (Figure 9) with droplets of liquid crystal dispersed in a polymer rich matrix. It is the size of these droplets which control the properties of the screen.

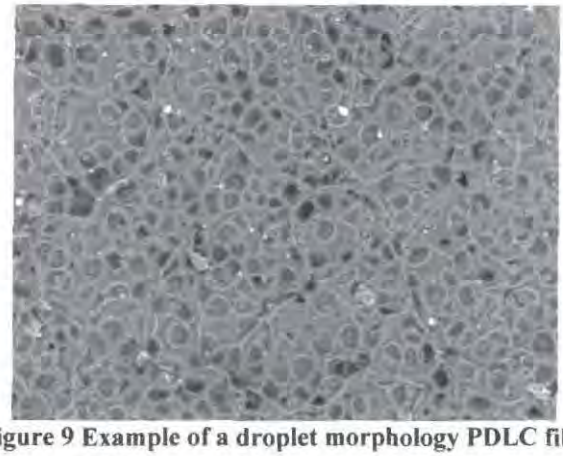

Figure 9 Example of a droplet morphology PDLC film

3.2.1 Contrast Ratio

The refractive index matching concepts work because the droplet sizes are an order of magnitude larger than the wavelength of the light being scattered, if the droplets are too small then the light waves will not experience the individual interfaces between droplets, just the film as a whole. As such, the light will only change speed and direction as it enters and leaves the film, so there is not the required number of scattering events to make the light reflect back in the direction it came from, and cause the screen to appear white. It has been shown[10, 22, 24] that this limit is generally reached at around 2 μm, and below this point the amount of light which can pass through the film in the off-state begins to increase, above this limit the amount of scattering decreases with increasing droplet size. This is due to the fact that the larger

the droplets the lower the likelihood that incident light will hit enough interfaces to be reflected back towards the viewer. It has been shown[10, 22, 24] that this starts to become significant around 5 μm and at around 10 μm it is the case that the morphology size is large enough that the individual components of the film become identifiable to the eye. At this point the droplets are of a large enough size compared to the wavelength of light that incident rays only experience one component species upon passing through film and light is no longer scattered back towards the observer. It has been shown therefore that the ideal morphology size for optical properties is in the range of 2-5 μm. The effect of morphology size upon transmission in the on state is minimal as there should be no interfaces to cause scattering in the on state.

3.2.2 Electronic properties

As with the optical properties, the electric field and speeds at which the PDLC films switch are dependent upon the size of the droplets. There are two effects to consider; firstly switching to the on-state, which relates to the magnitude of electric field required and the rate at which the liquid crystals switch (rise time) and secondly the switching to off-state which relates only to the time required for the liquid crystals to switch back (fall time). The property which controls these is the same, but the reverse effect in each case. When encapsulated within the polymer, the liquid crystals experience ordering effects from the polymer interface, to get the liquid crystal to switch to the on-state these ordering effects have to be overcome so that all the liquid crystals are pointing in the same direction and presenting the same refractive index to incident light. Equally to return back to the off-state requires the polymer interface to exert its ordering effect, this occurring upon removal of the electric field, resulting in the liquid crystal molecules becoming unaligned as a whole. Therefore in the former case the less interface area exerting an ordering force upon the liquid crystal the better, and in the latter case the more the better.

This effect for the encapsulated droplets of liquid crystals in PDLCs can be thought of in terms of the ratio of the volume of liquid crystal in the droplets to the area of the interface between the liquid crystal and polymer. The higher the ratio (larger the droplet size) the less disordering effects to overcome per volume of liquid crystal and therefore the lower the field strength required to bring about switching and the faster switching is achieved. Equally the higher the ratio, the slower the droplets of liquid crystals will switch back to their previous disordered state. As such the two effects

are actually contrary to each other, to make the film switch faster and at a lower voltage by increasing the droplet size means that it will switch back to the off-state slower. This has been shown to be the case by many studies[5, 9-11, 22, 24].

Overall this means that the two most important properties required of a PDLC screen, low switching field and contrast ratio are actually dependent upon contradictory requirements, for the former a large droplet size is required and the latter a small (but larger than 2 μm) droplet size is required. It is therefore of great interest to be able to optimise between the two requirements, or to determine a way in which one of the two properties can be improved without the requirement of changing the droplet size.

4 PDLC Formulation Techniques

Three techniques have been proposed for the formulation of PDLCs. The first[2, 4] works on the basis of forming an emulsion of liquid crystal and polymer in a solvent (usually water) and then evaporating the solvent off to leave a dispersed film. The second method is thermally induced phase separation[1, 7] (TIPS), a blend of liquid crystal and polymer are heated up to above the phase mixing temperature and then the melt is cooled below the phase mixing temperature again. The phase separation thermodynamics and mechanism cause the liquid crystal rich phase to separate out into droplets within the polymer rich phase.

The final formulation method is polymerisation induced phase separation (PIPS), this can either be through the use of photo-polymerisation[3, 6, 8-11, 13, 15, 20, 21] or thermally induced polymerisation[1, 7, 25, 26]. In this method a completely phase mixed starting solution of monomer in liquid crystal is prepared; the monomer is subsequently polymerised until a point is reached where it becomes thermodynamically unfavourable for the polymer chains to remain dissolved in the liquid crystal and phase separation occurs. As for thermally induced phase separation the thermodynamics and mechanism of phase separation control the morphology formed. Photo-polymerisation induced phase separation is by far the most popular technique for forming PDLCs as it is relatively easy and does not require the high temperatures necessary for both thermally induced phase separation and thermal polymerisation phase separation techniques. It also provides consistency of morphology and droplet size which has been shown to be lacking films formed by emulsion evaporation

preparation techniques[4, 5]. Evaporation techniques also have the disadvantage of forming oblique droplets of liquid crystal due to the structural collapse of the film as the solvent evaporates off[5]. For these reasons it is the PIPS technique which is utilised in the work presented in this report.

5 Aims of Work

The aims of the work presented in this report are fourfold; the main aim of the work is to examine PDLCs in terms of formation mechanism with the aim of determining the mechanism by which PDLC films form and the dependence of the phase separation mechanism upon composition, cure temperature and cure UV intensity. This phase separation mechanism is also to be related to the type and size of morphology formed which in turn is to be related to the electro-optical properties of the films. This work is presented in Section B of the report. As the effect of phase separation conditions is being investigated it is important to understand the phase properties of the monomer/liquid crystal and polymer liquid crystal systems from which they are formed. As such Section A presents work determining the phase diagrams for a series of monomer/liquid crystal pairs and relates these to phase mixing theory, and in particular the effect of the liquid crystalline species upon the phase mixing thermodynamics. The final aim is an attempt to improve the electro-optical properties of the PDLC films by changing the chemistry of the monomer/liquid crystal pair and in particular the effect of having both a fluorinated monomer and liquid crystal species as the components of the PDLC films. This is investigated in terms of both the effect of the chemistry upon phase properties and separation mechanism, and to see if the fluorination can affect the disordering effect at the polymer/liquid crystal interface; this work is presented in Section C.

Bibliography

1. Drzaic, P. S., *Liquid crystal dispersions*. World Scientific: Singapore ; London, 1995; p xv,429p.
2. Fergason, J. L. *SID Int. Symp. Dig. Tec.* **1985,** 85, 68-70.
3. Doane, J. W.; Vaz, N. A.; Wu, B. G.; Zumer, S. *Applied Physics Letters* **1986,** 48, 269-271.
4. Drzaic, P. S. *Journal of Applied Physics* **1986,** 60, 2142-2148.
5. Coates, D. *Journal of Materials Chemistry* **1995,** 5, 2063-2072.
6. Doane, J. W.; Golemme, A.; West, J. L.; Whitehead Jr., J. B.; Wu, B. G. *Molecular Crystals and Liquid Crystals* **1988,** 165, 511-532.
7. West, J. L. *Molecular Crystals and Liquid Crystals* **1988,** 157, 427-441.
8. Amundson, K. *Physical Review E* **1996,** 53, 2412-2422.
9. Amundson, K.; vanBlaaderen, A.; Wiltzius, P. *Physical Review E* **1997,** 55, 1646-1654.
10. Carter, S. A.; LeGrange, J. D.; White, W.; Boo, J.; Wiltzius, P. *Journal of Applied Physics* **1997,** 81, 5992-5999.
11. LeGrange, J. D.; Carter, S. A.; Fuentes, M.; Boo, J.; Freeny, A. E.; Cleveland, W.; Miller, T. M. *Journal of Applied Physics* **1997,** 81, 5984-5991.
12. Nwabunma, D.; Chiu, H. W.; Kyu, T. *Journal of Chemical Physics* **2000,** 113, 6429-6436.
13. Nwabunma, D.; Chiu, H.-W.; Kyu, T. *Macromolecules* **2000,** 33, 1416-1424.
14. Nwabunma, D.; Kyu, T. *Macromolecules* **1999,** 32, 664-674.
15. Nwabunma, D.; Kyu, T. *Polymer* **2001,** 42, 801-806.
16. Beni, G.; Hackwood, S. *Applied Physics Letters* **1981,** 38, 207-209.
17. Craighead, H. G.; Cheng, J.; Hackwood, S. *Applied Physics Letters* **1982,** 40, 22-24.
18. Maier, W.; Saupe, A. *Zeitschrift Fur Naturforschung Part a-Astrophysik Physik Und Physikalische Chemie* **1959,** 14, 882-889.
19. Maier, W.; Saupe, A. *Zeitschrift Fur Naturforschung Part a-Astrophysik Physik Und Physikalische Chemie* **1960,** 15, 287-292.
20. Masutani, A.; Roberts, T.; Schuller, B.; Yasuda, A.; Sakaigawa, A. *IDRC* **2003**, 6.2.
21. Masutani, A.; Roberts, T.; Yasuda, A.; Sakaigawa, A.; Cross, G.; Bloor, D. *22nd International Display Research Conference Proceedings* **2002**, 47-50.
22. Grand, C.; Achard, M. F.; Hardouin, F. *Liquid Crystals* **1997,** 22, 287-296.
23. Lovinger, A. J.; Amundson, K. R.; Davis, D. D. *Chemistry of Materials* **1994,** 6, 1726-1736.

24. Nomura, H.; Suzuki, S.; Atarashi, Y. *Japanese Journal of Applied Physics Part 1-Regular Papers Short Notes & Review Papers* **1990,** 29, 522-528.

25. Smith, G. W.; Vaz, N. A. *Liquid Crystals* **1988,** 3, 543-571.

26. Chien, L. C.; Lin, C.; Fredley, D. S.; Mccargar, J. W. *Macromolecules* **1992,** 25, 133-137.

Experimental

1 Materials

1.1 Morphological Work

For studying the phase separation mechanism, morphology of PDLC films and electro-optical properties the liquid crystal species used is the Merck halogenated blend TL213. Chosen for its desirable properties to Sony[1, 2] as a liquid crystal blend for an active matrix display; TL213's ordinary refractive index of 1.53 is a good match for the type of polymer species used and has a nematic range of ~275K to 354K ideal for the working temperature range of a display screen device. The exact composition of TL213 is unknown, but is known to contain halogenated terphenyl molecules including 2',2'',4''-trifluoro-4-propyl-1,1':4'1''-terphenyl (Figure 1) and 4-chloro-2',2''-difluoro-4''-pentyl-1,1':4',1''-terphenyl (Figure 2).

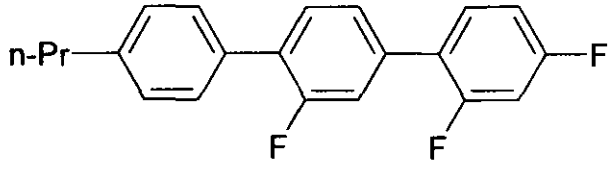

Figure 1 2',2'',4''-trifluoro-4-propyl-1,1':4'1''-terphenyl

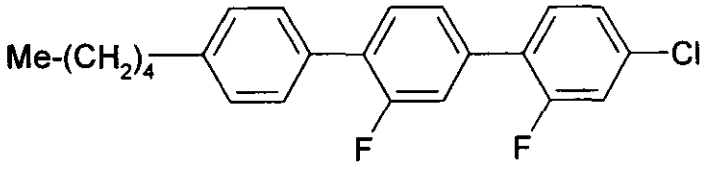

Figure 2 4-Chloro-2',2''-difluoro-4''-pentyl-1,1':4',1''-terphenyl

Given that the liquid crystal species is to a large degree unknown, it is considered important that the polymer species is precisely known, so the commercial photo initiated pre-polymer PN393[1, 2] utilised in many PDLC studies is not used in this work. The monomer 2-ethylhexyl acrylate (EHA) (Figure 3) (refractive index 1.436) was used with the crosslinking species trimethylol propane triacrylate (Figure 4) (both sourced from Aldrich Chemicals) as these are known to be the main constituent species of PN393[3]. This combination however lacks the liquid crystalline monomer species present in PN393 which improve PDLC electronic and optical properties, but it allows for control of both the crosslink density and the amount of initiator present. The initiator used is a combination of 4-(dimethylamino)-benzophenone and the co-

initiator N-methyldiethanol-amine) (sourced from Aldrich Chemicals). All chemicals were used as supplied.

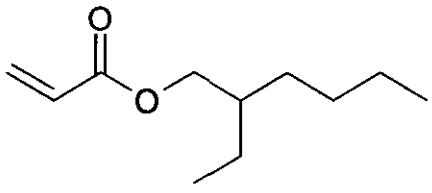

Figure 3 2-ethylhexyl Acryl ate

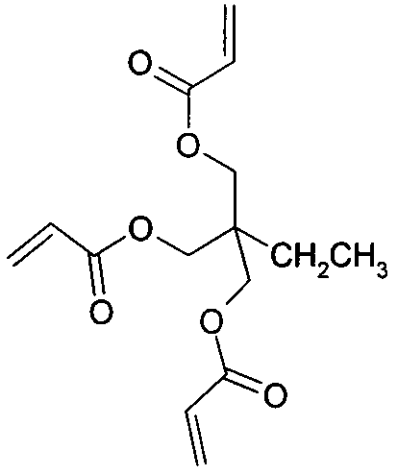

Figure 4 Trimethylol propane triacrylate

1.2 Phase Property Investigations

For small angle light scattering studies of phase properties the materials investigated are the same as those used in other studies described above and below as the phase diagram is used as a tool to understand further results. In studies where small angle neutron scattering is used to determine fundamental properties of species it is necessary – as described later – to have a deuterated species, limiting choice to availability. Phase property investigations by SANS are limited to the test system of the single deuterated cyano-biphenyl liquid crystal species 4-cyano-4'-n-pentyl-d_{11}-diphenyl (d5CB) (Figure 5) (CDN Isotopes) and the polymer poly(butyl acrylate) (Figure 6) of molecular weight 3650 $gmol^{-1}$ (Polymer Source). All chemicals were used as supplied

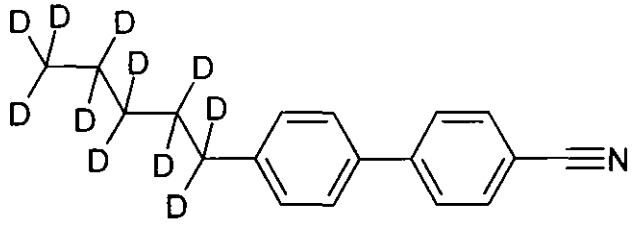

Figure 5 4-cyano-4'-n-pnetyl-d_{11}-diphenyl

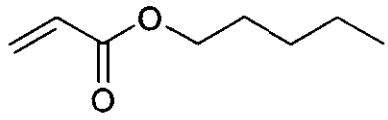

Figure 6 Butyl Acrylate

1.3 Polymer Fluorination Studies

For experimental studies presented where the polymer species is doped by a fluorinated monomer during cure, 2,2,3,3,4,4,4-heptaflurobutyl acrylate (HFBA) (Figure 7) and 2,2,3,3,4,4,5,5,6,6,7,7,7-dodecafluoroheptyl acrylate (DDFHA) (Figure 8) are used as the dopant species (both sourced from Aldrich Chemicals).

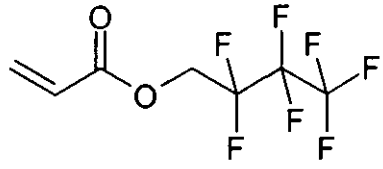

Figure 7 2,2,3,3,4,4,4-heptafluorobutyl acrylate

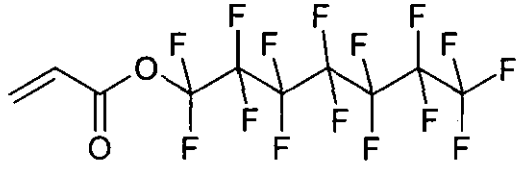

Figure 8 2,2,3,3,4,4,5,5,6,6,7,7,7-dodecafluroheptyl acrylate

2 Small Angle Light Scattering

Small angle light scattering (SALS) is a commonly used technique in polymer physics studies as it non-invasively elucidates a number of significant properties in polymer systems. In terms of the type of phase separation and morphological work presented within this thesis there are three applications of SALS; determination of phase separation temperatures and times, morphological size determination, and phase separation mechanism determination.

2.1 SALS Concept

When incident light enters a film containing two dispersed species with differing refractive indices, the light will be refracted at the interface between the two species scattering at an angle dependent upon its incident angle and the refractive indices of the two species. This is demonstrated schematically in Figure 9, k_i represents the incident wave vector; the wave vector of light scattered by an angle θ is represented by k_s.

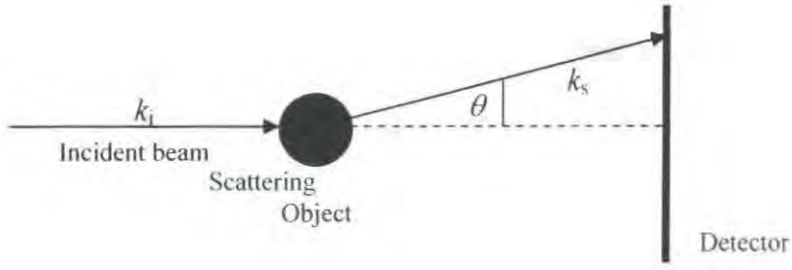

Figure 9 Schematic geometry of a scattering event

The resultant vector defined by;

$$q = k_s - k_i \tag{1.1}$$

is referred to as the scattering vector q and can be calculated by,

$$q = \frac{4\pi}{\lambda}\sin\theta \tag{1.2}$$

where λ is the wavelength of the incident light.

Different light waves scattered by different interfaces will be out of phase and as such will undergo interference. For a regular lattice type system – such as is the case for a polymer film with a regular morphology – this can be understood in terms of Bragg scattering (Figure 10),

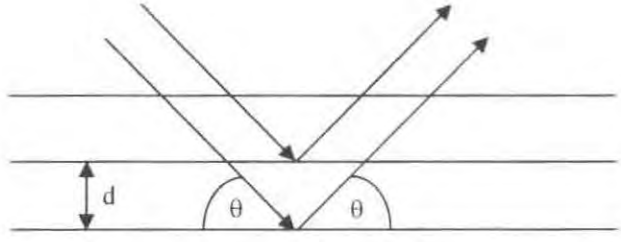

Figure 10 Schematic representation of Bragg Scattering

The observed scattering pattern will demonstrate its highest intensity only when two scattered light waves are in-phase with each other causing constructive interference and lowest intensity when two perfectly out of phase waves interfere destructively. According to Bragg's law, for a regular lattice constructive interference will occur when the following condition is met,

$$n\lambda = 2d\sin\theta \tag{1.3}$$

where d is the domain size of the lattice, n an integer number of wavelength path-length difference between the two diffracting light waves and θ the scattering angle. If the system is made up of a regular morphology then you would expect constructive

interference rings, with the separation of the rings determined by the domain size of the scattering material. By combining equations (1.2) and (1.3) it is possible to relate the scattering vector to the length-scale of the morphology,

$$d = \frac{2\pi}{q} \tag{1.4}$$

2.2 Phase Separation Temperature and Time Determination

As light scattering requires at least two species to be present of differing refractive index the technique can be used as a simple and effective method for determining when two species have phase separated. As long as the phase mixed system has a refractive index that light can pass through (i.e. the sample is transparent) there will be no scattering when the sample is homogenously mixed. When the system is changed either by reaction or temperature such that phase separation is initiated, domains of two new phases with usually differing refractive index will be formed and the sample will begin scattering. Through the use of a temperature control stage to ramp the sample through a temperature range and correlating the point at which scattering begins to the temperature it is possible to determine the type of temperature/composition phase diagram discussed later in Section A. Equally initiating curing and observing the time of initial scattering can be used to determine polymerisation induced phase separation times.

2.3 Determination of Morphology Size

As discussed if a system exhibits a consistent morphology size throughout the sample then scattering is described by Bragg's laws, and the scattering vector at which a peak is observed is related to the morphology size. By using a diffraction grating of known width (d) and applying equation (1.4) it is possible to calibrate the experimental set up so that radial distance (number of pixels away from centre) can be related to the scattering vector, and in turn the morphology size. In the case where the morphology is not of a consistent size scattering will not result in a peak in the interference pattern and therefore it is not possible to gain any morphology size evidence via light scattering.

2.4 Elucidation of Phase Separation Mechanism

As will be discussed in further detail in Section B some mechanisms of phase separation form by their nature a consistent morphology size which is indicative of the mechanism. As such the presence or lack of a scattering ring denotes whether or not morphology is consistent in size and the likelihood of a particular phase separation mechanism occurring.

2.5 Experimental Set-Up

The light scattering set-up consists of a Siemens 5 mW HeNe laser source of wavelength 635 nm set to pass perpendicular through the sample under test. The sample is placed upon a Linkam THMS 600 temperature control stage to allow control to ± 0.1K. The scattered light is projected onto a screen with a beam stop through the centre to avoid saturation of the CCD camera used to record the scattering patterns by the central unscattered beam. The images captured by the CCD can then be computer analysed to produce a radial scattering average from which a plot of intensity against scattering vector is possible.

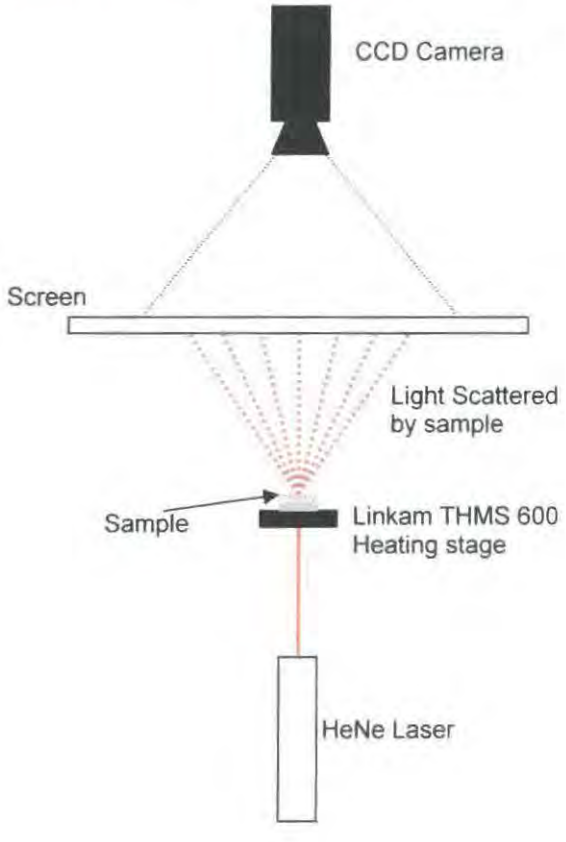

Figure 11 Small angle light scattering experimental set-up

2.6 Sample Preparation

Liquid crystal/monomer solutions of appropriate composition are prepared by mixing until homogeneous (transparent); 10 μl of the sample is pipetted onto a glass slide prepared with an adhesive, a second glass slide is placed on top and closed to a separation of ~50 μl by pressure to form a cell. The cell is placed on the Linkam heating stage and caused to phase separate either via a temperature change, or at a constant temperature by polymerisation induced by irradiating with a 365 nm UV-LED of known intensity.

3 Environmental Scanning Electron Microscopy

3.1 SEM Concept

Scanning Electron Microscopy (SEM) is a technique used to examine the surface structure of materials where the structural properties of interest are too small to be observed via optical microscopy or the refractive index of the material makes optical microscopy indistinct. The technique works by firing a beam of electrons at the sample under study and through the use of a series of detectors observing their behaviour after interacting with the sample. Depending upon the type of detector used it is possible to determine two main properties of a material under study; the surface topography and the relative electron density of a species to give an approximate idea of composition. When the electron interacts with an atom in the sample there are four possible results; **i.** the electron is absorbed and therefore no information can obtained about the sample. **ii.** The electron collides with the atom's nucleus and is scattered back towards the source where it is measured by the use of a backscatter detector. A higher atomic mass species will appear brighter as its larger nucleus will have a higher probability of interacting with an incident electron. **iii.** Electrons interact with electrons within the atom passing on energy to them, causing a secondary electron to be emitted. The low energy of emitted electrons mean that they are unable to travel far from the surface so the population at a given distance from the sample provides information on topography. **iv.** In the case where a secondary electron is emitted it is possible that the atom needs to release energy to regain equilibrium and will therefore emit either an X-ray quantum or a photon. All of these results are dependent to some degree upon both the topography of the system and the atomic mass of the atoms they are interacting with. In general use is

made mainly of backscattered and secondary electrons in comparison to total emitted electrons (accounts for absorbed electrons) to generate the image.

A scanning technique is applied to increase the area it is possible to probe on a sample. Electric fields are used to deflect the incident electron beam to scan a series of sites on the sample with the number of backscattered and/or secondary electrons counted for that site so a topographical image can be built up.

3.2 Environmental SEM

For standard SEM to work a high vacuum is required as electrons will be quickly absorbed by any atmospherically dispersed species and as such alter the image. This means that samples must be perfectly dry so any volatile species does not become atomised at low pressure. Equally the sample must be electrically conductive otherwise the sample will charge up and degrade; this is normally overcome by sputtering the surface with a conductive material such as gold. If the sample to be examined requires that a volatile species or insulator be imaged it is possible to utilise Environmental Scanning Electron Microscopy (ESEM). The technique works by separating the main gun column which is under full vacuum from the scanning chamber which is flooded at very low pressure (0.1-1 Torr) with water vapour. This water vapour acts as an amplifier for secondary electrons; the original secondary electrons in turn cause the production of secondary electrons in the water vapour molecules causing a cascade effect back to the detector. By emitting these secondary electrons the water molecules become positively charged and can therefore neutralise the charge build up on the sample allowing insulators to be imaged.

3.3 Sample Preparation and Imaging

To image PDLC morphologies after formation via reaction induced phase separation the cells are broken open and the free liquid crystalline phase is washed out using methanol to leave only the relief surface of the polymer rich phase. The sample is left to dry for a minimum of 24 hours to allow any surface methanol to evaporate off. Experiments are performed in a Phillips FEI XL30 Environmental Scanning Electron Microscope, operating in environmental mode at a water vapour pressure of ~0.3 Torr, an acceleration voltage of normally 15.0 kV, but between 10 and 25 kV depending upon the sample and conditions. While both backscattered and secondary electrons provide the desired topographical images it is found that the backscatter

detector provides the superior images at the relatively low magnifications required for the systems under study and is utilised for this study. Magnification is generally between 50x and 500x, with most images being taken at 200x; magnification up to 1000x was possible but any greater than this causes the degradation of the sample without providing any further useful information.

4 Small Angle Neutron Scattering

Neutron scattering has proved to be of great interest for polymer research[4-6], it can provide a variety of information including; the use of neutron reflection to determine depth composition information[7], neutron spectroscopy to determine polymer dynamics[4], and neutron scattering to determine the arrangement and crystal structures of polymers[4]. Of interest in studying PDLCs is Small Angle Neutron Scattering (SANS), which provides a method of quantifying the phase mixing properties of a system independent of it's composition[8-11].

Neutrons have wavelengths varying between 1 and 20 Å, the same order of magnitude as for inter-atomic distances, and as such can be used to investigate local molecular motions. Knowledge of molecular diffusion (localised composition) can therefore be obtained. And through the use of deuterium doping it is also possible to differentiate between two hydrocarbon rich species.

Small angle neutron scattering is analogous to small angle light scattering (as in Figure 9), a neutron of known wavelength is propelled incident to a scattering centre (in this case the nucleus of a constituent atom of a polymer chain), and will be scattered with a wave amplitude defined by the type of nucleus it has been scattered by. This amplitude is quantified by the scattering length b; for[10] hydrogen -3.741 x 10^{-15} m and deuterium 6.671 x 10^{-15} m. The fact that hydrogen is negative and deuterium positive provides the strong contrast required between two hydrocarbon rich species to see them separately. The scattering length is most relevantly applied in the form of the scattering length density ρ for a given type of molecule,

$$\rho = n\sum_i b_i = \frac{\sum_i b_i}{v} \tag{1.5}$$

Where n is the number concentration of the scattering centre, i is the constituent atom of the molecule, and v the volume of a single molecule.

The scattered neutrons are detected by a large 2D array detector which measures the population of neutrons of a given wavelength scattered through a given angle, in a given time frame. This is quantified by the differential scattering cross-section $\frac{\partial \Sigma}{\partial \Omega}(|q|)$. As analogous with SALS, scattering properties are related to the detector population via a scattering vector q, and can be interpreted in terms of Bragg scattering as in equations (1.2) (1.3) (1.4). For SANS, due to the much smaller wavelength d is a molecular-level length scale. For isotropic systems interpretation is in terms of the modulus of the scattering vector $|q|$. This is equal to the modulus of the difference between the scattered and incident vectors,

$$|q| = |k_s - k_i| = \frac{4\pi}{\lambda}\sin\theta \tag{1.6}$$

The way in which these scattered neutron waves constructively and destructively interfere can be used to determine localised structural and compositional properties.

4.1 Small Angle Neutron Scattering to Determine Interaction Parameters

As will be discussed in further detail in Section A the interaction of two species in a solution can be quantified using Flory-Huggins theory. In particular for two given species their enthalpic interaction is quantified by an interaction parameter χ. SANS[8-11] can be used to determine this parameter independent of the compositional fitting to phase diagrams method usually applied. The method works by examining localised fluctuations in the composition of a one phase system, with the neutrons able to probe these fluctuations on a molecular level.

To link the differential scattering cross-section to the compositional fluctuations and subsequently the effective Flory-Huggins interaction parameter, de Gennes'[12] random phase approximation (RPA) is applied.

$$\frac{(\Delta\rho)^2}{\frac{\partial \Sigma}{\partial \Omega}(|q|)} = \frac{1}{N_1 v_1 \phi_1 P\left(|q|, R_{g,1}^2\right)_{Debye}} + \frac{1}{N_2 v_2 \phi_2 P\left(|q|, R_{g,2}^2\right)_{Debye}} - \frac{2\chi_{eff}}{v_{ref}} \tag{1.7}$$

where N_1, N_2 are the degrees of polymerisation of species 1 and 2 respectively, v is the monomer volume, ϕ the volume fraction, χ_{eff} the effective interaction parameter,

and $P\left(|q|, R_g^2\right)_{Debye}$ the Debye form factor. Importantly as can be seen with $|q|$ tending to zero the form factors tend to 1, so that,

$$\frac{(\Delta\rho)^2}{\frac{\partial\Sigma}{\partial\Omega}(0)} \approx \frac{1}{N_1 v_1 \phi_1} + \frac{1}{N_2 v_2 \phi_2} - \frac{2\chi_{eff}}{v_{ref}} \tag{1.8}$$

This analysis method gives the effective interaction parameter for a given set of conditions (composition and temperature), but the interaction parameter is temperature dependent and can be composition dependent. While it is the aim of the work presented to investigate the composition dependence, the temperature dependence can be easily interpreted. Phenomologically the interaction parameter is often written in the form,

$$\chi_{eff} = a + \frac{b}{T} \tag{1.9}$$

where a and b are constants, by running a series of experiments at different temperatures above the phase mixing temperature for a blend which phase separates on cooling it is possible to fit the results to gain values for a given system.

4.2 Experimental and Sample Preparation

SANS experiments were performed at the ISIS facility in Chilton, Berkshire, UK using the LOQ fixed geometry time of flight instrument. Samples are prepared with varying composition of deuterated 5CB and poly(butyl acrylate) as determined to be appropriate by the phase diagram and placed in Hellma cells of path length 1 mm. A neutron beam of 8 mm diameter is used giving a sample volume of 5.026 x 10^{22} Å^3. The scattering lengths of the two species are shown in Table 2

Element	Carbon	Deuterium	Hydrogen	Nitrogen	Oxygen
Atomic Scattering length/*m*	6.646E-15	6.671E-15	-3.741E-15	9.362E-15	5.803E-15

Table 1 Atomic scattering lengths

Species		Molecular scattering length/*m*
Deuterated 5CB	$C_{18}D_{11}H_8N_1$	1.724E-13
Poly(butyl acrylate)	$C_7H_{12}O_2$	1.324E-14

Table 2 Molecular scattering lengths of species under test

5 Rheology

5.1 Concept

Rheology[13, 14] is the study of the deformation and flow of matter, an ideal solid will undergo reversible elastic deformation upon the application of a stress, whereas an ideal fluid will behave as a viscous material and undergo irreversible flow deformation. In the case of polymer systems – in particular those which are in solution – this becomes more complicated as they cannot be considered as either an ideal solid or liquid and in fact have visco-elastic properties with a component of each type. It is possible through the use of appropriate rheological techniques to separate these two properties. This can be achieved by the use of oscillatory rheology between two plates, a lower stationary plate and an upper oscillating plate, this set up is capable of measuring the complex viscosity η^* of the system as defined by,

$$\eta^* = \frac{\left[(G')^2 + (G'')^2\right]^{\frac{1}{2}}}{\omega} \tag{1.10}$$

Where G' is the storage modulus which is related to the elastic properties of the system under test, G'' is the loss modulus which is related to the viscous properties and ω is the oscillatory frequency. It is possible to separate out these two components so that the two physical properties can be analysed separately.

5.2 Using Rheology to Determine Phase Separation Mechanics

While rheology is a useful tool for determining absolute physical properties of a material, the work presented is interested merely in relative effects during the polymerisation and phase separation processes, in particular the evolution of system viscosity with polymerization and morphology evolution. Therefore presented are viscosity and elasticity time dependent profiles, which show how these properties evolve during the curing process.

5.3 Experimental Set-Up and Sample Preparation

All experiments are performed on a TA Instruments AR2000 using a 40mm quartz plate geometry with a Peltier stage as the static plate to maintain cure temperature.

100 µl of LC/monomer solution is pipetted onto the Peltier stage and the quartz geometry lowered to a 10 µm gap. The sample undergoes an initial condition step for one minute at an angular velocity of 0.06 radians per second to reduce the chance of LC alignment having an effect on the results. The sample is irradiated with 365 nm UV of maximum intensity 700 mWm^{-2}, less than for other experiments performed due to structural restrictions of equipment (the proximity with which, to the sample, the UV LED can be placed). Simultaneously the upper geometry is oscillated at 1 Hz and an amplitude of 0.0174 radians (1 degree) and time dependent G' and G'' values recorded. These profiles can then be utilised to determine morphological rearrangements due to changes in the samples elastic properties and viscosity increases due to chain growth and system gelation.

6 Electro-Optical Measurements

There are three main electro-optical properties of interest for a PDLC system; **i**. the optical transmission in the on and off states (contrast ratio). **ii**. The electric field strength required to bring about switching between the on and off states. **iii**. The speed at which the system switches between the on and off states. It is possible to measure these three properties simultaneously; this is achieved by applying an electric field across the sample film and measuring the light transmission in relation to the applied field. Due to the S-shape (Figure 12) of the transmission voltage dependence, to generate the first and last 10% increases in transmission large field changes are required.

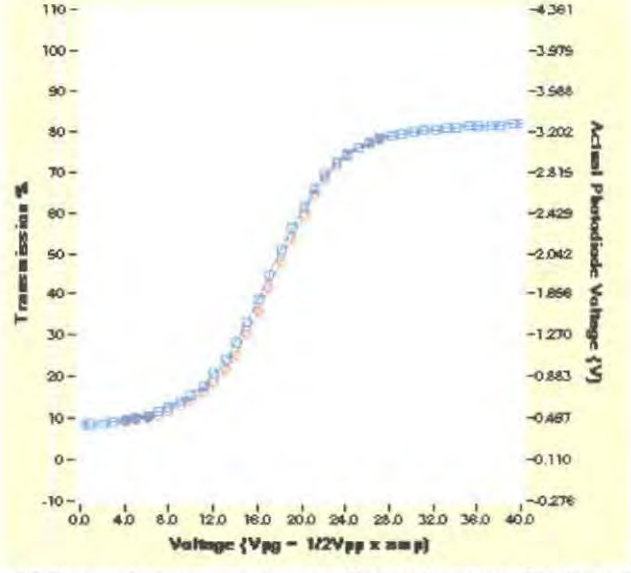

Figure 12 Example transmission applied voltage profile for a PDLC

Therefore instead of taking values for the electric field required to bring about full switching (100% of maximum transmission) measurements are taken in terms of E_{90} or the field required to bring about 90% of maximum transmission[1, 2, 15-17]. Equally switching times are measured between the 10% and 90% switching states. Equations have been derived[18-20] for the rise τ_{rise} and fall τ_{decay} times of encapsulated nematic liquid crystals,

$$\tau_{rise} = \frac{\gamma_1}{\frac{\Delta \in E^2}{4\pi} - \frac{K\left(L^2-1\right)}{R^2}} \tag{1.11}$$

$$\tau_{decay} = \frac{\gamma_1 R^2}{K\left(L^2-1\right)} \tag{1.12}$$

where γ_1 is a rotational viscosity coefficient for the liquid crystal, $\Delta \in$ the dielectric anisotropy of the liquid crystal, E the applied field, K a Frank elastic constant for distortion of the nematic field, L the droplet aspect ratio and R the characteristic droplet ratio. As can be seen from the equations the decay time is field independent and therefore purely a physical property of the film, as such it is possible to record the decay time as an average of a series of tests. The rise time however is field dependent and therefore a way is required to quantify the properties of a given film in a field independent manner. To do this a value is calculated for the elastic constant of the film rather than the actual rise time. As can be seen from equation (1.11) K is related to the applied field and the rise time; as such it is possible to determine a K value from the intercept of a graph of the reciprocal of the rise time against the square of the applied field.

6.1 Experimental Set-Up

The electro-optical results presented in this report were performed by the author at Sony Deutschland's Materials Science Laboratory in Stuttgart, Germany using their experimental set up[1, 2]. This consisted of a Leica DMR-X-HC confocal microscope working in transmission mode using a white light source, an Edmund Optics NT54035 photodiode to measure the percentage transmission of light through the film, and a Linkam LTS350 hot stage to maintain the sample cell at 35°C throughout testing. The whole device is driven using a National Instruments 6024E DAQ PCMCIA data logging card, which through the use of an in-house program is able to

apply a field across the film and correlate this to the light level received by the photodiode. The testing process works by initially applying an increasing field across the film to determine the absolute transmission of the film (as a percentage of the maximum light available), and from this it is possible to calculate the 10% and 90% transmission fields. Once the fields are known the difference is divided into 16 and a series of averaged switching tests are performed at these interval fields to determine the field dependent rise times and decay time for the film.

6.2 Sample Preparation

The samples are prepared as for the light scattering experiments, except that the solution is pipetted into E.H.C. Japan Liquid Crystal test cells of 10 μm separation with the interior of the cells having an ITO coating so that a field can be applied across the sample. As previously described these are cured for 30 minutes to form the film via phase separation, once cured the cells are left for at least 24 hours to allow equilibrium phase separation to be reached. They are then tested via the above method.

Bibliography

1. Masutani, A.; Roberts, T.; Schuller, B.; Yasuda, A.; Sakaigawa, A. *IDRC* **2003**, 6.2.
2. Masutani, A.; Roberts, T.; Yasuda, A.; Sakaigawa, A.; Cross, G.; Bloor, D. *22nd International Display Research Conference Proceedings* **2002**, 47-50.
3. Nephew, J. B.; Nihei, T. C.; Carter, S. A. *Physical Review Letters* **1998,** 80, 3276-3279.
4. Arrighi, V.; Fernandez, M. L.; Higgins, J. S. *Science Progress* **1994,** 77, 71-90.
5. Roe, R. J., *Methods of X-ray and neutron scattering in polymer science.* Oxford University Press: New York, 2000; p xiv, 331.
6. Pethrick, R. A.; Dawkins, J. V., *Modern Techniques for Polymer Characterisation.* 1st ed.; John Wiley & Sons: Chichester, 1999.
7. Bucknall, D. G., Neutron Reflection Studies of Polymers. In *Modern Techniques for Polymer Characterisation,* 1st ed.; Pethrick, R. A.; Dawkins, J. V., Eds. John Wiley & Sons: Chichester, 1999; pp 109-140.
8. Clark, J. N.; Fernandez, M. L.; Tomlins, P. E.; Higgins, J. S. *Macromolecules* **1993,** 26, 5897-5907.
9. Elliniadis, S.; Higgins, J. S.; Clarke, N.; McLeish, T. C. B.; Choudhery, R. A.; Jenkins, S. D. *Polymer* **1997,** 38, 4855-4862.
10. King, S. M., Small Angle Neutron Scattering. In *Modern Techniques for Polymer Characterisation,* Pethrick, R. A.; Dawkins, J. V., Eds. John Wiley and Sons Ltd: 1999; pp 171-232.
11. Warner, M.; Higgins, J. S.; Carter, A. J. *Macromolecules* **1983,** 16, 1931-1935.
12. de Gennes, P. G., *Scaling Concepts in Polymer Physics.* Cornell University Press: 1985.
13. Schramm, G., *A Practical Approach to Rheology and Rheometry.* 2nd ed.; Gebrueder HAAKE GmbH: Karlsruhe, 2000.
14. Sperling, L. H., Polymer Rheology. In *Introduction to Physical Polymer Science,* 3rd ed.; John Wiley & Sons: New York, 2001; pp 461-469.
15. Amundson, K.; vanBlaaderen, A.; Wiltzius, P. *Physical Review E* **1997,** 55, 1646-1654.
16. LeGrange, J. D.; Carter, S. A.; Fuentes, M.; Boo, J.; Freeny, A. E.; Cleveland, W.; Miller, T. M. *Journal of Applied Physics* **1997,** 81, 5984-5991.
17. Nomura, H.; Suzuki, S.; Atarashi, Y. *Japanese Journal of Applied Physics Part 1-Regular Papers Short Notes & Review Papers* **1990,** 29, 522-528.
18. Amundson, K. *Physical Review E* **1996,** 53, 2412-2422.
19. Drzaic, P. S.; Muller, A. *Liquid Crystals* **1989,** 5, 1467-1475.
20. Wu, B. G.; Erdmann, J. H.; Doane, J. W. *Liquid Crystals* **1989,** 5, 1453-1465.

Section A – Phase Properties of Monomer and Polymer Solutions

1 Background

1.1 Phase Properties and Morphology

As discussed in the introduction control of morphology is vital for controlling electronic and optical properties of PDLCs. This is in turn dependent upon the mechanism and conditions of phase separation, and an understanding of these are vital if controllable systems are to be achieved. To understand the phase separation properties of a system it is first necessary to understand the conditions under which a multi-component system will solvate and form a homogenous phase.

1.2 Miscibility of Multi-Component Systems

The state of a system is dependent upon whether the single phase or the combined immiscible phases have a lower free energy; the lower energy configuration being favoured. This can be thought of in terms of the compositional free energy profile, and whether it has one or more minima. In the circumstances that there is only one minima the lowest system energy is obtained by having a single homogenous phase of a composition equal to that of the minima (Figure 1a). Equally if the system has two or more minima then the lowest energy is achieved by having a multiphase system with phases of composition given by each of the minima compositions (Figure 1b).

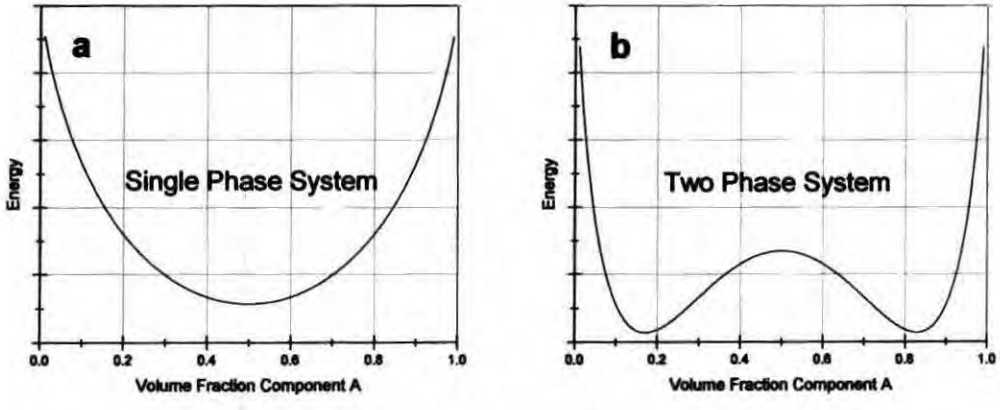

Figure 1 Example energy profiles of a, phase mixed system b, phase separated system

Gibbs[1] showed that it was possible to determine whether a system was thermodynamically stable or unstable by considering changes in free energy (G) with

changes in the density of a component (n – amount of component). If the free energy of a system increases with a change then it is considered to be energetically unfavourable to this change, i.e. a system is energetically stable under the condition,

$$\left(\frac{\partial G}{\partial n}\right)_{T,P} > 0 \tag{1.1}$$

This is what is known as the chemical potential of the component. Equally a system is thermodynamically favourable to a change in composition under the condition,

$$\left(\frac{\partial G}{\partial n}\right)_{T,P} < 0 \tag{1.2}$$

While the chemical potential demonstrates the conditions under which it is thermodynamically favourable for phase separation to occur it fails to take into account kinetic effects. It may be possible to form an energetically lower system by changing the local composition of one of the species, but there can be a localised kinetic barrier. This occurs when a system is in a meta-stable state, one which is defined by having a chemical potential of less than 0, but where the chemical potential initially increases upon a compositional change, mathematically defined as the second derivative of the free energy with respect to density. So a system is meta-stable when,

$$\left(\frac{\partial G}{\partial n}\right)_{T,P} < 0 \tag{1.2}$$

and

$$\left(\frac{\partial^2 G}{\partial n^2}\right)_{T,P} > 0 \tag{1.3}$$

For a system to be spontaneously unstable with respect to a compositional change then the chemical potential must decrease upon a change in density, so the mathematical conditions are,

$$\left(\frac{\partial G}{\partial n}\right)_{T,P} < 0 \tag{1.2}$$

and

$$\left(\frac{\partial^2 G}{\partial n^2}\right)_{T,P} < 0 \tag{1.4}$$

With the line between the unstable and meta-stable states known as the spinodal being defined by,

$$\left(\frac{\partial^2 G}{\partial n^2}\right)_{T,P} = 0 \tag{1.5}$$

and equally the line between the meta-stable and the stable, the binodal defined by,

$$\left(\frac{\partial G}{\partial n}\right)_{T,P} = 0 \tag{1.6}$$

This demonstrates the conditions under which a system will phase separate, it is now necessary to define the contributions to the free energy for a multi component system.

1.3 Mixing Thermodynamics

1.3.1 Flory-Huggins Theory

The work of Flory[2, 3] and Huggins[4] has applied mixing thermodynamics to derive an expression for the free energy for the specific cases of polymer solutions and polymer blends[5-8], which can then be applied to the above Gibbs equations. The model follows from the Gibbs equation for free energy,

$$\Delta G = \Delta H - T\Delta S \tag{1.7}$$

which shows that the free energy of a system consists of an enthalpic (H) and an entropic (S) term. The enthalpic term is determined to be the sum of the internal energies of all the possible interactions between molecules in the system, scaled by the likelihood of that interaction taking place. For a system consisting of two components A and B, there are three possible enthalpic interactions A with B, A with A, and B with B. The entopic term is determined by the use of statistical thermodynamics; the entropy of a system being defined by the Boltzmann equation,

$$S = k \ln Q \tag{1.8}$$

k is the Boltzmann constant, and Q is a partition function, the number of possible states a system can inhabit.

The Flory-Huggins model determines both the likelihood of an enthalpic interaction and the number of possible entropic states by imagining a three dimensional lattice (Figure 2), where each site on the lattice has a volume equal to either the volume of the repeat unit of the polymer, the solvent molecule, or a third reference volume.

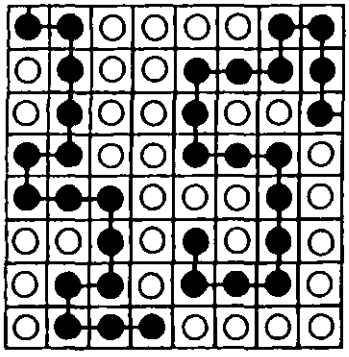

Figure 2 Schematic diagram of Flory-Huggins lattice

They propose that each lattice site will contain either a polymer repeat unit, or a solvent molecule, scaled against the reference volume; with the number of sites of each species proportional to the volume fraction of the species in the system under study. The number of ways it is possible to place the monomer units of the polymer chains and solvent molecules upon the lattice is equal to the number of possible entropic states.

For a monomer/solvent system where the volumes of the monomer and solvent can be considered to be approximately equal this is the number of possible ways to arrange n_m monomer molecules and n_s solvent molecules upon a lattice with $n_m + n_s$ sites. It can be shown that averaged over the entire system that the number of possible configurations for each molecule of a species is equal to the system population n_{Total} multiplied by the volume fraction (ϕ) of the species,

$$S_A = \sum_i k \ln n_{Total} \phi_A \tag{1.9}$$

The entropy of the system is equal to the sum of the entropies of the components, and given that the entropy of each molecule of the species is equal, the entropy of each species is then equal to the entropy of one molecule multiplied by the total number of molecules of that species. For a two component system this is,

$$\frac{S_{Total}}{k} = n_A \ln n_{Total} \phi_A + n_B \ln n_{Total} \phi_B \tag{1.10}$$

The entropy of mixing is given by the change in entropy between the phase mixed and phase demixed systems,

$$\frac{\Delta S_{mix}}{k} = \frac{S_{AB} - (S_A + S_B)}{k} = n_{Total} \ln n_{Total} - (n_A \ln n_{Total}\phi_A + n_B \ln n_{Total}\phi_B) \quad (1.11)$$

Which by application of log laws and averaged for a single lattice site simplifies to,

$$\frac{\Delta S_{mix}}{nk} = -(\phi_A \ln \phi_A + \phi_B \ln \phi_B) \quad (1.12)$$

In the case of polymer chains the second repeat unit of the polymer chain needs to be on a lattice site adjacent to the first repeat unit and so forth until the whole chain is placed on the lattice. This therefore modifies the number of possible configurations and subsequently the entropy of the system. It was shown by Flory and Huggins that this has the effect of scaling the entropic contribution of each species by the reciprocal of the chain length (degree of polymerization N), such that the entropy is now,

$$\frac{\Delta S_{mix}}{nk} = \frac{\phi_A}{N_A} \ln \phi_A + \frac{\phi_B}{N_B} \ln \phi_B \quad (1.13)$$

The enthalpic term's scaling is calculated by multiplying the number of molecules a molecule on the lattice is adjacent to (its coordination number z) by the probability that the molecule is of a given type which is assumed to be equal to it's volume fraction (the mean field approximation). So for a molecule of species A the enthalpy is given by,

$$H_A = z[\phi_A u_{AA} + \phi_B u_{AB}] \quad (1.14)$$

And for the total system,

$$\Delta H_{mix} = H_{AB} - (H_A + H_B) = \frac{z n_{Total}}{2} \phi_A \phi_B [2u_{AB} - u_{AA} - u_{AB}] \quad (1.15)$$

with the divisor by 2 to account for the double counting of interactions. The energy terms which are constant for a given set of species are usually grouped together in a temperature dependent interaction parameter χ_{AB},

$$\Delta H_{mix} = \chi_{AB} \phi_A \phi_B T \quad (1.16)$$

By applying equation (1.7) this gives the overall Flory-Huggins equation for the free energy of a two component polymer blend or solution as,

$$\frac{\Delta G_{mix}}{nkT} = \frac{\phi_A}{N_A} \ln \phi_A + \frac{\phi_B}{N_B} \ln \phi_B + \chi_{AB} \phi_A \phi_B \quad (1.17)$$

It is worth noting that for a system which consists of only two incompressible species, the volume fractions will sum to 1,

$$\phi_A + \phi_B = 1 \tag{1.18}$$

it is possible to rewrite the free energy equation in terms of one of the species,

$$\frac{\Delta G_{mix}}{nkT} = \frac{\phi_A}{N_A}\ln\phi_A + \frac{(1-\phi_A)}{N_B}\ln(1-\phi_A) + \chi_{AB}\phi_A(1-\phi_A) \tag{1.19}$$

As previously stated the lattice has a reference volume v_0 and as such equations (1.17) and (1.19) should be scaled by it,

$$\frac{\Delta G_{mix}}{nkT} = \frac{\phi_A v_o}{N_A v_A}\ln\phi_A + \frac{\phi_B v_0}{N_B v_B}\ln\phi_B + \chi_{AB}\phi_A\phi_B \tag{1.20}$$

$$\frac{\Delta G_{mix}}{nkT} = \frac{\phi_A v_0}{N_A v_A}\ln\phi_A + \frac{(1-\phi_A)v_0}{N_B v_B}\ln(1-\phi_A) + \chi_{AB}\phi_A(1-\phi_A) \tag{1.21}$$

The interaction parameter has been often phenomologically stated in the form,

$$\chi_{AB} = a + \frac{b}{T} \tag{1.22}$$

where a and b are constants for a given set of species.

1.3.2 Limitations of Model

While having proved itself to be a very effective model for analysing and predicting phase properties in polymer solutions and blends, it does have a number of occasionally significant limitations[5, 9-11]. In particular the model neglects possible compositional dependencies in the interaction parameter, which result from excluded volume effects.

1.4 Phase Diagrams

As previously discussed a system can either be in a stable, meta-stable, or unstable state and it is useful to be able to determine which state a system will be in under a given set of external conditions. It is possible to plot a temperature/composition phase diagram, which shows the boundary lines between the stable one phase region and the meta-stable two phase region (the binodal line), and the meta-stable two phase region and the unstable two phase region (the spinodal line).

1.4.1 Binodal Line

The binodal is the line which defines the first points at which phase separation is thermodynamically possible, and for this to be the case two new phases need to be formed which are of equal chemical potential,

$$\left(\frac{\partial G_{mix}}{\partial \phi_A{}'}\right)_{T,P} = \left(\frac{\partial G_{mix}}{\partial \phi_A{}''}\right)_{T,P} \tag{1.23}$$

This defines a line which is a tangent between two minima on the free energy profile (Figure 3)

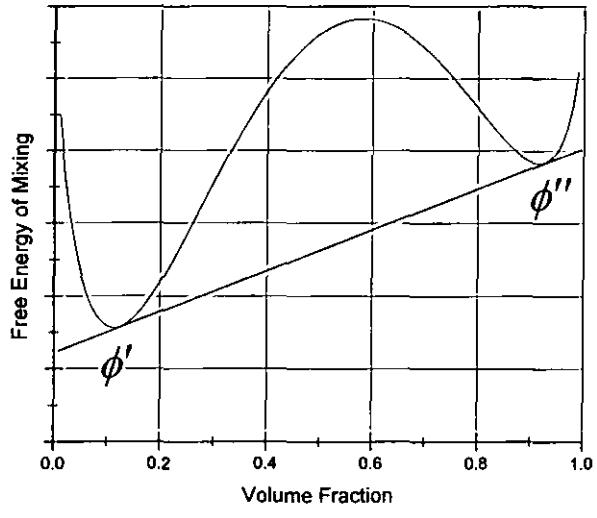

Figure 3 Schematic of tangent line linking a pair of equal chemical potential phases ϕ' and ϕ''

The chemical potential or first derivative with respect to the composition of one component in a two component system is given by,

$$\left(\frac{\partial G_{mix}/nkT}{\partial \phi_A}\right) = \frac{\ln \phi_A}{N_A} + \frac{1}{N_A} - \frac{\ln(1-\phi_A)}{N_B} - \frac{1}{N_B} + \chi_{AB}\phi_A(1-2\phi_A) \tag{1.24}$$

Using the temperature dependence of χ_{AB} (equation (1.22)), it is possible to solve a series of simultaneous equations (one for each component) to determine compositional pairs for each temperature, and plot a temperature/composition binodal graph,

$$\begin{aligned} &\frac{\ln \phi_A{}'}{N_A} + \frac{1}{N_A} - \frac{\ln(1-\phi_A{}')}{N_B} - \frac{1}{N_B} + \left(a + \frac{b}{T}\right)(1-2\phi_A{}') = \\ &\frac{\ln \phi_A{}''}{N_A} + \frac{1}{N_A} - \frac{\ln(1-\phi_A{}'')}{N_B} - \frac{1}{N_B} + \left(a + \frac{b}{T}\right)(1-2\phi_A{}'') \end{aligned} \tag{1.25}$$

1.4.2 Spinodal Line

The spinodal line bounds the meta-stable and the unstable regions, as previously stated this occurs when,

$$\left(\frac{\partial G_{mix}^2}{\partial^2 \phi_A}\right)_{T,P} < 0$$

which for a system where the mixing free energy is defined by (1.21) is equal to,

$$\frac{\partial G_{mix}^2}{\partial^2 \phi_A} = kT\left[\frac{1}{N_A \phi_A} + \frac{1}{N_B(1-\phi_A)} - 2\chi_{AB}\right] = 0 \qquad (1.26)$$

Adding the temperature dependence of the interaction parameter it is possible to rearrange to give a relation for the spinodal temperature T_S in terms of the composition,

$$T_S = \frac{2b}{\frac{1}{N_A \phi_A} + \frac{1}{N_B(1-\phi_A)} - 2a} \qquad (1.27)$$

The two binodal and spinodal lines can then be combined to produce one overall temperature/composition phase diagram which shows the stable, unstable and meta-stable regions (Figure 4)

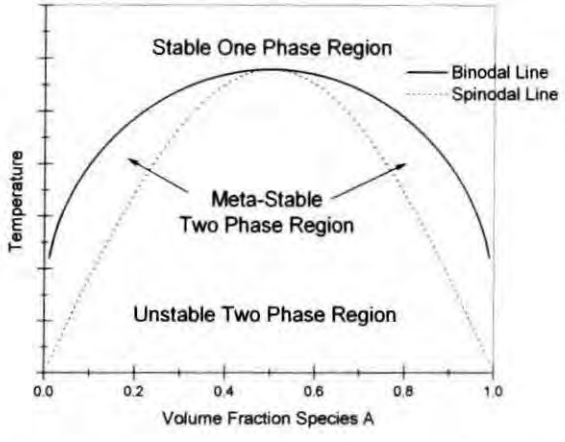

Figure 4 Example phase diagram for a symmetric blend ($N_A = N_B$)

2 Aims of Work

The main aim of the work presented within this section is to determine the explicit phase properties of those systems applied in sections B and C for determining phase separation mechanisms, morphological properties, and effects of fluorine doping in

PDLC systems. An attempt is made to mathematically fit the results to simple models to determine their effectiveness in explaining the thermodynamic properties of polymer/liquid crystal solutions; determined using both a composition dependent fitting technique and composition independent neutron scattering. Comment will also be made upon the unique phase properties demonstrated by solutions involving liquid crystalline species as a solvent.

3 Small Angle Light Scattering Studies

The temperature at which phase separation commences for a system at a number of compositions is observed by the use of small angle light scattering (SALS). The phase separation temperature is taken as the point at which scattering starts, due to the formation of interfaces between phases. The technique is applied as described in subsection 2 of the Experimental Section.

3.1 Liquid Crystal/Hydrogenous Monomer Phase Diagrams

3.1.1 TL213 with 2-Ethylhexyl Acrylate

This is the basic system utilised in most of the studies presented within this report, and in particular makes up the majority of the morphological and mechanism work. This system is utilised both in its pure form, and in the presence of a crosslinking species (trimethylol propane triacrylate), and which is therefore a ternary system. Two studies are performed upon the system once in the absence of crosslinker and once with the 2-ethylhexyl acrylate doped with 15 mol% crosslinker to determine the effect of the crosslinker on phase properties.

3.1.1.1 Results and Discussion

Figure 5 shows the phase properties for the system in the absence of the crosslinker and Figure 6 shows the properties with 15 mol% crosslinker. It can be clearly seen that the phase behaviour is effectively unmodified by the presence of the crosslinker. These results suggest it is reasonable to treat the ternary system of TL213, 2-ethylhexyl acrylate and trimethylol propane triacrylate as a pseudo binary system, with the two monomer species treated as one single species. It can be assumed the proportion the crosslinker is present in has no effect on the mixing thermodynamics.

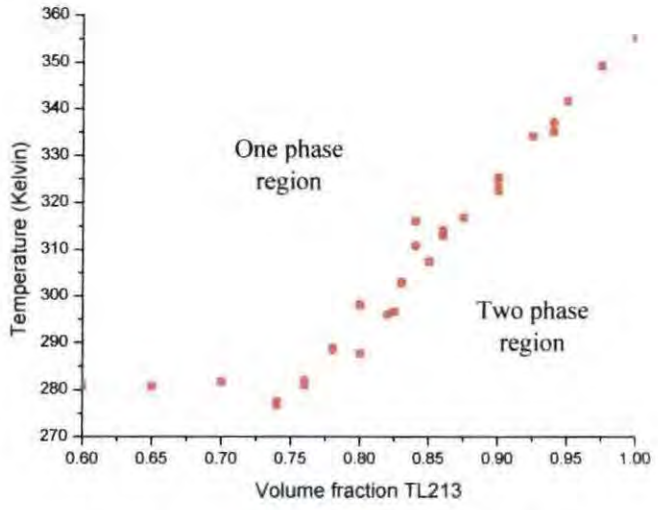

Figure 5 SALS determined phase diagram for TL213 with 2-ethylhexyl acrylate (in the absence of crosslinker)

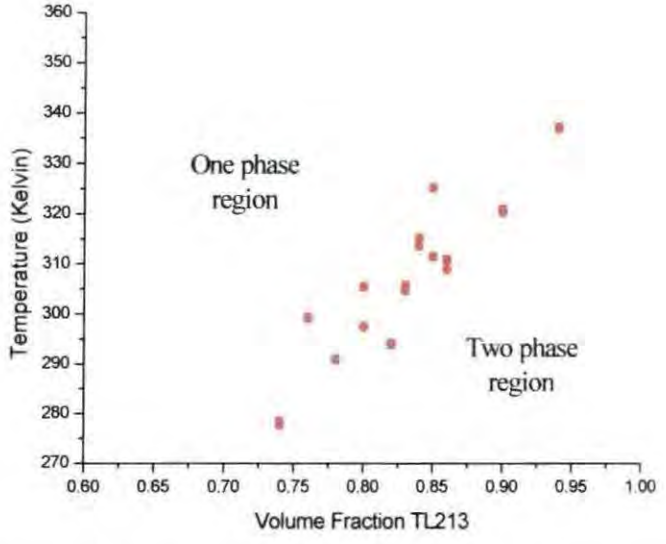

Figure 6 SALS determined phase diagram for TL213 with 2-ethylhexytl acrylate doped with 15 mol% trimethylol propane triacrylate

The profiles present an unusual phase dependence for a system where the two components are of roughly the same volume and degree of polymerization. A symmetric two component system which follows the Flory-Huggins model would be expected to demonstrate a phase diagram with a critical composition (curve peak) in the vicinity of volume fraction 0.5 (as exemplified by Figure 4), whereas the profiles shown do not appear to demonstrate any kind of critical composition. An attempt was made to fit the curves to Flory-Huggins theory, equation (1.27), using the parameters in Table 1, but this proved impossible.

Species	Monomer unit volume v (cm^3)	Reference Volume (cm^{-3})	Degree of polymerisation *N*
TL213	5.42E-22	1.00E-22	1
2-EthylHexyl Acrylate	3.46E-22	1.00E-22	1

Table 1 Flory-Huggins input fitting parameters for TL213 with 2-ethylhexyl acrylate monomer, refer to footnote[1]

Significantly the points at which light scattering first occurs at the highest liquid crystal volume fractions are very close to the nematic-isotropic transition temperature (T_{NI}) of pure TL213 (354 K). This suggests that what is being observed is the composition dependence of the T_{NI}, therefore it is difficult to determine that which is scattering due to the interfaces between differently aligned nematic domains and that due to the formation of two unique phases. There is a possibility of a change in the observed profile from that of the actual phase separation at lower ϕ_{LC} to that of the T_{NI} with concentration for TL213 at higher ϕ_{LC}. The significant change in trend at $\phi_{LC} \approx 0.75$ and temperature ~280 K coincides with the approximate freezing point of the liquid crystal. It would seem reasonable to presume that all the scattering points at these temperatures (those for compositions less than $\phi_{LC} = 0.75$) are due to the system freezing rather than a liquid-liquid phase demixing process.

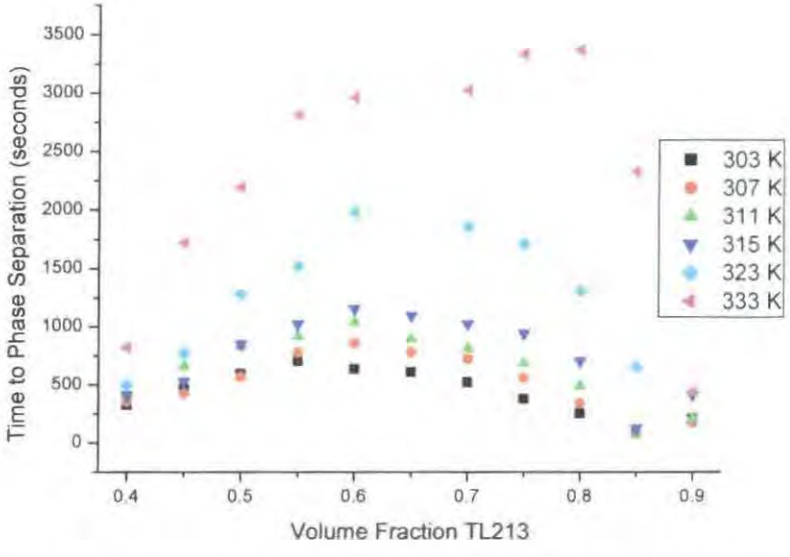

Figure 7 Phase separation times for TL213 with 2-EthylHexyl Acrylate (5mol% Trimethylol Propane Triacrylate) cured under 2000 mWm^{-2} UV

While most of these ideas are merely inferences which cannot be fully supported, evidence in terms of phase separation times (which will be fully explored in Section

[1] There is no accurate structural information for TL213, so it is assumed for calculations that it consists purely of the component species 2',2'',4''-Trifluoro-4-propyl-1,1':4',1''-terphenyl, with the parameters as per Table 1

B) would seem to support the idea that the points between $\phi_{LC} = 0.75$ and 0.85 are indicative of the phase separation curve. Figure 7 shows the phase separation times for TL213 with 2-ethylhexyl acrylate (doped with 5 mol% trimethylol propane triacrylate) at varying temperatures and compositions under a cure intensity of 2000 mWm^{-2}. As can be seen the time to initial phase separation decreases to a minimum for most temperatures at $\phi_{LC} \approx 0.85$, suggesting that this is the point at which the lowest degree of polymerization is required to cause phase separation. This would be expected to be the case for temperature composition points nearest to the phase curve, suggesting a peak and critical composition at $\phi_{LC} \approx 0.85$, and as such support the above interpretation. The decrease in phase separation time with increasing monomer composition is an effect of reaction rate and will be discussed in further detail in Section B.

There is much evidence in the literature for this interpretation with similar profiles observed for many systems including E7 with NOA65[12, 13] (Figure 8), 5CB with IDA[14], 5CB with 2-HEA[14], TL205 with 2-EHA[14] (Figure 10), TL205 with PN393[15], E44 with NOA65[16], K21 with NOA65[17].

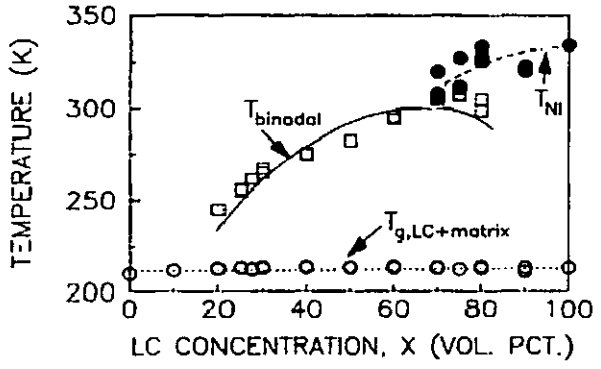

Figure 8 Phase diagram for E7 with uncured NOA-65 as determined by G. W. Smith[12, 13]

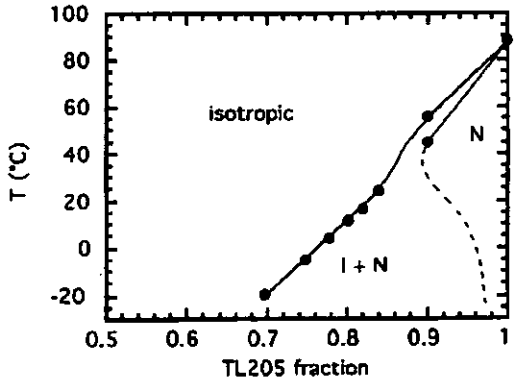

Figure 9 Phase diagram for TL205 with 2-ethylhexyl acrylate as determined by Amundson et al.[15]

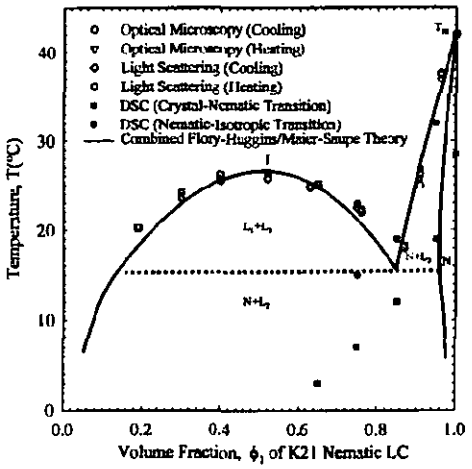

Figure 10 Phase diagram for K21 with NOA65 as determined by Nwabunma and Kyu[17]

Significantly the work of Smith[12, 13] was performed using differential scanning calorimetry (DSC), which is able to differentiate between thermal changes occurring in the same sample, whereas SALS is unable to differentiate between a nematic-isotropic temperature and a phase mixing temperature as both create scattering. Smith's results show the phase dependence beneath the T_{NI} dependence, which agrees with that which is inferred for the results presented.

Attempts to fit the overall profile prove to be impossible, so on the assumption that the shoulder at $\phi_{LC} = 0.85$ represents the start of the phase properties an attempt is made to fit values between 0.75 and 0.85. This was still not possible without allowing the degree of polymerization of the 2-ethylhexyl acrylate to be at least 80 (Figure 11). The results of the fit with $N_{TL213} = 80$, are shown below in Table 2

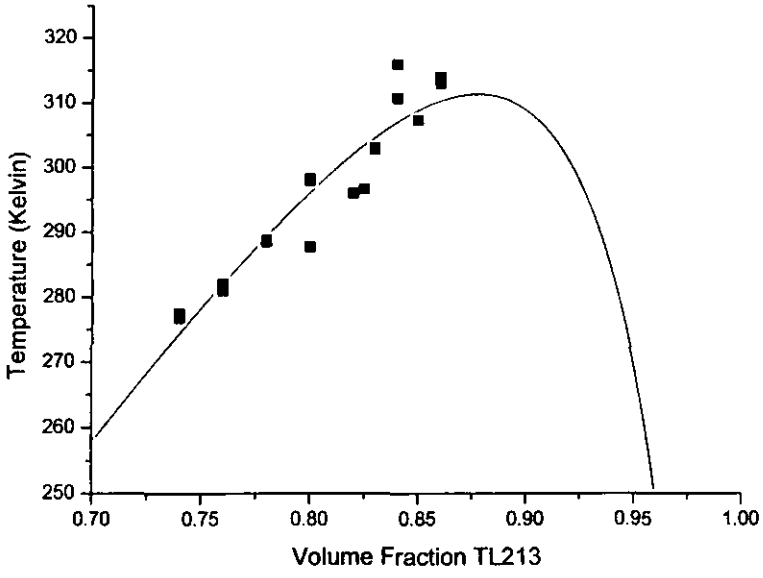

Figure 11 Attempted fit of TL213 with 2-ethylhexyl Acrylate to Flory-Huggins spinodal equation

Parameter	N_{TL213}	N_{EHA}	a	b	Chi2	R2
Fit Value	1	80	3.332E-02	26.960	19.140	0.889

Table 2 Output parameters for Flory-Huggins fit of phase diagram of TL213 with 2-EthylHexyl Acrylate

This would seem to support the idea that the behaviour of these systems is not explicable by the basic Flory-Huggins model. There are two possible explanations for this, the interaction parameter has a large compositional dependence, or the structural anisotropy of the liquid crystal modifies the thermodynamics. The former would seem unlikely as it would require a very large variation of the interaction parameter with composition, this will be looked into in further detail in the neutron scattering studies. The second has been considered by a number of models which are discussed in further detail in subsection 5 below.

3.2 Liquid Crystal/Fluorinated Monomer Phase Diagrams

Section C of this report focuses on fluorinating the polymer species and how this affects PDLC properties; an understanding of the effect of fluorine doping on the phase properties is required. An initial phase diagram is determined for TL213 with pure heptafluorobutyl acrylate, which is followed up by examining the effect of varying the degree of doping of 2-ethylhexyl acrylate with heptafluorobutyl acrylate and the more highly fluorinated species dodecaflurohеptyl Acrylate.

3.2.1 TL213 with Heptafluorobutyl Acrylate

3.2.1.1 Results and Discussion

TL213 with heptafluorobutyl acrylate (Figure 12) demonstrates very unusual phase behaviour, like with the 2-ethylhexyl acrylate results it is possible to observe a curve up to a maximum at high ϕ_{TL213} compositions. The values in this case however are higher than the T_{NI} of TL213 and would suggest that what is being observed are liquid-liquid phase demixing temperatures. More strikingly this dependence ends at $\phi_{TL213} = 0.6$, where there is then an almost linear increase in phase separation temperature (although with a high degree of scattering in data points) with decreasing ϕ_{TL213}. While it has not been possible to develop any conclusive explanation for why this phase behaviour is observed it is worth noting that the overall graph shows a similarity to the shape of a phase diagram for a system which contains two liquids which are miscible, but which become immiscible upon either

solidifying (Figure 13). The T_g of the monomer and the freezing points of both the monomer and liquid crystal are far lower than the values observed, and unless there is a phase demixing effect due to the formation of liquid crystalline phases this is an unlikely explanation.

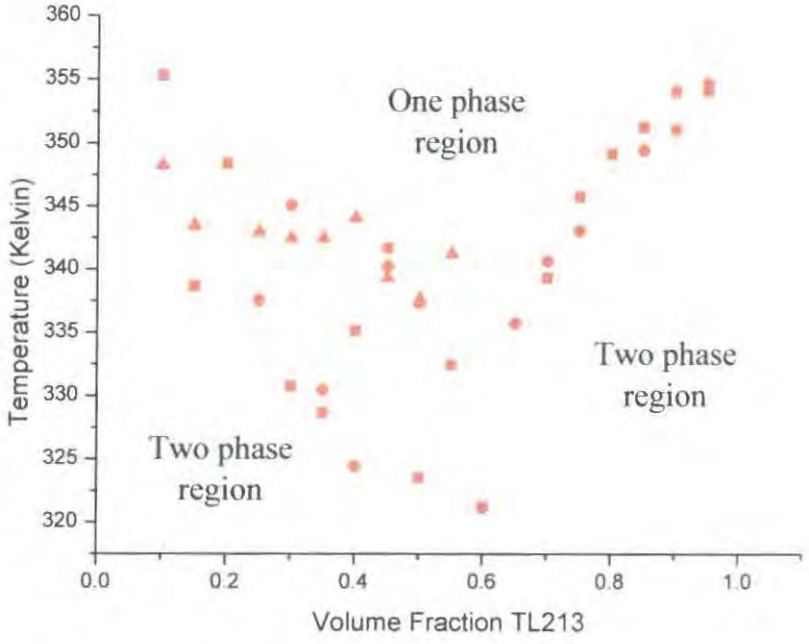

Figure 12 SALS determined phase diagram for TL213 with heptafluorobutyl acrylate

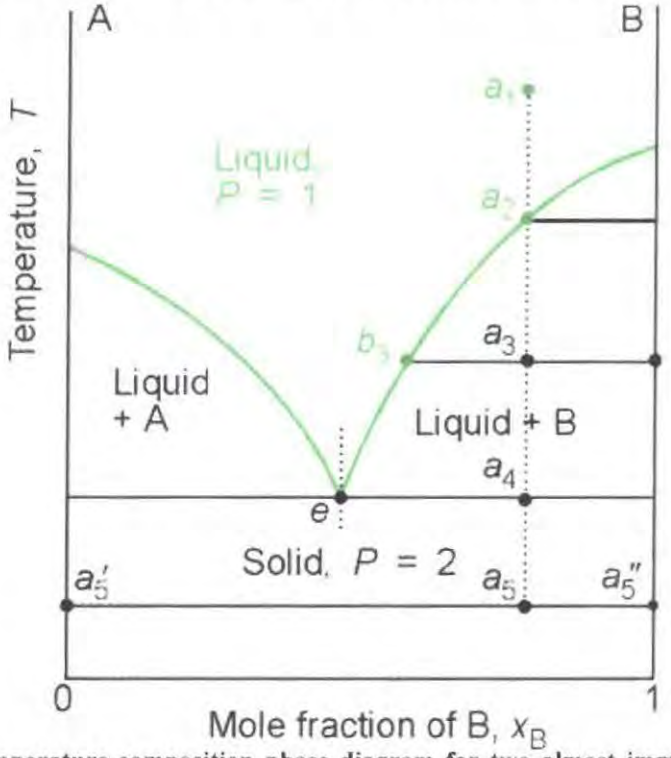

Figure 13 The temperature-composition phase diagram for two almost immiscible solids and their completely miscible liquids[18]

An initial fit is attempted to Flory-Huggins theory using the variables in Table 3, purely for the curve between $\phi_{TL213} = 0.6$ and 1 (Figure 14) which demonstrates phase behaviour similar to that for 2-ethylhexyl acrylate. Again as is the case for 2-ethylhexyl acrylate a fit is only possible if you allow the degree of polymerization of the monomer species to be high, in this case ~243 (See Table 4 for fit output data). This further adds to the evidence suggesting that the Flory-Huggins model is not applicable for liquid crystal/monomer solutions. An attempt has also been made to fit the values below $\phi_{TL213} = 0.6$ but any meaningful data was impossible to obtain. The same was true for an attempt to fit the entire data set.

Species	Monomer unit volume v (cm^3)	Reference Volume (cm^{-3})	Degree of polymerisation N
TL213	5.42E-22	1.00E-22	1
Heptafluoro butyl acrylate	2.97E-22	1.00E-22	1

Table 3 Flory-Huggins input fitting parameters for TL213 with heptafluorobutyl monomer

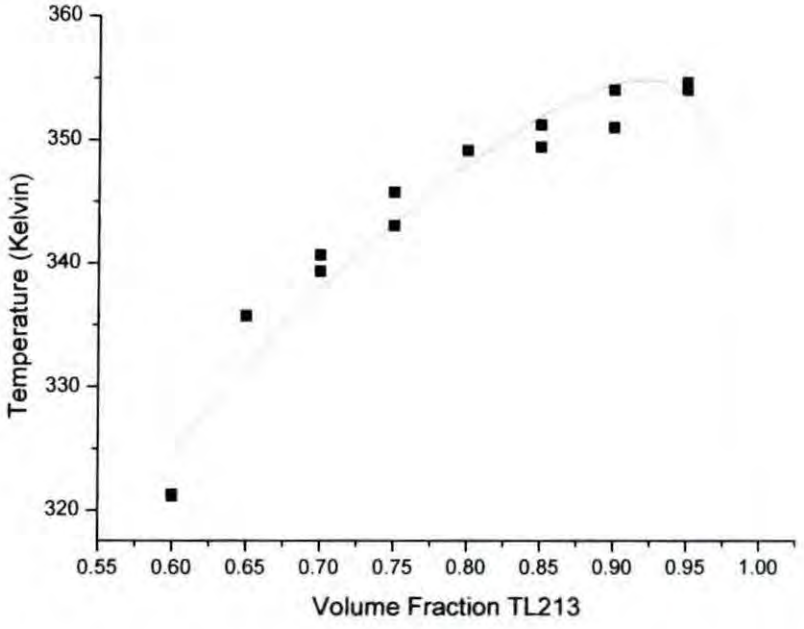

Figure 14 Attempt to fit TL213 with Heptafluorobutyl Acrylate phase properties to Flory-Huggins spinodal curve

Parameter	N_{TL213}	N_{HFBA}	a	b	Chi2	R2
Fit Value	1	243	-0.389	176.87	7.104	0.952

Table 4 Output parameters for Flory-Huggins fit of phase diagram of TL213 with heptaflurobutyl acrylate

3.2.2 TL213 with 2-Ethylhexyl Acrylate Doped with Heptafluorobutyl Acrylate

3.2.2.1 Results and Discussion

As can be seen from the profile overlaid of the phase dependency of pure 2-ethylhexyl acrylate (Figure 15) the effect of doping with small amounts of fluorinated monomer is not large. There is a noticeable trend for increasing phase separation temperature with increasing degree of fluorine doping, particularly from $\phi_{TL213} = 0.7$ to 0.85, although the increase is only small. It would suggest that in later reaction induced phase separation studies that for a given temperature and composition, phase separation should occur earlier and that analysis of morphologies can be understood in relation to this.

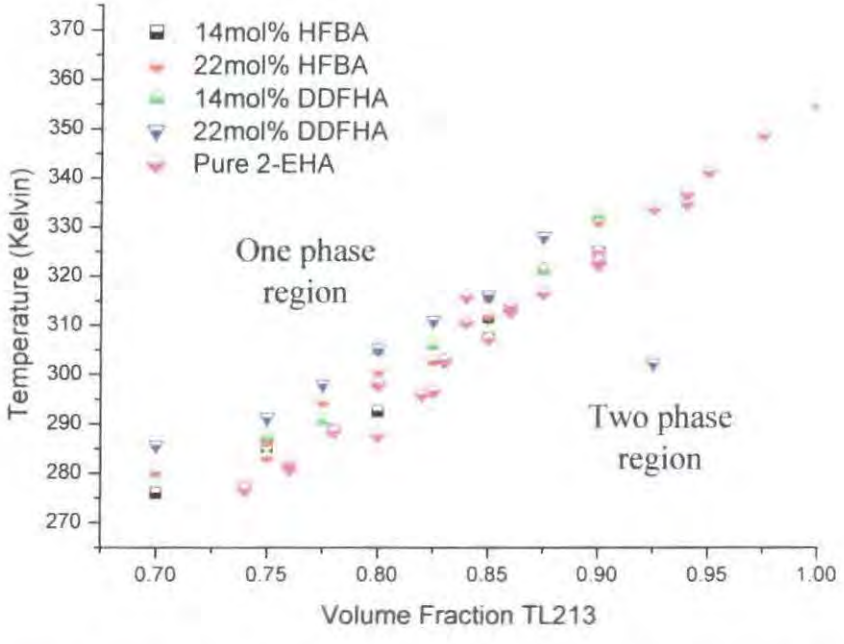

Figure 15 Phase diagram showing the effect of fluorine doping of 2-ethylhexyl acrylate when mixed with TL213

3.3 Liquid Crystal/Hydrogenous Polymer Phase Diagrams

3.3.1 TL213 with Poly(2-Ethylhexyl Acrylate)

To compare the phase properties of polymerized and unpolymerized systems the combination of TL213 with 2-ethylhexyl acrylate was repeated, this time with the polymerised form of molecular weight ($\bar{M}_n$) 92000 $gmol^{-1}$.

3.3.1.1 Results and Discussion

Figure 16 shows the SALS determined phase diagram for TL213 with 92000 $gmol^{-1}$ poly(2-ethylhexyl acrylate).

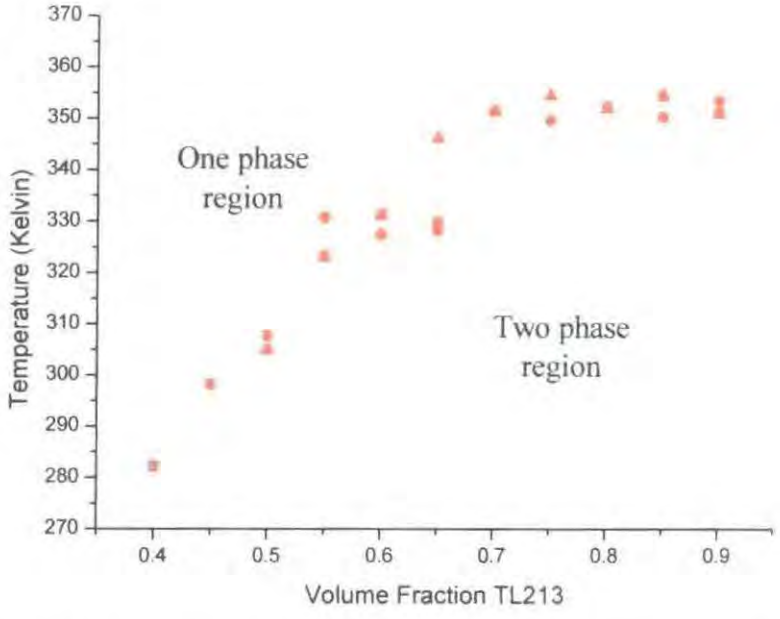

Figure 16 SALS determined phase diagram for TL213 with poly(2-ethylhexyl acrylate) (92000 $gmol^{-1}$)

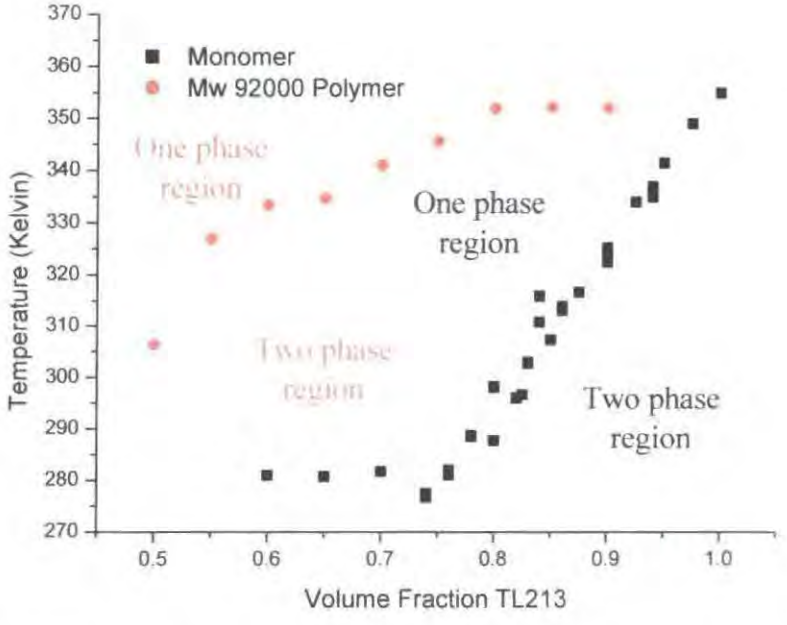

Figure 17 Comparison of the phase properties of 2-ethylhexyl acrylate with TL213 in the monomer and polymer forms

As can be seen from Figure 17 the phase separation temperatures of the polymerised form of 2-ethylhexyl acrylate (Mw 92000 $gmol^{-1}$) are all greater than those of the presumed T_{NI} temperatures determined in the unpolymerized study. This suggests

that what is now being observed are purely the liquid-liquid phase demixing temperatures.

An attempt has been made to fit the resultant curve to Flory-Huggins theory using the input variables in Table 5; unlike in the case of the unpolymerized form it is possible to fit the results to the theory (Figure 1) without having to use physical values – such as the degree of polymerization – which are impossible (for a monomer species). The fit resulted in the values $a = -0.414$ and $b = 186.5$ (see Table 6 for fitting output parameters).

Species	Monomer unit volume v (cm^3)	Reference Volume (cm^{-3})	Degree of polymerisation N
TL213	5.42E-22	1.00E-22	1
2-Ethylhexyl Acrylate	3.46E-22	1.00E-22	499.24

Table 5 Flory-Huggins input fitting parameters for TL213 with poly(2-ethylhexyl acrylate) (92000 $gmol^{-1}$)

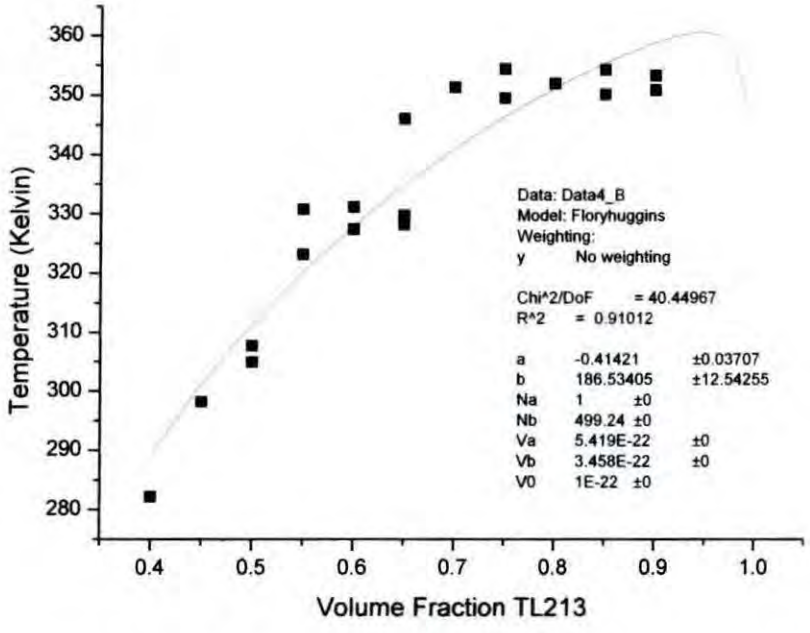

Figure 18 Attempted fit of TL213 with poly(2-EthylHexyl Acrylate) (Mw 92000) to Flory-Huggins spinodal equation

Parameter	N_{TL213}	N_{EHA}	a	b	Chi2	R2
Fit Value	1	243	-0.389	176.87	7.104	0.952

Table 6 Output parameters for Flory-Huggins fit of phase diagram of TL213 with 92000 $gmol^{-1}$ poly(n-butyl acrylate)

It would seem that liquid crystal/polymer solutions show a better correlation to Flory-Huggins theory than their monomer counterparts. The likelihood is that the problems associated with fitting of liquid crystal/monomer solutions are due to the previously discussed structural anisotropy of the liquid crystal species. When the second component species of the solution is a monomer which has a volume

significantly less than that of the liquid crystal the ordering effects of the anisotropy become very significant. As the degree of polymerization increases and the chain grows longer the significance of the anisotropy decreases compared to the structural effects of the increasingly long chains and it is their entropic contribution which dominates the free energy. Therefore as the length of the chain increases the fit to Flory-Huggins theory would be expected to become better.

Similar phase diagrams have been observed such as by Ahn et al.[19] for 7CB with PMMA (Figure 19) and polystyrene (Figure 20) and by Lee and Bae[20] for EBBA with polystyrene (Figure 21).

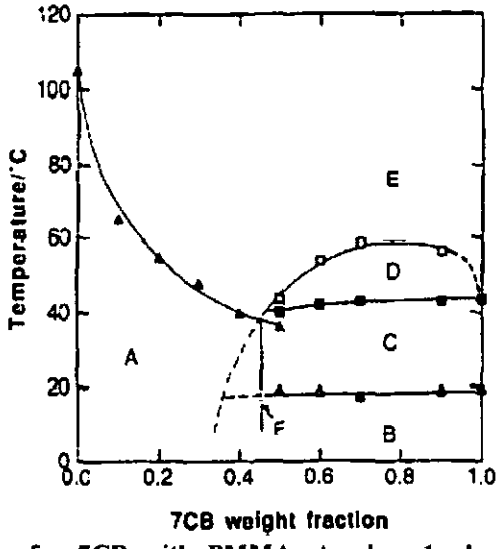

Figure 19 Phase diagram for 7CB with PMMA, A, glass 1 phase state; B, PMMA/solid crystalline 7CB 2 phase; C, PMMA/nematic 7CB 2 phase; D, PMMA/isotropic 7CB 1 phase; E, homogenous 1 phase. Ahn et al.[19]

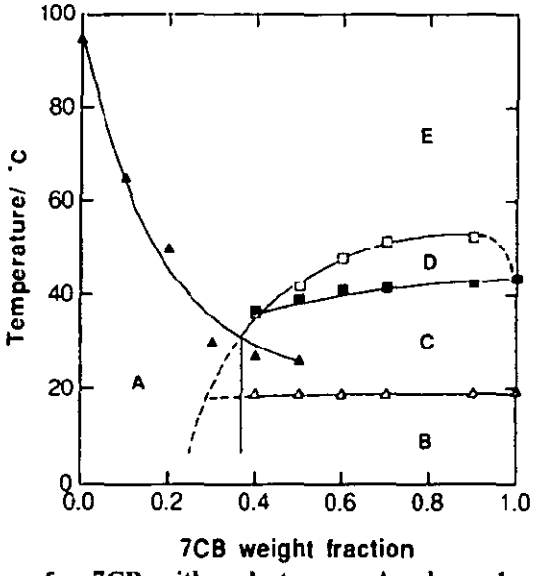

Figure 20 Phase diagram for 7CB with polystyrene; A, glassy 1 phase state; B, PS/solid crystalline 7CB phase 2 phase state; C, PS/nematic 7CB phase 2 phase state; D, PS/isotropic 7CB 2 phase state; E, homogeneous 1 phase state. Ahn et al.[19]

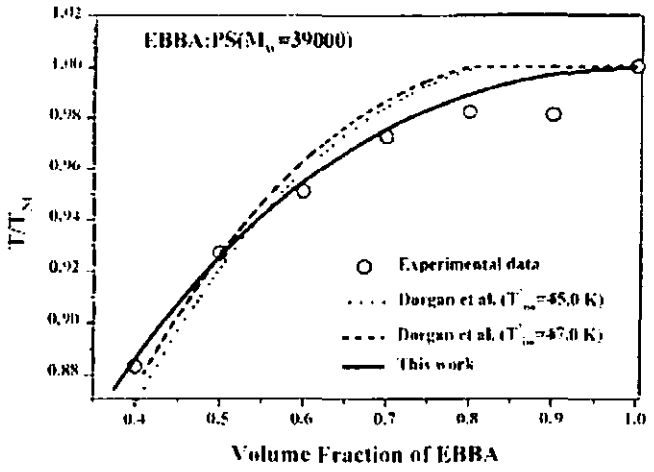

Figure 21 Phase diagram of EBBA:PS (Mw 39000) with temperature listed relative to the T_{NI} of the liquid crystal. Work of Lee and Bae[20]

The similarity at least in shape (critical composition), if not magnitude, between the phase curves for the unpolymerized and polymerised forms of 2-ethylhexyl acrylate will become significant in later morphological studies (Section B). In particular there is little movement of the critical composition point to affect the type of phase separation for a given temperature composition point.

3.3.2 TL213 with Poly(n-butyl Acrylate)

Given the conclusions of the previous study into the phase properties of poly(2-ethylhexyl acrylate) with TL213, a further study is performed with a polymer species of varying degree of polymerization. If the Flory-Huggins theory fits for polymer/liquid crystal solutions then the fit of the phenomological interaction parameter should be the same for all degrees of polymerization. Equally given the conclusions of the previous study it would be expected that the fit should improve with increasing degree of polymerization. The system chosen for the study is TL213 with poly(n-butyl acrylate) for its similarity in chemistry to systems used later in morphological studies and it's availability in a series of accurately known molecular weights.

3.3.2.1 Results and Discussion

Figure 22 shows that poly(butyl acrylate) has similar shaped phase curves to TL213 with poly(2-ethylhexyl acrylate); the phase separation temperatures increasing with degree of polymerization. The profiles in Figure 22 for molecular weight ($\bar{M}_w$) 1630 gmol^{-1} and 3650 gmol^{-1} would seem to suggest that above about $\phi_{TL213} = 0.9$ the observed dependence is that previously determined to be for the T_{NI} with

composition change. This seems to be confirmed by the fact it is impossible to make a fit for the whole profile to Flory-Huggins theory for a spinodal line, whereas the profile for molecular weight ($\bar{M}_w$) 14500 gmol^{-1} is above the T_{NI} at all compositions. An attempt is therefore made to fit the first two profiles below $\phi_{TL213} = 0.9$ and the latter to the entire data set.

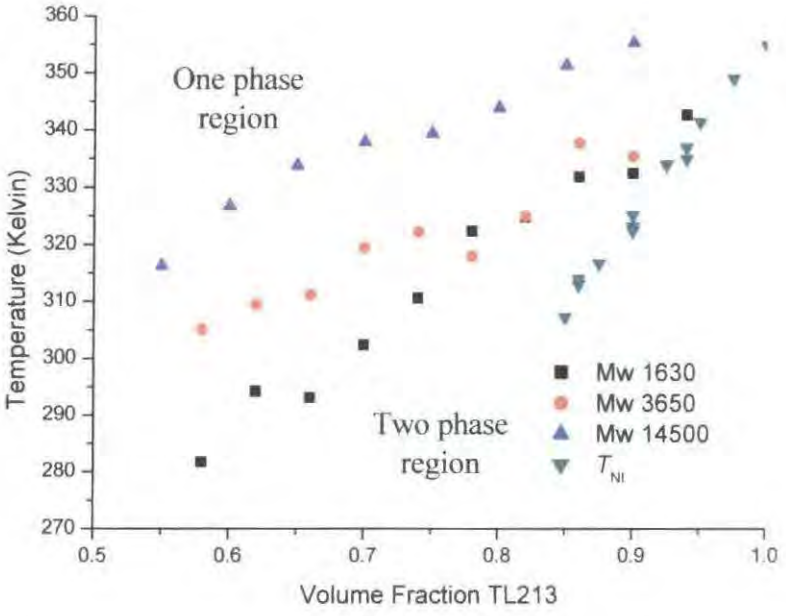

Figure 22 SALS determined phase diagram for TL213 with poly(n-Butyl Acrylate) of varying molecular weight

As with poly(2-ethylhexyl acrylate) it is possible to make a fit of the curves to Flory-Huggins theory (using the input parameters in Table 7) for the polymer of molecular weight 3650 gmol^{-1} (Figure 23a) and 14500 gmol^{-1} (Figure 23b). For the case of the 1630 gmol^{-1} (Figure 23c) system fitting is impossible without setting the degree of polymerization overly high or missing higher composition data points. This is analogous to the case of the phase properties of the monomer system of 2-ethylhexyl acrylate, and provides further evidence to the conclusion that the effectiveness of the Flory-Huggins fit is dependent upon the polymer's length.

Species	Monomer unit volume v (cm^3)	Reference Volume (cm^{-3})	Degree of polymerisation N
TL213	5.42E-22	1.00E-22	1
poly(n-butyl acrylate) 1630 gmol^{-1}	2.38E-22	1.00E-22	12.73
poly(n-butyl acrylate) 3650 gmol^{-1}	2.38E-22	1.00E-22	28.51
poly(n-butyl acrylate) 14500 gmol^{-1}	2.38E-22	1.00E-22	113.28

Table 7 Flory-Huggins input fitting parameters for TL213 with poly(n-butyl acrylate)

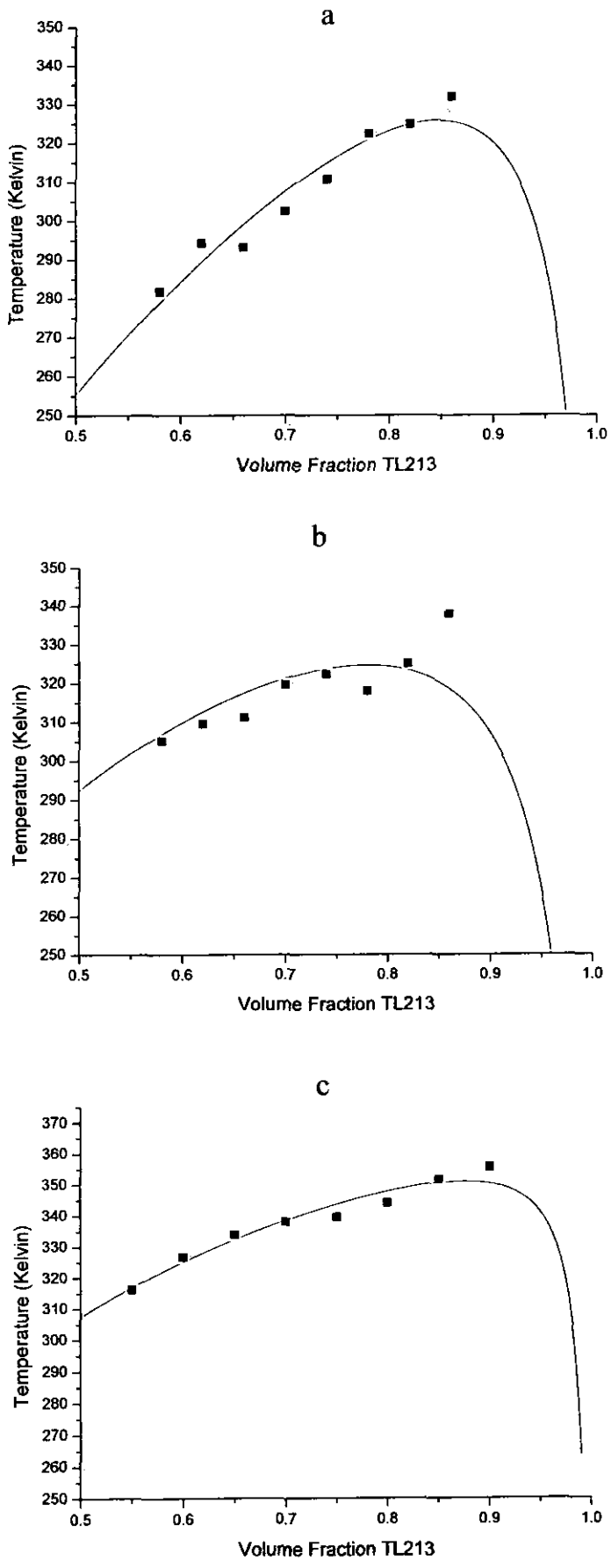

Figure 23 Attempted fits of TL213 with samples of poly(n-butyl acrylate) of varying molecular weight (a, 1630 $gmol^{-1}$, b 3650 $gmol^{-1}$, 14500 $gmol^{-1}$) to Flory-Huggins spinodal equation

Parameter	N_{TL213}	N_{PBA}	a	b	Chi2	R2
*1630 gmol^{-1}	1	70	-0.096	73.03	25.746	0.929
3650 gmol^{-1}	1	29	-0.277	139.20	139.230	0.361
14500 gmol^{-1}	1	113	-0.360	168.60	10.857	0.943

Table 8 Interaction parameter fitting results for TL213 with poly(n-butyl acrylate) of varying molecular weight, *Fit only possible by setting N_p = 70, equivalent of Mw 8962 gmol^{-1}

While the higher molecular weight polymers can both be fitted to a spinodal line as defined by Flory-Huggins theory, they result in *a* and *b* values (Table 8) which differ significantly with polymer weight. For the two higher molecular weight polymers tested the *a* values differ by a margin of 23% and the *b* values by 17%. They are however of the same magnitude, suggesting some degree of consistency with Flory-Huggins theory for higher molecular weight polymers in liquid crystalline solvents. They are also of the same magnitude and similar value to those gained fitting TL213 with poly(2-ethylhexyl acrylate), as would be expected for what are chemically very similar systems. Figure 24 shows the spinodal curves which would be generated by each of the two fittings if they were applied to the other two molecular weights.

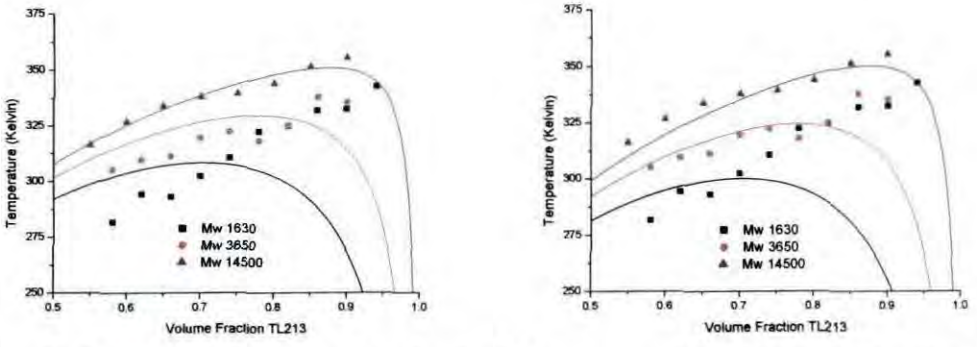

Figure 24 Comparison of fitting derived spinodal curves to original data; a, determined from Mw 14500; b, Mw 3650

It can be seen that the Mw 3650 gmol^{-1} fitting actually provides a reasonable fit for both the Mw 3650 gmol^{-1} and Mw 14500 gmol^{-1} systems, whereas the Mw 14500 gmol^{-1} fitting only really fits its own data well. That said both produce fittings in a similar region to the phase curves. It is not unreasonable to interpret the results of these experiments as supporting the hypothesis introduced as a conclusion to the TL213 with poly(2-ethylhexyl acrylate) studies. The values of the interaction parameters are similar suggesting that the Flory-Huggins theory can be a reasonable fit for polymer/liquid crystal systems, with different degrees of polymerization giving the same approximate results. Any difference in fittings can be put down to the second part of the hypothesis; the longer the polymer chain, the smaller the effect of the anisotropic ordering of the liquid crystal species and therefore the better the fit to Flory-Huggins theory.

It should also be taken into account when considering these results that the fit has been made upon the assumption that phase separation is only occurring by temperature quench once the system has entered the unstable region, and in fact the observed phase properties could be those for the binodal and not the spinodal.

3.3.3 5CB with Poly(n-butyl Acrylate)

As this is the test system which has been selected for the neutron scattering studies it is worth performing an initial SALS study of the system.

3.3.3.1 Results and Discussion

Figure 25 shows the SALS determined phase diagram for 5CB with 3650 $gmol^{-1}$ poly(n-butyl acrylate)

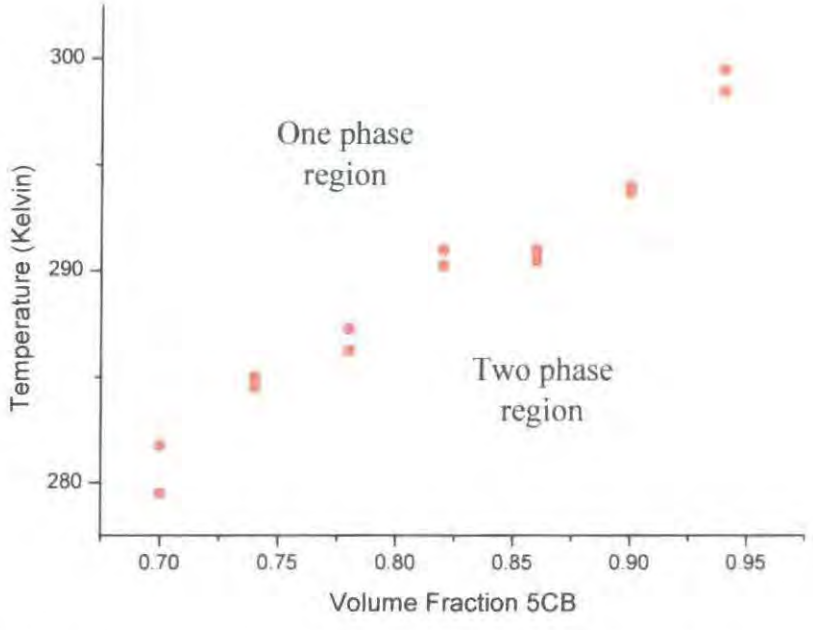

Figure 25 SALS determined phase diagram for 5CB with poly(n-butyl acrylate) (3650 $gmol^{-1}$)

An attempt is made to fit the coexistence curve to Flory-Huggins theory using the input parameters in Table 9. The results of the fitting for this system (Figure 26) should be read taking into account the fact that the data points are around the temperature at which 5CB freezes and as such it cannot be guaranteed that the values being fitted are in fact phase separation temperatures. Considering this however the values obtained $a = -0.173$ and $b = 106.4\,K$ (Table 10) are similar to those obtained for the halogenated liquid crystal blend TL213 with the same polymer, just slightly lower in magnitude as would be expected for a system which is more favourable to dissolution. The system is more favourable to mixing because the halogenated

TL213 blend has a larger number of repulsive highly electronegative centres than the cyanobiphenyl species 5CB. This provides a SALS determined pair of values for comparison with the SANS results presented below.

Species	Monomer unit volume v (cm^3)	Reference Volume (cm^{-3})	Degree of polymerisation N
5CB	3.98E-22	1.00E-22	1
poly(n-butyl acrylate) 3650 $gmol^{-1}$	2.38E-22	1.00E-22	28.51

Table 9 Input parameters for Flory-Huggins fit of phase diagram of 5CB with poly(n-butyl acrylate) (3650 $gmol^{-1}$)

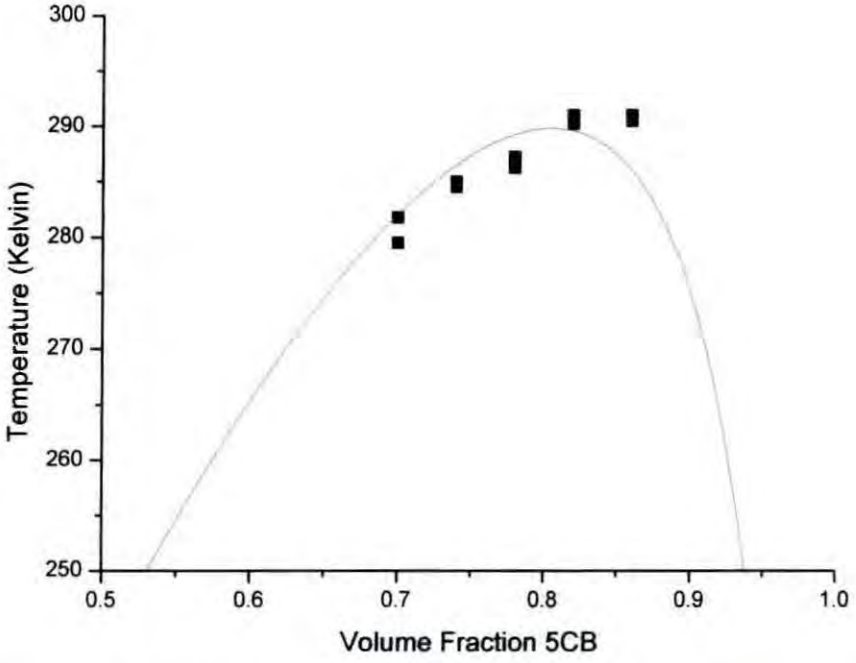

Figure 26 Attempt to fit phase properties of 5CB with Mw 3650 $gmol^{-1}$ poly(n-butyl acrylate) to Flory-Huggins spinodal curve

Parameter	N_{5CB}	N_{PBA}	a	b	Chi2	R2
Fit Value	1	29	-0.173	106.38	9.152	0.507

Table 10 Output parameters for Flory-Huggins fit of phase diagram of 5CB with 3650 $gmol^{-1}$ poly(n-butyl acrylate)

3.4 Fluorinated Polymers

Following on from the previous fluorinated monomer studies, attempts were made to determine the phase properties of fluorinated polymers. Unfortunately the phase mixing temperatures for such systems proved to be above the degradation temperatures of the liquid crystal species and measurements could therefore not be taken.

4 Small Angle Neutron Scattering Studies

As discussed, the Flory-Huggins model for polymer solution thermodynamics has proved to be of only limited success in attempting to fit the presented results. There are two possible explanations as to why; a composition dependence of χ_{AB}, or a structural effect resulting from the rod like nature of liquid crystal molecules requiring a different or modified model to describe the solution thermodynamics. To investigate the possibility of the former of these an attempt is made at utilising a composition independent SANS technique (as discussed in the Experimental section) to determine the interaction parameter for a system.

4.1 Deuterated 5CB with Poly(n-butyl Acrylate) (3650 $gmol^{-1}$)

Solutions of deuterated 5CB with 3650 $gmol^{-1}$ poly(n-butyl acrylate) are made up at compositions of 85:15, 90:10 and 95:5 and small angle neutron scattering profiles obtained at various temperatures above the phase mixing temperature.

As discussed in the experimental section, the De Gennes random phase approximation is applied to obtain temperature dependent χ_{eff} values. To gain temperature independent parameters for the liquid crystal/polymer pair, these are then fitted to the phenomological equation for the interaction parameter,

$$\chi_{eff} = a + \frac{b}{T} \tag{1.22}$$

4.1.1 Results and Discussion

Figure 27 shows the χ_{eff} dependency with temperature for each composition calculated by applying the De Gennes random phase approximation to the results of the SANS experiments performed. Table 11 summarises the phenomological fits of the temperature dependent χ_{eff} values to equation (1.22) to give temperature independent coefficients (a & b).

Composition	a	b
85:15	0.0406	30.73
90:10	-0.2399	96.12
95:5	0.0725	-94.45

Table 11 Tabulated values for 'a' and 'b' to SANS data

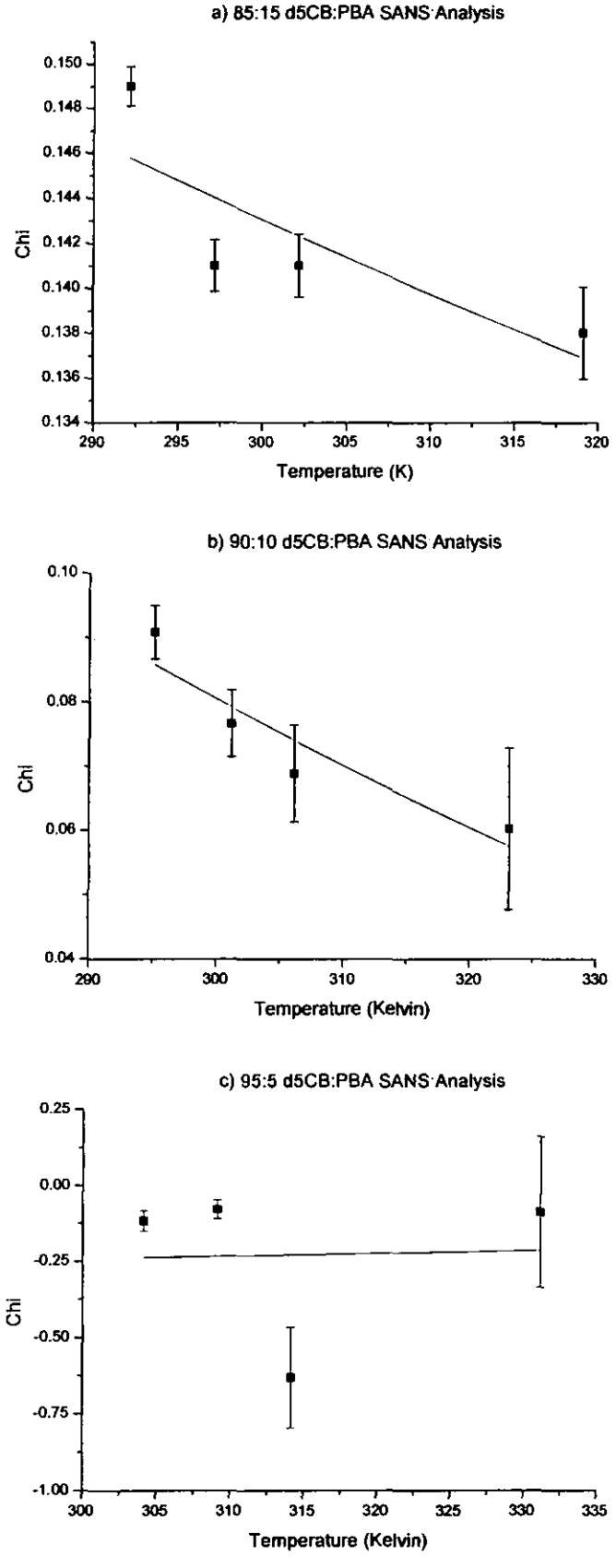

Figure 27 Fit of SANS data to phenomological interaction parameter equation for d5CB with poly(n-butyl acrylate) (Mw 3650 gmol^{-1}) of composition; a, 85:15; b, 90:10; c, 95:5

It can be clearly seen from the large errors bars and large scatter of data points with temperature which do not fit easily to the model, that the accuracy of the experiments

performed is quite limited. However an attempt is made to interpret the results to see if any useful conclusion can be reached.

The experiments performed for a composition of 95:5 5CB:PBA produce a set of fitting values which are *impossible* as they require that the system has phase behaviour described by a spinodal curve consisting of values less than absolute zero (Figure 28).

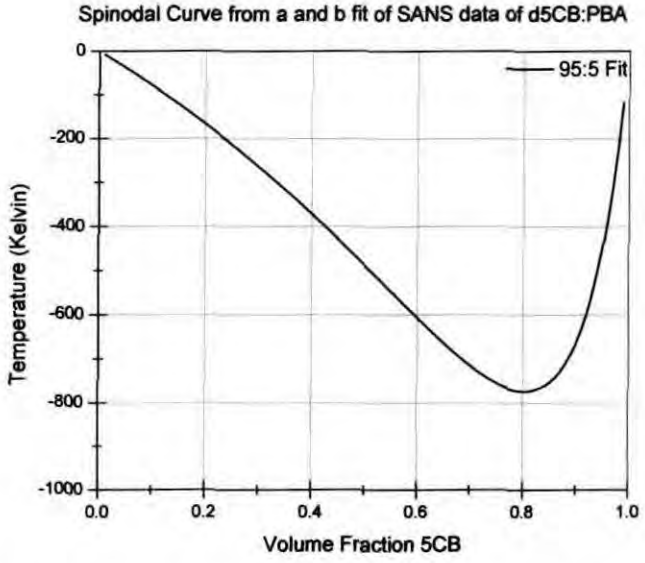

Figure 28 Spinodal curve generated from the fitting data of 95:5 d5CB:PBA

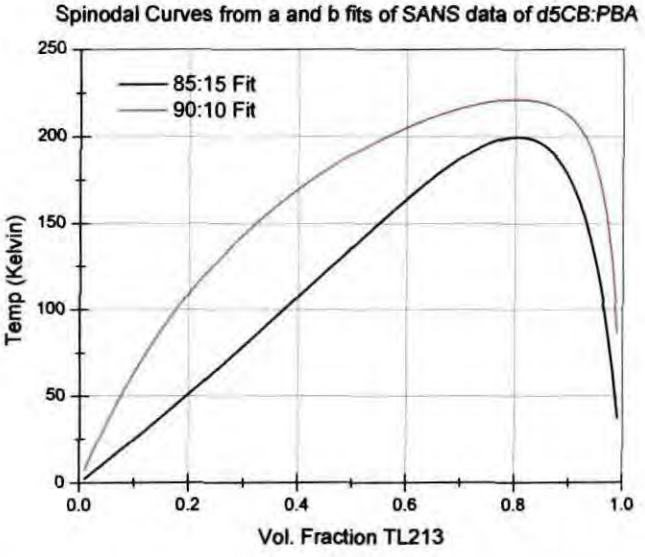

Figure 29 Spinodal curves generated from the fitting data of 85:15 and 90:10 d5CB:PBA

As it is possible to perform SANS experiments on polymer solutions of composition less than 1% polymer by volume it would seem unlikely that the composition is beyond the reliable extents of the technique. Instead it would seem more likely that

the technique is not applicable to the system under test. Further evidence to support this view can be observed in Figure 29 which shows the spinodal curves generated by the fitting data for the 85:15 and 90:10 d5CB:PBA samples. While in this figure the fitting parameters define spinodal curves of a shape expected for Flory-Huggins theory, the phase mixing temperatures are significantly (>100K) less than those observed experimentally using the SALS technique.

It is the view therefore of the author that, as the model used to interpret the raw data of the experiments is based upon Flory-Huggins theory for polymer solution thermodynamics, Flory-Huggins theory is not applicable to a polymer solution where the solvent is a structurally anisotropic *liquid crystalline* species. While the results are inconclusive due to their lack of accuracy and therefore could support the interpretation that the properties observed are due to a very large concentration dependence of the interaction parameter, they would seem to support the view another model is required to accurately describe the phase curves of polymer/liquid crystal and monomer/liquid crystal solutions.

5 Liquid Crystal Solution Thermodynamics

The results presented above suggest that Flory-Huggins theory can be a poor fit for systems which involve liquid crystals as a solvent. This is due to the structural anisotropic nature of liquid crystals, which can be analogised to being rod like in structure, rather than the spherical shape associated with most simple molecules. This has a significant effect on their energetics as they are able to obtain a lower energy configuration by forming domains of similarly aligned molecules, as such their phase properties are significantly modified. The extent of this modification is that a liquid crystal species itself has a series of different solid, liquid crystalline and liquid phases, the most significant of these being the liquid crystalline phases. In the liquid crystalline phases, energy of phase mixing will be significantly modified by the presence of the ordering energetics. There have been two different models applied to PDLC systems to account for these ordering effects upon the mixing thermodynamics, the first is a combination of the Flory-Huggins solution theory with the ordering effect accounted for by Maier-Saupe theory[16, 21, 22, 23] and the second is Flory's own liquid crystal solution lattice based model[20, 24-31].

5.1 Maier-Saupe Approach

This approach assumes that the ordering effect of the anisotropic liquid crystal molecules doesn't modify the phase mixing properties, but merely adds to the phase diagram the effects of ordering of the liquid crystal (i.e. the T_{NI} dependence) as demonstrated in Figure 30.

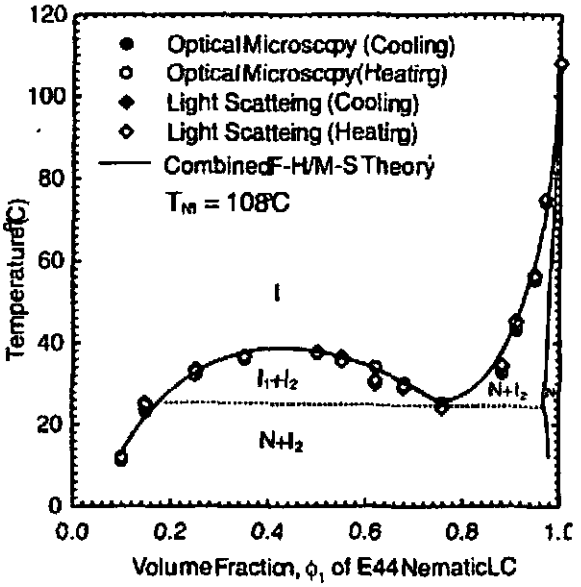

Figure 30 Example of a phase diagram fit to the combined Flory-Huggins/Maier-Saupe theory. E44 with NOA65, work of Nwabunma and Kyu[16].

The model works by assuming that the free energy of the system consists of an isotropic and a nematic component,

$$\Delta G_{mix} = \Delta G^{i} + \Delta G^{n} \tag{1.28}$$

Flory-Huggins theory is applied for the phase mixing energetics of the two component species under isotropic conditions, as defined by equations (1.19), (1.24), and (1.26). The Maier-Saupe[32, 33] mean field theory of liquid crystal ordering is used to define the nematic energetics,

$$\frac{\Delta G^{n}}{nkT} = \frac{\phi_A}{N_A}\left[-\ln Q + \frac{1}{2}v\phi_A S^2\right] \tag{1.29}$$

A is the liquid crystalline species, Q is the anisotropic partition function, v the Maier-Saupe quadropole interaction parameter and S the orientational order parameter. The Maier-Saupe quadropole interaction parameter is liquid crystal species dependent and defined by,

$$v = C_{LC}\frac{T_{NI}}{T} \tag{1.30}$$

C_{LC} is a dimensionless constant for a given liquid crystal species, which for example is 4.54 for the blend E7. The orientational order parameter is given by,

$$S = \frac{1}{2}\left[3\left\langle \cos^2\theta \right\rangle - 1\right] \tag{1.31}$$

where θ is the angle of a liquid crystal molecule to a reference director. The energies of the population of liquid crystal molecules is averaged by use of a partition function, defined by,

$$Q = \int e^{-U(\theta)/(kT)} d\cos\theta \tag{1.32}$$

with the internal energy of a molecule of given orientation described by,

$$U(\theta) = -\frac{m}{2}\left[3\cos^2\theta - 1\right] \tag{1.33}$$

where m is a proportionality parameter. By combining the above equations (1.30), (1.31), (1.32), (1.33), and applying the Boltzmann equation for entropy (1.8) equation (1.29) is reached.

This model is a very simplified approach to the problem, as it fails to take a number of properties into account. There is no consideration of the physical structure of the molecules, so the different ordering effects involved with species of different axial ratios is ignored. The effects of the shape of the liquid crystalline molecules on other species in the solution, such as excluded volumes effects, are also ignored. This is of particular importance when studying polymer/liquid crystal solutions. The model ignores the permanent dipole moments present in many liquid crystalline species, instead modelling only the effect of induced dipoles.

5.2 Flory Liquid Crystal Lattice Model

The Flory approach to modelling the thermodynamics of liquid crystal solutions is an extension of the approach devised for isotropic solutions (Section 1.3.1). Again the model works by producing a combinatorial contribution to the entropy defined by the way molecules fit onto the lattice, but in this case the rod like properties of the liquid crystal molecules need to be accounted for. As with the polymer molecules each member of the chain needs to occupy a site adjacent to the previous unit, in this case it also needs to be in a line along the director of the liquid crystal domain.

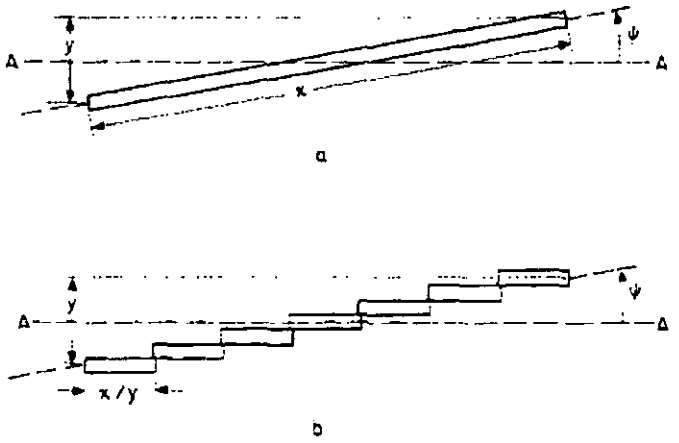

Figure 31 Schematic representation of the way a rod like molecule is treated in Flory Lattice theory[26]

This thus modifies the number of ways of fitting the molecules onto the lattice; Figure 31 shows how a liquid crystal molecule is treated in the Flory model. The molecule is divided up into (x/y) units, where y is the length of a lattice site, and these are then placed on the lattice so as to maintain the angle ψ along the chain. It can be shown that the combinatorial partition function is then given by,

$$Q_{comb} = \frac{(n_s + n_{LC}\bar{y})!}{n_s!\, n_x!} n_0^{\,n_{LC}(1-\bar{y})} \tag{1.34}$$

n_s, n_{LC} and n_0 are the number of molecules of solvent (monomer or polymer), liquid crystal and in total respectively, $\bar{y}$ is the mean value of y, which is dependent upon the angle of displacement of the liquid crystal molecule.

To calculate the entropy of the system it is also necessary to define a term for the orientational component, which is given by,

$$Q_{orient} = \prod_y \left(\sigma \sin\psi_y \frac{n_{LC}}{n_{LCy}} \right) \tag{1.35}$$

σ being an arbitrary constant.

By applying the Boltzmann equation, and Stirling's approximation it can shown that overall the entropic contribution is,

$$\begin{aligned} S = {} & n_s \ln\phi_s + n_{LC} \ln\left(\frac{\phi_{LC}}{x}\right) - (n_s + n_{LC}\bar{y}) \ln\left[1 - \phi_{LC}\left(1 - \frac{\bar{y}}{x}\right)\right] \\ & + n_{LC}(\bar{y} - 1) + n_{LC} \sum_y \frac{n_{LCy}}{n_{LC}} \ln\left(\frac{n_{LC} y}{n_{LC} \sin\psi_y}\right) - n_{LC} \ln\sigma \end{aligned} \tag{1.36}$$

The phase diagram as defined by the Flory lattice model is composed of two parts, a line defined by the equivalency of chemical potentials between the anisotropic and isotropic phases,

$$\left(\mu_s - \mu_s^0\right)_{aniso} = \left(\mu_s - \mu_s^0\right)_{iso} \tag{1.37}$$

$$\left(\mu_{LC} - \mu_{LC}^0\right)_{aniso} = \left(\mu_{LC} - \mu_{LC}^0\right)_{iso} \tag{1.38}$$

and a second defined by the equivalency of chemical potential between two anisotropic phases,

$$\left(\mu_s - \mu_s^0\right)_{aniso} = \left(\mu_s - \mu_s^0\right)_{aniso} \tag{1.39}$$

$$\left(\mu_{LC} - \mu_{LC}^0\right)_{aniso} = \left(\mu_{LC} - \mu_{LC}^0\right)_{aniso} \tag{1.40}$$

This therefore requires two forms of the free energy equation, one where the alignment of the rod like molecules are isotropic and another where the rods are in their equilibrium ordered state (anisotropic). The isotropic free energy is given by setting $n_{LCy} / n_{LC} = \sin\psi_y$, which results in an entropy of,

$$S_{iso} = n_s \ln\phi_s + n_{LC}\left(\frac{\phi_{LC}}{x}\right) + n_{LC}(x-1) - n_{LC}\ln\sigma \tag{1.41}$$

To determine the free energy for the anisotropic phase it is first necessary to introduce the thermotropic contribution to the free energy which is achieved through the use of a term for the ordering effect of one rod upon its neighbours,

$$s_{LC} = \left(3\left\langle\cos^2\psi_y\right\rangle\right) \tag{1.42}$$

This can then be used to give the enthalpic contribution to orientation energy,

$$H_{orient} = -\frac{1}{2}xn_{LC}kT_{NI}s_{LC}^2 \tag{1.43}$$

For the anisotropic free energy the distribution of orientations for such a system is given by,

$$\frac{n_{LCy}}{n_{LC}} = f_1^{-1}\sin\psi_y \exp\left[\ln\left[1-\phi_{LC}\left(1-\frac{\bar{y}}{x}\right)\right]y - \frac{3}{2}\frac{\bar{y}sx}{\tilde{T}}\sin^2\psi_y\right] \tag{1.44}$$

$\tilde{T}$ being the reduced volume, and f_1 given by,

$$f_1 = \int_0^{\psi_{max}} \sin\psi_y \exp\left[\frac{4}{\pi} x \ln\left[1-\phi_{LC}\left(1-\frac{\bar{y}}{x}\right)\right]\sin\psi_y - \frac{3}{2}s\tilde{T}^{-1}\sin^2\psi_y\right] d\psi_y \quad (1.45)$$

Overall it can be shown that this yields a free energy for the liquid crystal in equilibrium alignment given by,

$$\begin{aligned}\frac{G}{kT} &= -n_s \ln\left[1-\phi_{LC}\left(1-\frac{\bar{y}}{x}\right)\right] + n_s \ln n_s - (n_s + n_{LC})\ln n_{Total} \\ &+ n_{LC}\bar{y} - n_{LC} + n_{LC}\ln n_{LC} - n_{LC}\ln(\sigma f_1) - \frac{\phi_{LC} x n_{LC} s\left(1-\frac{s}{2}\right)}{\tilde{T}}\end{aligned} \quad (1.46)$$

With $\tilde{y}$ and s minimised for the system.

Once these terms are known it is possible to calculate the chemical potentials and apply equations (1.37) to (1.40) to generate phase diagrams. As with Flory-Huggins theory it is possible to scale the entropic contributions by the reciprocal of the degree of polymerization to account for changes due to increasing chain length.

Dorgan[30] has used this model to produce phase diagrams to demonstrate the effect of polymer chain length on the phase properties of rod like liquid crystals in solution with them (Figure 32 (in figure θ is the reduced temperature).

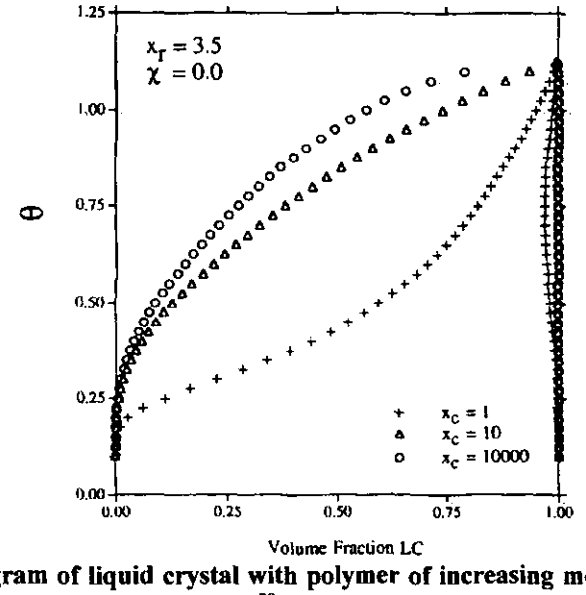

Figure 32 Phase diagram of liquid crystal with polymer of increasing molecular weigth (x_c), as derived from Flory lattice theory by Dorgan[30] (θ is the reduced temperature)

This phase diagram demonstrates the type of behaviour observed in the experimental results previously presented. In particular the importance of ordering due to rod like molecules upon the phase mixing temperatures is accounted for, which is not the case from simply combining Flory-Huggins theory with Maier-Saupe theory. This

results in the observed migration of the critical composition to high liquid crystal volume fractions, rather than $\phi_{LC} \approx 0.5$ as would be expected from Flory-Huggins theory.

Although not covered in this thesis, it would be of great interest to attempt to apply the Flory lattice model for liquid crystals to the systems under experimental study, by the use of computational modelling. The aim being to provide greater evidence to support the supposition that this model is the most appropriate to apply to PDLC systems and to investigate the likely effect of changing the physical and chemical properties of potential monomer/liquid crystal solutions. This is discussed in greater detail in the further work section at the end of this thesis.

6 Conclusions

It has been demonstrated that due to presence of a structurally asymmetrical species the mixing thermodynamics of liquid crystal/monomer solutions cannot be explained by the normally applied Flory-Huggins theory for solutions. The result of this asymmetry is to produce phase diagrams which are skewed to the high ϕ_{LC} compositions, which will have a significant effect on the reaction induced phase properties and morphologies formed.

Further work into the phase properties of polymer/liquid crystal solutions demonstrated that as the degree of polymerization increases the fit to Flory-Huggins theory improves. This is believed to be the result of increasing chain length making the entropic constraints of the polymer species more important than those of the much shorter anisotropic liquid crystal molecules.

The results of SANS studies and the ability of the Flory lattice model for liquid crystal solutions to demonstrate the experimentally observed phase behaviour would suggest that the limitations in the Flory-Huggins model in this instance are due to structural asymmetry and not a composition dependent interaction parameter.

Bibliography

1. Gibbs, J. W., In *Collected Works*, Yale University Press: New Haven, 1948; Vol. 1, pp 105-115.
2. Flory, P. J. *Journal of Chemical Physics* **1941,** 9, 660-661.
3. Flory, P. J. *Journal of Chemical Physics* **1942,** 10, 51-61.
4. Huggins, M. L. *Journal of Chemical Physics* **1941,** 9, 440.
5. Balsara, N. P.; Jonnalagadda, S. V.; Lin, C. C.; Han, C. C.; Krishnamoorti, R. *Journal of Chemical Physics* **1993,** 99, 10011-10020.
6. Rubinstein, M.; Colby, R. H., Thermodynamics of Mixing. In *Polymer Physics*, Oxford University Press: Oxford, 2003; pp 137-170.
7. Cowie, J. M. G., In *Polymers: Chemistry & Physics of Modern Materials*, 2nd ed.; CRC Press: Boca Raton, 1991; pp 315-317.
8. Balsara, N. P., Thermodynamics of Polymer Blends. In *Physical Properties of Polymers Handbook*, Mark, J. E., Ed. AIP Press: New York, 1996; pp 257-268.
9. Muller, M. *Macromolecular Theory and Simulations* **1999,** 8, 343-374.
10. Muthukumar, M. *Journal of Chemical Physics* **1986,** 85, 4722-4728.
11. Yamamoto, T.; Narita, T.; Nobe, M.; Dobashi, T. *Macromolecules* **2004,** 37, 3475-3486.
12. Smith, G. W. *Physical Review Letters* **1993,** 70, 198-201.
13. Smith, G. W. *Molecular Crystals and Liquid Crystals Science and Technology Section a-Molecular Crystals and Liquid Crystals* **1994,** 239, 63-85.
14. Grand, C.; Achard, M. F.; Hardouin, F. *Liquid Crystals* **1997,** 22, 287-296.
15. Amundson, K.; vanBlaaderen, A.; Wiltzius, P. *Physical Review E* **1997,** 55, 1646-1654.
16. Nwabunma, D.; Kyu, T. *Polymer* **2001,** 42, 801-806.
17. Nwabunma, D.; Kim, K. J.; Lin, Y. H.; Chien, L. C.; Kyu, T. *Macromolecules* **1998,** 31, 6806-6812.
18. Atkins, P. W., Phase Diagrams. In *Physical Chemistry*, 6th ed.; Oxford University Press: Oxford, 1998; pp 191-214.
19. Ahn, W.; Kim, C. Y.; Kim, H.; Kim, S. C. *Macromolecules* **1992,** 25, 5002-5007.
20. Lee, J. C. *Physical Review E* **1999,** 60, 1930-1935.
21. Nwabunma, D.; Chiu, H.-W.; Kyu, T. *Macromolecules* **2000,** 33, 1416-1424.
22. Shen, C. S.; Kyu, T. *Journal of Chemical Physics* **1995,** 102, 556-562.
23. Benmouna, F.; Bedjaoui, L.; Maschke, U.; Coqueret, X.; Benmouna, M. *Macromolecular Theory and Simulations* **1998,** 7, 599-611.
24. Ballauff, M. *Molecular Crystals and Liquid Crystals* **1986,** 136, 175-195.

25. Flory, P. J. *Journal of the American Chemical Society* **1956,** 78, 5222-5234.

26. Flory, P. J.; Abe, A. *Macromolecules* **1978,** 11, 1119-1122.

27. Flory, P. J.; Ronca, G. *Molecular Crystals and Liquid Crystals* **1979,** 54, 289-309.

28. Flory, P. J.; Ronca, G. *Molecular Crystals and Liquid Crystals* **1979,** 54, 311-330.

29. Warner, M.; Higgins, J. S.; Carter, A. J. *Macromolecules* **1983,** 16, 1931-1935.

30. Dorgan, J. R. *Journal of Chemical Physics* **1993,** 98, 9094-9106.

31. Yoon, D. K.; Lee, Y. S.; Bae, Y. C. *Macromolecular Chemistry and Physics* **2002,** 203, 41-47.

32. Maier, W.; Saupe, A. *Zeitschrift Fur Naturforschung Part a-Astrophysik Physik Und Physikalische Chemie* **1959,** 14, 882-889.

33. Maier, W.; Saupe, A. *Zeitschrift Fur Naturforschung Part a-Astrophysik Physik Und Physikalische Chemie* **1960,** 15, 287-292.

Section B – Phase Separation Mechanism and Morphology

1 Background

1.1 Importance of Morphology Control

As previously discussed, to make PDLCs applicable as a display screen technology a balance between lowering the switching voltage and increasing film optical contrast needs to be achieved. To this end control needs to be maintained over morphology size and phase purity during the formation process; in the work presented formation is by the phase separation of a homogeneous monomer/liquid crystal solution into polymer rich and liquid crystal rich phases. A larger morphology results in a lower switching voltage, but also a lower contrast ratio. To be able to control film morphology it is first necessary to understand the mechanisms by which phase separation occurs.

1.2 Phase Separation of Polymer Solutions and Blends

1.2.1 Phase Mixing Energetics

As previously discussed in section A the phase properties of a classical solution – in which the monomers can be considered to be approximately spherical and the inter-diffusion of the species unhindered – can be understood by applying the Flory-Huggins theory of polymer solution thermodynamics. A system will remain phase mixed so long as the entropy gain from forming a disordered system is greater than any enthalpic loss due to two or more species being placed in unfavourable contact. Equation 1.1 for a polymer solution shows the entropic contribution is degree of polymerization dependent while the enthalpic contribution is constant for a given set of chemical species.

$$\frac{\Delta G_{mix}}{kT} = \underbrace{\frac{\phi_A}{N_A}\ln\phi_A + \frac{\phi_B}{N_B}\ln\phi_B}_{\text{Entropic}} + \underbrace{\chi_{AB}\phi_A\phi_B}_{\text{Enthalpic}} \qquad (1.1)$$

where ϕ_A & ϕ_B are the volume fractions of species A and B respectively, N_A, N_B the degrees of polymerization, and χ_{AB} the interaction parameter between the two species.

The χ_{AB} term can be phenomologically considered inversely proportional to temperature.

$$\chi_{AB} \cong a + \frac{b}{T} \tag{1.2}$$

a and b are constants for a given set of species 'A' and 'B'.

Phase separation becomes energetically favourable once the overall energy of two new phases is less than that of the system in a single phase, although this does not mean phase separation will be spontaneous as there may still be a kinetic barrier to the lower energy configuration. This energetic behaviour can be summarised through the use of a temperature/composition phase diagram. Phase separation can be initiated either by a thermal/compositional change such that the conditions are now below the phase mixing boundary – known as thermally induced phase separation (TIPS) – or through a change in the position of the curve. The latter is generally initiated by polymerization of a monomeric or oligomeric species such that the degree of polymerization (N) increases until it reaches a critical value and phase separation occurs. This is commonly referred to as either Reaction (RIPS) or Polymerization (PIPS) Induced Phase Separation, and is the focus of the work presented within this section. Phase separation is classically considered to occur by one of two mechanisms 'Nucleation and Growth' or 'Spinodal Decomposition'. The type of mechanism being determined by the system's energetic properties and thus the conditions under which you enter the two phase region.

1.2.2 Nucleation and Growth

Nucleation and Growth[1-3] occurs when a system is thermodynamically meta-stable; a lower energy system can be achieved by a single phase separating into two distinct phases, but only after overcoming an initial energy barrier. As can be seen in Figure 1, the energy gain from forming phase ϕ' isn't large enough to overcome the energy barrier to phase ϕ'' even though both are of lower energy than the initial system. This occurs in the binodal region of the temperature/composition phase diagram. For phase separation to occur an initial nucleus of one of the two novel phases needs to be formed, and it is in this initial nucleation that an energy barrier must be overcome. Once formed phase separation is spontaneous by diffusion to overcome the large

energy gradient created at the interface. Phase separation and domain growth will continue until either equilibrium is reached or diffusion is somehow restricted.

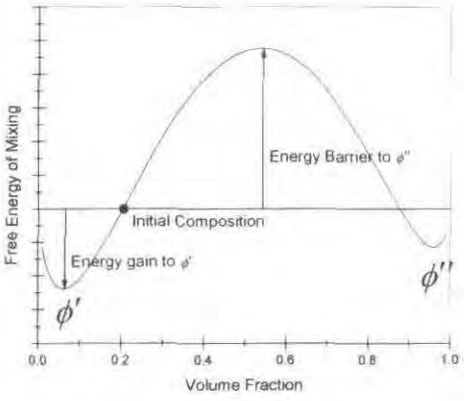

Figure 1 Energy profile of a meta-stable system capable of undergoing phase separation via nucleation and growth

This type of phase separation mechanism results in what is known as a droplet morphology, with the phase which initially nucleates out forming droplets within a matrix of the second phase (Figure 2). In most systems this form of phase separation will not occur as there will be either no source of external energy or the build up of a large enough composition fluctuation to overcome the barrier to nucleus formation, as such phase separation will not normally occur until the unstable spinodal region is reached.

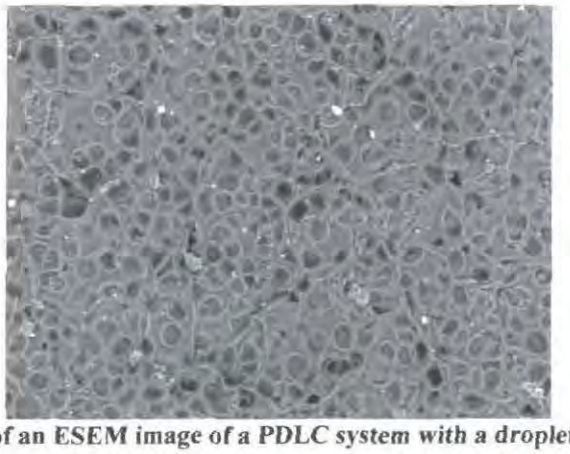

Figure 2 Example of an ESEM image of a *PDLC system with a droplet type morphology*

1.2.3 Spinodal Decomposition

Upon entering the unstable spinodal region phase separation becomes spontaneous as there is no energy barrier and a lower system energy can be achieved by phase separation. Under these conditions spinodal decomposition[2, 4, 5] occurs; thermal perturbations cause the formation of local composition fluctuations leading to a lowering of free energy. These fluctuations proceed via diffusion to grow into a

preferred length scale as different length scales grow at different rates. The larger the length scale the greater the distance over which the component species needs to diffuse to equilibrate the system, whereas a smaller length scale requires the formation of a large number energetically unfavourable composition gradients. Overall short length scales are suppressed and larger length scales do not have time to grow leaving one preferred length scale.

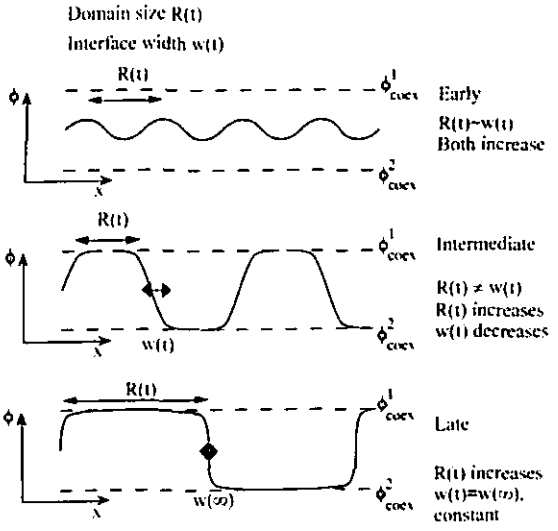

Figure 3 Schematic representation of spinodal decomposition in terms of domain size. Figure reproduced from Polymers at Surfaces and Interfaces, Jones and Richards[2]

As a result of this preferred length scale the initial morphology has a consistent size. Once this length scale is established the domains increase in amplitude (purity of the phase increases) and coarsen as the two component species interdiffuse. During the intermediate stage the wavelength grows so as to reduce the energetically unfavourable interfacial gradient between the two phases. During the final stage of phase separation agglomeration of droplets occurs to reduce the interfacial energy, by reducing the interfacial area to volume ratio. Figure 3 shows an overview of the spinodal decomposition domain growth mechanism.

The formation of a consistent initial morphology size can be observed by small angle light scattering[6-8] through the formation of what is known as a spinodal ring (Figure 4) in the 2D scattering profile at a maximum scattering vector q_{max} related to the length scale λ_{max} (1.3) of the morphology by,

$$q_{max} = \frac{2\pi}{\lambda_{max}} \tag{1.3}$$

The coarsening can be observed via small angle light scattering as the domain length scale increases the scattering vector decreases and the ring collapses into the beam.

The appearance of a ring in the phase separation process is generally considered to indicate that phase separation has occurred via spinodal decomposition. This has been the subject of some controversy with the belief that nucleation and growth can also produce a scattering ring[9, 10], and it is also possible that spinodal decomposition is occurring without a ring being observed if the initial length scale is large enough that q_{max} is too small to observe. Overall the presence of a ring is a strong suggestion that spinodal decomposition is occurring, and its absence would suggest that nucleation and growth is at the very least a possibility. Maugey and co-workers[8] have shown that if a ring is observed then it is possible to determine whether or not it is due to spinodal decomposition as at a fixed value of q there will be an exponential growth in intensity, during the early stages of phase separation.

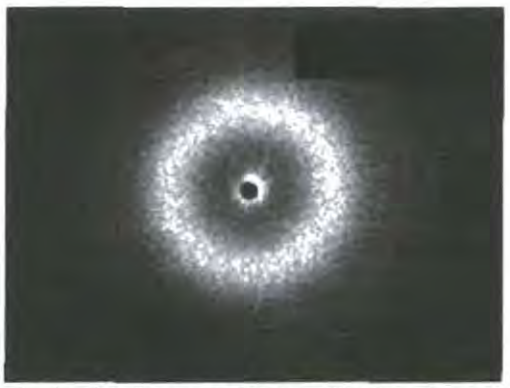

Figure 4 Example of spinodal decomposition scattering ring, reproduced from ref[7]

1.2.4 Lever Rule

The type of morphology formed by spinodal decomposition is dependent upon the relative compositions and hence relative volumes of the two new phases formed[4, 5], which is in turn dependent upon the free energy of the system.

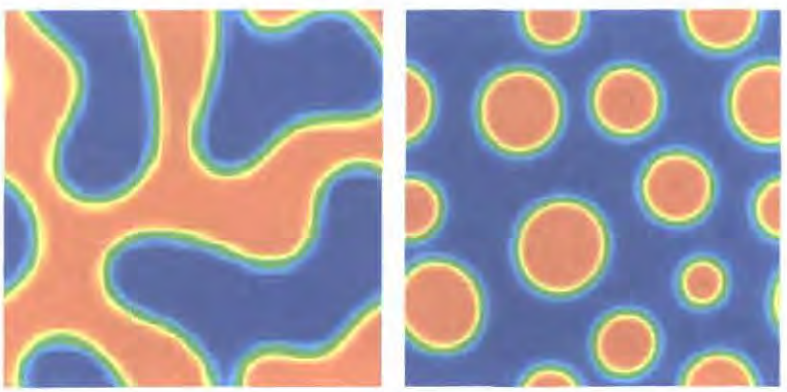

(a) (b)

Figure 5 Computational simulations of spinodal decomposition morphologies. (a) Co-continuous network, (b) droplet morphology. With thanks to Dr Ian Henderson

In the circumstances that the volumes of the two new phases formed are identical, the lowest interfacial energy is gained by the phases being completely interconnected, and forming what is known as a co-continuous network. If one phase is of a larger volume than the other then the lowest interfacial energy is achieved by the formation of a droplet morphology, where the lower volume phase forms droplets within a matrix of the larger volume phase (Figure 5).

The volume of each phase is given by the Lever rule; the two new phases have to produce a balanced system such that total volume and individual volume fractions are conserved upon phase separation.

$$V_{tot} = V' + V'' \tag{1.4}$$

$$V\phi_A = V'\phi_A' + V''\phi_A'' \tag{1.5}$$

where V' and V'' are the volumes of the two new phases formed and ϕ_A' and ϕ_A'' the volume fractions of species A in each new phase. By rearrangement of equations (1.4) and (1.5),

$$V'' = \frac{\phi_A'' - \phi_A}{\phi_A'' - \phi_A'} \tag{1.6}$$

and,

$$V' = \frac{\phi_A - \phi_A'}{\phi_A'' - \phi_A'} \tag{1.7}$$

For a pair of novel phases to have the same volume the system needs to start from an initial volume fraction ϕ_A which is an average of the two new volume fractions,

$$\phi_A = \frac{\phi_A'' + \phi_A'}{2} \tag{1.8}$$

This behaviour can be correlated to the phase diagram of the system as demonstrated schematically in Figure 6. For a blend of monodisperse polymers the volume fractions in the coexisting phases is independent of the bulk composition. Hence only if phase separation via spinodal decomposition initiates under the conditions of the central line will a co-continuous morphology will be generated, otherwise a droplet morphology result.

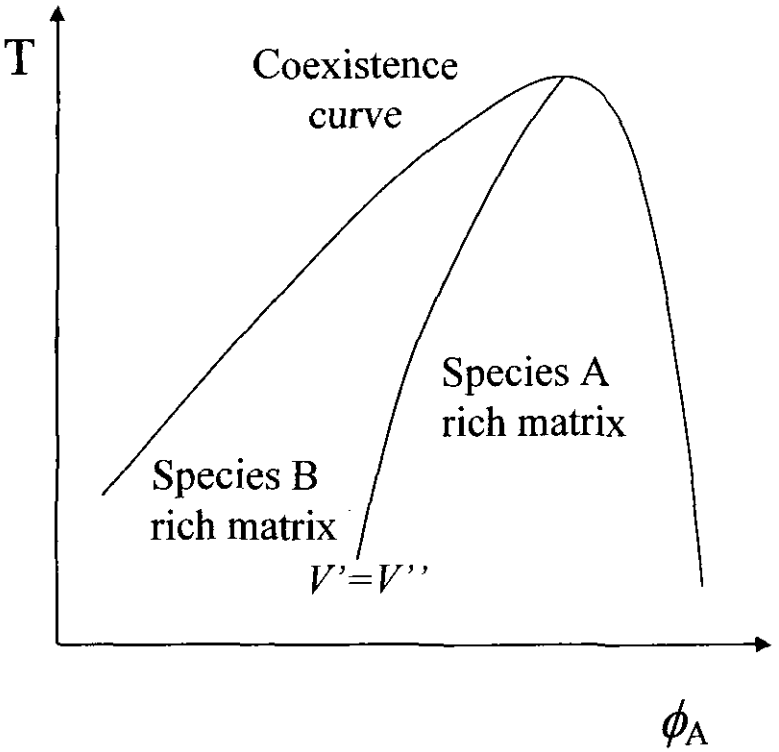

Figure 6 Schematic diagram showing morphology determination in a system undergoing spinodal decomposition

It is possible to determine which new phase will form the matrix in a droplet morphology as it will be the phase which has the larger volume. As shown by the lever rule this will be the phase where the difference between the bulk volume fraction and the volume fraction in the coexisting phase is the smallest.

1.3 Phase Separation in Polymer Gels

In most cases phase separation can be explained by the liquid-liquid demixing mechanisms described above, but another property needs to be considered for the work presented herein. For PDLCs to work as display devices it is necessary for their two phases to form a permanent morphological structure. To this end a tetra-functional (or greater) monomer species is mixed in with the bi-functional monomer/liquid crystal solution, and this species acts to link together individual polymer chains to form a polymer network. This network cannot dissolve in a solvent like a linear polymer, such mixing solvation would require the breaking of covalent bonds which requires a large input of energy. Instead the network is capable of swelling[11-18]; a solvent molecule can solvate within the different chains of the network, resulting in an elongation of the component chains (swelling of the network), as shown schematically in Figure 7.

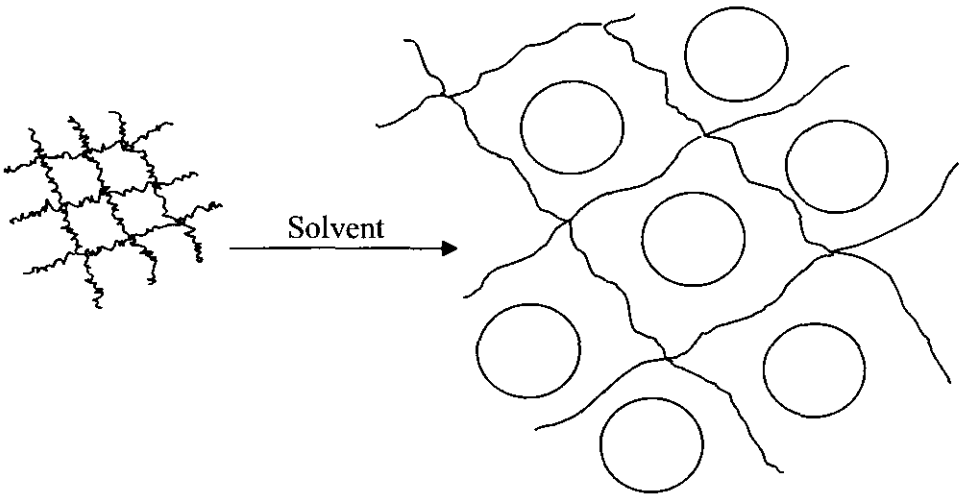

Figure 7 Schematic diagram of the effect of chain elongation of phase mixing in polymer gels

This ability to absorb solvent by network swelling means that the system's phase behaviour and mechanism of separation become more complex. Phase separation is now highly dependent upon the elastic properties of the polymer network, by swelling the polymer network the chains are being perturbed from their equilibrium conditions and as such being placed into a higher energetic state. While the system wants to reduce energy by de-swelling, it can also be the case that the polymer network can act against phase separation. If the network is universal (homogeneous throughout) within a system then it will require greater stretching of the chains for a domain of a new solvent phase to form within the network, which will lead to an increase of the energy of the polymer chains and therefore the network[19].

If, as is the case for the experiments presented, the network is formed while in solution the chains will already be in a swollen state and therefore will be looking to form an energetically lower state by phase separation. Therefore provided, as described above, conditions aren't such that phase separation is suppressed by elasticity, the polymer chains will look to contract upon phase separation to form two relatively pure phases, one which is purely solvent and unreacted monomer and one which is mainly polymer.

1.3.1 Polymer-Gel Thermodynamics

This stretching of the polymer chains which form the network results in a modification of the thermodynamic properties of the solvated system. A relatively simple model has been devised through the work of Flory[14, 15, 18, 20] and Dušek[11, 12, 21, 22]. The model assumes that the network formed is perfect (all possible bonds are

formed and no loops), and that all chains between crosslinks are of the same length. Equally the model also ignores any contribution to elastic forces from what are known as transient crosslinks, where two chains are able to entwine and act temporarily like a crosslink until they un-entangle again. The model starts from the principle that the free energy of the system consists of a mixing term for the solvent with the polymer network and an elastic term for the stretching of the chains.

$$\Delta G = \Delta G_{mix} + \Delta G_{el} \tag{1.9}$$

The mixing free energy is considered to be an evolution of the Flory-Huggins mixing energy of a polymer solution (equation 1.1), but as the individual chains of the polymer network are crosslinked together they are considered as one infinitely long chain and hence have no entropic contribution, such that,

$$\frac{\Delta G_{mix}}{kT} = \frac{\phi_{solv}}{N_{solv}} \ln \phi_{solv} + \chi \phi_{solv} \phi_{pol} \tag{1.10}$$

The free energy due to chain stretching is approximated to purely the entropic contribution, as, for an ideal polymer, no bonds are broken or formed during stretching and as such no change in internal energy occurs. According to the Flory approach[15] the entropy has two components, a term for the configurational entropy of the chains in the network, and a second to account for the random distribution of the crosslinks over the total volume of the sample. Other derivations have taken different approaches and determined different terms for the stretching entropy[17, 23, 24] The configurational entropy is calculated by assuming that each chain between crosslinks is Gaussian and has been shown to be given by,

$$\Delta S_{el} = \left(\frac{-kn_c}{2} \right) \left(\lambda_{ix}^2 + \lambda_{iy}^2 + \lambda_{iz}^2 - 3 \right) \tag{1.11}$$

where, n_c is the number of chains in the system, and λ_{ix} λ_{iy} λ_{iz} are the Cartesian stretching factors of the chain.

While equation 1.11 takes account of the entropy change due to all the chains present it does not account for the entropic loss due to crosslinking monomers going from being freely dispersed to being constrained within the network. A second term is needed for the distribution of the crosslinks going from the total volume V_0 to a constrained volume V, which is given by,

$$\Delta S = \frac{k2n_c}{f}\left[\ln V - \ln V_0\right] \tag{1.12}$$

where f is the functionality of the crosslinking species.

As the system's total volume does not change upon stretching (assuming no excluded volume effects), V_0 is constant and therefore the term does not change upon stretching and can be ignored. Combining equations (1.11) & (1.12) gives,

$$\Delta S_{el} = kn_c\left[\left(\frac{1}{2}\right)\left(\lambda_{ix}^2 + \lambda_{iy}^2 + \lambda_{iz}^2 - 3\right) + \left(\frac{2}{f}\right)\left(\ln V\right)\right] \tag{1.13}$$

The model as currently presented assumes that the network has been formed under perfect dry conditions; this is not always going to be the case. As has been discussed by Dušek[11] if a diluent species, that is a good solvent, is present during the network formation the equilibrium, and as such reference state is going to be more stretched. To take this into account a value is included for the volume fraction of the polymer at the point of network formation Φ_0. It can be shown that by relating the expansion of the network to the volume fraction of the network (ϕ_{pn}) the following expression for the elastic entropy is found[21],

$$\Delta S_{el} = -kn_c\left[\left(\frac{3A}{2}\right)\Phi_0^{2/3}\left(\phi_{pn}^{-2/3} - 1\right) - B\ln\left(\phi_{pn}\right)\right] \tag{1.14}$$

As previously discussed the model presented is for a perfect network which contains all possible chains and no loops. To take account of this, the constants A and B are introduced; the actual values of these are the subject of much discussion [17, 21, 23, 25, 26]. As the model being presented is deliberately the simplest possible the values of A and B shall be those presented by Flory,

$$A = 1 \tag{1.15}$$

$$B = \frac{2}{f} \tag{1.16}$$

Thus the network is considered to have no defects and the expression for B is simply a consequence of the relation between the number of chains and the number of crosslinks.

1.4 Phase Separation Mechanism and Morphology Control in Polymer Dispersed Liquid Crystal Systems

As discussed in the introduction, the control of morphology is vital in controlling the electro-optical properties of films for display applications. As a result much work has been performed in the last twenty years into this area both in terms of the effect of composition and cure temperature upon final morphology and into the mechanisms by which they form and the effect of mechanism upon end morphology.

1.4.1 Control of Morphology in PDLC Formation

Most work into the formulation of PDLC films involves the application of polymerization induced phase separation (PIPS)[27-37] methodologies as opposed to thermally induced phase separation (TIPS)[27, 28], or solvent evaporation induced phase separation (SIPS)[27, 28, 38, 39]. This can be ascribed to the simplicity of method, relative cheapness of fabrication, ease of control of variables and flexibility of the methodology[27, 28, 36, 37]. Significantly most work, including that presented within this report, utilise radical as opposed to step-growth or condensation polymerization, again due to flexibility and ease of method, although at the cost of full control over polymerization[40].

All work described starts from a system in the one phase region before cure; this removes the possible formation of large uneven domains of one or other phase caused by the polymerization of an already phase separated system[41-44]. The exact effect of composition and temperature of cure upon morphology is very much system dependent as phase properties will vary depending upon polymer and liquid crystal chemistry[34, 43]. Even considering this there are some notable trends observed in the literature. Most work suggests the morphology type to be droplet with a liquid crystal rich phase dispersed within a network formed of a polymer rich phase[5, 27, 28, 30, 33-37, 43, 45-50], with no reference to co-continuous networks. Amundson and co-workers[36] ascribe this type of morphology to being that which would be expected by application of the lever rule; it has however also been observed under conditions for which the lever rule would prescribe a liquid crystal rich matrix. At high polymer content there has also been the observance of non-display device applicable spherulitic morphologies[37]. It should be pointed out that this in itself is not evidence

for any one phase separation mechanism as all are capable of forming a droplet type morphology as will be discussed in further detail later.

The work presented in Section A of this report showed that the rod-like properties of the liquid crystalline species have a dramatic effect upon the unpolymerized phase diagram, driving the phase curve to the high liquid crystal volume fraction extreme of composition for most systems. Most work presented in the literature is based on the assumption that morphology size is controlled by the time between initial phase separation and polymer gelation[30, 36]; a longer time resulting in a larger morphology size as domains are able to grow in this time by both diffusion and coalescence of droplets. Therefore as the phase curve is higher in temperature as you move to the higher liquid crystal compositions you would expect morphology growth to occur for a longer time and a larger morphology size to be formed as a result. This indeed has been frequently observed for various systems, including the epoxy based pre-polymer NOA65 (Norland) with the cyanobiphenyl liquid crystal blend E7 (Merck)[34, 37], K21 (4-*n*-heptyl-4'-cyanobiphenyl) (BDH Chemicals)[35], and the acrylate based pre-polymer PN393 (Nematel) with TL213[30, 34], TL205 (halogenated liquid crystal blend) (Merck)[36].

Both Amundson et al.[36] (pre polymer PN393 with liquid crystal TL205) and Carter et al.[30] (PN393 with TL213) have reported the importance of viscosity effects in the domain growth process. They claim to consider contradictory effects to be important, in the case of Amundson and co-workers they suggest that the degree of polymerization at the point of phase separation is important as the polymer species will be of a much lower viscosity at lower degrees of polymerization. This they believe allows for the rapid growth of domains by both diffusion of phases and coalescence. Their results for higher liquid crystal composition systems would seem to support this view as a lower degree of polymerization is required for phase separation and large droplets and coalescence are observed as a result. They attempted to further prove this view by performing a series of lower temperature studies where a lower viscosity would be expected from a lower degree of polymerization at the phase separation point; counter to expectation they actually observed smaller droplet sizes. Carter et al. observed similar results but interpreted them slightly differently, suggesting that viscosity variation was in fact an effect of temperature and as cure temperature increased, viscosity decreased accounting for the larger droplet sizes at higher temperatures.

An earlier piece of work by Amundson et al.[37] into the effect of cure temperature on morphology for a system of E7 with NOA-65 showed the seemingly contradictory result that for a 65:35 liquid crystal:monomer system a higher cure temperature resulted in a smaller droplet size. This is however a system of much lower liquid crystal composition, and as such suggests evidence for the effect of temperature being also composition dependent. Given that the results are reported in different papers no explanation is presented for this apparent behaviour.

Comment has been made upon the fact that the shape of the droplets formed is composition dependent; higher liquid crystal composition systems displaying a more polygonal or honeycomb like structure than the more perfectly spherical structure of those of lower liquid crystal volume fraction[30, 35, 36, 46]. This change is usually ascribed to impingement effects; as the monomer component is decreased the volume of the polymer rich phase formed decreases too, with the result there is less polymer phase between the LC rich droplets and the droplets start to impinge upon each other causing deformation. Amundson[36] and co-workers have taken this further and suggest the polygonal structure is a result of the previously mentioned viscosity effects resulting from the low functionality of the acrylate monomers. When the viscosity at phase separation is low such as is the case for high liquid crystal volume fraction systems the liquid crystal droplets grow quickly and fill all the space available, resulting in a polygonal structure as the most efficient packing. If the functionality were higher, such as with a greater proportion of crosslinker the morphology would be more spherical as solidification would occur before great growth could take place. Equally this would suggest that for the low liquid crystal volume fraction systems, where phase separation and gelation are close together, the droplets should be spherical as well, as has been observed.

Increasing the crosslinker mole fraction has been shown[46, 47] to have the intuitively expected effect of decreasing droplet size. The greater the crosslinking component the faster the network grows and the shorter the time between phase separation and gelation.

1.4.2 Spinodal Decomposition and Nucleation & Growth in PDLCs

Early work[27, 28] into PIPS assumed that morphology growth occurred by a system reaching a point of thermodynamic meta-stability (Nucleation and Growth)[27, 30, 31, 34] or instability (Spinodal Decomposition)[32, 33, 40, 51] resulting in initiation of phase

separation. Domains of the two phases would then proceed to grow by the appropriate mechanism until the polymer reached a degree of polymerization whereby gelation occurred. Upon gelation it was believed that the film would freeze in its final morphology, unable to rearrange due to the infinite viscosity of the polymer species.

The work of Kim et al.[32, 33] has appeared to demonstrate the presence of a peak in small angle light scattering studies during phase separation, suggesting that phase separation is via a spinodal decomposition mechanism. Significantly they used a monomer which underwent polymerization via a condensation reaction and not a radical reaction. Other papers based on radical polymerization provide evidence to the contrary with morphologies which shouldn't be possible for systems phase separating via spinodal decomposition under those temperature and compositional conditions[30, 31, 34-37, 43]. Carter et al.[30, 31, 34] have reported the observance of droplet formation followed by coalescence, which is indicative of a morphology formed by droplets being nucleated and allowed to grow, an observation also made by Nwabunma and Kyu[43]. Equally Amundson and co-workers discuss the idea of nucleation of droplet domains in their studies of systems involving E7 with NOA65[37] and TL205 with PN393[36]. They state that nucleation is evidenced by the way the morphology develops after initial phase separation; initially nucleated domains grow little in size, but new smaller drops are nucleated. This is an unlikely observation for a system undergoing spinodal decomposition. Further their observations suggest that nucleation is a quicker process than growth by diffusion and is a kinetically favourable event, which overcomes the normal barrier to nucleation and growth type mechanisms.

Similarly modelling investigations have been performed, again with disagreement over the type of phase separation mechanism. Generally this is because modellers have only looked to form morphology types rather than accurately recreate the trends in morphology size with composition and temperature observed experimentally. The type of morphology generally observed for PDLC systems is droplets of a liquid crystal rich phase dispersed within a matrix of a polymer rich phase. As has been previously discussed it is possible to form a droplet type morphology from either spinodal decomposition[5, 52-55] or nucleation and growth[5, 48] with, in the case of spinodal decomposition, the matrix species being determined by the system thermodynamics. In some cases such as in the work of Chan and Rey[54, 55] they have

been able to show similar morphology types even in the absence of a proper representation of the phase mixing thermodynamics, ignoring the nematic effect.

The work of Ohta et al.[5, 48] on nucleation and growth would seem to suggest that phase separation initiates by nucleation of droplets of the nematic phase with the energy required for nucleation possibly originating from the energetic gain produced by the ordering of the liquid crystalline molecules.

Overall a full understanding of the concepts behind the phase separation process is still wanting.

1.4.3 Elastic Contribution and Gel Effects in PDLC Phase Separation

While many researchers have made mention of the importance of a crosslinking species in the gelation of the polymer phase to freeze the network morphology[5, 30, 34-37, 43, 48], little consideration has been given to the effect that network and gel effects have upon the phase separation process itself. Most work as so far discussed is interpreted in terms of simple liquid-liquid demixing and spinodal decomposition or nucleation and growth. As discussed in the section on polymer solution phase separation mechanism, when a crosslinker is present in the monomer solution, elastic forces become significant in the phase separation mechanism. This has been observed to be the case for PDLC systems; Boots et al.[46] suggest that coalescence is absent for systems with relatively low liquid crystal volume fractions, demonstrating that network gelation has occurred before phase separation, changing the mechanism from liquid-liquid demixing to gel-liquid demixing. They practically demonstrate the importance of gel effects in liquid crystal solvation by demonstrating the further deswelling of the network and resultant liquid crystal rich phase domain growth when the temperature of the final film is reduced. Upon increasing the liquid crystal volume fraction they observe larger droplet sizes; this they suggest is explained by a greater dilution of the monomer leading to greater cyclisation and suppression of network gelation. This along with thermodynamic considerations increases the time between phase separation and gelation, and increases domain growth. Phase separation is believed to be occurring before gelation as coalescence of droplets is observed, hence giving a different morphology type.

Nwabunma et al.[35] briefly discuss the thread like nature of the polymer network in high liquid crystal volume fraction systems, which is a sign of a polymer phase which has collapsed in volume due to the shrinkage associated with gel-liquid deswelling. Carter et al.[34] in their work comment on the importance of elastic forces and gel deswelling in systems which are polymerized above the phase mixing temperature of the final film and as such only phase separate once cooled. They then go onto show the significance of composition in terms of gel effects; they suggest, similar to Boots et al., that at greater monomer volume fractions gelation occurs before phase separation, and this leads to elastic forces becoming significant in phase separation mechanisms.

Ohta et al.[5, 48] have produced probably the most comprehensive and effective model of PDLC phase separation to date including some consideration of gel effects and the effect of phase separation and gelation time upon morphology. While they deal with gelation solely as a point at which phase separation is suppressed they have backed up their modelling results with some experimental work where they demonstrate the effect of gelation time in relation to phase separation time on morphology. They suggest that phase separation before gelation results in the formation of a monomer rich phase which then proceeds to gelate quickly due to radical concentration therefore encouraging gel-liquid demixing leaving a relatively pure polymer phase of limited volume.

2 Aims of Work

As discussed the understanding of the phase separation mechanisms involved in PDLC morphology formation is still very confused, with particular controversy as to the importance of gelation and whether phase separation begins in the meta-stable or unstable domain. There is also still little work on attempting to link an understanding of final morphology to the mechanism of phase separation and as such the electronic and optical properties of a resultant film. It is therefore the aim of the work presented herein to produce a systematic study of phase separation under different conditions and attempt to produce comprehensive explanation as to why certain morphologies occur and under what conditions. In particular the work aims to ascertain whether the initial phase separation occurs via spinodal decomposition or nucleation and growth, and the extent to which chain swelling either encourages or suppresses phase separation. It is also the aim of the work to illuminate on the unusual temperature

dependence of the morphology and the seemingly contradictory behaviour at different compositions.

3 Phase Separation Times Overview Investigation

3.1 TL213 with 2-Ethylhexyl Acrylate (5% b/v Crosslinker)

An initial investigation is undertaken to ascertain the major trends in phase separation times and morphologies, with the aim of determining the areas of greatest interest for further study. This was achieved by analysing the SALS determined phase separation times for TL213 with 2-ethylhexyl acrylate (with 5% by volume crosslinker) at compositions from $\phi_{TL213} = 0.4$ to 0.9, at 0.05 intervals. Values less than 0.4 were not investigated as it has been shown by the work of Amundson et al.[37] that systems of these compositions are of no interest for PDLC display applications, and above 0.9 phase separation time determination becomes impossible due to nematic scattering (refer to section A). Investigations were performed at 303, 307, 311, 315, 323, and 333 K, and samples were irradiated under 2000 mWm^{-2} UV (365 nm) light. Selected samples were subsequently examined by ESEM to determine their morphologies.

3.1.1 Results and Discussion

Figure 8 shows the polymerization time at which phase separation initially commences; there are four significant trends. Firstly as cure temperature increases the time to initial phase separation increases. Secondly the phase separation times at all temperatures decrease from a peak at $\phi_{TL213} \approx 0.60$ down to 0.40. Thirdly for lower temperature cures above $\phi_{TL213} \approx 0.60$ there is also a decrease down to a minimum in phase separation time at $\phi_{TL213} \approx 0.85$ (phase separation times above $\phi_{TL213} > 0.85$ are ambiguous as it is hard to differentiate between a phase separation point due to polymerization and an isotropic-nematic phase change, refer to section A). The fourth significant observation is that at 333 K the second trend is not observed, phase separation times are still long and in fact increase with TL213 volume fraction to a peak at $\phi_{TL213} \approx 0.80$.

There are two main factors which affect the time taken for phase separation to initiate. The first is the extent of polymerization for the temperature and composition

of the system, required to enter the meta-stable or unstable (depending upon by which mechanism phase separation occurs) region. While, as discussed previously, this is classically considered under Flory-Huggins theory to be the degree of polymerization (the number of monomer repeat units per polymer chain) for a number of reasons, including the use of crosslinking species and the limited control afforded by radical polymerization, the term extent of polymerization is used instead. This is a qualitatively term to explain the effect of the increasing conversion of monomer units into bulk polymer. This concept will be discussed in greater detail later in relation to the system under investigation later. The second is the rate at which the monomer reacts to reach the phase separation extent of polymerization.

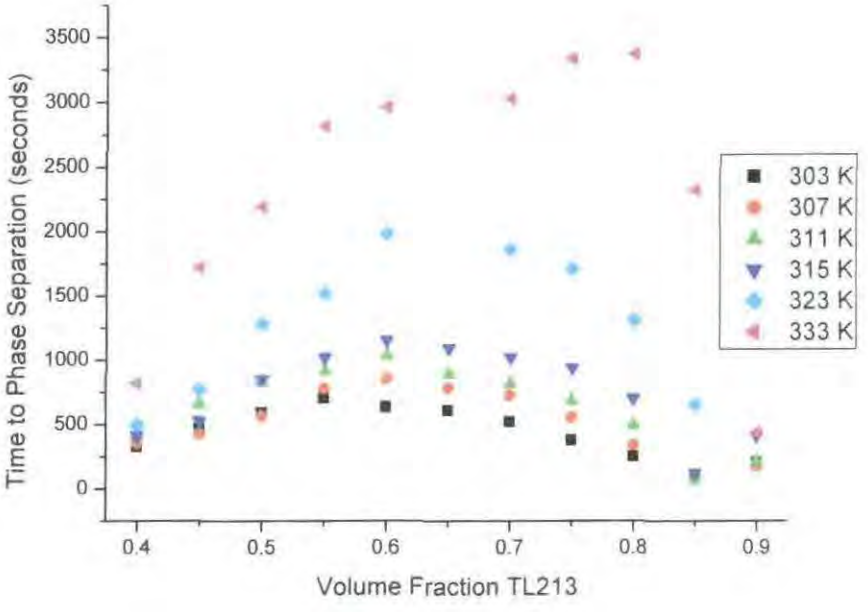

Figure 8 SALS determined phase separation times for TL213 with 2-ethylhexyl acrylate (5% b/v Crosslinker) irradiated at 2000 mWm^{-2}

The first trend, of increasing phase separation time with increasing cure temperature, can be simply ascribed to the upper critical separation temperature nature of the system, i.e., solvation of the system increases with increasing temperature (Figure 9). The higher the temperature, the greater the extent of polymerization which is required for phase separation to be initiated, so higher temperatures result in much longer phase separation times.

$$k = Ae^{\frac{-E_a}{RT}} \tag{1.17}$$

where k is the rate constant, A is the Arrhenius pre-exponential factor (constant for a given system), E_0 is the reaction activation energy, R is the gas constant, and T is the temperature.

As shown by Arrhenius equation (1.17) for the relationship between reaction rate constant and temperature, an increase in temperature will also result in an increase in reaction rate and therefore a given extent of polymerization should be reached faster at higher temperatures. The fact that there is still a significant increase in phase separation times at higher temperatures would suggest that the increase in required extent of polymerization is much more significant than any increase in reaction rate due to increased temperature.

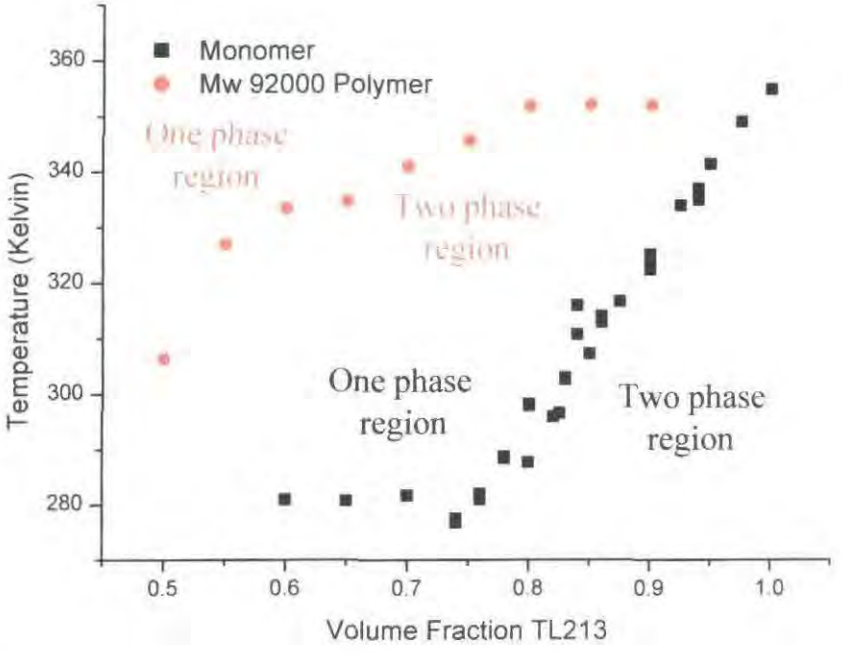

Figure 9 Temperature/Composition Phase Curves for TL213 with 2-ethylhexyl acrylate in monomer and Mw 92000 states

The second observed trend of decreasing initial phase separation time with decreasing liquid crystal composition can be explained by reaction kinetics. As can be seen from the phase curves in Figure 9, as the liquid crystal composition decreases the phase curve falls away, so that as ϕ_{TL213} decreases the extent of polymerization required to initiate phase separation should increase. This can be seen schematically in Figure 11 below, which shows phase separation temperatures for different degrees of polymerisation. It would be expected therefore that the initial phase separation time should equally increase greatly, this is not the case.

The theoretical rate of polymerization is given by[56],

$$r_{pol} = k_p \left[\frac{n\Phi k_d I_0 [I]}{2k_t} \right]^{\frac{1}{2}} [M] \qquad (1.18)$$

where k_p, k_d, and k_t are the polymerization, initiator decomposition and termination rate constants respectively, $[I]$ is the initiator concentration, $[M]$ is the monomer concentration (either free or in a polymer chain), Φ is the quantum yield (the number of radicals formed which cause polymerization, constant for a given initiator), and n is the number of radicals produced by the initiation reaction, in the case of the system presented this is 1, I_0 is the intensity of the incident light (constant for a given set of experiments). The temperature dependence of the reaction is contained within the rate constants as defined above in the Arrhenius equation (1.17). The initiator is present in the monomer at 5mol%, therefore it follows that as monomer concentration increases so does initiator concentration.

As per equation (1.18) reaction rate will increase as the monomer concentration increases (i.e. lower ϕ_{TL213}), as a result of both $[I]$ and $[M]$ increasing, although the effect of $[M]$ increasing is the far greater. This relatively large increase in reaction rate means that the high extents of polymerization required to initiate phase separation at lower ϕ_{TL213} are quickly reached and phase separation times are significantly shorter. The increase in reaction rate with temperature can also be observed by the greater decrease in high temperature phase separation time with increasing monomer concentration as compared to lower temperatures. This is shown schematically below in Figure 10 which shows the reaction rate for a polymerisation reaction relative to the temperature of cure and concentration of monomer. The curves have been generated by combining the Arrhenuis equation (1.17) and the above equation for polymerisation reaction rate (1.18), where approximate values appropriate to an acrylate polymerisation have been used for the constants.

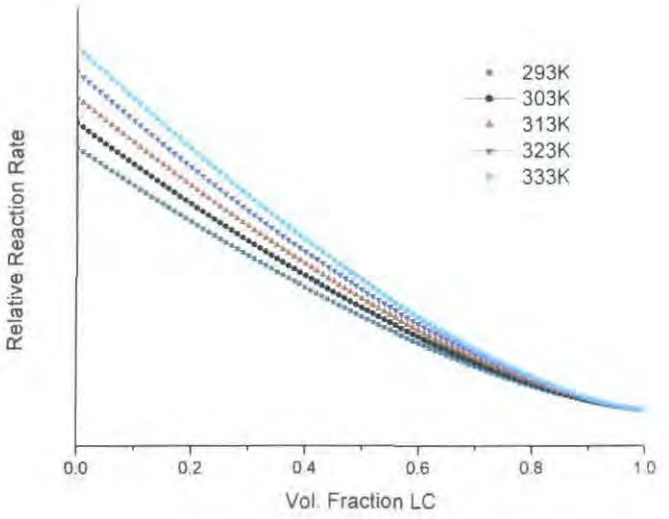

Figure 10 Schemiatic representation of the relationship between relative reaction rate, monomer concentration, and cure temperature. The curves have been generated based upon a combination of the polymerisation rate equation and the temperature dependent *Arrenhius* equation for rate constants. Approximate values of the correct proportions have been used for all values except temperature, and monomer concentration (where the values are those as shown on the graph, and initiator concentration which was set at 5% of monomer concentration.

Although not presented in this thesis, it would be possible to provide further evidence to support the above two conclusions by performing experiments to track the extent of the polymerisation reactions with time under different conditions. This is discussed in greater detail in further work section at then end of this thesis, where potential approaches to obtain the required data are discussed.

The decrease in phase separation times at higher ϕ_{TL213} is simply a result of the phase separation temperature increasing at higher liquid crystal volume fractions and as such low extents of polymerization are required to initiate phase separation. So while polymerization rate is slower the required extent of polymerization is reached much faster. It is also significant that while at temperatures of 315 K and below, phase separation is of a similar time for all runs, that for runs at 323 K and 333 K phase separation times are much greater. Figure 11 shows the Flory-Huggins spinodal curves which would be predicted for varying degrees of polymerization (in this instance actual degree of polymerization figures are applied rather than the extent of polymerization concept, so that curves can be computationally generated) based upon the experimental fit determined for TL213 with poly(2-EthylHexyl Acrylate) of molecular weight 92000 $gmol^{-1}$ in Section A.

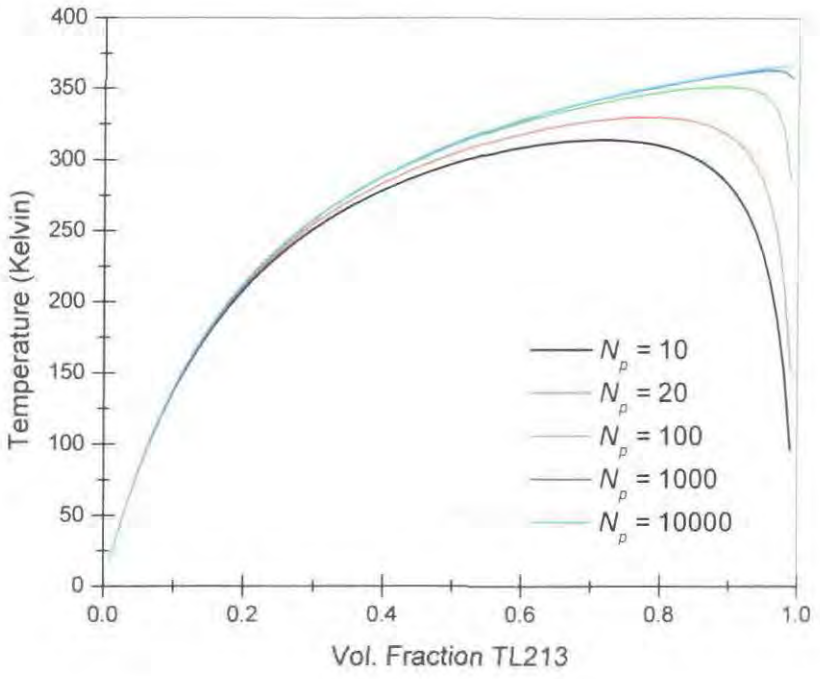

Figure 11 Predicted Flory-Huggins spinodal curves at varying degrees of polymerization based upon fit of TL213 with Mw 92000 gmol^{-1} poly(2-ethylhexyl acrylate)

While bearing in mind that the Flory-Huggins fit at low degrees of polymerization is poor for liquid crystal solutions with the phase curve artificially pushed to high ϕ_{LC} values, it can be seen that at around $\phi_{TL213} = 0.85$ at low degrees of polymerization (N_p = 10 to 100), small changes in N_p result in very large changes in the position of the phase curve. This means that for the temperature range 303 K to 315 K very little change in the degree of polymerization (in actuality extents of polymerization) is required to move the phase curve sufficiently that the two phase region is entered. Above N_p = 100, there is very little change in the position of the phase curve with large changes in the degree of polymerization, as such at higher temperatures it requires a very great increase in degree of polymerization (extent of polymerization to bring about a phase separation.

It should be born in mind that analysis using Figure 9 is based upon the assumption that phase separation is occurring via spinodal decomposition in the unstable region rather than by nucleation and growth in the meta-stable region, although similar trends will be observed for both.

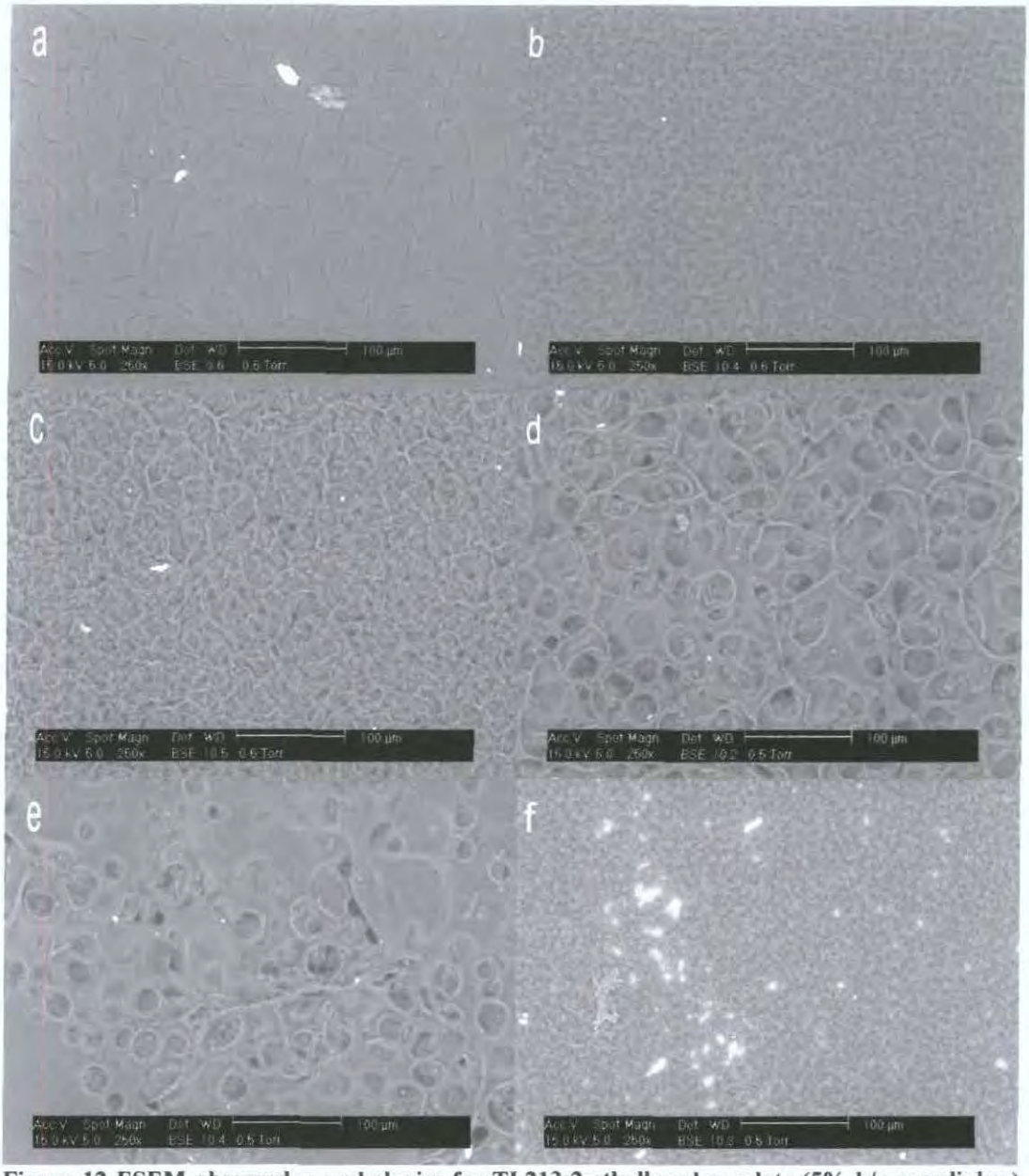

Figure 12 ESEM observed morphologies for TL213:2-ethylhexyl acrylate (5% b/v crosslinker) polymerized at 303 K under 2000 mWm^{-2} UV (365 nm); a, 55:45; b, 70:30; c, 75:25; d, 80:20; e, 85:15; f, 90:10. All images 250x magnification, measure bar s 100 μm

Figure 12 shows the ESEM observed morphologies of a series of films cured at 303 K of varying composition (TL213:2-EHA – 55:45, 70:30, 75:25, 80:20, 85:15 and 90:10). Firstly it can be seen that at low ϕ_{TL213} compositions (0.55) the film morphology is of a size beyond the capability of the ESEM to observe for these materials, as at magnification greater than 1000x the film degrades in the electron beam. All that is observed is a smooth film with a few surface indentations and defects. This would suggest a morphology size (liquid crystal droplet size) of less than 1μm, with the sample appearing as a near continuous film to the ESEM. It is the view of the author that the observed surface defects are likely to be as a result of the use of solvents in the preparation of samples for ESEM imaging. As discussed in the

experimental section the PDLC films are prepared for imaging by washing out any free liquid crystal present using methanol. As, the LC crystal droplet size is likely to be so small that the PDLC acts as a continuous film the methanol is likely to loosen the PDLC film from the glass substrate, allowing stretching and contraction. The methanol will also swell the polymer film, and once left to dry the subsequent evaporation of the methanol is going to lead to film shrinkage and the observed uneven surface.

From $\phi_{TL213} = 0.70$ to 0.85 it can be seen that morphology is of a droplet type, with droplet size increasing with increasing liquid crystal volume fraction, from about 1-2 μm to greater than 20 μm. The morphology in the region of $\phi_{TL213} = 0.70$ is quite indistinct, with the boundaries between phases being quite difficult to observe, suggesting two rather impure phases (i.e. both have a high polymer component which cannot be washed out). The boundaries between phases for higher liquid crystal volume fractions 0.80 and above are very sharp suggesting the formation of two relatively pure phases. Above $\phi_{TL213} = 0.90$ the morphology appears to be indistinct, suggesting that at such high liquid crystal compositions there is not enough polymer present to form a matrix to properly encapsulate the liquid crystal.

Figure 13 and Figure 14 show the morphologies of films formed by polymerization of 70:30 and 85:15 TL213:2-ethylhexyl acrylate solutions respectively at temperatures 303, 307, and 333K. While Figure 14 shows that for 85:15 composition films there is an obvious trend of increasing droplet size with increasing cure temperature, Figure 13 would suggest that for 70:30 composition films either the droplet size is unchanged with increasing cure temperature, or shows a slight decrease. This would suggest that there is a difference in the way in which systems phase separate depending upon composition; this will be examined in the rest of this section.

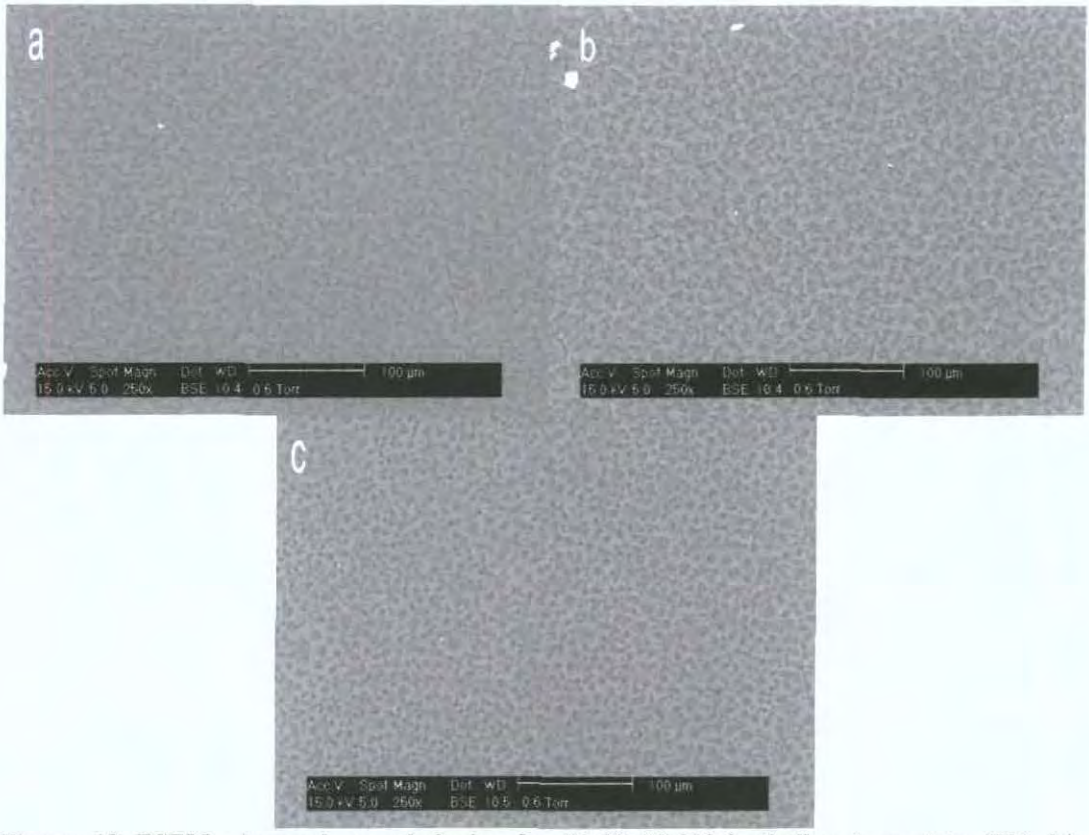

Figure 13 ESEM observed morphologies for 70:30 TL213:2-ethylhexyl acrylate (5% b/v Crosslinker), polymerized under 2000 mWm^{-2} UV (365 nm); a, 303K; b, 307 K; c, 333 K. All images 250x magnification, measure bar 100 μm

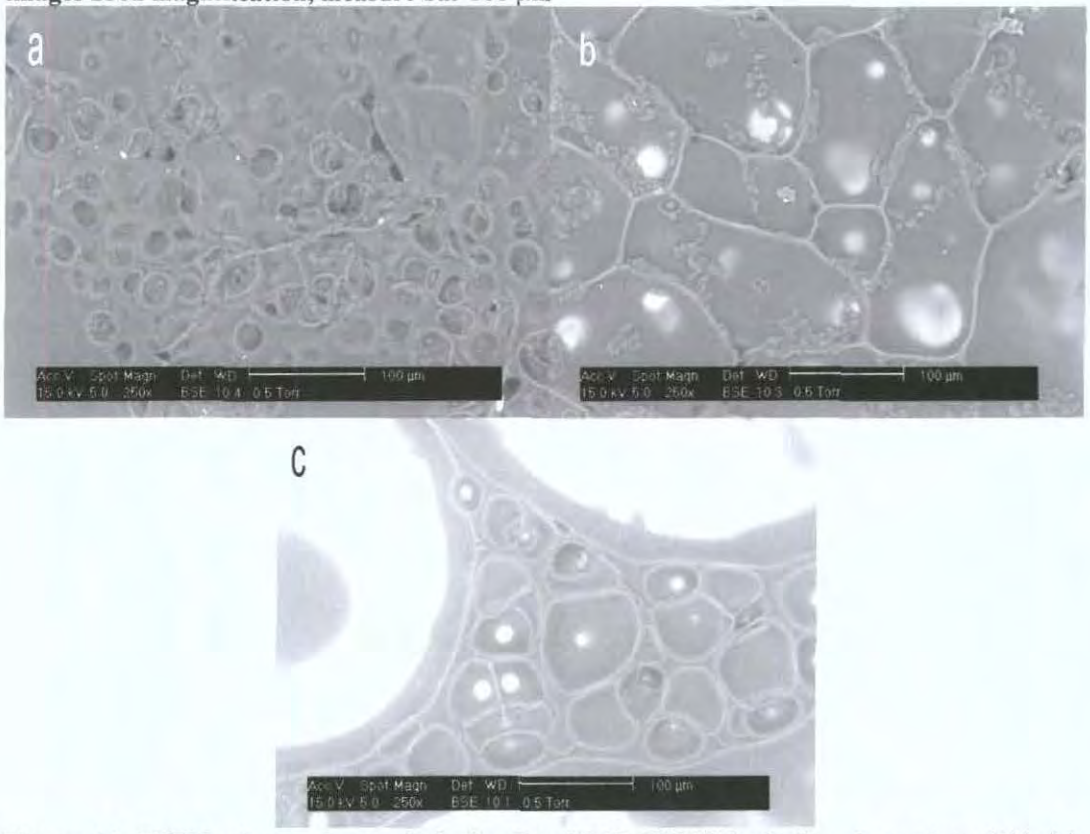

Figure 14 ESEM observed morphologies for 85:15 TL213:2-ethylhexyl acrylate (5% b/v crosslinker), polymerized under 2000 mWm^{-2} UV (365 nm); a, 303 K; b, 307 K; c, 333 K

As discussed in the introduction there is a specific range of morphology sizes of interest for PDLC based display screen devices, this being 2-10 μm, and generally a droplet morphology is required to provide the uniform fast liquid crystal switching required for the technology. The liquid crystal phase also needs to be relatively pure to make low voltage switching possible. For these reasons the compositional range $\phi_{TL213} = 0.70 \text{ to } 0.85$ appears to be the area of most interest for applying PDLCs as display screen devices, and it also shows the greatest change in morphology type and size. Therefore it constitutes the majority of the studies presented herein, with attempts to determine the factors which affect the type and size of morphology formed; the effect of each of these on the film's electro-optical properties, and to explain these in terms of the mechanism by which the systems phase separate.

4 In-Depth $\phi_{TL213} = 0.70$ to 0.85 Morphology Study

4.1 TL213 with 2-Ethylhexyl Acrylate (15% b/v Crosslinker)

As the range $\phi_{TL213} = 0.70 \text{ to } 0.85$ has already been shown to be the region of most interest for application as PDLC based display screen devices it has been decided to perform a comprehensive morphological study. Films are prepared from solutions of TL213 with 2-ethylhexyl acrylate at $\phi_{TL213} = 0.01$ intervals between $\phi_{TL213} = 0.70 \& 0.85$, cured at 2000 mWm^{-2} and 303K. The 2-ethylhexyl acrylate monomer was doped with 15% by volume crosslinker (this was an amount chosen because as it will be shown later it provides the appropriate droplet size for useful electro-optical properties). The films are subsequently observed using ESEM to determine morphology trends.

4.1.1 Results and Discussion

Based on the observations in the first set of experiments presented in this section, the expectation was that the morphology size would increase with increasing liquid crystal volume fraction. This is based upon the assumption as discussed in the background section[30, 36] that morphology size is controlled purely by the time between phase separation and gelation. Therefore, as shown in Section A, as the phase separation temperature increases with increasing liquid crystal component, phase separation should occur at a lower extent of polymerization and the time

between phase separation and gelation should be longer, giving a larger morphology size.

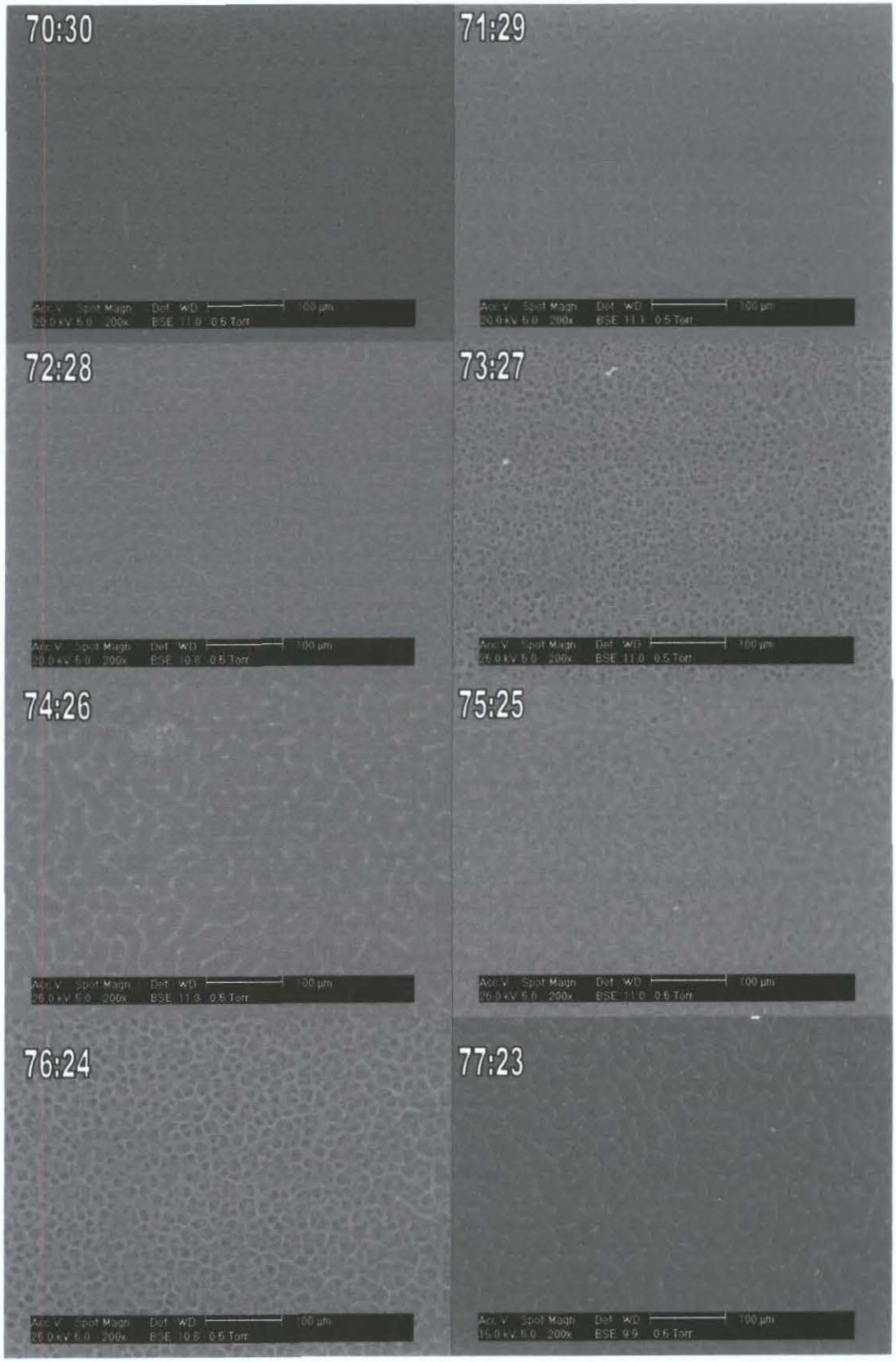

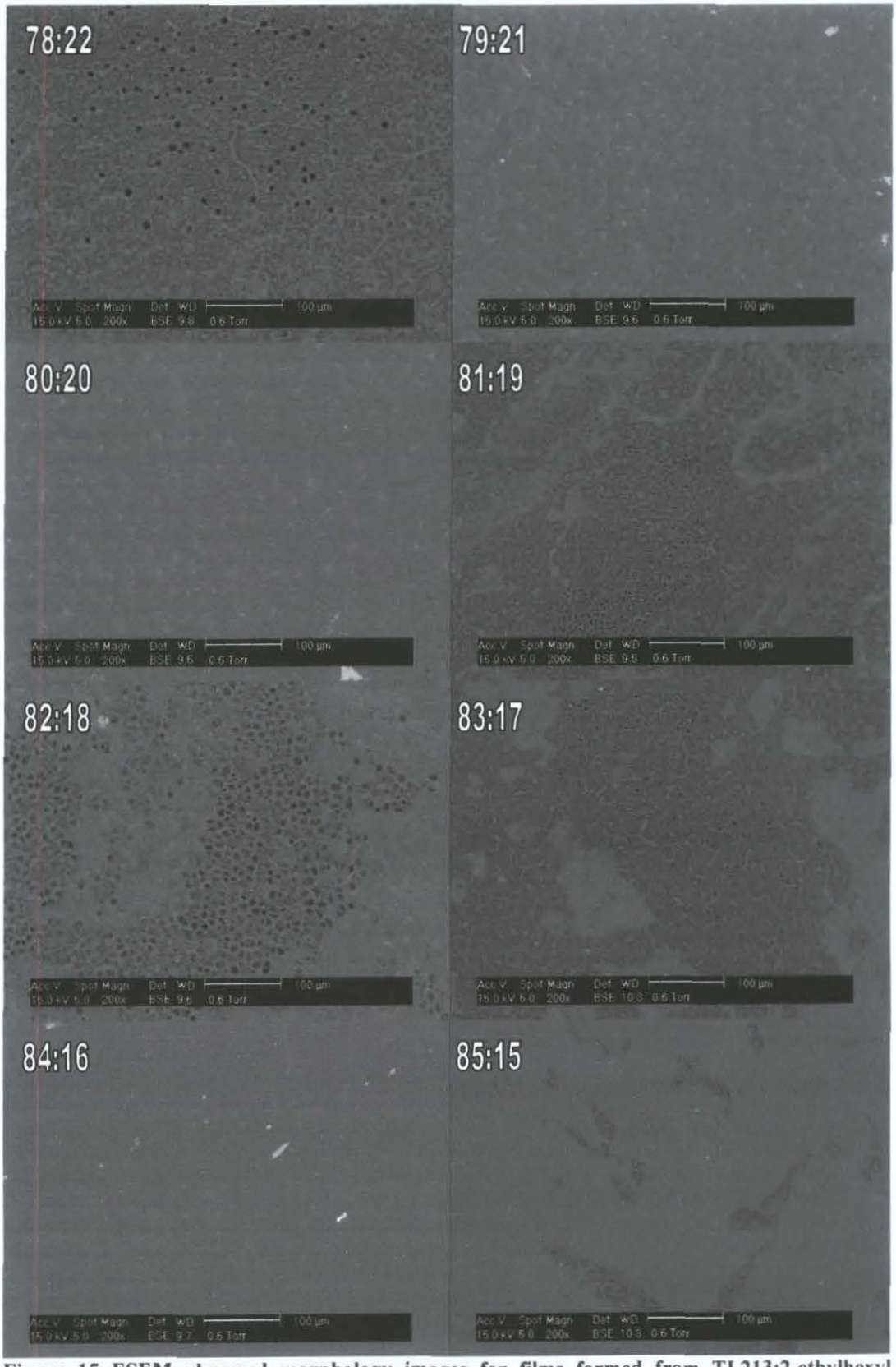

Figure 15 ESEM observed morphology images for films formed from TL213:2-ethylhexyl acrylate (15% b/v crosslinker) cured at 303 K, under 2000 mWm^{-2} intensity UV (365 nm) at compositions 70:30 to 85:15 at 1% intervals

While this general trend can be observed going from $\phi_{TL213} = 0.70$ to 0.85, it can be seen from Figure 15 that this is not a continuous trend. An initial increase in

morphology size can be observed going from $\phi_{TL213} = 0.70$ to 0.72, but the morphology size decreases again at 0.73. It is also observed that with increasing liquid crystal volume fraction the morphology also becomes more distinct, suggesting that a much purer liquid crystal phase has been formed which is more easily washed out as it does not have a high polymer content. I would conclude from this that there is a difference in the way the systems phase separate depending upon composition, suggesting possible differences in phase separation mechanism. This is explained in further detail below.

Above $\phi_{TL213} = 0.80$ the films start to develop a patchy morphology where some areas appear to have one type of structure and droplet size, whilst other may be completely different. This is likely to be due to the temperature being near either the phase mixing temperature or the nematic-isotropic temperature for that composition, so that before polymerization begins there is either nematic ordering in areas or the system is already partially phase separated. This will result in uneven phase separation with areas of different morphologies as suggested by Nwabunma et al.[35, 43]

5 Phase Separation Mechanism Determination

To properly interpret the results presented in this section into morphology and phase separation time, it is first necessary to gain an understanding of the mechanism by which phase separation is occurring. To this end an analysis is made of the type and profiles of scattering observed during phase separation by Small angle light scattering (SALS).

5.1 Small Angle Light Scattering Study

5.1.1 Results and Discussion

5.1.1.1 In the Presence of Crosslinker

Figure 16 is indicative of the type of SALS patterns observed under all conditions for the polymerization induced phase separation of TL213:2-ethylhexyl acrylate (with crosslinker) solutions. As can be observed, as phase separation commences initial scattering appears as a gradient of light going out from a peak at the centre point (Figure 17), there cannot at any point be observed a spinodal ring.

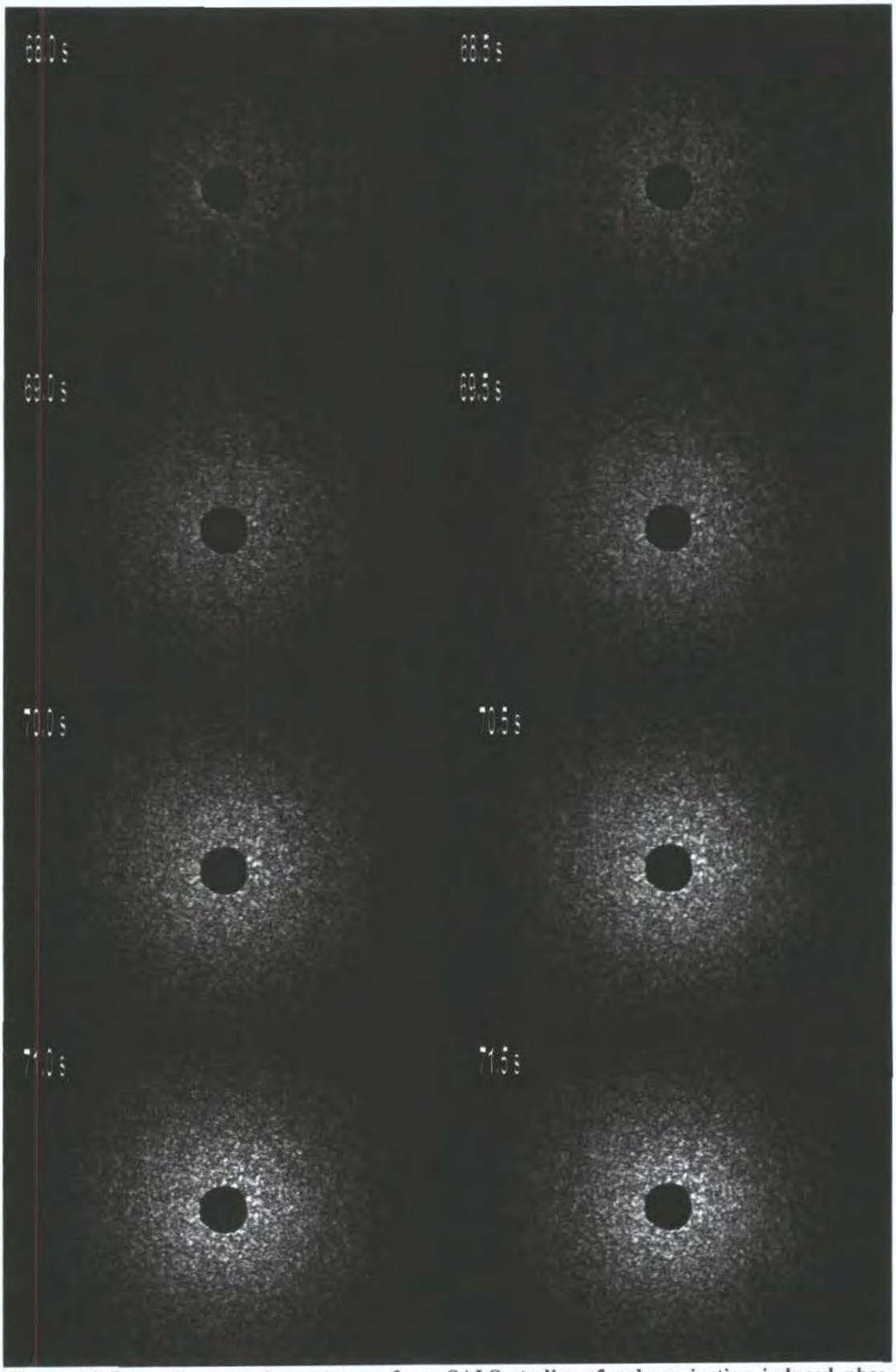

Figure 16 Example scattering patterns from SALS studies of polymerization induced phase separation of monomer/liquid crystal solutions. 70:30 TL213:2-ethylhexyl acrylate (15% by volume crosslinker) 303 K 5000 mWm^{-2} UV (365 nm)

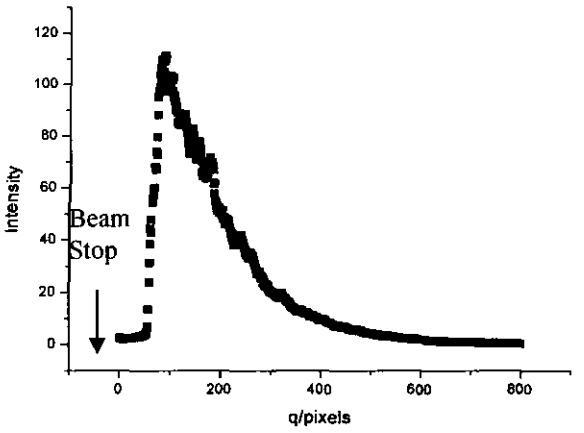

Figure 17 Scattering profile after 72 seconds of polymerization induced phase separation of 70:30 TL213:2-ethylhexyl acrylate (15% by volume crosslinker) polymerized at 303 K under 5000 mWm^{-2} UV (365 nm)

This suggests that either the initial domain size formed upon phase separation via spinodal decomposition is large enough that the ring peak occurs below the beam stop or that there is no ring present. Figure 18 is a calibration scattering profile for the set-up determined using a diffraction grating of 100 lines per millimetre, it can be seen that a peak occurs at 449 pixels from the centre point, from this it can calculated using equations (1.19) and (1.20), that alpha (a correlation function) is equal to $1.4\times10^{-3}\,\mu m^{-1}$

$$q = \alpha p \tag{1.19}$$

$$q_1 = \frac{2\pi}{d} \tag{1.20}$$

where p is the number of pixels, α a ratio constant, q_1 is the q value of the first peak, and d is the line spacing of the grating.

This would require an initially formed spinodal domain to be of size greater than 97.6 μm to form under the beam stop which occurs below 46 pixels. While domains of such size are not impossible, it would seem highly unlikely given that the formation of larger domains is suppressed by the distance over which the component species would have to diffuse. It has also been shown in previous results presented, that the final morphologies are not this large either. It should be brought into consideration that while the liquid crystal species maintains relatively low viscosity throughout allowing quick diffusion, the polymer species will be reaching very high viscosities under certain conditions before phase separation occurs suppressing the formation of large domains. Therefore it can be reasonably considered the case that spinodal rings are not observed.

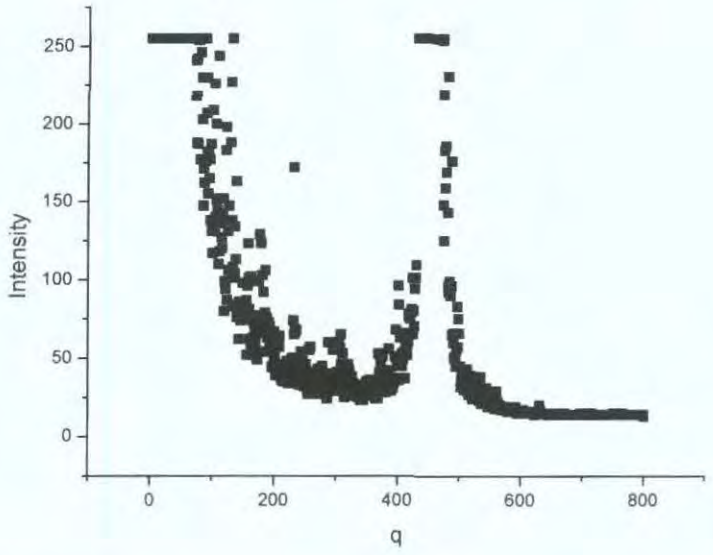

Figure 18 Calibration scattering profile of 10 μm diffraction grating

While the lack of a spinodal ring is not evidence in itself that the more commonly observed spinodal decomposition mechanism is not occurring, it does act as evidence to suggest this is the case. The regularly sized domains associated with the spinodal decomposition mechanism are also not formed. This would suggest that nucleation and growth should be seriously considered as the phase separation mechanism even with its kinetic restrictions.

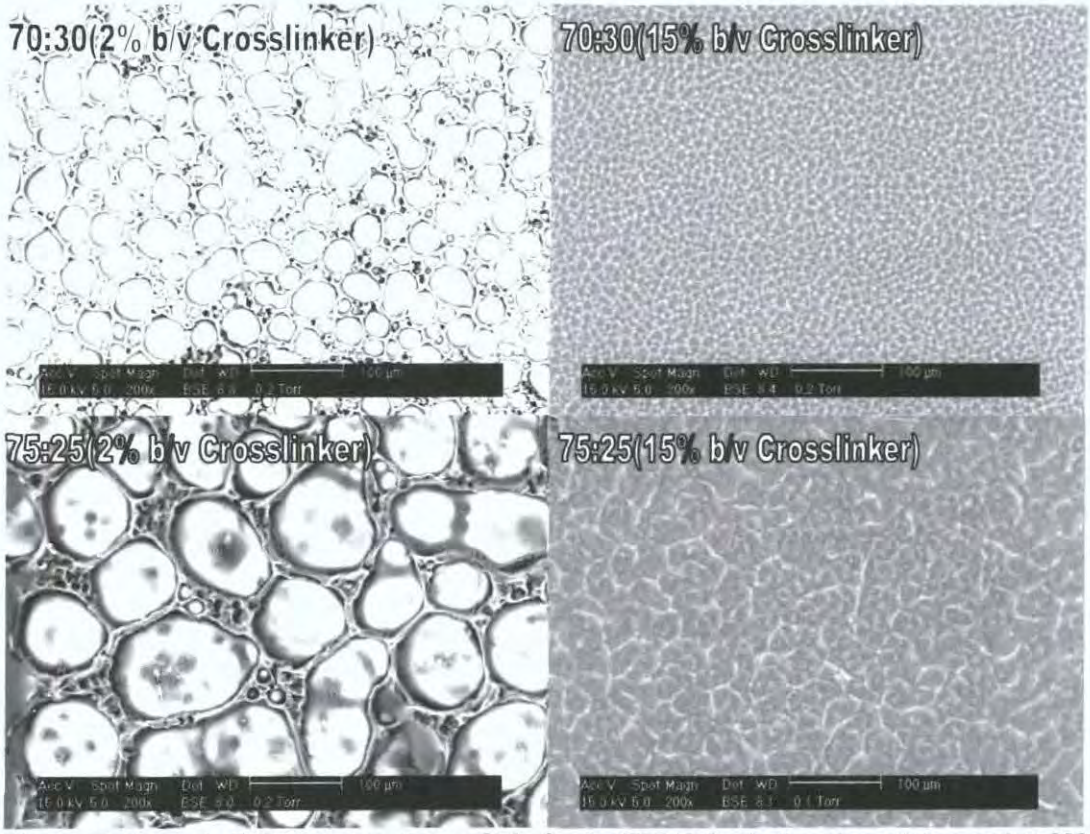

Figure 19 Example ESEM observed morphologies for TL213:2-ethylhexyl acrylate cured at 303 K under 2000 mWm^{-2} UV (365 nm)

Figure 19 shows example film morphologies, and it can be seen that the morphologies formed do indeed have a variety of droplet sizes present within the same section of film. Whilst some of this variety in droplet sizes can be ascribed to the formation of primary and secondary phase separation morphologies, in many films there are significantly larger and smaller droplets present, within each of the primary and secondary morphologies there is a great variety of droplet sizes. This is still possible in a system which has undergone spinodal decomposition as after the initial domain formation droplets coarsen and enlarge to form the lowest energy configuration, including undergoing droplet coalescence. Whilst there is no definitive evidence to suggest that spinodal decomposition is not occurring, or that nucleation and growth is, the fact that there is no positive evidence in favour of spinodal decomposition leads the author to believe that, due to two properties distinctive to the system under study described below, phase separation is occurring via a nucleation and growth mechanism.

The first is the presence of the liquid crystalline solvent, which is capable of making an energetic gain by the molecules nematically aligning in the droplets. This results from the entropic gain to be had from the reduction in excluded volume effects due to alignment, which under the right conditions (temperature and concentration) overcomes the loss due to translational entropy from the more ordered alignment of molecules. This in theory should overcome much of the kinetic barrier to the formation of droplets, as it should, under the right conditions, be kinetically favourable to form liquid crystalline nuclei.

The second is the presence in the monomer species of a crosslinking agent, which means instead of forming many freely dispersed long chain polymers, the system actually forms a large polymer network. This combined with the, in relation to the polymer network, low viscosity of the liquid crystalline species, means that the system is acting like a polymer gel rather than a polymer solution. It has been discussed by Tanaka[57] that the formation of a polymer network leads to the suppression of phase separation by spinodal decomposition as it is possible for the localised concentration fluctuations caused by thermal perturbations which initiate spinodal decomposition, to be absorbed by the swelling properties of the network. It should be possible for the network to stretch to make the solvation of more of the solvent species possible and suppress these localised compositional changes and as

such create a kinetic barrier to phase separation via spinodal decomposition as well as nucleation and growth.

It is therefore the belief of the author that the initial mechanism of phase separation is via nucleation and growth with droplets of liquid crystal solvent able to form within the not universally formed polymer network. Growth over time then occurs due to energetically favourable diffusion. The apparent difference in mechanism depending upon composition and temperature of cure is likely to be a result of the differing extent of network present at the point phase separation occurs; either acting to promote phase separation by de-swelling or suppressing it due to phase separation requiring the formation of solvent droplets within the stretched polymer network. As discussed in sub-section 1.4, such a view is supported by the work of other researchers, in particular Amundson and co-workers with their studies of morphologies formed by E7 with PN393[31] and TL205 with PN393[36] where they observed by the use of confocal microscopy the initial formation of droplets. They suggest that it is possible to observe the formation of initial droplets which grow in size only slowly, and that subsequent nucleation of droplets is observed before great increases in size of the initial droplets. This formation of subsequent nucleus droplets is strong evidence for nucleation and growth as opposed to spinodal decomposition as it would be expected that the latter would occur universally throughout the sample at the same point, without further phase separation occurring so soon after. Secondary phase separation has been observed during spinodal decomposition[58], it therefore is still possible that these smaller droplets are the result of secondary phase separation via spinodal decomposition, but this would seem unlikely.

It is for this reason that, for the system under investigation, it is not appropriate to discuss the point at which phase separation becomes thermodynamically favourable in terms of degree of polymerisation, but instead in terms of extent of polymerisation (or extent of network formation). The presence of a crosslinking species means that the polymer is not present in the form of free polymer chains but instead as an extended network. It is the formation of this network and it's extent of formation which controls not only the point at which phase separation becomes thermodynamically and kinetically favourable, but also whether phase separation is suppressed or promoted.

5.1.1.2 In the Absence of Crosslinker

Given that the nucleation and growth mechanism observed in the presence of a crosslinking species is ascribed to the gel like nature of the system, it would be

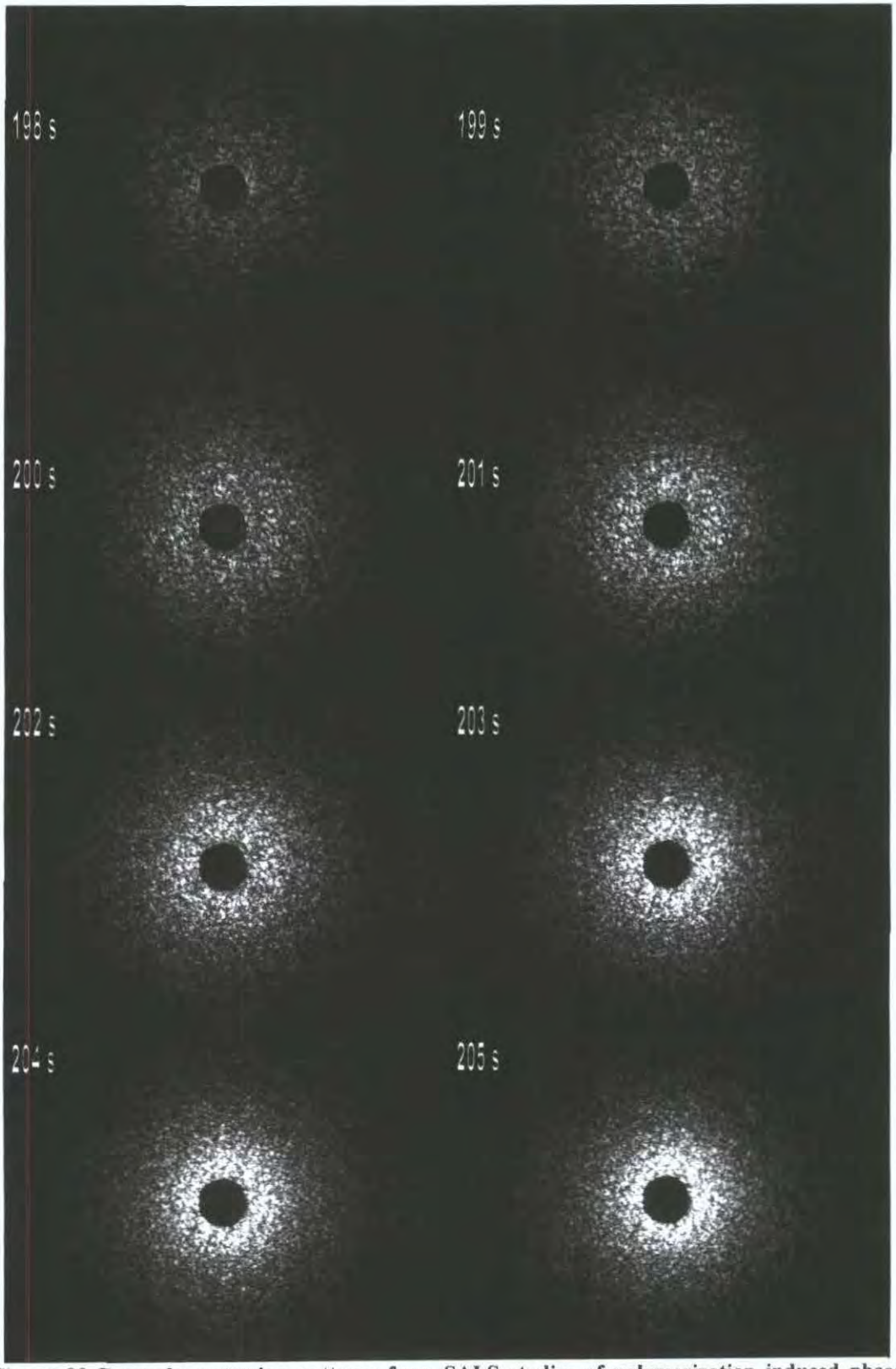

Figure 20 Example scattering patterns from SALS studies of polymerization induced phase separation of monomer/liquid crystal solutions. 70:30 TL213:2-ethylhexyl acrylate (0% crosslinker) 303 K 5000 mWm^{-2} UV (365 nm)

reasonable to presume that for a system in which there are no monomers of functionality greater than two present that phase separation would be via a classic spinodal decomposition mechanism. Again however when the scattering patterns are observed from the polymerization induced phase separation process (Figure 20) there is a lack of any spinodal rings observed. This can be further observed in the scattering profiles (Figure 21) where it can be seen during initial phase separation there is an increase in scattering intensity, but no obvious peak, and equally no movement of peak with domain growth.

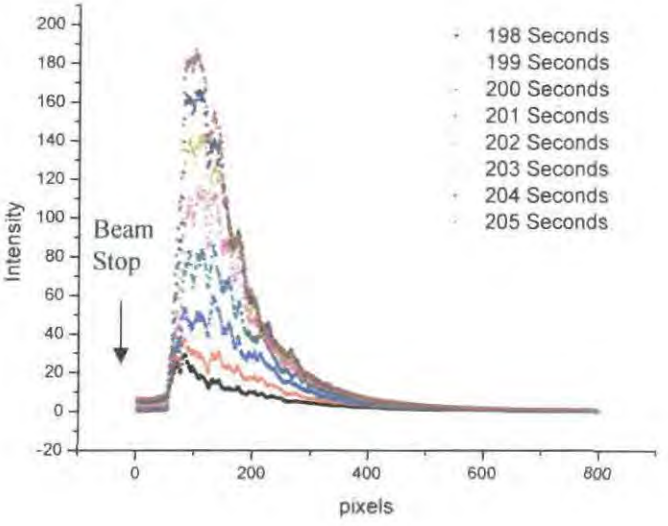

Figure 21 Scattering profiles during polymerization induced phase separation of 70:30 TL213:2-ethylhexyl acrylate (0% by volume crosslinker) polymerized at 303 K under 5000 mWm^{-2} UV (365 nm)

As discussed above, the morphologies formed from the phase separation of monomer/liquid crystal solutions by PIPS in the absence of a crosslinking species, are short lived, as would be expected due to the low viscosity of the solvent. Diffusion is fast and the formation of the two unique phases in separated bulk is observed. When observed before forming this final fully phase separated form (within a few hours of polymerization), the morphology observed is that of polymer droplets within a sea of liquid crystal. If as the scattering evidence suggests spinodal decomposition is still not occurring, it would seem odd for such a morphology to be formed by a classic nucleation and growth mechanism where droplets of liquid crystal are formed within a matrix of polymer. Therefore some other form of explanation is required, and one has been provided by the work of Tanaka[57, 59-62] into what is known as Viscoelastic phase separation, or phase separation by the formation of a transient gel state.

5.1.2 Viscoelastic Phase Separation

The viscoelastic phase separation mechanism is the result of viscosity asymmetry between two species undergoing phase separation. Long polymer chains are capable of forming transient crosslinks due to the entanglement of two or more chains, when this occurs it is possible for the polymer chains to form a temporary network-like structure. If the characteristic relaxation time of these entanglements is longer than the phase separation times then it becomes the case that phase separation can no longer be described by simple diffusion driven phase demixing dynamics, the system instead starts acting like a polymer gel. As is the case with a polymer gel it is possible for the chains to stretch and swell to overcome the compositional fluctuations suppressing spinodal decomposition, it is again expected that phase separation is occurring by the formation of a solvent droplet within the polymer matrix. Unlike in the case of gel-liquid demixing where there is a permanent network structure present, eventually the chains will become disentangled and the network structure will breakdown. So whereas, in the presence of a crosslinking species gelation occurs and the polymer matrix freezes, the polymer chains are still capable of rearrangement.

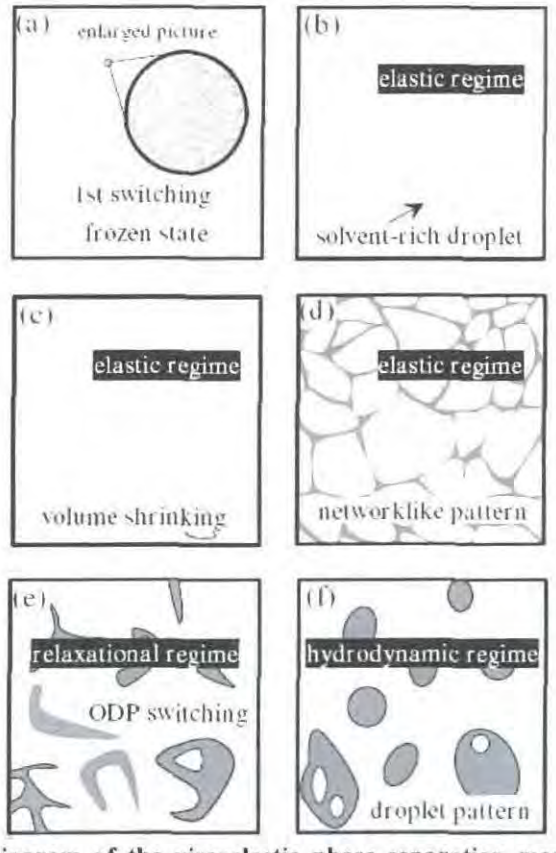

Figure 22 Schematic diagram of the viscoelastic phase separation mechanism, sourced from review by Tanaka[57]

Given that the solvent species is of a much lower viscosity than the polymer species, the polymer-rich phase is able to undergo great rearrangement in its macro scale structure unhindered by the solvent-rich phase. The polymer chains which when entangled were in an energetically unfavourable configuration then relax and contract causing the breakdown of the network structure. This results in an inversion in the system morphology as the matrix phase breaks up and forms spherical droplets which are able to form easily within the low viscosity solvent-rich phase, and what Tanaka[57] describes as a hydrodynamic regime is formed where the polymer-rich droplets are free to move within the solvent-rich phase. This process is illustrated in Figure 22. Such behaviour has been observed by Tanaka in systems which undergo phase separation initiated by temperature quench[59, 61] (Figure 23) and has also been observed in systems which undergo phase separation initiated by polymerization[63-66].

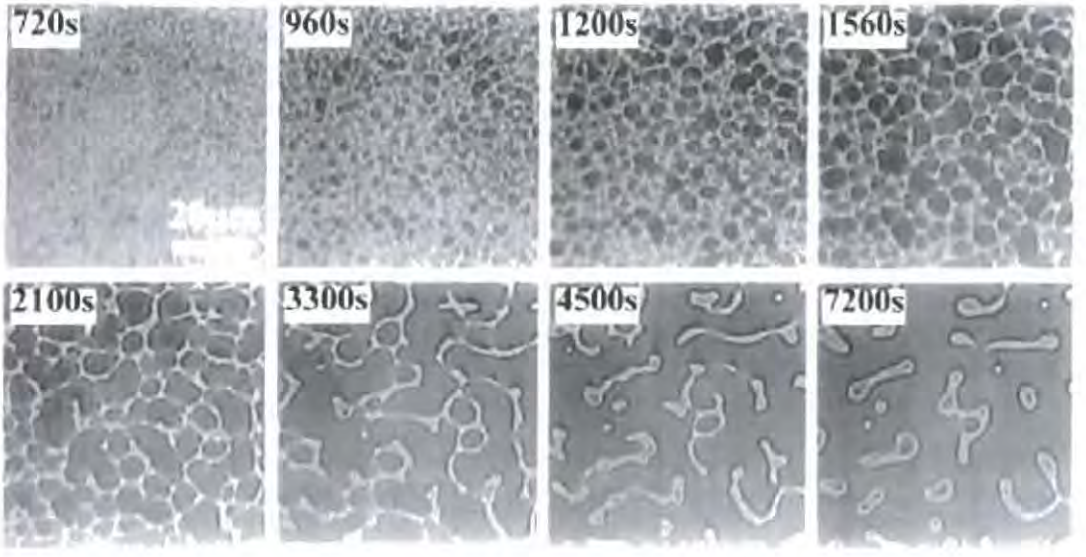

Figure 23 Viscoelastic phase separation mechanism as observed by Tanaka using video phase-contrast microscopy of a polystyrene/poly(vinylmethylether) mixture undergoing a temperature quench[61]

5.2 Rheological and Optical Microscopy Studies

To test the above theories on the phase separation mechanism, and in particular the presence of viscoelastic effects when there is either no or limited crosslinker present, a series of rheology and optical microscopy experiments to observe the formation of physical properties during the phase separation process are performed. The aim is to observe, in systems without a crosslinker species present, the phase inversion discussed above which would be indicative of phase separation occurring via a viscoelastic mechanism. As discussed in the experimental section the G' value is the storage modulus and is related to the elastic properties of the system and G'' is the

loss modulus, which is related to the viscous properties of the system. As such it is the latter of these which is of interest for the study of viscoelastic phase separation, it is expected that it should be possible to observe a phase inversion as a change in viscous properties of the sample during phase separation[66]. Samples of varying composition 70:30 to 80:20 TL213:2-ethylhexyl acrylate (with either 0 or 15% crosslinker) are polymerized within the rheometer, while undergoing oscillation to determine G'' at 303K, under 700 mWm^{-2} (due to the structural constraints of the set-up, this is the highest intensity possible). The time dependence of G'' is then observed.

5.2.1 Rheology Results and Discussion

Figure 24 shows the loss modulus time dependence during the phase separation of TL213 with 2-ethylhexyl acrylate when the monomer is doped with 15% by volume of a crosslinking species.

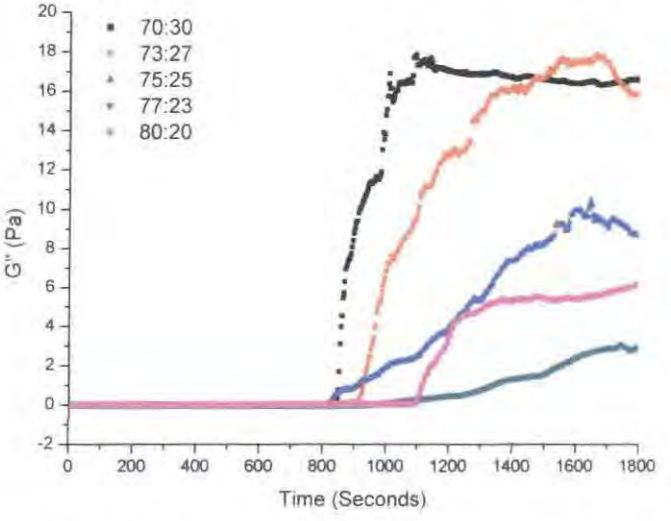

Figure 24 Time dependent G'' values for varying compositions of TL213:2-ethylhexyl acrylate (15% b/v crosslinker) during polymerization induced phase separation, under 700 mWm^{-2} UV (365 nm)

As can be seen the loss modulus stays at approximately zero until at a given point a sharp increase in loss modulus is observed. This massive increase in storage modulus is due to the formation of an approximately infinite polymer network within the system due to the presence of the crosslinking species. The greater the extent of polymerization, the greater the extent of the network, and as such the greater the contribution to the storage modulus up to the point at which the system can be considered to have gelated and form a relatively solid system. At the point of gelation the oscillatory motion of the rheometer has the effect of actually breaking

the sample on a macroscopic scale and therefore any values after this point should be disregarded, these being the points at which noisy plateaus in the profiles can be observed.

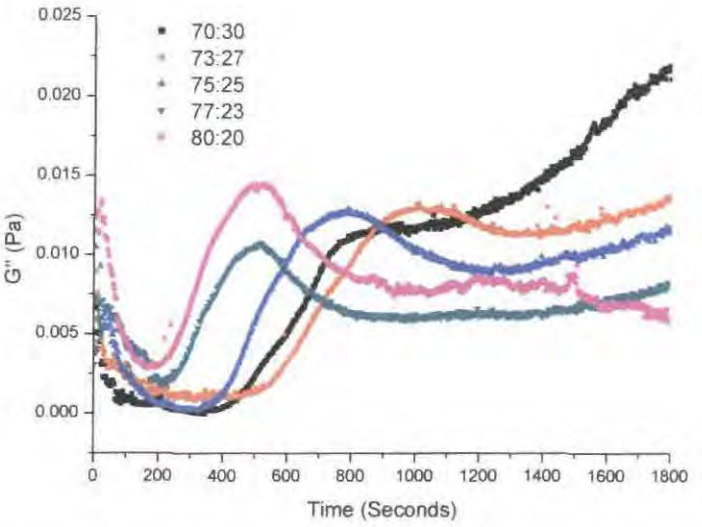

Figure 25 Time dependent G'' values for varying compositions of TL213:2-ethylhexyl acrylate (0% *crosslinker*) during polymerization induced phase separation, under 700 mWm^{-2}

Figure 25 shows a very different set of behaviours, for samples where there is no crosslinking species present to cause the dramatic increase in viscosity as the network is formed and as such has loss modulus values of much lower magnitude. What is being observed can be considered to be the behaviour in viscosity due to morphological factors.

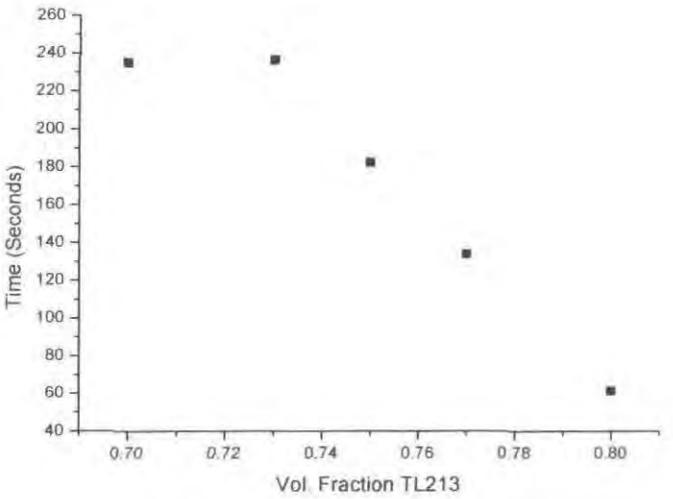

Figure 26 SALS determined phase separation times for TL213:2-ethylhexyl acrylate (0% crosslinker) undergoing polymerization induced phase separation at 303 K and under 2000 mWm^{-2} UV (365 nm)

Support for this view comes from the fact that all the profiles after an initial decrease in value, show a subsequent significant increase at a given point; Figure 26 shows the

phase separation times for solutions without crosslinker polymerized at 303 K (these results are presented in greater detail later in this report) and the points at which the loss modulus increase occur correlate to the phase separation times relative to composition. (A direct comparison is not possible as cure intensity is different due to experimental set-up limitations) An increase is observed at the earliest time for a solution of composition 80:20, slightly later for 77:23 and so forth down to 73:27, comparing this to Figure 8, this is what would be expected if they were due to phase separation times. If this dependency were due to an increase in viscosity merely due to the increasing length of polymer chains, it would be expected that an increase would be seen first in the system which has the highest polymer content, and as such the greatest polymer contribution to viscosity and the fastest reaction rate and therefore viscosity increase. The fact that the dependency is observed earlier for the 70:30 system than the 73:27 system is likely to be due to the increased reaction rate at the lower liquid crystal volume fraction resulting in an earlier phase separation time, and/or an increase in the contribution to the loss modulus due to the formation of a transient network by temporary interlinks between chains.

Significantly after the initial increase in loss modulus there can be seen, in all but the 70:30 case, a subsequent decrease. It is the belief of the author that this is representative of a phase inversion indicative of viscoelastic phase separation and that the initial build up of loss modulus is due to the formation of the phase separated transient network. Subsequently inversion of the morphology occurs to form a hydrodynamic phase in which the movement of polymer droplets in a sea of liquid crystal results in a much lower loss modulus. It should be noted that the 70:30 system does not show this same inversion and it is possible that in this case the amount of polymer present means that the formation of interlinks is much greater than is the case for higher liquid crystal composition systems, as such the lifetime of the transient network is much longer as more interlinks need to be broken down for inversion to occur. Therefore it is likely that inversion is occurring much later and as such is not observed in this study.

It is also worthy of note that in all cases there is an initial decrease in loss modulus at the start of all the experiments, while a definitive explanation for this is lacking the author suggests the following possible explanation. The separation between Peltier plate and rheometer geometry is very small at 10 μm, as such it is of a small enough size that alignment effects in the liquid crystal are likely to make a contribution to the

loss modulus. It is therefore hypothesised that the decrease is due to alignment effects in the liquid crystal molecules upon the initial application of the oscillatory motion. While this is worthy of note it is not going to be the case in normal phase separation experiments where no shear is applied to the samples under cure, and as the expected behaviour due to the phase separation's viscoelastic nature appears to be present, it is felt that this reduction can be reasonably disregarded.

5.2.2 Optical Microscopy Resuilts and Discussion

Figure 27 shows the progression of phase separation for a film formed from an initial solution of 80:20 TL213:2-ethylhexyl acrylate (15% by volume crosslinker) cured at 303 K, by optical microscopy. It can be seen, as had been predicted, that initial phase separation is by the formation of small nucleus droplets, the number of which grow over time (which would not be the case for spinodal decomposition).

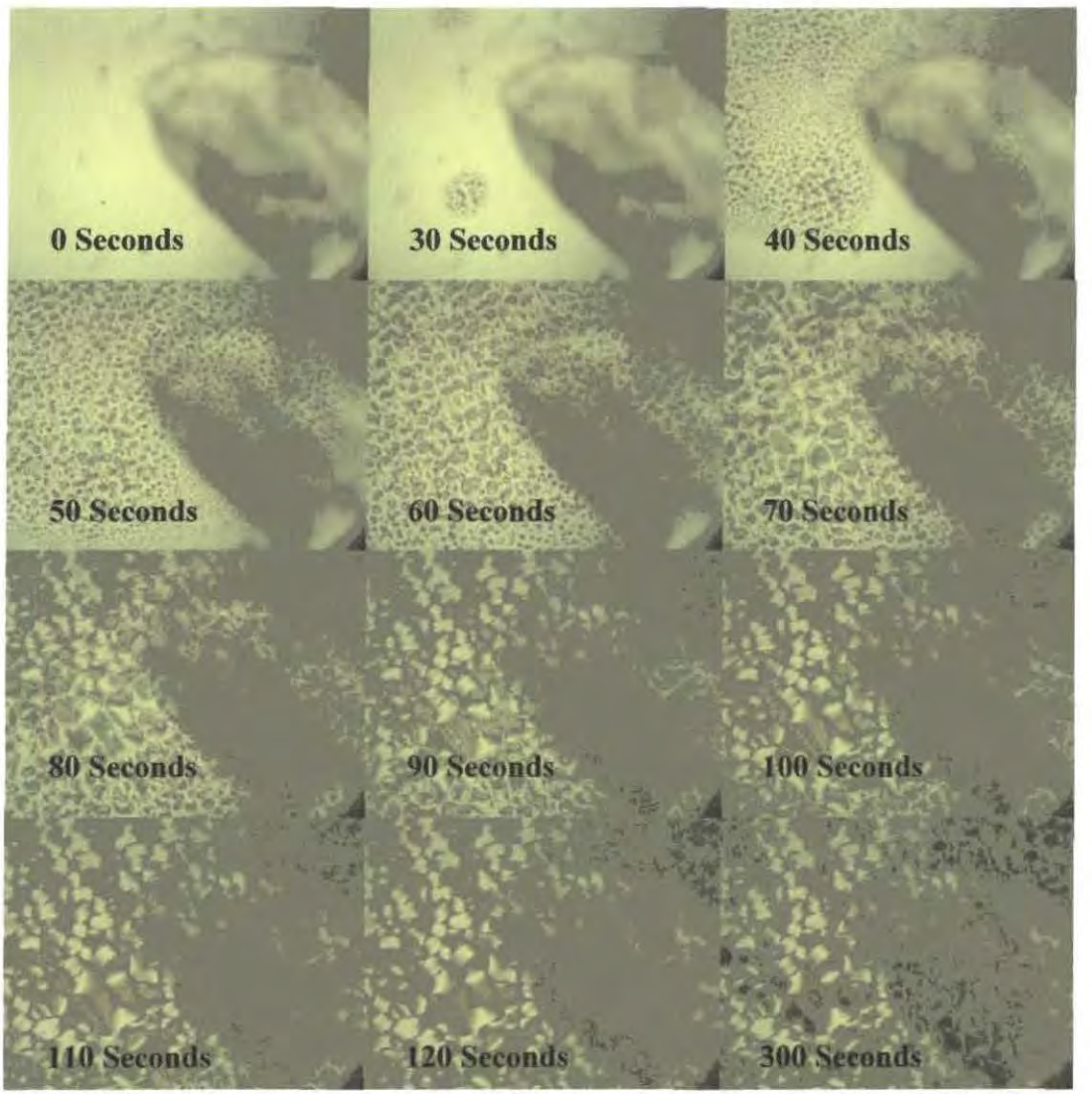

Figure 27 Morphology images observed with time by optimcal microscopy (4x magnificantion) of 80:20 TL213:EHA (15% by volume crosslinker) polymerized at 303K under 2000 mWm^{-2} UV intensity

These droplets then proceed to grow in size as a result of deswelling of the polymer phase at first and then subsequently by coalescence of liquid crystal droplets to form larger droplets as the polymer phase shrinks back to deswell further. Therefore all the mechanistic properties which would be expected to be observed for a system phase separating by a polymer gel deswelling mechanism as discussed above can be seen and this provides strong evidence that this is the mechanism by which phase separation is occurring.

5.3 Conclusions

The evidence presented above would seem to support the suggestion that phase separation initiated by the photo-polymerization of acrylate monomer/liquid crystal solutions is occurring by one of two mechanisms depending upon the amount of crosslinking monomers present in solution. In the absence of a crosslinking species it has been observed that phase separation occurs via a transient gel viscoelastic phase separation mechanism and in the presence of high crosslinker concentration via a polymer gel-liquid demixing mechanism. It would not be unreasonable to presume from this that there is a gradiented effect as the amount of crosslinker present increases with a combination of the two processes effecting the final morphology. In effect, in both cases the initial phase separation mechanism is the same as either crosslinks or transient crosslinks formed by chain entanglements suppress the initiation of phase separation via spinodal decomposition. The number of permanent crosslinks present determines how far the phase separation mechanism can proceed as in all cases the stretched polymer chains will look to contract to lower their energetic state. The greater the degree of crosslinking the sooner gelation will occur and the greater the degree of network development to suppress rearrangement.

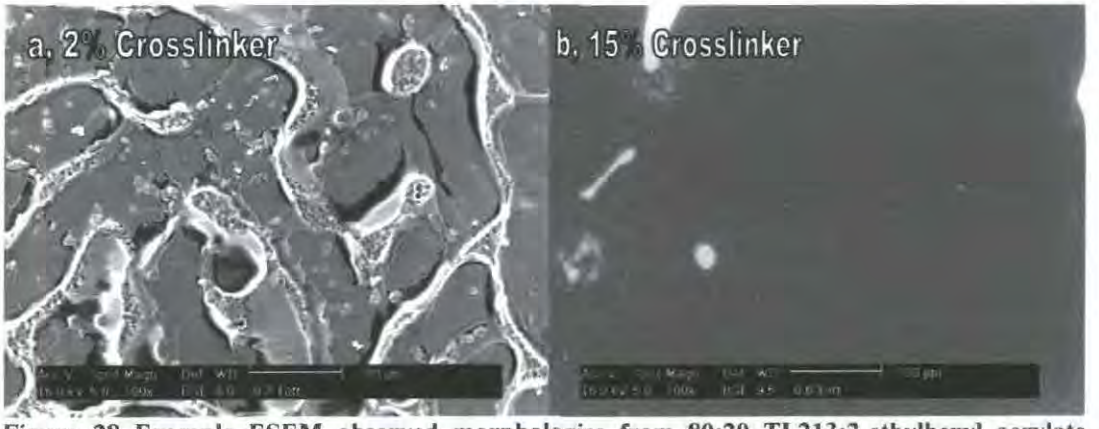

Figure 28 Example ESEM observed morphologies from 80:20 TL213:2-ethylhexyl acrylate solutions cured at 303 K under 2000 mWm^{-2} UV (365 nm), with the monomer doped with a, 2 % and b, 15 % by volume crosslinker

Figure 28 shows the ESEM observed morphology of films of composition 80:20 TL213-ethylhexyl acrylate cured at 303 K under 2000 mWm^{-2} intensity UV (365 nm) with the monomer doped with 2 and 15 % by volume respectively, with crosslinker. As can be seen the 15 % crosslinker film demonstrates a droplet type morphology, but the 2 % crosslinker film can clearly be seen to be frozen midway through the morphological inversion process with the initial solvent-rich droplets coalescing and polymer-rich droplets forming.

The above theory is further put to the test below as an attempt is made to interpret the phase separation times and morphologies of films formed at varying compositions, cure temperature, UV intensity and crosslink density in terms of mechanism.

6 Mechanism and Morphology

6.1 TL213 with 2-EthylHexyl Acrylate, Variable Crosslink Density SALS and ESEM Study

Based upon the observations that different morphology types are formed at different pre-polymer solution compositions an attempt is made via the use of small angle light scattering and ESEM to ascertain the mechanism via which phase separation proceeds. As discussed in the background chapter of this section, crosslinking has a significant effect upon the type and size of morphology formed, it affects how soon gelation occurs and as such the size of domains, but as discussed in sub-section 5 could also be acting against or in favour of demixing depending upon the extent of the network formed. For this reason a series of experiments with the pre-polymer containing varying amounts of hexa-functional monomers as crosslinking agent are performed to determine its effect on morphology and likely phase separation mechanism.

The study consists of SALS determined phase separation times, an analysis of the time dependent scattering profiles from the SALS studies and analysis of morphology structure and size through the use of ESEM. An initial study is performed with films formed by curing solutions of TL213 with 2-ethylhexyl acrylate under 2000 mWm^{-2} UV intensity (365 nm), with the monomer containing by volume 0, 2, or 15 % trimethylol propane triacrylate crosslinker. These were used at compositions of TL213:monomer of 70:30, 73:27, 75:25, 77:23, 80:20 to cover the range of most interest for display device morphologies, and cured at temperatures of

303, 313, 323, and 333 K. The study was subsequently further extended to determine the effect of cure rate on morphology, by repeating the series of experiments, but with a UV cure intensity of 5000 mWm^{-2} instead.

6.1.1 Results and Discussion

A complete set of morphology images covering the entire scope of the work presented in this section can be found in **Appendix A**, selected images are used and presented in the discussion below.

6.1.1.1 Cure Intensity

Figure 29 shows the SALS observed phase separation times for cells prepared with 2% by volume crosslinker under a UV cure intensity of 2000 mWm^{-2} while Figure 30 shows the same, but cured under UV of intensity of 5000 mWm^{-2}.

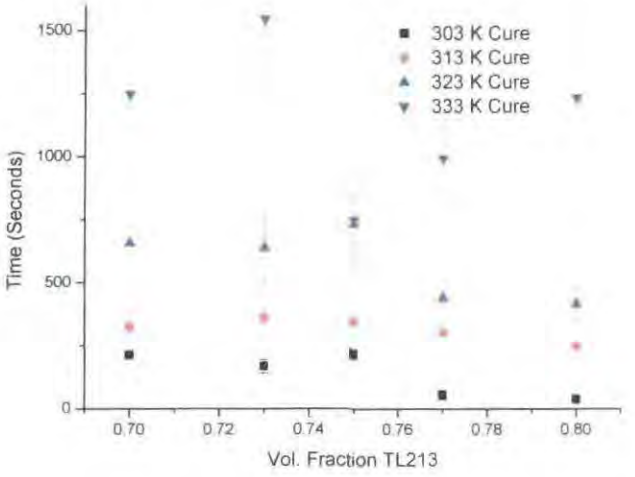

Figure 29 SALS determined phase separation times for TL213 with 2-ethylhexyl acrylate (2% b/v crosslinker) cured under 2000 mWm^{-2} UV

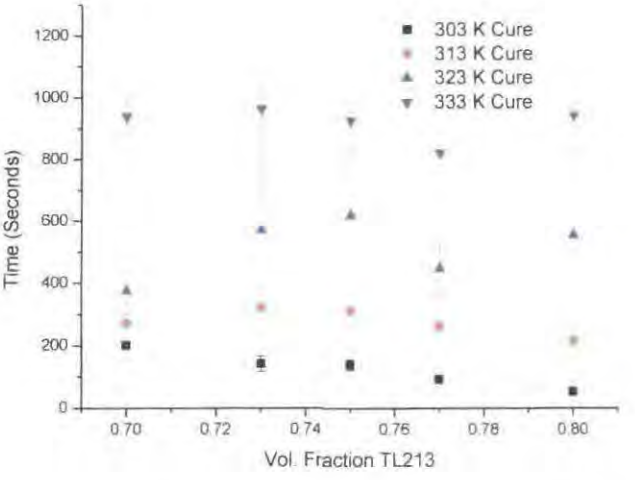

Figure 30 SALS determined phase separation times for TL213 with 2-ethylhexyl acrylate (2% b/v crosslinker) cured under 5000 mWm^{-2} UV

Figure 31 and Figure 32 show the same for films containing polymer doped with 15% by volume crosslinker cured at 2000 mWm^{-2} and 5000 mWm^{-2}. In both cases it can be seen that increasing the cure intensity has the effect of decreasing the time to initial phase separation. This effect is more pronounced at higher temperatures where the time to initial phase separation is much greater in all cases as a result of, as discussed earlier, higher temperatures being further from the unpolymerized coexistence curve and therefore requiring a greater extent of polymerization for phase separation to become favourable.

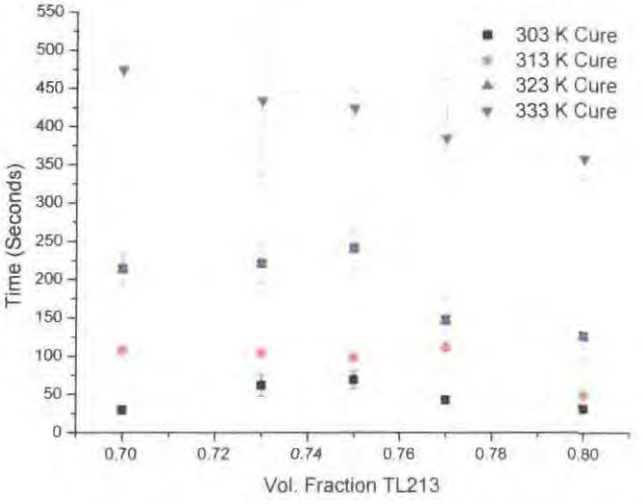

Figure 31 SALS determined phase separation times for TL213 with 2-ethylhexyl acrylate (15% b/v crosslinker) cured under 2000 mWm^{-2} UV

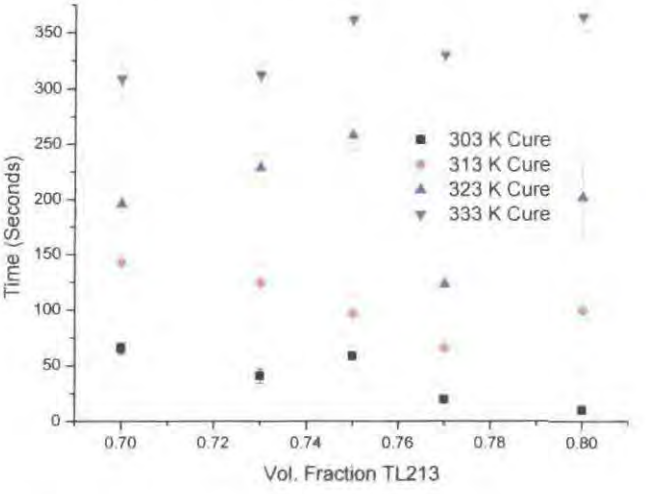

Figure 32 SALS determined phase separation times for TL213 with 2-ethylhexyl acrylate (15% b/v crosslinker) cured under 5000 mWm^{-2} UV

The greater cure intensity results in a faster polymerization rate and the required extent of polymerization is reached more rapidly. As shown previously in this section the reaction rate of polymerization is given by the following equation;

$$r_{pol} = k_p \left[\frac{n\Phi k_d I_0 [I]}{2k_t} \right]^{\frac{1}{2}} [M]$$

Assuming that all other terms are constant the increase in UV cure intensity from 2000 mWm^{-2} to 5000 mWm^{-2} will result in an increase in reaction rate by a factor of 1.58, as shown below;

$$\frac{r_{5000 mWm^{-2}}}{r_{2000 mWm^{-2}}} = \frac{k_p \left[n\Phi k_d \times 5000 mWm^{-2} \times [I] \right]^{\frac{1}{2}} [M]}{k_p \left[n\Phi k_d \times 2000 mWm^{-2} \times [I] \right]^{\frac{1}{2}} [M]}$$

$$\frac{r_{5000 mWm^{-2}}}{r_{2000 mWm^{-2}}} \approx \frac{\left[5000 mWm^{-2} \right]^{\frac{1}{2}}}{\left[2000 mWm^{-2} \right]^{\frac{1}{2}}}$$

$$\frac{r_{5000 mWm^{-2}}}{r_{2000 mWm^{-2}}} \approx \frac{70.71}{44.72}$$

$$\frac{r_{5000 mWm^{-2}}}{r_{2000 mWm^{-2}}} \approx 1.58$$

The improvement is less pronounced at lower temperatures as here the extent of polymerization required is much lower and therefore is reached quite quickly regardless of cure intensity. It can also be seen that for some of the samples with higher ϕ_{TL213} the phase separation time at lower cure temperatures is actually quicker for the lower cure intensity. In these cases the extent of polymerization required for phase separation to become favourable is very low as the coexistence curve is almost at room temperature, therefore the differences are well within experimental error.

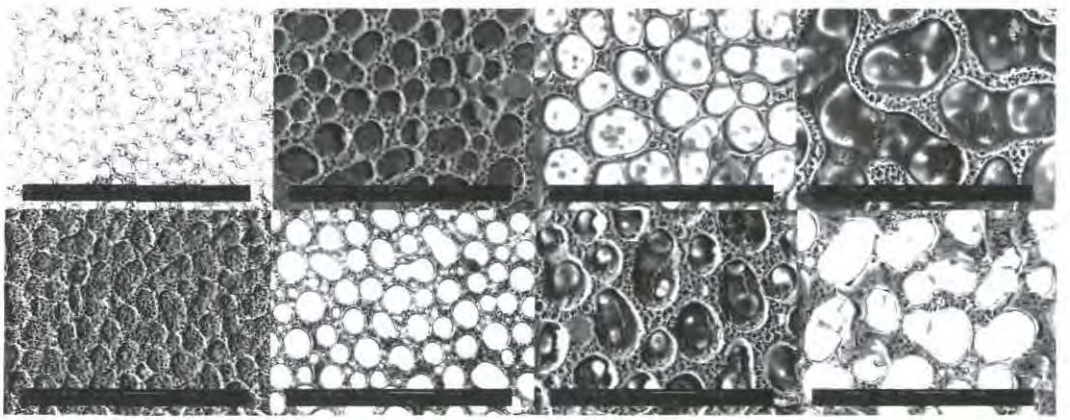

Figure 33 Comparison of morphologies of PDLC films formed from TL213 and 2-ethylhexyl acrylate with 2% b/v crosslinker cured 2000 mWm^{-2} and 5000 mWm^{-2} (303 K). Top row cured at 2000 mWm^{-2} bottom row at 5000 mWm^{-2}, from left to right 70:30, 73:27, 75:25, 77:23

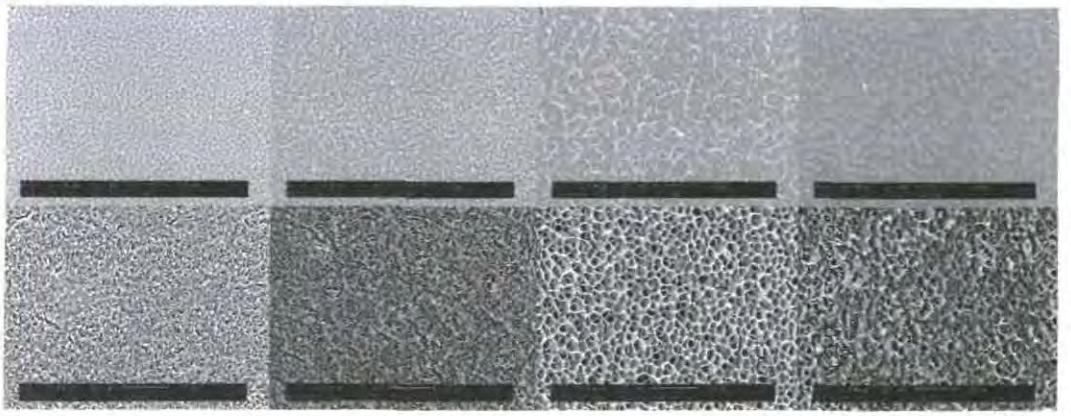

Figure 34 Comparison of morphologies of PDLC films formed from TL213 and 2-ethylhexyl acrylate with 15% b/v crosslinker cured 2000 mWm^{-2} and 5000 mWm^{-2} (303 K). Top row cured at 2000 mWm^{-2} bottom row at 5000 mWm^{-2}, from *left to right* 70:30, 73:27, 75:25, 77:23

It has been shown that increasing cure intensity has the effect of speeding up the initiation of phase separation; Figure 33 shows a comparison of the morphologies formed from liquid crystal/monomer solutions of varying compositions where the monomer contains 2% by volume crosslinker under cure intensities of 2000 mWm^{-2} and 5000 mWm^{-2} (303 K) and Figure 34 shows the same but where the crosslinker is present at 15% by volume. It can be seen that in both cases the increasing of the cure intensity has little or no effect on the type or size of morphology formed, suggesting that morphology is not related to cure rate only phase separation thermodynamics. Figure 35 shows the same is true for 15% crosslinker films formed at 333K, so that even at the higher temperatures where the effect of cure rate is more noticeable on phase separation time, it is still thermodynamics which control the type of morphology formed.

Figure 35 Comparison of morphologies of PDLC films formed from TL213 and 2-ethylhexyl acrylate with 15% b/v crosslinker cured 2000 mWm^{-2} and 5000 mWm^{-2} (333 K). Top row cured at 2000 mWm^{-2} bottom row at 5000 mWm^{-2}, from left to right 70:30, 73:27, 75:25, 77:23

6.1.1.2 Effect of Composition

Figure 33 and Figure 34 show the effect of increasing TL213 volume fraction on the morphologies formed and the droplet size for systems with 2 and 15% by volume crosslinker respectively. As has been previously discussed increasing the liquid crystal volume fraction has the effect of increasing the droplet size as the initial composition/temperature point gets closer to the coexistence curve. A lower extent of polymerization is required for phase separation to become favourable, this means that the degree of network formation at the point of phase separation is lower and it therefore acts to promote, not suppress phase separation, and larger droplet sizes are formed. From Figure 35, which shows the same dependencies for a cure temperature of 333 K, it can be seen that interestingly this trend is less pronounced when polymerization occurs at a higher temperature until reaching much higher liquid crystal volume fractions. This is investigated further below.

This behaviour can be seen in the SALS observed phase separation time results. The general trend observed for the systems studied is that as the volume fraction of TL213 increases, the time to phase separation decreases. This suggests that the extent of polymerization required to make phase separation favourable is much less at these compositions (ignoring the reaction rate effects which come into effect at higher polymer volume fractions, where a greater polymer concentration means that the radical concentration is higher and, as reaction rate has a $[R\cdot]^2$ relationship with radical concentration, reaction rate is higher).

6.1.1.3 Effect of Temperature

As discussed above increasing cure temperature has the effect of changing the size of morphology formed. Figure 36 shows examples of the morphologies formed at different temperatures for a 70:30 initial composition system cured at 303, 313, 323 and 333 K, it can be seen that as the cure temperature increases there is an a corresponding decrease in the morphology size. Figure 37 again shows the effect of changing cure temperature on morphology but this time for a starting composition of 73:27. As previously discussed the morphology size has become greater with the increasing TL213 volume fraction, as the initial temperature/composition points are nearer to the coexistence curve and the degree of network formation upon phase separation is less. The temperature trend as observed for solutions of composition

70:30 can again be seen for the 73:27 system, with a higher cure temperature leading to a decrease in droplet morphology size.

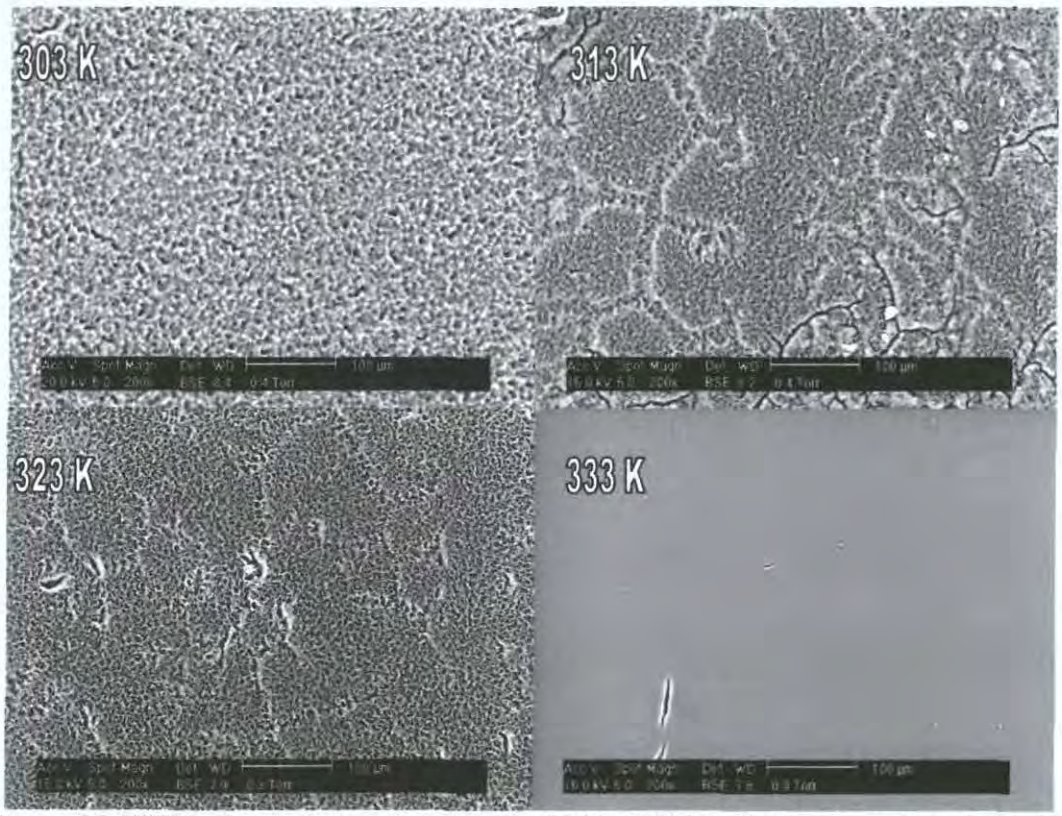

Figure 36 ESEM observed morphologies for 70:30 TL213:2-ethylhexyl acrylate (15% b/v crosslinker) polymerized under 5000 mWm^{-2} UV (365 nm) at varying temperatures. All images 200x magnification, measure bar is 100 μm

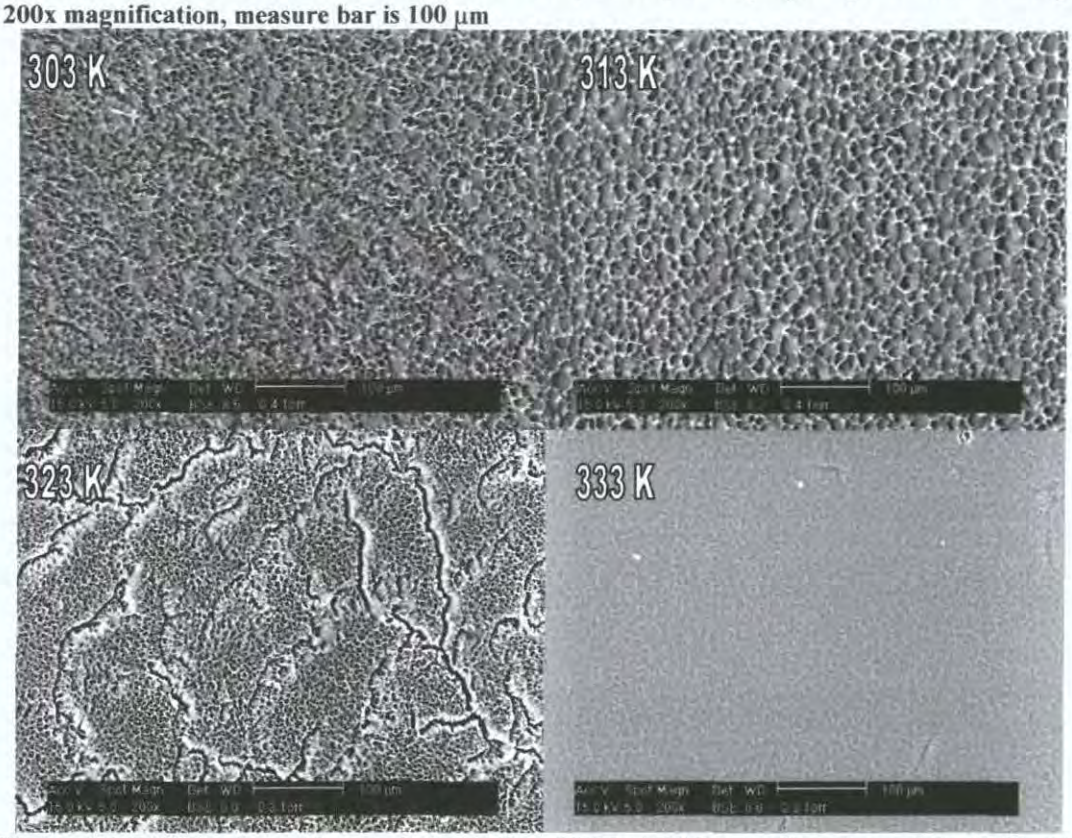

Figure 37 ESEM observed morphologies for 73:27 TL213:2-ethylhexyl acrylate (15% b/v crosslinker) polymerized under 5000 mWm^{-2} UV (365 nm) at varying temperatures. All images 200x magnification, measure bar is 100 μm

Again in Figure 38 the same trend can be observed for cells formed from an initial composition of 75:25; at this composition however the morphology has become larger and better defined at all cure temperatures and does not appear as featureless as the films formed at 333 K for lower TL213 volume fraction systems.

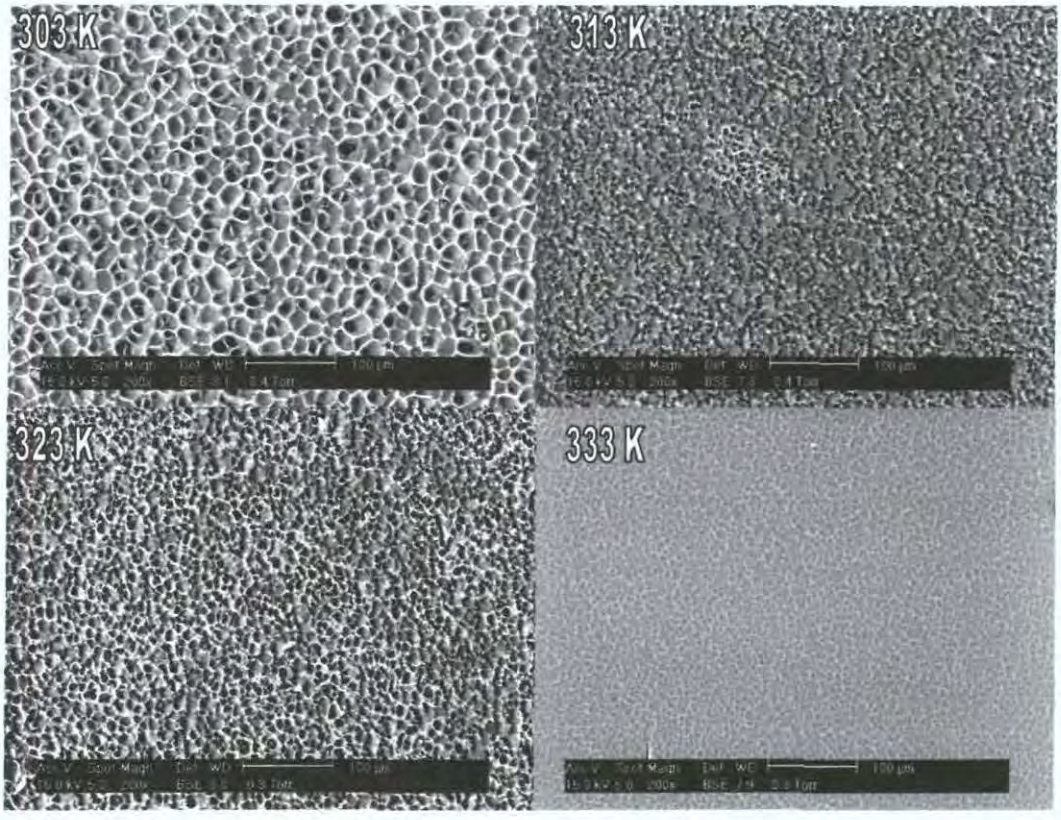

Figure 38 ESEM observed morphologies for 75:25 TL213:2-ethylhexyl acrylate (15% b/v crosslinker) polymerized under 5000 mWm^{-2} UV (365 nm) at varying temperatures. All images 200x magnification, measure bar is 100 μm

When the volume fraction of TL213 in the initial solution is increased further to 77:23 (Figure 39) there can be observed a change in the trend in morphology droplet size as temperature increases. While the films formed at 323 and 333 K are smaller in droplet size than for that formed at 303 K, the 313 K film demonstrates a morphology droplet size which is actually larger than that for the film cured at 303 K. For films formed from a solution of composition 80:20 this behaviour becomes even more pronounced (Figure 40), there can be observed significant increases in droplet size with increase in cure temperature from 303 K to 313 and 323 K. Once the cure temperature is increased to 333 K the droplet size once again decreases to a size much smaller than that for the film cured at 303 K.

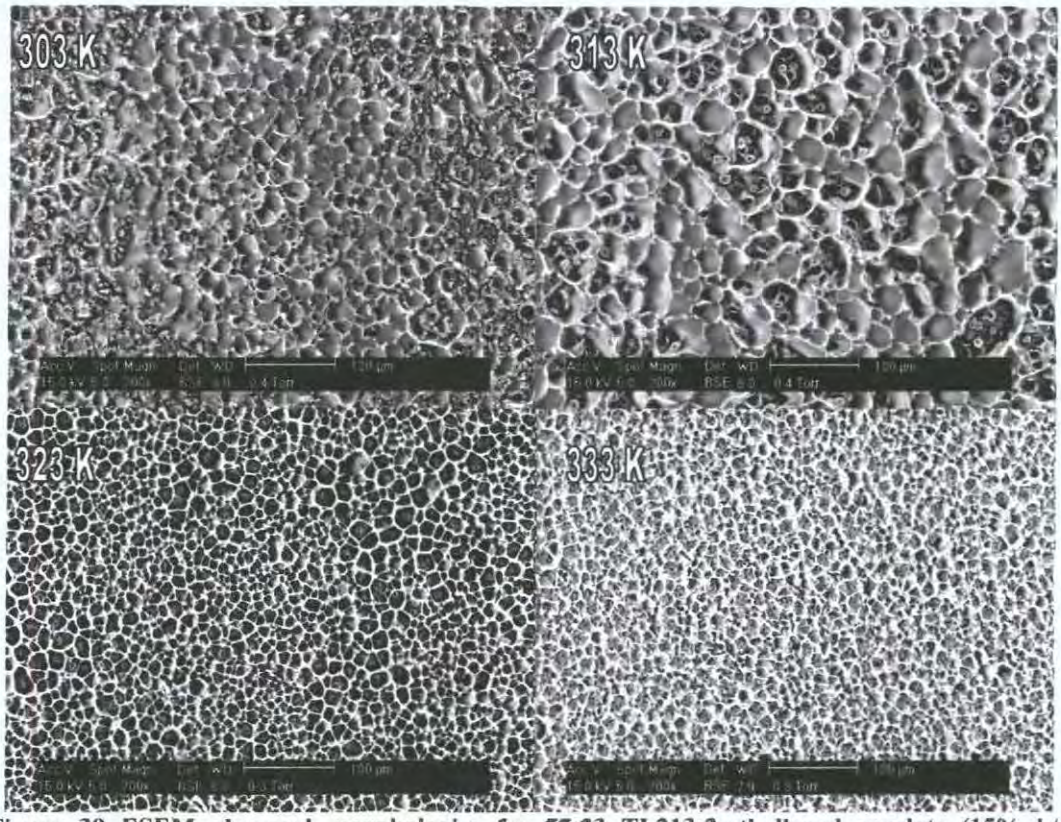

Figure 39 ESEM observed morphologies for 77:23 TL213:2-ethylhexyl acrylate (15% b/v crosslinker) polymerized under 5000 mWm^{-2} UV (365 nm) at varying temperatures. All images 200x magnification, measure bar is 100 μm

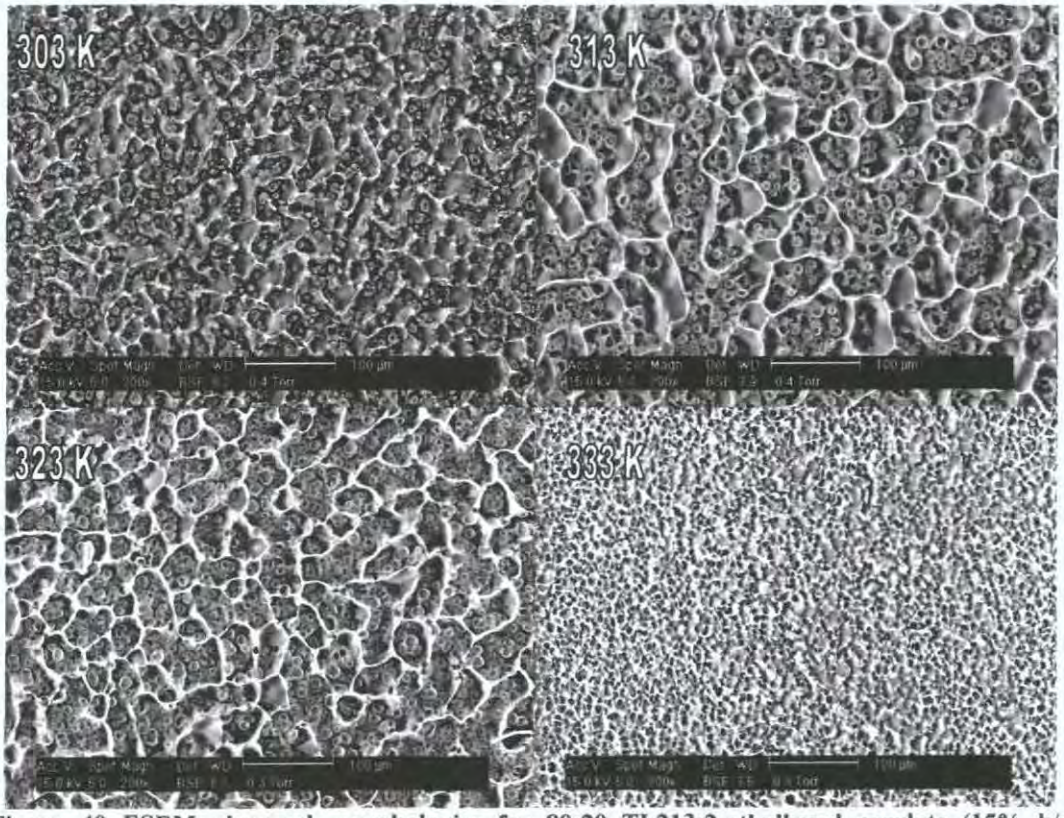

Figure 40 ESEM observed morphologies for 80:20 TL213:2-ethylhexyl acrylate (15% b/v crosslinker) polymerized under 5000 mWm^{-2} UV (365 nm) at varying temperatures. All images 200x magnification, measure bar is 100 μm

The reason for the observed behaviour is once again to do with the distance of the initial temperature/composition point from the unpolymerized coexistence curve. Figure 41 shows the unpolymerized phase diagram for TL213 with 2-ethylhexyl acrylate; as has been previously discussed the coexistence curve moves to higher temperatures as the TL213 volume fraction increases. This has the effect of at lower TL213 volume fractions, making the initial composition/temperature points far from the coexistence curve; as a result a very large extent of polymerization is required for phase separation to become favourable. Therefore at the point of phase separation the degree of polymer network formation is greater, and has the effect of suppressing phase separation resulting in smaller droplet sizes.

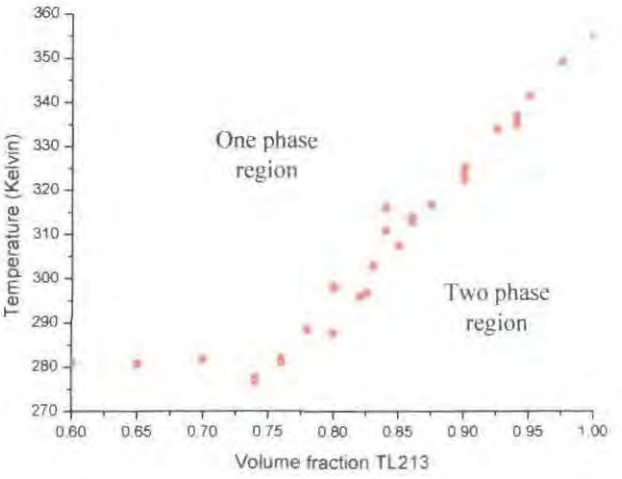

Figure 41 Phase diagram for TL213 with unpolymerized 2-ethylhexyl acrylate

As the cure temperature increases the distance from the coexistence curve at a given temperature increases, and so does the extent of polymerization required to make phase separation favourable. Therefore the degree of network formation at phase separation is greater and the suppression to phase separation is greater also and as a result the morphology size is smaller by comparison. Figure 42 shows the dependence with degree of polymerization (in this instance a quantitative degree of polymerization rather than a qualitative extent of polymerization is used as the model is based upon free chains) of the coexistence curve for TL213 with 2-ethylhexyl acrylate based upon Flory-Huggins theory for spinodal curves (as extrapolated from a fit of an experimentally determined phase curve). It has already been shown that Flory-Huggins theory cannot be used to accurately describe the phase mixing properties and phase separation mechanisms of polymer dispersed liquid crystals, equally the presence of a crosslinking species means that a model based upon free chain degrees of polymerization is not directly applicable. However it does provide a

useful understanding of the effect of extent of polymerisation upon the phase separation temperature for a given composition.

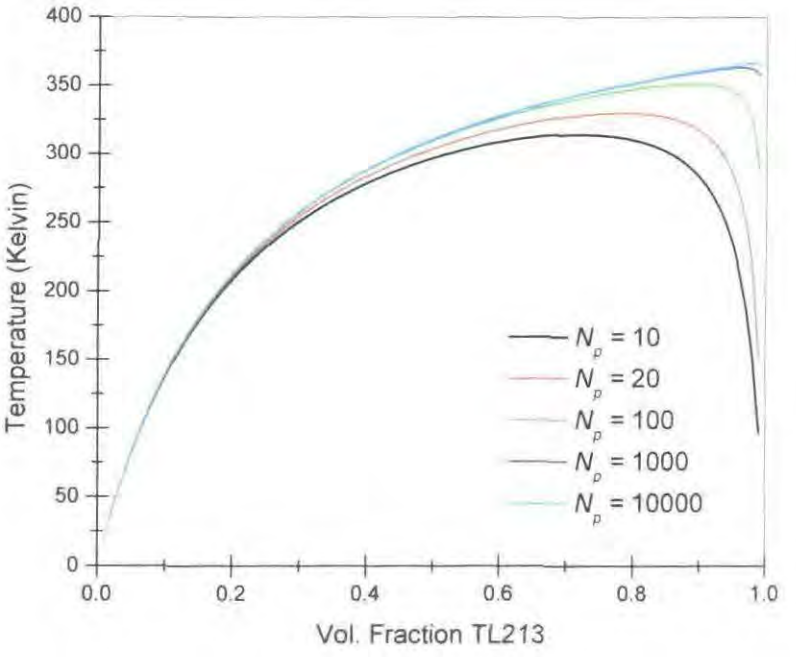

Figure 42 Predicted Flory-Huggins spinodal curves for TL213 with 2-ethylhexyl acrylate at varying degrees of polymerization based upon fit of TL213 with Mw 92000 gmol^{-1} poly(2-ethylhexyl acrylate)

Figure 42 shows that the increase in degree of polymerization required for phase separation to become favourable is not linear with increase in temperature. A change of a few Kelvin in temperature can result in increases of orders of magnitude in the phase separation degree of polymerization. The rate of this increase in phase separation degree of polymerization with temperature also varies from composition to composition. As the volume fraction of liquid crystal increases, larger increases in temperature are required for the same increases in the phase separation degree (extent) of polymerization. This relationship will work the other way round, so for solutions of high TL213 volume fractions, the increase in the degree (extent) of polymerization required to make phase separation favourable will be much less than for initial compositions of lower TL213 volume fraction. This is the case when comparing cells formed from solutions of composition 70:30 and 80:20 and is the reason for the observed differences in the effect of cure temperature on morphology type and size.

As can be seen from Figure 36 for compositions of 70:30 the decrease in morphology size as cure temperature increases is only slight, whereas in Figure 38 which shows the morphologies for films formed from an initial composition of 75:25 the decrease

in droplet size is quite marked. This is because at 70:30 for a cure temperature of 303 K the initial temperature/composition point is already a significant distance from the coexistence curve and the extent of polymerization required to make phase separation favourable is already of a very high order of magnitude. Therefore upon phase separation the degree of polymer network formation will already be high (and near universal) and act significantly against phase separation. So while small increases in temperature result in significant increases in the extent of polymerization required to make phase separation favourable, the increase in the degree of network formation will not be great by comparison. So the forces acting against phase separation will not be significantly larger and the droplet size will not significantly decrease. For systems of composition 75:25 and above, as can be seen from Figure 41, at 303 K the initial temperature/composition points are much nearer to the coexistence curve; so increases in cure temperature result in increases in phase separation extent of polymerization which have a much more significant effect upon the type of phase separation mechanism and morphology formed than would be the case at cure temperatures much further from the coexistence curve. At 303 K these systems are so near the coexistence curve that the degree of network formation, at the point of phase separation, is quite low and as such acts to promote phase separation, (as can be seen from the fine ribbon like structures of the polymer matrices) resulting in relatively large droplet sizes. So as the cure temperature increases, and the phase separation extent of polymerization increases, the degree of network formation at the point of phase separation becomes much greater and starts to act against phase separation resulting in the observed decrease in morphology size. As can be seen for the 75:25 film cured at 333 K the morphology loses its well defined polymer matrix structure, as the polymer network development becomes highly advanced.

It would be expected that this behaviour should be observed for all compositions of volume fraction higher than 75:25; this does not prove to be the case as can be seen in Figure 39 and Figure 40; instead initial increases in morphology droplet size are observed with increasing temperature. At these compositions, for cure temperatures of 303 K, as can be seen from the type of morphologies formed with very large droplet sizes and well defined polymer structures, the extent of polymerization required for phase separation to become favourable is very low, as is the degree of network formation. As can be seen in Figure 42 increases of cure temperature do not require very large increases in extent of polymerization for phase separation to

become favourable, this means that the effect of greater network formation is only slight and not large enough to change its effect from that of overall promotion to overall suppression of phase separation. The observed increase in droplet size therefore with initial increases in cure temperature at compositions of 77:23 and 80:20 can be explained in one of two ways. Firstly, it could be the case, as described above, that the formation of a more advanced polymer network at the point of phase separation has the effect of increasing the driving force for the liquid crystal solvent to be forced out from the polymer phase. Since the network is not yet fully developed, it does not act greatly against droplet nucleation and suppress phase separation significantly; this results overall in a net gain in the promotion of phase separation, and thus a larger morphology size. The second is a hypothesis put forward by the groups lead by Amundson[36] and Carter[30], they believe that at these compositions viscosity effects become important in the phase separation process. As the extent of polymerization at phase separation is so low for systems polymerized at 303 K and 313 K for solutions of composition 80:20, the polymer chains will still be relatively short and the formation of a polymer network still inadvanced. This means that the viscosity of the polymer phase will be low, and diffusion of the liquid crystal out of the polymer phase will be fast by comparison to systems where the polymer network is more highly developed. An increase in temperature will bring about further decrease in the viscosity of the polymer phase; at these low phase separation degrees of polymerization. If decreases in viscosity are greater than the increases in the suppressive effect of the formation of the polymer network then the overall effect will be to make the growth of the liquid crystal droplets quicker and therefore larger morphologies will develop before gelation occurs.

It is likely to be the case that both of these phenomena are to an extent of importance for those systems where morphology size increases with increased cure temperature. For both 77:23 and 80:20 compositions there can still be observed significant decreases in morphology sizes at higher cure temperatures, for 77:23 at 323 K and for 80:20 at 333 K. This is because, as previously discussed, the increase in extent of polymerization required to make phase separation favourable with increasing temperature is not a linear relationship, and, as can be seen from the approximate behaviour as demonstrated in Figure 42, at all compositions a point is reached where small increases in temperature result in very large increases in the extent of polymerization at the phase separation point, and degree of network formation

6.1.1.4 Effect of Crosslinker Percentage

Figure 43 shows the morphologies formed at 303, 313, 323 and 333 K for 70:30 TL213:2-ethylhexyl acrylate with 2% by volume crosslinker, and Figure 44 and Figure 45 show the same but for initial compositions of 73:27 and 75:25 respectively. As can be seen by comparing to the equivalent film morphologies with 15% by volume crosslinker (Figure 37 and Figure 38), there is no longer observed a decrease in droplet size with increasing cure temperature. In fact phase separation becomes more advanced as the cure temperature increases with large areas of polymer and liquid crystal phases which do not really form a droplet morphology, but rather two distinct phases. This suggests that phase separation has not at any point been greatly suppressed. This is a result of the low crosslinker density; as the crosslinker is only present in the initial monomer at 2% by volume there is never enough network formation at the point of phase separation for it to act to suppress phase separation and in fact is always acting to promote it (by encouraging gel deswelling).

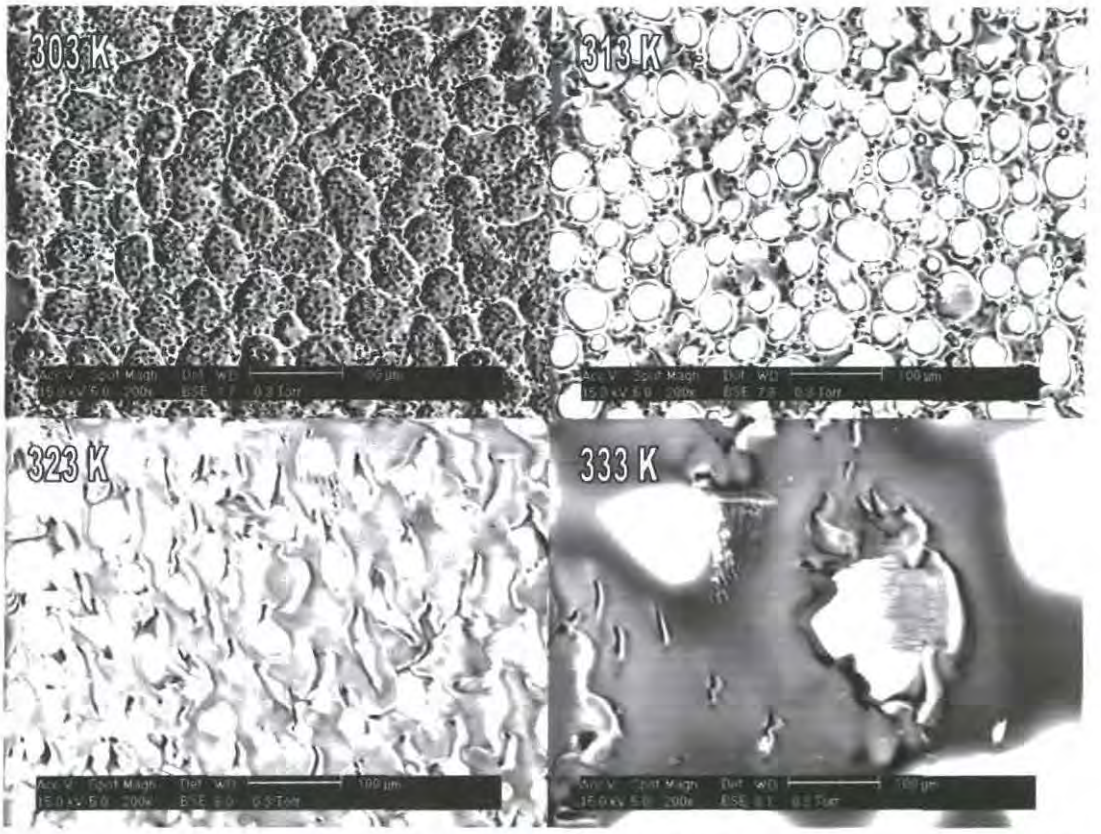

Figure 43 ESEM observed morphologies for 70:30 TL213:2-ethylhexyl acrylate (2% b/v crosslinker) polymerized under 5000 mWm^{-2} UV (365 nm) at varying temperatures. All images 200x magnification, measure bar is 100 μm

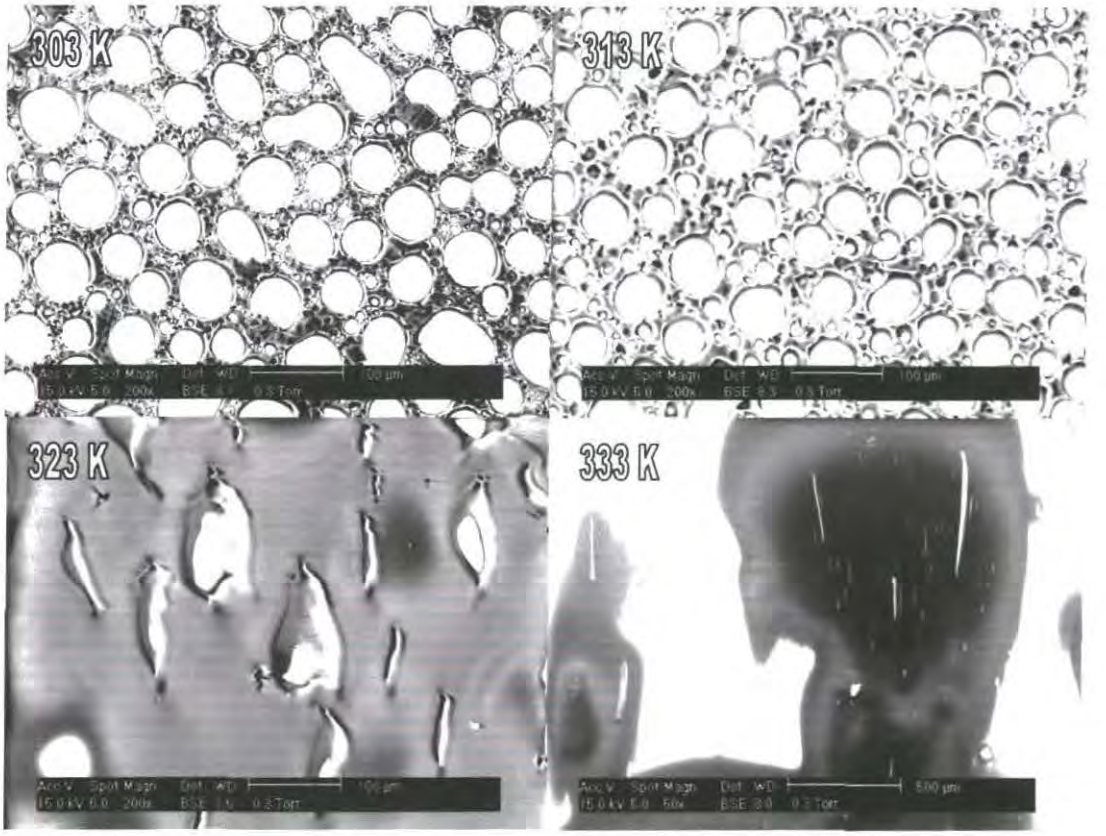

Figure 44 ESEM observed morphologies for 73:27 TL213:2-ethylhexyl acrylate (2% b/v crosslinker) polymerized under 5000 mWm^{-2} UV (365 nm) at varying temperatures. All images 200x magnification, *measure bar is 100 μm*

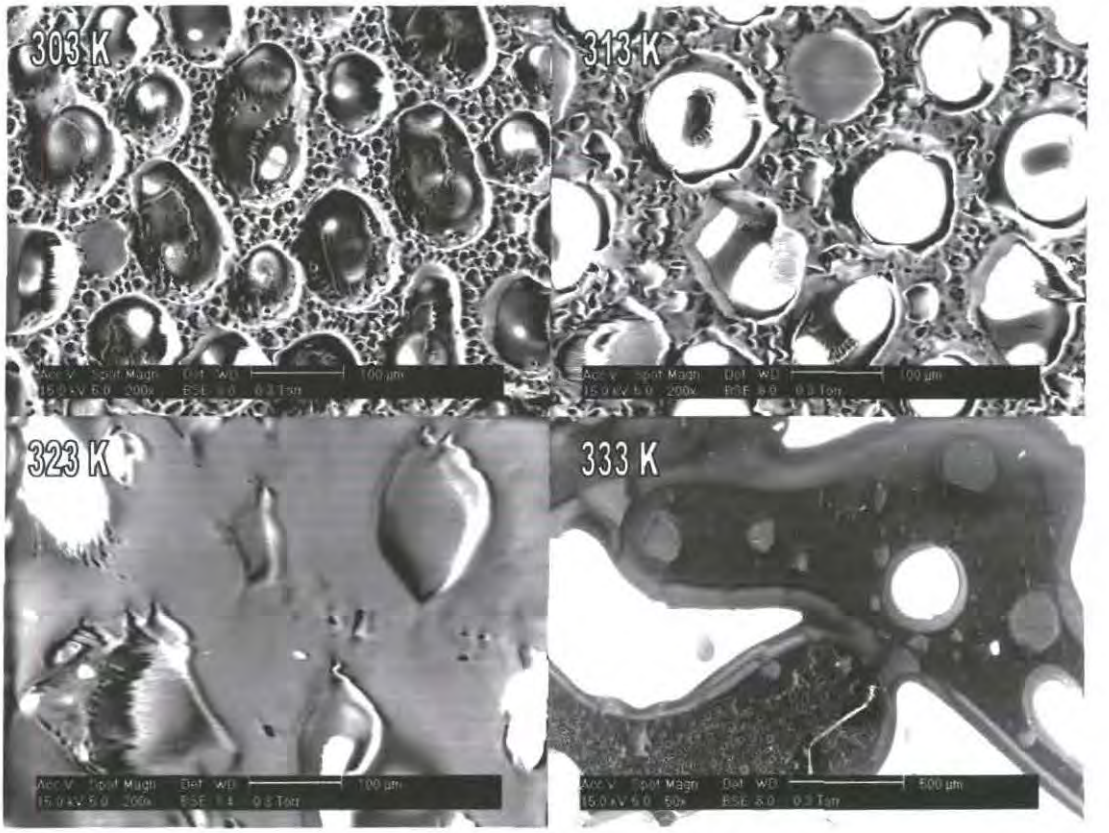

Figure 45 ESEM observed morphologies for 75:25 TL213:2-ethylhexyl acrylate (2% b/v *crosslinker)* polymerized under 5000 mWm^{-2} UV (365 nm) at varying temperatures. All images 200x magnification, measure bar is 100 μm

This has resulted in the large droplet morphologies observed at low temperatures, and the highly phase separated morphologies observed at high temperatures, where, as discussed above, a combination of higher network development at the phase separation point (increasing phase separation promotion) and temperature dependent viscosity effects have resulted in greater phase separation before gelation.

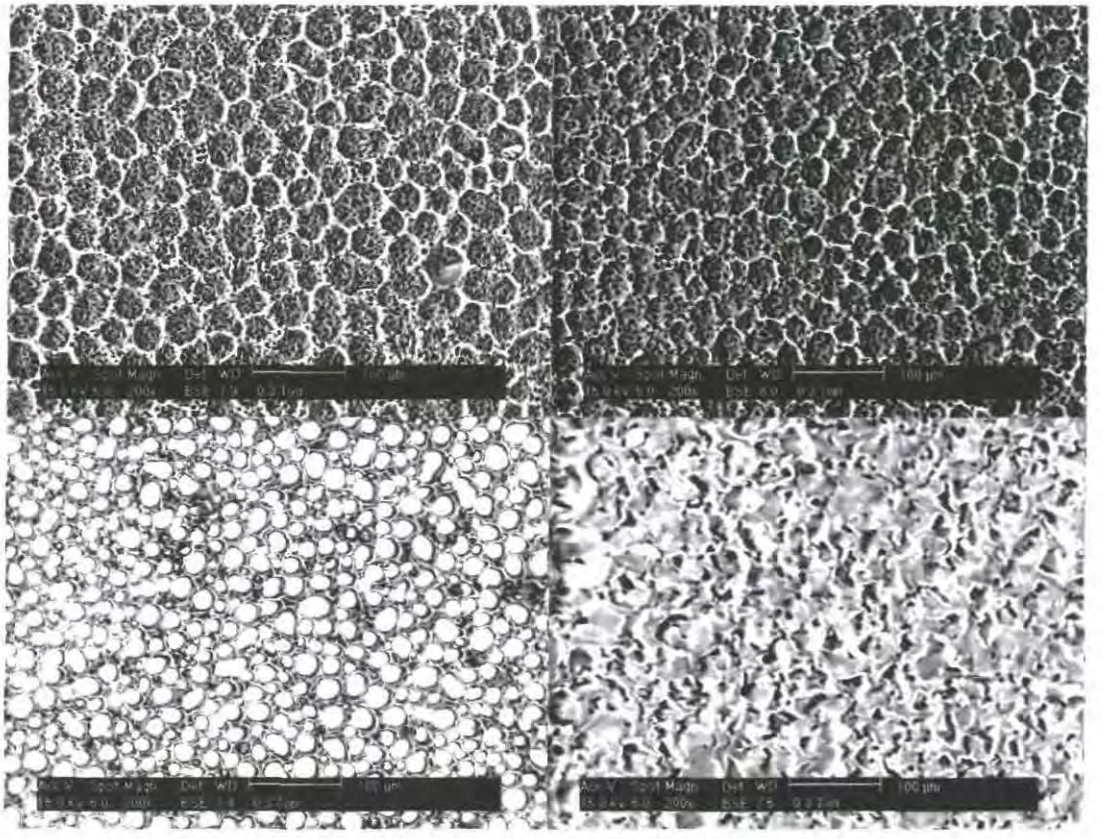

Figure 46 ESEM observed morphologies for 70:30 TL213:2-ethylhexyl acrylate (5% b/v *crosslinker) polymerized under* 5000 mWm^{-2} UV (365 nm) at varying temperatures. All images 200x magnification, measure bar is 100 μm

Figure 46 shows the temperature dependent morphologies for 70:30 initial composition but with the crosslinker present at 5% by volume. It can be seen that the increased crosslinker density has had the effect of, as the temperature increases, decreasing the droplet size as the polymer network becomes more developed and suppresses phase separation. The relatively large droplet size, compared to the 15% by volume crosslinker films, suggests that even at this crosslink density the overall effect of the polymer network is to initially promote (rather than suppress) phase separation. This shows that a relatively large crosslink density is required to form the type of films of use for display screen devices.

Figure 47 shows the time at which phase separation commences for films cured under 2000mWm^{-2} UV intensity at varying temperatures and compositions for initial liquid crystal/monomer solutions which contain no crosslinking species. When

compared to Figure 29 (2% by volume crosslinker) and Figure 31 (15 % by volume crosslinker) it can be seen that the phase separation commencement times for *solutions without* crosslinker and with 2% by volume crosslinker are very similar. This contrasts to the much shorter phase separation times for the solutions which contain 15% by volume (e.g. for 75:25 solutions cured at 303 K the 15% films phase separate after ~60 seconds compared to ~200 seconds for the 2% and 0% solutions). This supports the theory that at low crosslinker compositions when phase separation becomes favourable there is very little network formation. In fact the results suggests that phase separation is actually proceeding via a viscoelastic phase separation mechanism as has been shown to occur in systems where there is an absence of crosslinker (sub-section 5.2) as the phase separation commencement times are so similar, whereas those for 15% by volume crosslinker solutions where a gel deswelling mechanism is occurring are significantly lower.

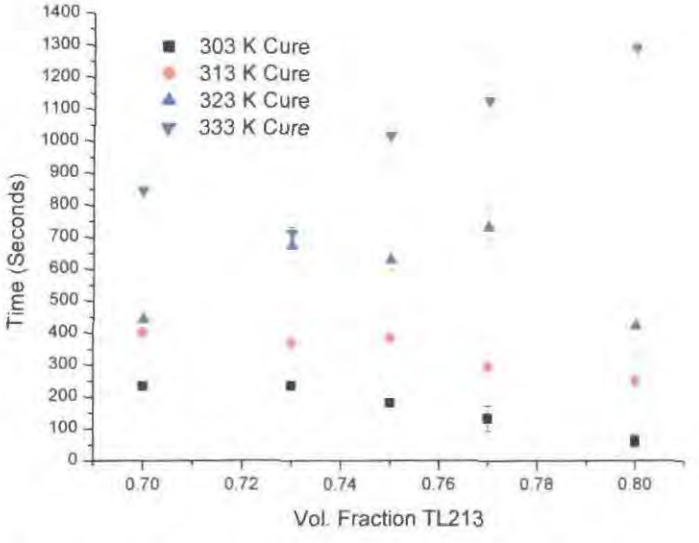

Figure 47 SALS determined phase separation times for TL213 with 2-ethylhexyl acrylate (0% crosslinker) cured under 2000 mWm^{-2} UV

6.1.2 Conclusion

It has been shown by the work in this sub-section that, as hypothesised in subsection 5 on the phase separation mechanism, the most important factor in the type of morphology formed is the degree of network formation at the point of phase separation. This supports the belief that phase separation proceeds by a polymer gel deswelling mechanism and not a spinodal decomposition mechanism. The results presented have also backed up the interpretation that the presence of a polymer network can have both the effect of promoting phase separation (when the network is

not greatly developed, it wants to contract to force out the solvent (liquid crystal)), or suppress it (network development is advanced and therefore to form solvent droplets within it would require significant entropically unfavourable chain stretching).

Whether or not the presence of a crosslinking species is acting to promote or suppress phase separation has been shown to be related to the distance of the initial composition temperature point to the unpolymerized coexistence curve. When the initial point is close to the curve, the extent of polymerization required for phase separation to become favourable is low and as such polymer network development will be limited. This leads to the network acting to promote rather than suppress phase separation. As you move further from the coexistence curve either by decreasing the liquid crystal volume fraction or increasing the temperature of cure the extent of polymerization to make phase separation favourable becomes greater, and as such the network is more developed at the point of phase separation. It therefore starts to act against phase separation, resulting in a smaller droplet size. It is also the view of the author that these general trends are limited by a couple of factors; for high liquid crystal volume fraction compositions increased temperatures can result in decreased viscosity and therefore increased diffusion rate, which allows the formation of large droplet sizes before gelation. Secondly, if the increase in polymer network development at the point of phase separation is only small it will not be great enough for it to act to suppress phase separation, but will increase the driving forces acting to promote phase separation. Both of these factors mean that small increases in cure temperature, when cure temperature is close to the coexistence curve, will result in initial increases in droplet size rather than the overall trend for droplet size to reduce with increasing cure temperature.

7 Electro-Optical Study

To be applicable to the design of display screen devices the above results and conclusions need to be correlated to the electro-optical properties of PDLC films; to this end a series of test cells are synthesised and their optical transmission and electronic switching fields and times measured. The aim is twofold, firstly to correlate trends in electro-optical properties to phase separation mechanism and morphology size, and secondly to determine the optimum synthesis conditions and composition for the system under study.

7.1 TL213 with 2-Ethylhexyl acrylate Variable Temperature and Composition Study

All the cells prepared for this study are done so under 5000 mWm^{-2} UV (365 nm) light for 30 minutes, with the monomer doped at 15% by volume with a crosslinking monomer and in ITO cells to make electro-optical testing possible. A series of cells is prepared at temperatures and compositions to correlate with those used in the study in sub-section 6, further compositions and temperatures are also incorporated into the study as they are in the areas which show most interest and potential for display devices. The cells are then tested as described in the experimental section.

7.1.1 Results and Discussion

7.1.1.1 303 K Variable Composition Study

Cells of compositions from 70:30 to 80:20, at 1% by volume intervals, TL213:2-ethylhexyl acrylate are prepared at a cure temperature of 303 K, and tested for their electro-optical properties and example cells then imaged by ESEM.

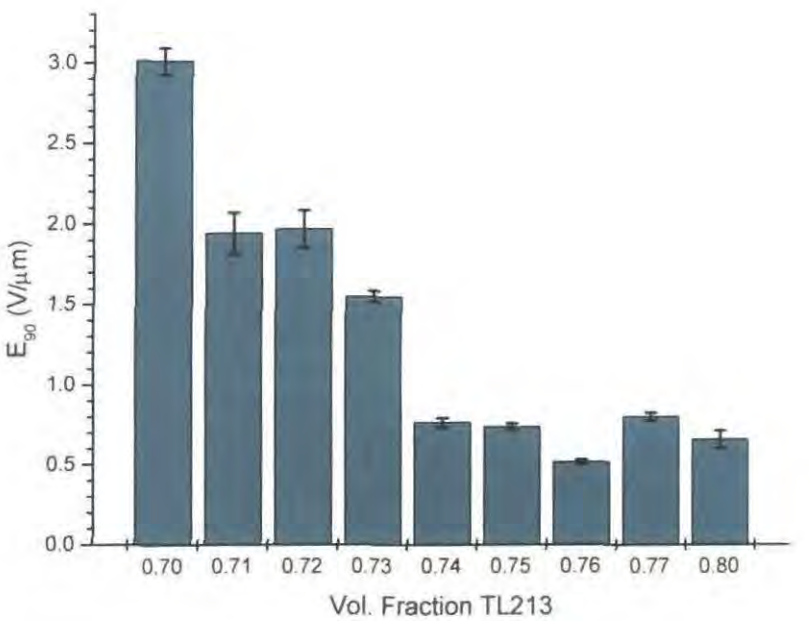

Figure 48 E_{90} switching fields for TL213:2-ethylhexyl acrylate(15% b/v crosslinker) cells of varying composition cured at 303 K under 5000 mWm^{-2} UV (365 nm)

Figure 48 shows how the field required to result in 90% switching changes with composition for films of TL213 with 2-ethylhexyl acrylate (15% by volume

crosslinker), which are cured at 303 K. As discussed in the introduction the field required to bring about switching of the liquid crystals encapsulated in a droplet is related to the size of the droplet. In particular it is the droplet volume to interfacial area that is of importance, the greater the interfacial area the greater the disordering effect for a given volume. It is therefore expected that a lower field will be required to bring about switching in a larger droplet. The results presented above in sub-section 4 shows that for films cured at 303 K droplet size generally increases from about 1-2 μm for a 70:30 composition system up to about 20-30 μm for 80:20 (with a slight deviation in this trend around 72:28, where there is a decrease in droplet size). It would therefore be expected that the required 90% switching field should decrease with increasing liquid crystal volume fraction from 70:30 to 80:20, as is indeed what is observed.

While the general trend in decreasing switching field with increasing liquid crystal volume fraction can be seen, it is not a smooth decrease, instead there are a couple of steps in the dependence. A large decrease can be observed between 70:30 and 71:29, with a subsequent large decrease between 73:27 and 74:26.

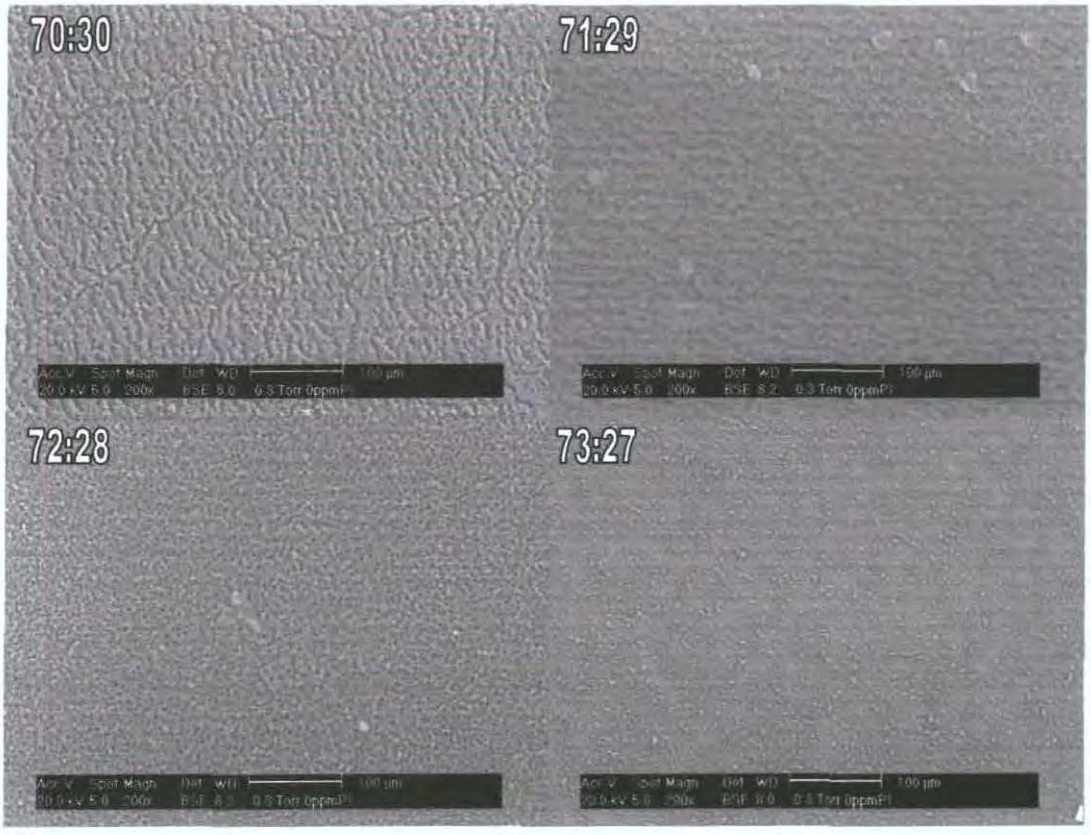

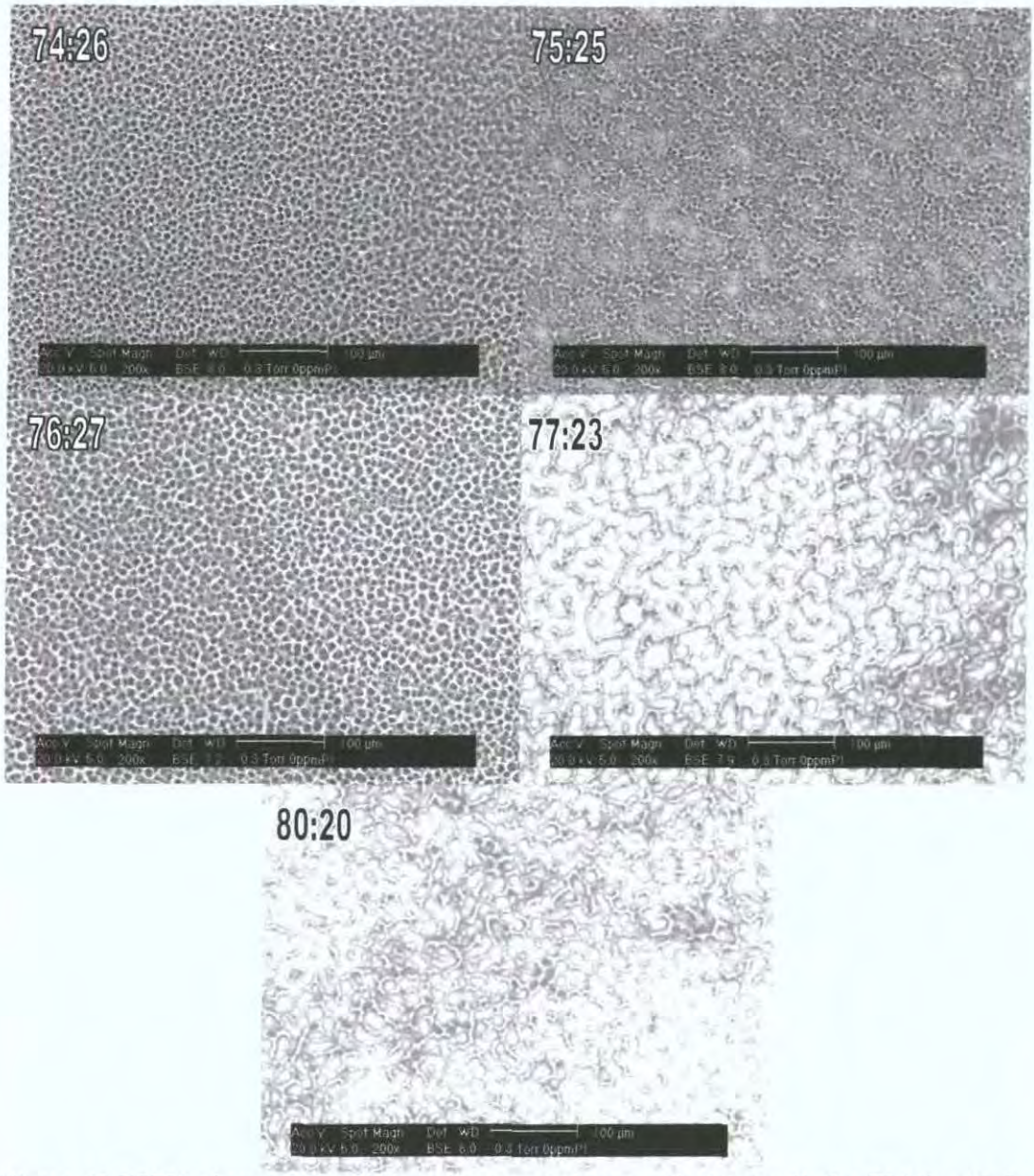

Figure 49 ESEM observed morphology images of electro-optical test cells for TL213 with 2-ethylhexyl acrylate (15% b/v *crosslinker*) *cured at* 303 K *under* 5000 mWm^{-2} intensity UV (365 nm), all images 200x magnification, measure bar is 100 μm

Figure 49 shows the ESEM observed morphologies for example test cells, and it can be seen that between 70:30 and 71:29 there is a suggestion of a possible change in the morphology type, with the two phases becoming much more distinct. As discussed in sub-section 6 this is as a result of phase separation occurring earlier, due to the unpolymerized phase mixing properties, for the higher liquid crystal composition system. As such the network is formed to a lesser degree at the point of phase separation, and therefore acts to promote phase separation via deswelling and a relatively pure liquid crystal-rich phase is formed compared with the lower liquid crystal composition system. This purer liquid crystal-rich phase will have less point defects and as such a lower field is required to overcome disordering of the liquid

crystal and bring about switching. Between 73:27 and 74:26 can be observed a significant change in morphology droplet size from about 2-3 μm to 3-5 μm, this results in a further reduction in switching field at this point in the trend. As is shown in sub-section 6 these large changes in morphology are as a result of the phase mixing temperature of the unpolymerized system coming closer to 303 K as ϕ_{TL213} increases. As such the degree of network formation is less at the point of phase separation and therefore acts to promote phase separation. The fact that the switching field does not show any further significant reduction beyond this composition even though there can be observed a further increase in droplet size, would suggest that above a certain point the size of droplet becomes less significant as the surface area to volume ratio goes below some critical value where it starts to behave more like an impure bulk liquid crystal species which has disordering centres within it, than an encapsulated species.

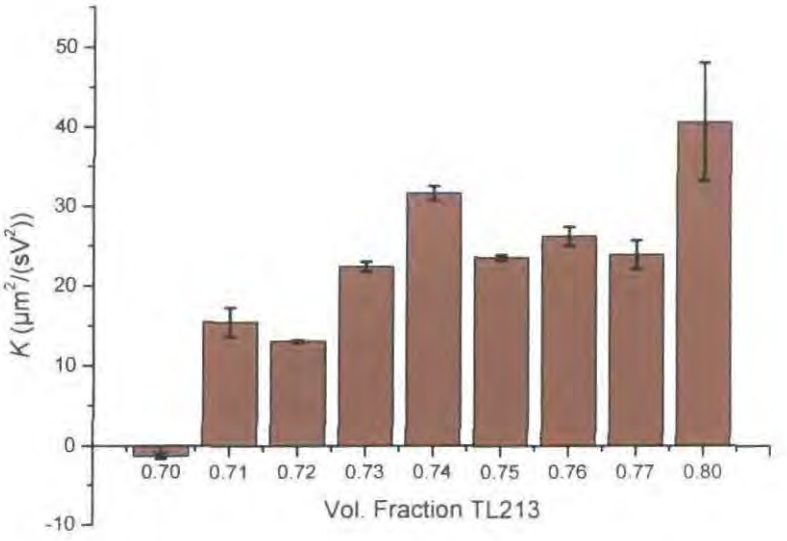

Figure 50 *K* values (related to rise switching rate) for TL213:2-ethylhexyl acrylate (15% b/v crosslinker) cells of varying composition cured at 303 K under 5000 mWm^{-2} UV (365 nm)

Figure 50 shows the *K* speed factor values for each of the compositions. Given that like the applied field, the speed at which the system switches depends upon the amount of disordering which needs to be overcome, it is to be expected that the speed factor (the higher the value, the faster the switching rate) increases going from low to high liquid crystal volume fraction, as the droplet size increases and disordering effect decreases. The negative value for the systems of composition 70:30 would seem to suggest that the model used to derive the *K* values breaks down

for such system, possibly suggesting that the behaviour of the liquid crystals change once encapsulated in such a small sized droplet. This would also provide an explanation for why there is a 50% change in the required switching field going from composition 70:30 to 71:29, as the dopant size becomes large enough that it becomes more like a normal display type PDLC.

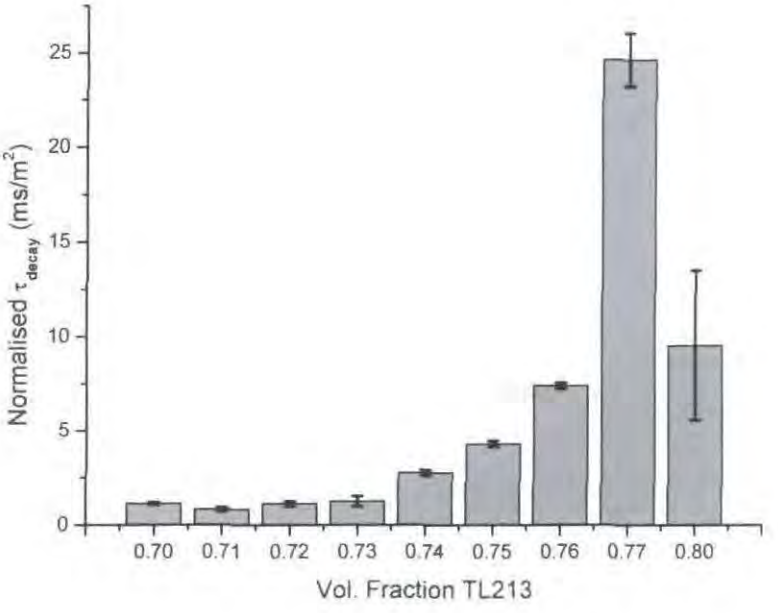

Figure 51 Normalised decay times (τ_{decay}) from 90% switching for *TL213:2-ethylhexyl acrylate* (15% b/v crosslinker) cells of varying composition cured at 303 K under 5000 mWm^{-2} UV (365 nm)

As with the speed factor the interpretation of the normalised 90% switching decay times (Figure 51) is quite simple, the greater the disordering surface to volume ratio the faster the system will relax back to its equilibrium configuration upon removal of the switching field. Therefore the decay time increases as the liquid crystal volume fraction and thus the droplet size increases reducing the surface to volume ratio. The anomalous drop at 80:20 can be ascribed to the fact that the test cells appear to the eye uneven in their composition, with areas which appear to the eye to have different structures. This would suggest that due to the proximity of the initial temperature composition point to the coexistence curve that the system was not properly phase mixed upon polymerization and as such the morphology developed unevenly. Therefore it could be the case that the areas under study represented morphologies of types associated with a lower liquid crystal volume fraction systems. This can be

seen in the large error bars associated with these results suggesting that each of the test cells was of a different morphology.

As discussed in the introduction, low switching fields and fast switching times are two of the three main requirements of a PDLC based display device, the third is a high contrast ratio. A PDLC film is of no use as a display if it switches quickly and at low field, but has either an off state which scatters only limited light and does not appear white to the eye, or has a high degree of scattering in the on-state and does not appear transparent and colourless. So whilst the switching field results presented above would suggest that the larger droplet sizes at higher liquid crystal volume fractions are better, consideration of the respective transmission properties of the cells needs to be made. Figure 52 shows the on and off state transmissions of systems of each composition along with the contrast ratio (the ratio of the on to the off state transmissions). As would be expected, the smaller the droplet size (lower liquid crystal volume fraction) the greater the number of scattering interfaces, the lower the off state transmission and the whiter the film appears. This is up to the point at which the droplets sizes are less then ~2 μm where the droplets are no longer large enough compared to the wave-length of light that a significant amount of scattering occurs and the film appears less white. This is the reason why the downward trend in off state transmission with decreasing liquid crystal volume fraction demonstrates a turning point at $\phi_{TL213} = 0.72$ as the droplet size becomes too small and transmission starts to increase again.

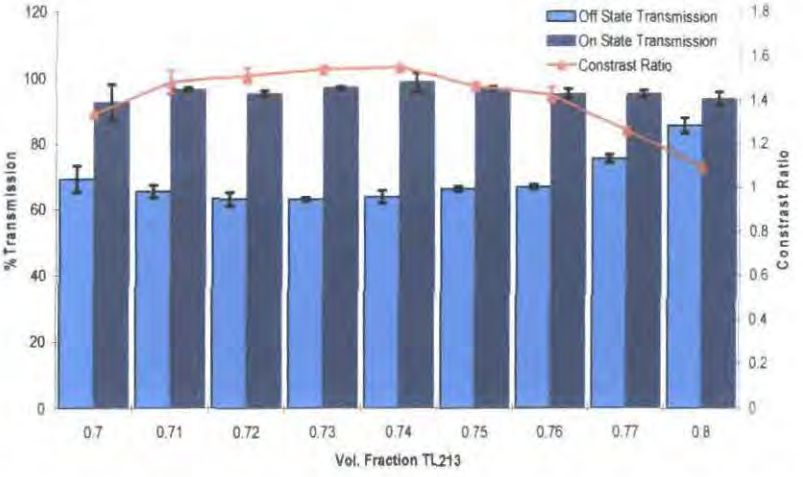

Figure 52 Off and on state %transmissions, and contrast ratios for TL213:2-ethylhexyl acrylate (15% b/v crosslinker) cells of varying composition cured at 303 K under 5000 mWm^{-2} UV (365 nm)

For on-state transmission there is very little difference between films, generally in the range 93-98% of total light. As such it is the off-state transmission which makes the greatest contribution to the contrast ratio. It can be seen that the contrast ratio follows the same trend as the off-state transmission in terms of the films at the two extremes of the compositions studied being the least favourable. As such it can be seen from both a transmission point of view that the best systems are those with compositions in the range 72:28 to 76:24, with an optimum of approximately 73:27. Given that the switching field and rise switching rate improve with increasing liquid crystal volume fraction (although with a plateauing in the E_{90} field at $\phi_{TL213} \approx 0.74$) it would seem that a balance between the electronic and optical properties of the systems can be achieved with a composition of 74:26 or 75:25.

7.1.1.2 Variable Temperature Studies

The initial study has shown that the compositions of most interest for systems cured at 303 K, are those which produce morphologies of size in the range 2-6 μm, which corresponds to systems of composition 73:27 to 75:25. It is shown in sub-section 6, that the morphology is highly dependent upon cure temperature in the composition range of 70:30 to 75:25, it is therefore of interest to see how the electro-optical properties of these systems vary with temperature. Therefore more samples were prepared for systems of composition 70:30, 73:27 and 75:25 at cure temperatures of 293, 313 and 323 K and tested for their electro-optical properties.

Figure 53 to Figure 55 show the electro-optical properties of the films cured at different temperatures for the same composition. The switching field results show interesting trends, for the 73:27 and 75:25 composition cells there is an obvious temperature dependence, as cure temperature increases so does the field required to bring about 90% switching. Whereas for 70:30 films at 303 K and above there is no discernable differences between switching field with temperature change, but when the film is cured at 293 K there is a highly significant drop in switching field from about 3 $V\mu m^{-1}$ to 0.5 $V\mu m^{-1}$. Again as with the compositional switching field studies, the observed results can be explained in terms of the morphological trends previously discussed in subsection 6.

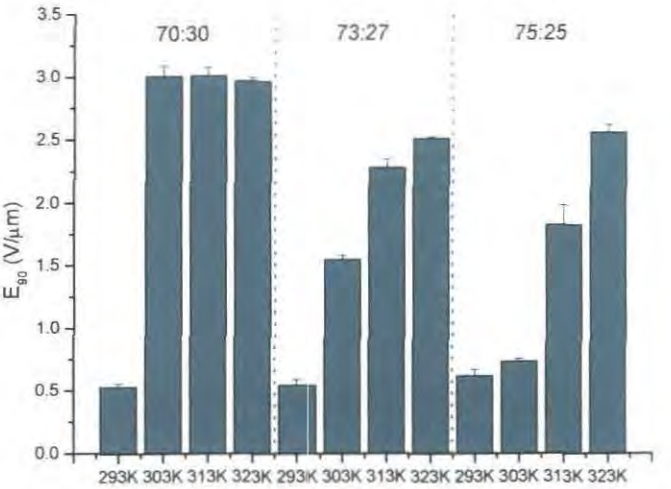

Figure 53 E_{90} switching fields for TL213:2-ethylhexyl acrylate (15% b/v crosslinker) cells of varying composition and cure temperature, cured under 5000 mWm^{-2} UV (365 nm)

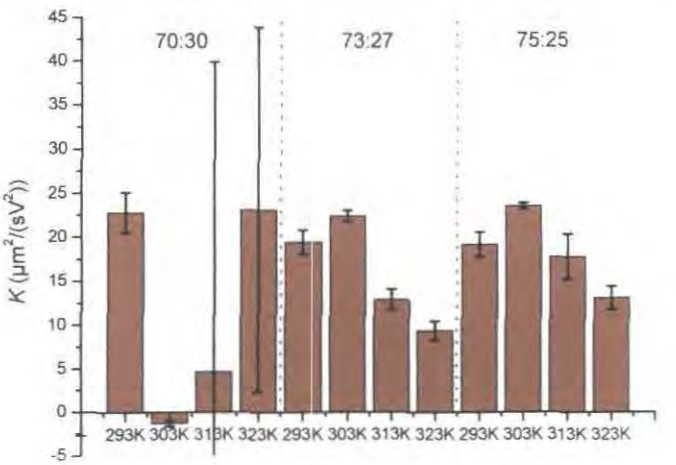

Figure 54 *K* values (related to rise switching rate) for TL213:2-ethylhexyl acrylate (15% b/v crosslinker) cells of varying composition and cure temperature, cured under 5000 mWm^{-2} UV (365 nm)

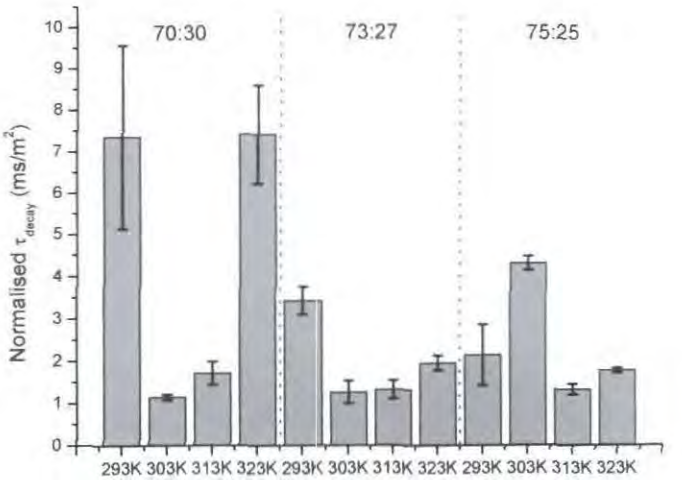

Figure 55 Normalised τ_{decay} for TL213:2-ethylhexyl acrylate (15% b/v crosslinker) cells of varying composition and cure temperature, cured under 5000 mWm^{-2} UV (365 nm)

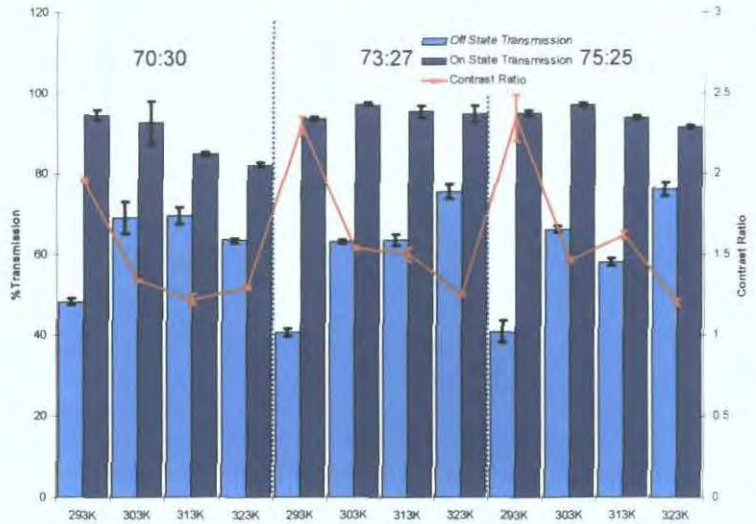

Figure 56 Off and on state %transmissions, and contrast ratios for TL213:2-ethylhexyl acrylate (15% b/v crosslinker) cells of varying composition and cure temperature, cured under 5000 mWm^{-2} UV (365 nm)

Figure 57 shows the ESEM observed morphologies of 70:30 compositional cells cured at difference temperatures, as can be observed the morphologies at cure temperatures of 303 K and above are as normally observed for films of this composition with very small droplet sizes due to the high degree of polymer network formation before phase separation occurs.

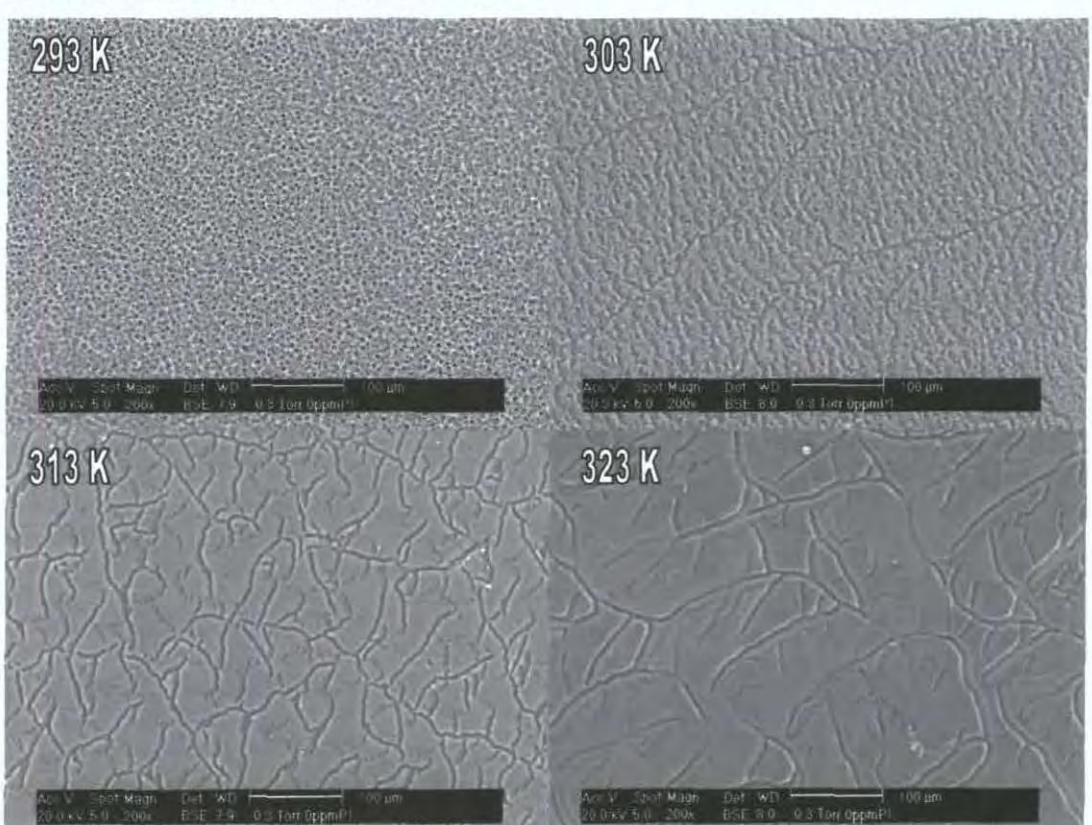

Figure 57 ESEM observed morphology images of electro-optical test cells for TL213 with 2-ethylhexyl acrylate (15% b/v crosslinker) of composition 70:30 cured under 5000 mWm^{-2} intensity UV (365 nm), all images 200x magnification, measure bar is 100 μm

This high degree of network formation acts to suppress phase separation leading to small droplet sizes and a relatively impure liquid crystal phase. This results in the high fields observed to bring about 90% switching. The film cured at 293 K demonstrates a significantly different morphology type than previously observed for 70:30 composition films, there is a well defined droplet morphology of size in the range 3-5 μm. As for other conditions which result in a similar morphology size and structure, these cells have a relatively low 90% switching field, particularly in comparison to other 70:30 composition films. It is the belief of the author that this has resulted from the movement of the initial temperature composition point to much nearer the coexistence curve for the system. So whereas for the films cured at 303 K and above the thermodynamic properties of the system meant that a near infinite network was required to be formed before phase separation became favourable, now a much lower extent of polymerization is required at 293 K. The network now acts to promote phase separation via a gel-demixing mechanism, so these films have a much more well defined and larger droplet morphology and a much purer liquid crystal phase. As observed for the variable composition studies both of these properties act to bring down the field required to bring about 90% switching.

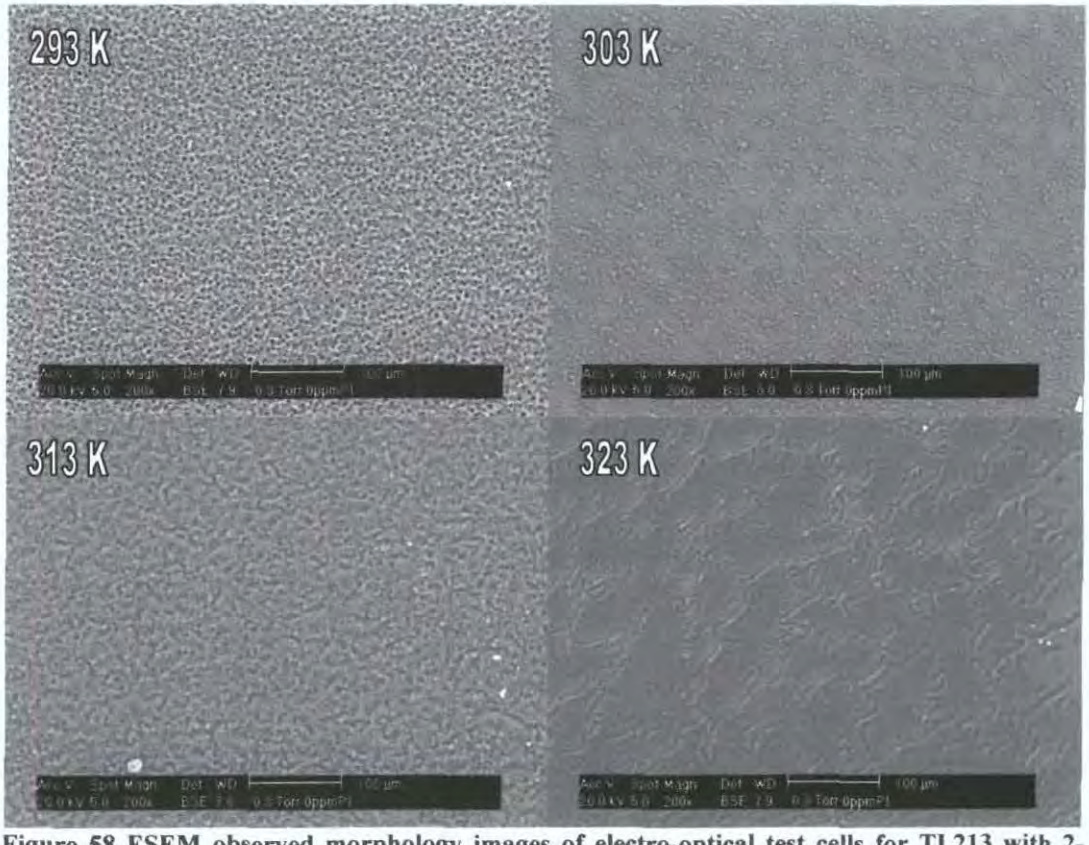

Figure 58 ESEM observed morphology images of electro-optical test cells for TL213 with 2-ethylhexyl acrylate (15% b/v crosslinker) of composition 73:27 cured under 5000 mWm^{-2} intensity UV (365 nm), all images 200x magnification, measure bar is 100 μm

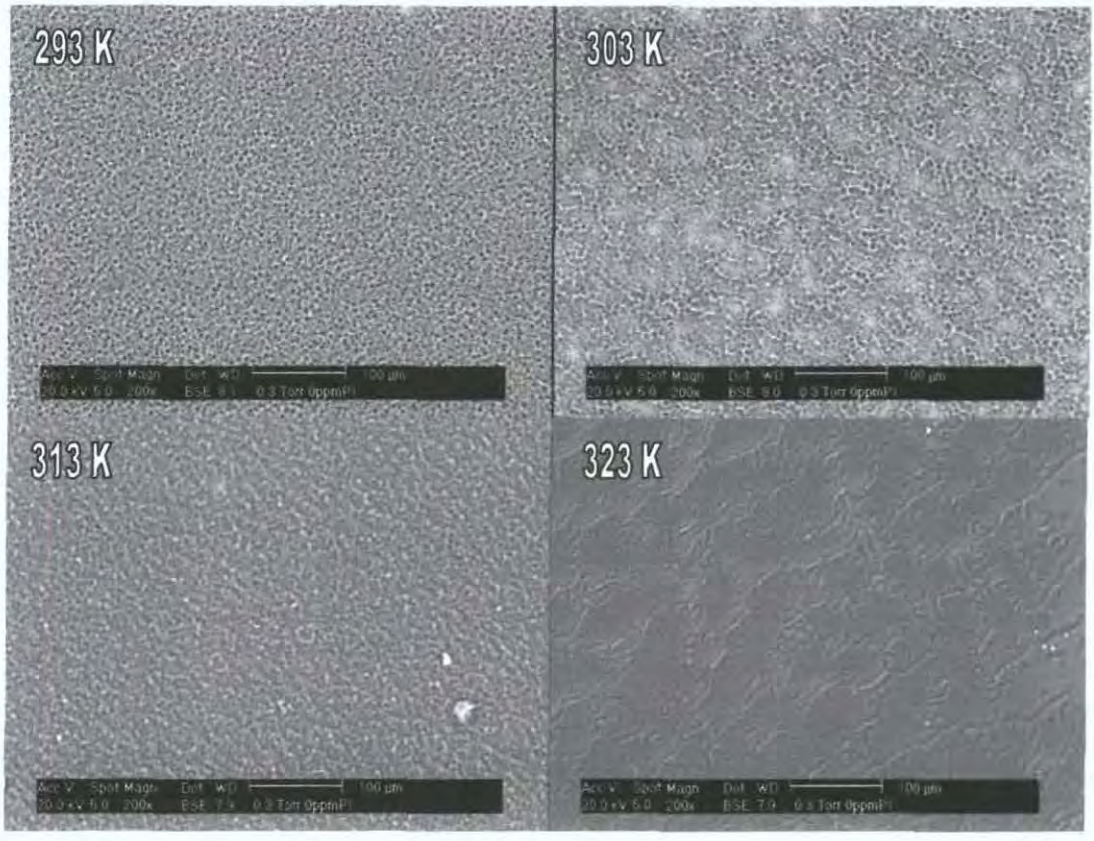

Figure 59 ESEM observed morphology images of electro-optical test cells for TL213 with 2-ethylhexyl acrylate (15% b/v crosslinker) of composition 75:25 cured under 5000 mWm^{-2} intensity UV (365 nm), all images 200x magnification, measure bar is 100 μm

Figure 58 and Figure 59 show the ESEM observed morphologies of example films formed by starting solutions of composition 73:27 and 75:25 at varying cure temperatures. In both instances the morphology size decreases as cure temperature increases as has been previously demonstrated for films of this composition. So the observed increase in E_{90} with increasing cure temperature is due to the decreased volume to interface ratio, which provides more disordering effects which have to be overcome to cause the liquid crystals to switch. For 73:27 the difference in the E_{90} switching field between the 313 K and 323 K films is relatively small compared to that between the 313 K and 303 K films and between the 303 K and 293 K films. This combined with the morphologies observed in Figure 59 which with increasing cure temperature begin to resemble those of the higher cure temperature 70:30 films, with the morphology becoming indistinct and no longer appearing obviously droplet in their form, supports the interpretation of two differing phase separation mechanisms occurring depending upon distance from the coexistence curve. For the higher cure temperature films the thermodynamics of the systems at these temperatures means that the network structure is near universally pervasive when

phase separation becomes favourable suppressing good phase separation, whereas at the lower cure temperatures the network acts to promote phase separation.

As the initial composition of liquid crystal to monomer increases, as shown in section A, the coexistence curve moves closer to room temperature and as such much lower extents of polymerization are required for phase separation to become favourable. This explains why the difference in the switching field for 75:25 composition films cured at 293 K and 303 K is very small (as opposed to quite large for 73:27), and it can be seen from the examples in Figure 59 that the films are both of a droplet morphology type of similar size. It is the belief of the author therefore that as the coexistence curve at this composition is so close to the initial cure temperatures that the difference in the required extent of polymerization to cause phase separation to occur is quite small between the two cure temperatures. The phase separation mechanisms for the two types of films are therefore similar, resulting in very similar physical properties. Combining this with the results for the 73:27 composition films suggests that the relationship of cure temperature with the extent of polymerization required to make phase separation favourable is not linear, and by extension the mechanism by which phase separation occurs and the morphology type formed. It would in-fact appear from the switching field experiments that the dependence is S-shaped with changes in cure temperatures near to the coexistence curve not having much effect as only small increases in the extent of polymerization are needed to initiate phase separation and therefore network formation acts to promote phase separation resulting in relatively large droplet morphologies. As cure temperature is increased a point is reached where the phase separation extent of polymerization starts to increase at a much faster rate due to the entropic contribution to phase mixing becoming more significant than the enthalpic contribution. At this point small increases in cure temperature start to result in very large changes in morphology, with droplet size decreasing significantly, this continues until a temperature is reached where the extent of polymerization required to make phase separation energetically favourable is so high that it is not reached at any temperature above this point until the polymer network formed is near universal. This, as previously discussed, results in phase separation occurring by a different mechanism. The network acts to suppress phase separation giving a morphology which has smaller droplet sizes and a relatively impure liquid crystal phase. Any subsequent increase in cure temperature as such has little effect on the type and size

of morphology formed and therefore a levelling off of switching field at the higher cure temperatures is observed. This is shown schematically in Figure 60 which gives a very approximate relationship between cure temperature and phase separation extent of polymerization – this is only a very schematic relationship based upon interpretation of experimental results and not a mathematical model of the relationship, which is highly complex due to the inclusion of both mixing and polymer network effects, which is beyond the scope of the work presented here.

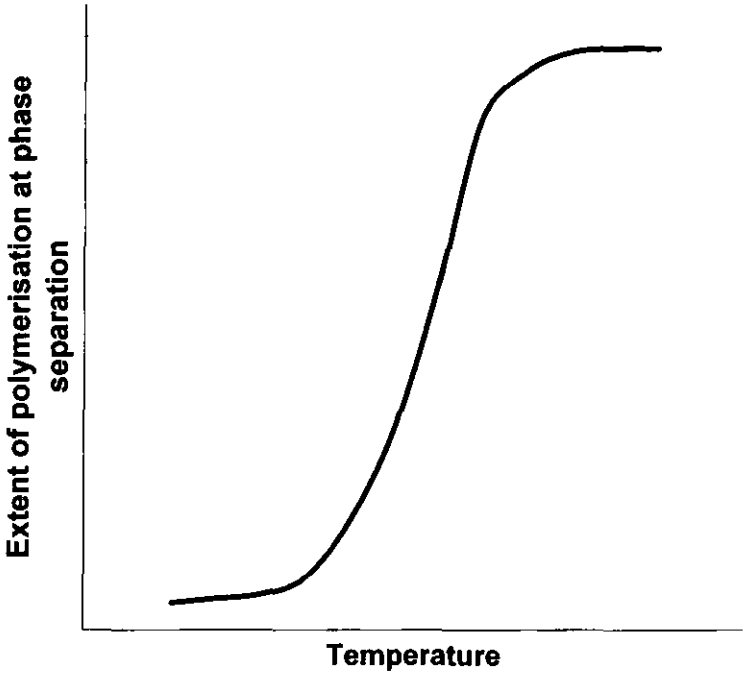

Figure 60 Schematic of the approximate behaviour of phase separation extent of polymerization with cure temperature for a monomer/liquid crystal system for a fixed composition

Figure 54 shows the *K* value switching rates dependence with cure temperature at each composition, as would be expected given the above interpretation of the switching field results for the 73:27 and 75:25 composition films show a decrease in switching rate as cure temperature increases, due to the smaller droplet size. Again as shown by the compositional studies already presented the results for the 70:30 films would suggest that the morphology is of a type and size whereby the *K* value model breaks down.

Figure 55 and Figure 56 show the decay times and optical transmissions and contrast ratios respectively, for different composition films cured at different temperatures. These show rather surprising behaviours, most strikingly there are no real discernable trends in the normalised decay times with changes in temperature of cure. The results would seem to suggest that there is something which is affecting the

decay time performance of the films tested with cure temperature which is independent of the morphology size. A hypothesis for why this occurs is discussed below. Equally the results for the on and off state transmissions seem counterintuitive with off state transmission seeming to increase with increasing cure temperature which is unexpected given that it would be expected that morphology size should get smaller with increasing cure temperature as has been observed. This is countered by the fact that at very small morphology sizes (less than 2 μm) the light is no longer scattered as much due to its closeness in size to the wavelength of light. The on-state transmissions, much like for the composition studies, vary little with varying cure temperature as in all cases little light should be scattered.

As has previously been discussed in Section A, the alignment of liquid crystal molecules is strongly dependent upon temperature. As the temperature increases the enthalpic gain which comes from the liquid crystals being ordered decreases compared to the entropic desire to form a disordered system. It is therefore hypothesised that at higher temperatures it is likely that the liquid crystal will be more disordered during the cure and as such will not create any kind of ordering effect at the polymer liquid crystal interface upon phase separation. As there is less ordering of the polymer during phase separation there will be less ordering effects from the polymer/liquid crystal interface so the contrast in refractive indices is likely to be less. This could equally explain the increase in relaxation time observed with higher cure temperatures for some of the test cells as the polymer interface will be less ordering, and the driving force to disorder will as such be less.

7.2 Conclusion

It has been shown by the work presented above that small changes in cure temperature and initial starting composition can have significant effects on the physical and electro-optical properties of PDLC films. It has also been shown that the changes in properties are due to changes in morphology type and size and as such the type of phase separation mechanism which occurs under each condition. At higher temperatures of cure the extent of polymerization required to make phase separation favourable is large enough that the polymer network is near universal at the point of phase separation and therefore suppresses phase separation resulting in small droplet size and poor switching properties. Whereas at lower temperatures (nearer the coexistence curve) the phase separation extent of polymerization is lower

and as such the polymer network acts to promote phase separation resulting in morphologies with good electro-optical properties. The compositional studies show similar results, with the best shown when the starting point is near to the coexistence curve allowing the polymer network to promote phase separation once it becomes energetically favourable.

Overall it is difficult to define optimal cure conditions and composition for any polymer and liquid crystal system due to the differing thermodynamic dependencies at each composition. This means that the best cure temperature at one composition will be different to that for another composition, and may again be completely different for a chemically different liquid crystal/monomer mix. From the work presented the optimum conditions for TL213 with 2-EthylHexyl Acrylate are for ϕ_{TL213} 0.73 to 0.76 and cure temperature in the range 293 K to 303 K.

8 Conclusions

It has been shown through the work presented in this section that the morphology of a PDLC films is highly dependent upon the mechanism by which phase separation occurs, and that by extension the electro-optical properties which are dependent upon the morphology are also dependent upon the phase separation mechanism.

It is the belief of the author that phase separation occurs by one of two main mechanisms, a gel deswelling mechanism or a viscoelastic transient gel mechanism, with a third mechanism demonstrating a hybrid of the properties of the first two mechanisms. Both the main mechanisms are based around the concept of a polymer network being able to stretch to absorb a solvent species; in a gel deswelling mechanism the network is formed by permanent chemical crosslinks and in the viscoelastic by the formation of transient crosslinks from two polymer chains entwining. In the former case the polymer network acts to suppress phase separation as for phase separation to occur requires the formation of solvent droplets within the polymer network resulting in significant energetically unfavourable polymer chain stretching. The result of this is that when PDLCs phase separate by this mechanism the morphologies formed are generally of a small droplet size and have a relatively impure liquid crystal phase, leading to high switching fields and slow rise times. In viscoelastic phase separation as the crosslinks are only temporary so the network can break up to allow solvent droplets to nucleate; as such the network acts to promote

phase separation as it is energetically favourable for the polymer chains to contract and force out the solvent. This mechanism only occurs in its truest form when there is no crosslinker present, this means there is nothing to cause phase separation to cease and freeze the morphology. As such phase separation continues until an equilibrium state of a polymer rich phase within a sea of liquid crystal is formed. This is of no use for display devices made from PDLCs.

As stated there is, depending upon conditions, a third mechanism combining properties of both the two former mechanisms. Under the right composition and temperature conditions phase separation can be initiated in a liquid crystal/polymer solution, which contains a crosslinker, before the polymer network has had a chance to significantly form. In these circumstances the network which has formed will act to promote phase separation, as in viscoelastic phase separation, giving the larger droplet sizes required for good switching fields, while the presence of the crosslinking species means the morphology is frozen before it is able to reach an equilibrium state and loose its morphological structure.

The work presented has shown that in the presence of a crosslinker the mechanism by which phase separation occurs depends upon the distance of the initial composition temperature point from the coexistence curve. The further the initial point from the curve the higher the extent of polymerization required for phase separation to become favourable and therefore the more extensive will be the development of the polymer network. As such the further you are initially from the coexistence curve the smaller the droplet size and the more impure the liquid crystal phase.

The work in the final part of this section has shown that the morphologies which provide the most favourable switching fields are those which undergo phase separation by the hybrid mechanism and form relatively large (3-5 μm) sized droplets and pure liquid crystal phases. As such the best conditions for the formation of PDLCs are to be found at those temperature composition points which are near to the coexistence curve, although if it is too near to the coexistence curve the network development won't be great enough to freeze the morphology at a droplet size small enough to give good optical contrast.

Bibliography

1. Cahn, J. W.; Hilliard, J. E. *Journal of Chemical Physics* **1959,** 31, 688-699.
2. Jones, R. A. L.; Richards, R. W., Polymer/polymer interfaces. In *Polymers at Surfaces and Interfaces*, 1st ed.; Cambridge University Press: Cambridge, 1999; pp 152-183.
3. Matsuyama, A.; Evans, R. M. L.; Cates, M. E. *European Physical Journal E* **2002,** 9, 89-95.
4. Cahn, J. W. *Journal of Chemical Physics* **1965,** 42, 93-&.
5. Nakazawa, H.; Fujinami, S.; Motoyama, M.; Ohta, T.; Araki, T.; Tanaka, H.; Fujisawa, T.; Nakada, H.; Hayashi, M.; Aizawa, M. *Computational and Theoretical Polymer Science* **2001,** 11, 445-458.
6. Johnson Jr., C. S.; Gabriel, D. A., *Laser Light Scattering*. 1st ed.; Dover Publications Inc.: 1981.
7. Maugey, J.; Navard, P. *Polymer* **2002,** 43, 6829-6837.
8. Maugey, J.; Van Nuland, T.; Navard, P. *Polymer* **2001,** 42, 4353-4366.
9. Elicabe, G. E.; Larrondo, H. A.; Williams, R. J. J. *Macromolecules* **1997,** 30, 6550-6555.
10. Elicabe, G. E.; Larrondo, H. A.; Williams, R. J. J. *Macromolecules* **1998,** 31, 8173-8182.
11. Dusek, K. *Journal of Polymer Science Part C-Polymer Symposium* **1967,** 1289-&.
12. Dusek, K.; Patterso.D. *Journal of Polymer Science Part a-2-Polymer Physics* **1968,** 6, 1209-&.
13. Flory, P. J. *Journal of Chemical Physics* **1950,** 18, 108-111.
14. Flory, P. J., In *Principles of Polymer Chemistry*, 1st. ed.; George Banta Publishing: Menasha, 1953; pp 577-593.
15. Flory, P. J. *Journal of the American Chemical Society* **1956,** 78, 5222-5234.
16. Flory, P. J.; Rehner, J. *Journal of Chemical Physics* **1944,** 12, 412-414.
17. Hermans, J. J. *Journal of Polymer Science* **1962,** 59, 191-&.
18. Flory, P. J.; Rehner, J. *Journal of Chemical Physics* **1943,** 11, 521-526.
19. Henderson, I. C.; Clarke, N. *Journal of Chemical Physics* **2005,** 123, -.
20. Flory, P. J.; Rehner, J. *Journal of Chemical Physics* **1943,** 11, 512-520.
21. Moerkerke, R.; Koningsveld, R.; Berghmans, H.; Dusek, K.; Solc, K. *Macromolecules* **1995,** 28, 1103-1107.
22. Dusek, K.; Prins, W. *Advanced Polymer Science* **1969,** 6, 1-102.
23. James, H. M.; Guth, E. *Journal of Chemical Physics* **1953,** 21, 1039-1049.
24. James, H. M.; Guth, E. *Journal of Chemical Physics* **1947,** 15, 669-683.
25. Gottlieb, M.; Gaylord, R. J. *Macromolecules* **1984,** 17, 2024-2030.

26. Petrovic, Z. S.; Macknight, W. J.; Koningsveld, R.; Dusek, K. *Macromolecules* **1987,** 20, 1088-1096.

27. West, J. L. *Molecular Crystals and Liquid Crystals* **1988,** 157, 427-441.

28. Golemme, A.; Zumer, S.; Doane, J. W.; Neubert, M. E. *Physical Review A* **1988,** 37, 559-569.

29. Doane, J. W.; Vaz, N. A.; Wu, B. G.; Zumer, S. *Applied Physics Letters* **1986,** 48, 269-271.

30. Carter, S. A.; LeGrange, J. D.; White, W.; Boo, J.; Wiltzius, P. *Journal of Applied Physics* **1997,** 81, 5992-5999.

31. LeGrange, J. D.; Carter, S. A.; Fuentes, M.; Boo, J.; Freeny, A. E.; Cleveland, W.; Miller, T. M. *Journal of Applied Physics* **1997,** 81, 5984-5991.

32. Kim, J. Y.; Cho, C. H.; Palffymuhoray, P.; Mustafa, M.; Kyu, T. *Physical Review Letters* **1993,** 71, 2232-2235.

33. Kim, J. Y.; Palffy-Muhoray, P. *Molecular Crystals and Liquid Crystals* **1991,** 203, 93-100.

34. Nephew, J. B.; Nihei, T. C.; Carter, S. A. *Physical Review Letters* **1998,** 80, 3276-3279.

35. Nwabunma, D.; Chiu, H.-W.; Kyu, T. *Macromolecules* **2000,** 33, 1416-1424.

36. Amundson, K.; vanBlaaderen, A.; Wiltzius, P. *Physical Review E* **1997,** 55, 1646-1654.

37. Lovinger, A. J.; Amundson, K. R.; Davis, D. D. *Chemistry of Materials* **1994,** 6, 1726-1736.

38. Drzaic, P. S. *Journal of Applied Physics* **1986,** 60, 2142-2148.

39. Rajesh, K.; Kikuchi, H.; Stark, M.; Guckenberger, R.; Kajiyama, T. *Molecular Crystals and Liquid Crystals Science and Technology Section a-Molecular Crystals and Liquid Crystals* **1999,** 329, 783-+.

40. Coates, D. *Journal of Materials Chemistry* **1995,** 5, 2063-2072.

41. Smith, G. W. *Physical Review Letters* **1993,** 70, 198-201.

42. Smith, G. W. *Molecular Crystals and Liquid Crystals Science and Technology Section a-Molecular Crystals and Liquid Crystals* **1994,** 239, 63-85.

43. Nwabunma, D.; Kyu, T. *Polymer* **2001,** 42, 801-806.

44. Nwabunma, D.; Kim, K. J.; Lin, Y. H.; Chien, L. C.; Kyu, T. *Macromolecules* **1998,** 31, 6806-6812.

45. Bhargava, R.; Wang, S. Q.; Koenig, J. L. *Macromolecules* **1999,** 32, 2748-2760.

46. Serbutoviez, C.; Kloosterboer, J. G.; Boots, H. M. J.; Touwslager, F. J. *Macromolecules* **1996,** 29, 7690-7698.

47. Grand, C.; Achard, M. F.; Hardouin, F. *Liquid Crystals* **1997,** 22, 287-296.

48. Motoyama, M.; Nakazawa, H.; Ohta, T.; Fujisawa, T.; Nakada, H.; Hayashi, M.; Aizawa, M. *Computational and Theoretical Polymer Science* **2000,** 10, 287-297.

49. Serbutoviez, C.; Kloosterboer, J. G.; Boots, H. M. J.; Paulissen, F. A. M. A.; Touwslager, F. J. *Liquid Crystals* **1997,** 22, 145-156.

50. Nwabunma, D.; Kyu, T. *Macromolecules* **1999,** 32, 664-674.

51. Smith, G. W. *Molecular Crystals and Liquid Crystals* **1993,** 225, 113-130.

52. Teixeira, P. I. C.; Mulder, B. M. *Journal of Chemical Physics* **1996,** 105, 10145-10152.

53. Dorgan, J. R. *Journal of Chemical Physics* **1993,** 98, 9094-9106.

54. Chan, P. K.; Rey, A. D. *Macromolecules* **1996,** 29, 8934-8941.

55. Chan, P. K.; Rey, A. D. *Macromolecules* **1997,** 30, 2135-2143.

56. Young, R. J.; Lovell, P. A., Rate of Polymerization. In *Introduction to Polymers*, 2nd ed.; Chapman & Hall: London, 1991; pp 47-50.

57. Tanaka, H. *Journal of Physics-Condensed Matter* **2000,** 12, R207-R264.

58. Henderson, I. C.; Clarke, N. *Macromolecules* **2004,** 37, 1952-1959.

59. Tanaka, H. *Physical Review Letters* **1993,** 71, 3158-3161.

60. Tanaka, H. *Journal of Chemical Physics* **1994,** 100, 5323-5337.

61. Tanaka, H. *Physical Review Letters* **1996,** 76, 787-790.

62. Tanaka, H. *Physical Review E* **1997,** 56, 4451-4462.

63. Gan, W. J.; Yu, Y. F.; Wang, M. H.; Tao, Q. S.; Li, S. J. *Macromolecules* **2003,** 36, 7746-7751.

64. Murata, K.; Sachin, J.; Etori, H.; Anazawa, T. *Polymer* **2002,** 43, 2845-2859.

65. Wang, M. H.; Yu, Y. F.; Wu, X. G.; Li, S. J. *Polymer* **2004,** 45, 1253-1259.

66. Yu, Y. F.; Wang, M. H.; Gan, W. J.; Tao, Q. S.; Li, S. J. *Journal of Physical Chemistry B* **2004,** 108, 6208-6215.

Section C – Effect of Fluorine Doping of the Polymer Matrix on PDLC Morphological and Electro-optical Properties

1 Background

1.1 Concept

The work presented in the majority of this report is concerned with the effect of physical variables upon both the morphological and electro-optical properties of PDLCs, and as such has centred on a single monomer liquid crystal pair. No work has as yet been presented herein into the effect of chemistry upon both the way in which phase separation occurs, the morphologies formed and the effect upon the switching properties of the liquid crystals.

As discussed in the main introduction, one of the aims of the work is to reduce the electric field strength and the time required to achieve 90% switching to the on state, which is dependent upon the disordering effects at the liquid crystal/polymer interface which act against ordering the liquid crystal molecules. It is therefore the main aim of the work presented in this section to see if the introduction of a highly fluorinated monomer species, which will be highly electronegative and therefore electronically repulsive to the halogenated liquid crystal species, will have the effect of reducing the anchoring energy at the interface and therefore the disordering force. Much work[1-4] has been performed into the effects of different liquid crystal species upon the electro-optical properties of PDLCs; including the use of halogenated liquid crystals[3] and the improvements in performance these give. Little work has been performed with the specific aim of attempting to control electro-optical properties through the use of chemically different monomer species and in particular fluorinated monomer species.

Previous work into the area has been performed by Heavin et al.[5] looking at the fluorine doping of thermo-polymerised epoxy polymers with the cyano-biphenyl based liquid crystal blend E7. In their study they noted that the fluorine doping resulted in an increase in switching voltages, but that this was matched by an improved phase separation evidenced by improved contrast ratios resulting from the sharper polymer/liquid crystal interface giving more off state scattering. Schulte et al.[6, 7], have also performed studies into fluorine doping of the polymer species in

PDLCs; their work was centred on holographic-PDLCs, these are PDLC films which have been selectively cured to form nano-scale arrays of distinct polymer and liquid crystal lines for use as volume gratings, this field of study is beyond the scope of this report. The work was also performed using a 50:50 liquid crystal:monomer system which resulted in a bead type morphology, with domain size in the order of 100s of nanometres (a result of the desire to produce HPDLCs) rather than the micrometer scale droplet morphologies more normally associated with optimum display screen applications. Again the liquid crystal used was E7, and their results showed that there was a slight decrease in switching voltage with increased fluorine doping. They also noted as Heavin et al. did that morphology size increased with increased fluorine doping, but did not relate this to the effects of fluorine on the phase properties of the system and subsequently the way in which the system phase separated.

The work of both groups was performed using the cyano-biphenyl liquid crystal blend E7, and not with a halogenated species. All the work noted the effect of fluorine doping upon morphologies formed, and sometimes the subsequent improvements in switching voltages, but that this was not necessarily the case. These results would appear to dispel the idea that fluorine doping has the effect of reducing the anchoring energy with liquid crystals. This work however has not investigated the use of halogenated liquid crystals with fluorinated polymers, which should, it is hoped, due to their equally high electronegativities be more repulsed by the fluorinated polymer and the anchoring energy be thus reduced.

None of these papers which have identified the effect of fluorine doping upon PDLC morphology have attempted to relate these changes to the effect of fluorine monomers upon the liquid crystal/monomer phase properties and subsequently the mechanism by which phase separation occurs. This leaves an area of great interest to be investigated, which is a focus of the work presented.

2 Aims of Work

It is the aim of the work presented herein to investigate the effects of fluorination of the monomer species of PDLCs formed from an acrylate monomer with a halogenated liquid crystal blend, using initial compositions and cure temperatures which are most applicable for display screen devices, on PDLC electro-optical properties. It is the subsequent aim to be able to attempt to explain these in terms of the effect of fluorination upon anchoring energy, phase separation mechanism and

therefore morphologies formed, and finally to appraise on the possibility of using fluorine doping as a method for improving PDLC display screen technologies.

Three particular areas of interest have been identified in selecting the system for study; these are to investigate the effect of fluorine doping the polymer matrix when the liquid crystal blend contains halogenated species. Secondly to investigate the important of phase properties in the way that fluorine doping affects the morphologies of PDLCs, and finally to investigate the affect of fluorine doping upon the, as discussed in section B, interesting morphological properties of PDLC films formed from TL213 with acrylate monomers at high liquid crystal volume fractions.

3 Systems under Study

As for most of the previous studies presented in this report the liquid crystal/monomer system to be used as the base for the all experiments is TL213 liquid crystal blend with 2-EthylHexyl Acrylate so as to make comparison possible. Two fluorinated monomer species have been used 2,2,3,3,4,4,4-heptafluorobutyl acrylate (HFBA) and 2,2,3,3,4,4,5,5,6,6,7,7,7,-dodecafluoroheptyl acrylate (DDFHA), their structures can be found in the experimental section. The aim of using two different fluorinated monomer species is to make it possible to determine whether the effects of fluorination are related to the amount of fluorine present, or the number of fluorinated monomer units as a proportion of total monomer units; as HFBA and DDFHA have seven and thirteen fluorine atoms per monomer unit respectively. It is hoped that this will help in determining if the effect of fluorination is as a result of reduced anchoring energy or morphological properties.

All cells under test are prepared at 75:25 TL213:monomer, cured at 303K under 5000 mWm^{-2} as this has been shown by the work presented in section B to produce good electro-optical properties for the undoped 2-ethylhexyl acrylate PDLCs at 303 K. Cells are prepared containing an undoped monomer solution, and 4, 8, 14, 22mol% of each of the two fluorinated monomer species, so as to give a spread of fluorine doping amounts to see if any trends can be discerned. Electro-optical testing as previously described in the experimental section is then performed.

4 Electro-optical Studies

4.1 Results and Discussion

It can be seen in Figure 1 and Figure 2 that compared to undoped PDLC samples both heptafluorobutyl acrylate and dodecafluoroheptyl acrylate can result in a reduction in the E_{90} switching field. It is not however a simple relationship with increasing fluorine doping resulting in decreasing switching field.

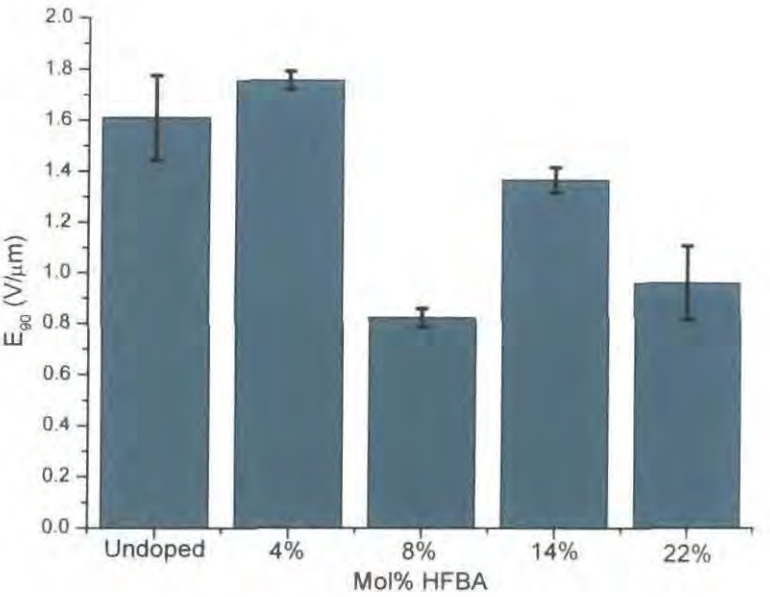

Figure 1 E_{90} switching fields for 75:25 TL213:2-ethylhexyl acrylate (15% b/v crosslinker) doped with varying mol% of heptafluorobutyl acrylate, cured at 303 K under 5000 mWm^{-2} UV (365 nm)

For heptafluorobutyl acrylate there is an increase in the switching field for 4mol% doping compared to the undoped film, this is likely to be due to experimental error rather than an effect of the doping as the increase is so small compared to the undoped cells. It can be reasonably assumed at this low doping percentage that there is no great effect. Upon 8mol% doping there is an approximately 50% drop in E_{90} from 1.6 V/μm to 0.8 V/μm, suggesting that the fluorine doping has had a significant effect upon some property of the PDLC films. Subsequently there is an increase in the switching field as doping increases to 14mol%.

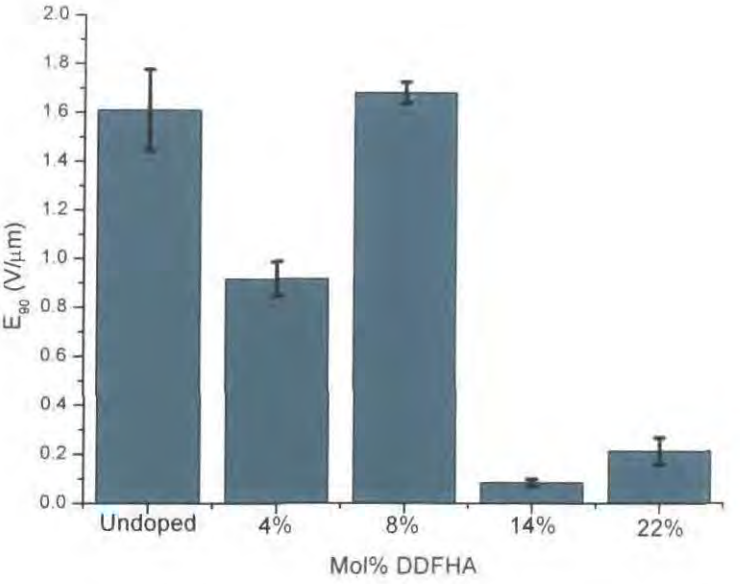

Figure 2 E_{90} switching fields for 75:25 TL213:2-ethylhexyl acrylate (15% b/v crosslinker) doped with varying mol% of dodecafluoroheptyl acrylate, cured at 303 K under 5000 mWm^{-2} UV (365 nm)

Equally in Figure 2 for dodecafluoroheptyl acrylate there is similar decrease in switching field compared to the undoped PDLCs for 4mol% doping and then again an increase in field with additional doping to 8mol%. Unlike for the heptafluorobutyl acrylate, there is a significant decrease in switching field with dopings of 14 & 22 mol%. This suggests that there has been a significant change in the system at these dopings.

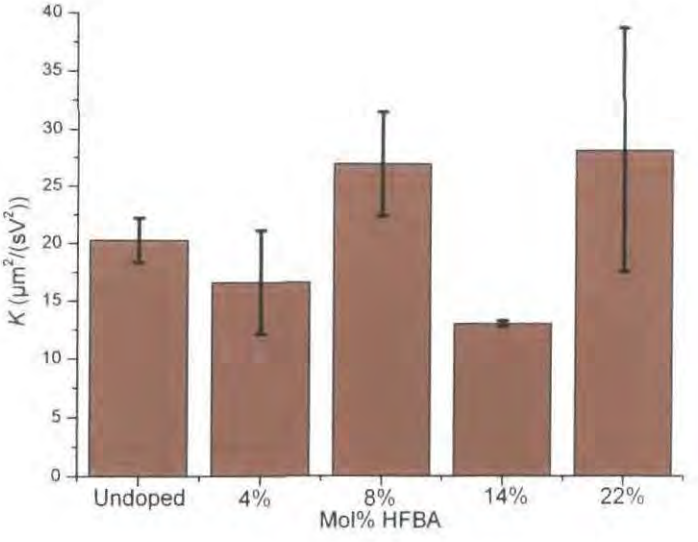

Figure 3 *K* values for 75:25 TL213:2-ethylhexyl acrylate(15% b/v crosslinker) doped with varying mol% of heptafluorobutyl acrylate, cured at 303K under 5000 mWm^{-2} UV (365 nm)

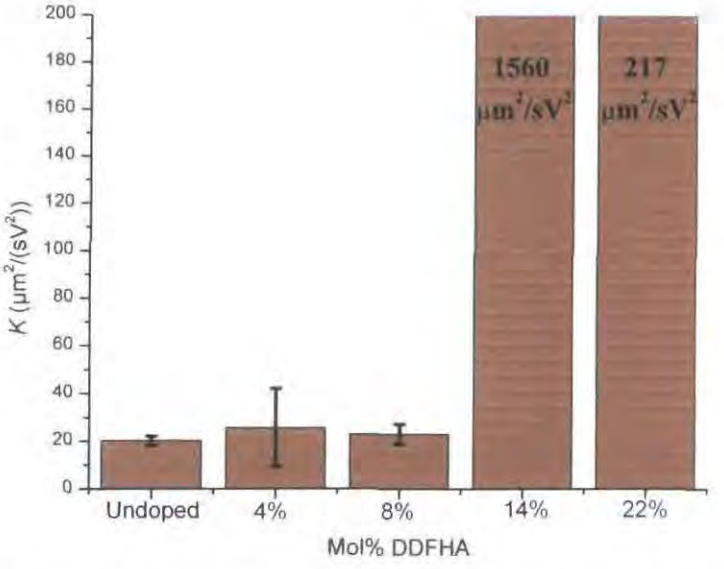

Figure 4 *K* values for 75:25 TL213:2-ethylhexyl acrylate (15% b/v crosslinker) doped with varying mol% of dodecafluoroheptyl acrylate, cured at 303K under 5000 mWm^{-2} UV (365 nm). The results for 14 mol% & 22mol% are much larger than the maximum of the graph

Figure 3 and Figure 4 show that similar reciprocal behaviours can be seen for the *K* value switching rates (low switching field has a high switching rate), with dopings of 8mol% heptafluorobutyl acrylate and 4mol% dodecafluoroheptyl acrylate showing significant increases compared to the undoped films. These results suggest one of two possibilities, that the decreases observed in switching field are either due to a reduction in the anchoring energy at the interface or a change in the morphology. As there is a subsequent increase in switching field with increasing mol%, it would seem more likely that the observed changes are due to morphology effects as you would expect if it were an anchoring energy effect that E_{90} would continue to decrease with increasing mol%. Figure 5 shows the ESEM observed morphologies of films doped with varying amounts of heptafluorobutyl acrylate, it can be seen that with 4 and 8mol% HFBA doping the size of the droplets have increased. This therefore suggests that the observed decrease in switching field with 8mol% doping of heptafluorobutyl acrylate compared to undoped films is as a result of a larger volume to disordering interface ratio. Therefore there are less disordering forces to overcome to achieve 90% switching, and as such a lower field is required. It can also be seen that upon increasing the doping to 14mol% there is a change in the morphology again; it appears to become more indistinct and have a smaller droplet size, this explains the observed subsequent increase in the switching field at 14mol% doping as the smaller droplets will have a lower volume to disordering interface ratio and therefore more disordering effects to overcome.

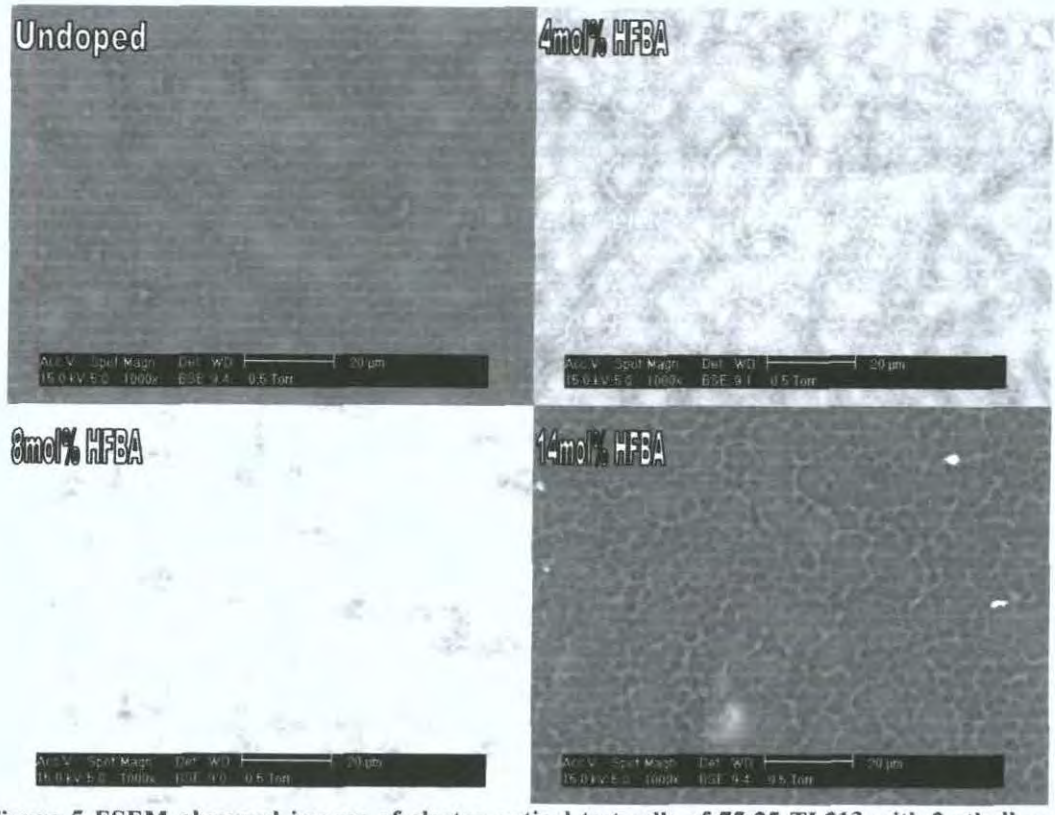

Figure 5 ESEM observed images of electro-optical test cells of 75:25 TL213 with 2-ethylhexyl acrylate (15% b/v crosslinker) with varying doping mol% of heptafluorobutyl acrylate, all films cured at 303 K under 5000 mWm^{-2} UV (365 nm), 1000x magnification, measure bar is 20 μm

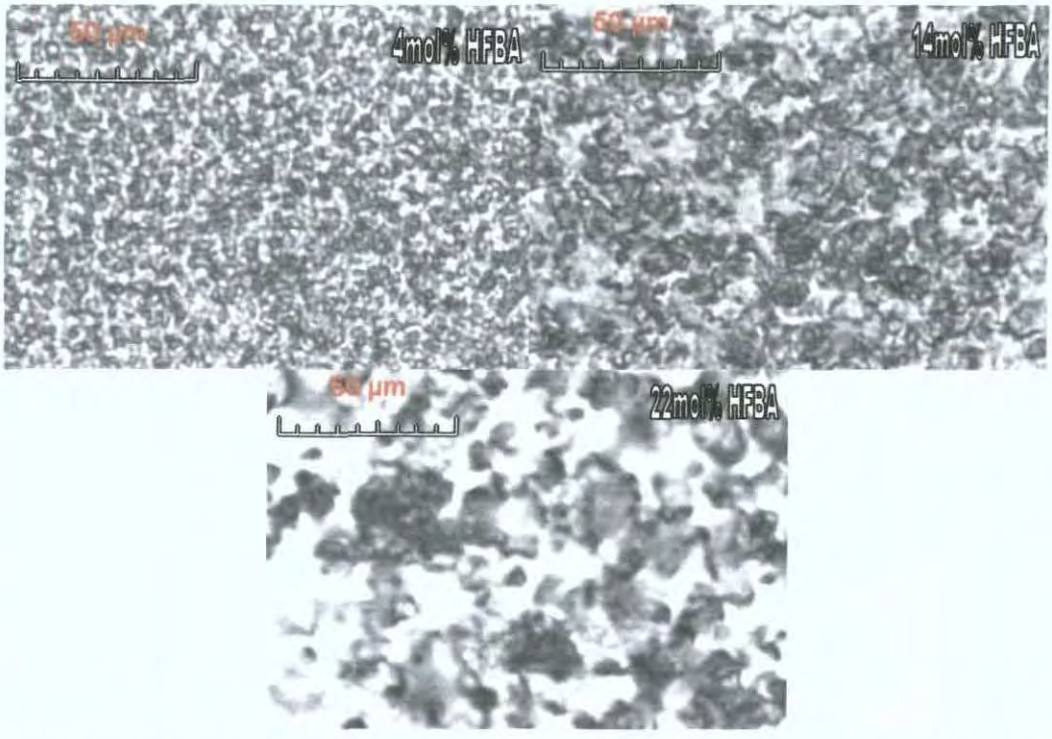

Figure 6 Confocal microscope observed images of electro-optical test cells of 75:25 TL213 with 2-ethylhexyl acrylate (15% b/v crosslinker) with varying doping mol% of heptafluorobutyl acrylate, all films cured at 303 K under 5000 mWm^{-2} UV (365 nm)

At 22mol% doping when observed with the naked eye the PDLCs appear to have formed two distinct morphological areas which cannot be imaged well by ESEM, instead Figure 6 shows confocal microscope observed images of films with 4mol%

14mol% and 22mol% doping. It can be clearly seen in these images that the morphologies formed at 14 and 22mol% are no longer the droplet type morphologies observed at lower doping mol% which provide the desired electro-optical properties for display devices. As the 22mol% cells lack any consistent morphology their electro-optical results cannot be effectively interpreted.

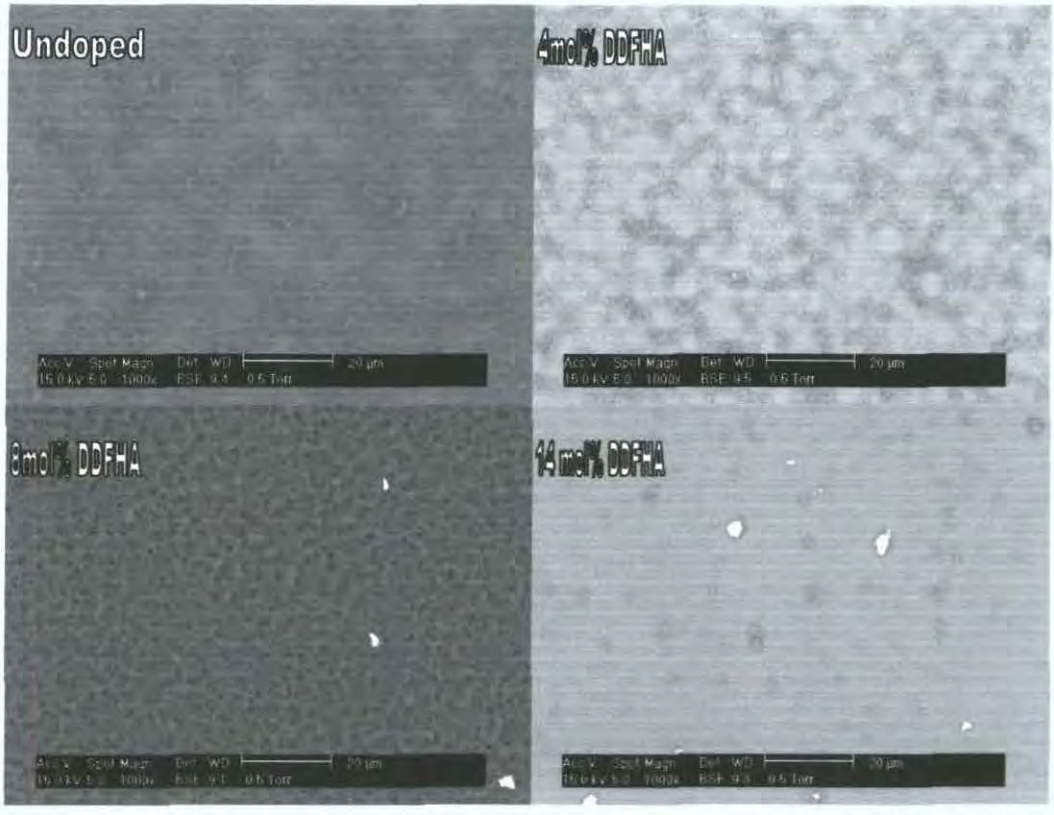

Figure 7 ESEM observed images of electro-optical test cells of 75:25 TL213 with 2-ethylhexyl acrylate (15% b/v crosslinker) with varying doping mol% of dodecafluoroheptyl acrylate, all films cured at 303 K under 5000 mWm^{-2} UV (365 nm), 1000x magnification, measure bar is 20 μm

Figure 7 shows the ESEM observed images for the dodecafluoroheptyl acrylate doped films, again as for the heptafluorobutyl acrylate doped films it can be seen that initial doping with fluorinated monomer results in an increase in droplet size (4mol% doping). Upon 8mol% doping a similar morphology type as for 14mol% of heptafluorobutyl acrylate can be observed, with the smaller droplet size. As for the heptafluorobutyl acrylate this morphology type results in an increase in the switching field required to obtain 90% switching back up to the field required for undoped samples. This would seem to support the hypothesis that the observed improvements in switching field and *K* value switching rates with fluorine doping are as a result of changes in the film morphology rather than changes in the liquid crystal anchoring energy at the interface.

It can be seen from Figure 2 that for films doped with 14 and 22mol% dodecafluoroheptyl acrylate that the switching field drops significantly to fields in the range 0.1 to 0.2 V/μm. These are switching fields which are more commonly associated with pure liquid crystal cells, rather than a polymer encapsulated liquid crystal; this suggests that the morphology formed is no longer that of a droplet PDLC. The results in Figure 4 also show that the switching rates are so fast compared to the lower doping mol% films that they cannot be shown effectively on the same graph. The ESEM images in Figure 7 for 14mol% doping are unclear as to the kind of morphology formed; after opening the cells and washing out the free liquid crystal what is left appears to be a thin polymer film of indistinct morphology, with possible droplets of polymer.

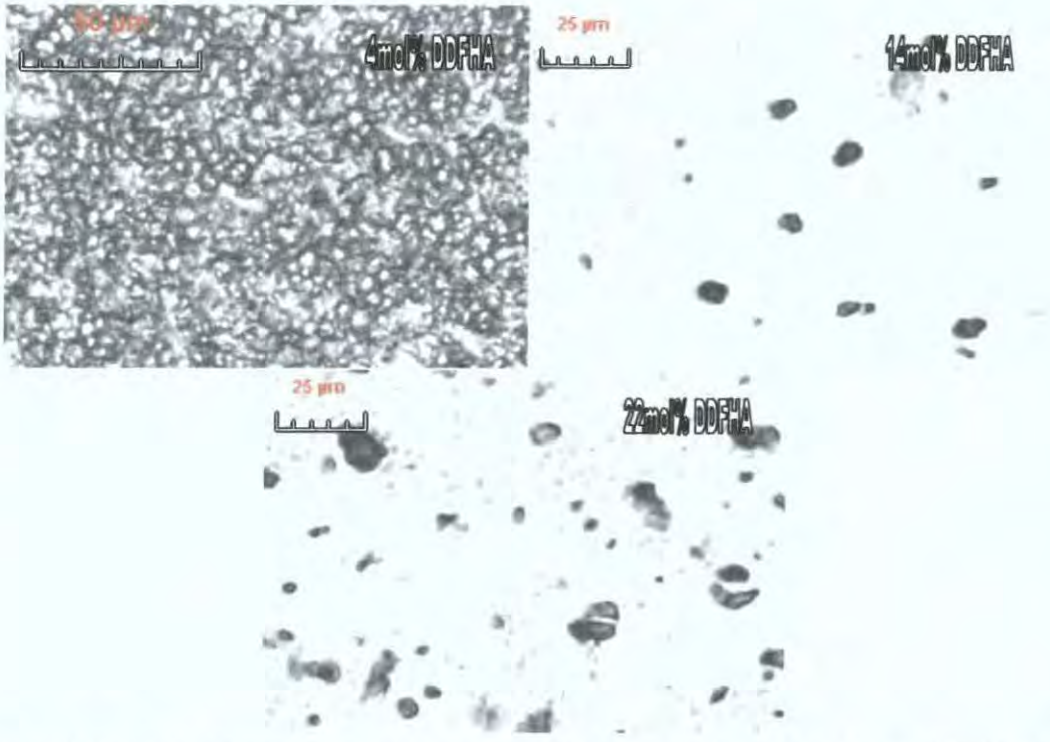

Figure 8 Confocal microscope observed images of electro-optical test cells of 75:25 TL213 with 2-ethylhexyl acrylate (15% b/v crosslinker) with varying doping mol% of dodecafluoroheptyl acrylate, all films cured at 303 K under 5000 mWm^{-2} UV (365 nm)

Figure 8 shows confocal microscope images of cells with 4, 14 and 22mol% doping; this technique doesn't require the cells to be broken open and the liquid crystal washed out, so the morphology can be observed in-situ. From the 4mol% doped film, which has a classic PDLC droplet morphology, it can be seen that the polymer under the confocal microscope forms dark areas whereas the free liquid crystal forms light areas, based upon this the microscope images of the 14 and 22mol% films would appear to suggest that what has formed is droplets of polymer within a sea of liquid crystal, rather than the droplets of liquid crystal encapsulated within a polymer

network. This was confirmed by observing the film under the microscope with polarizers. For this reason the sample cells are no longer acting as PDLCs but liquid crystals in the presence of disordering point defects in the form of the polymer droplets; this results in the significantly lower switching fields and higher K value switching rates for these systems, as less disordering forces need to be overcome. The reason for this change in morphology type with increasing fluorine doping is likely to be as a result of changes in phase properties of the uncured system with increasing fluorine doping. It is shown in Section A that as the mol% of fluorine doped in the monomer fraction increases so does the phase mixing temperature for a given liquid crystal volume fraction.

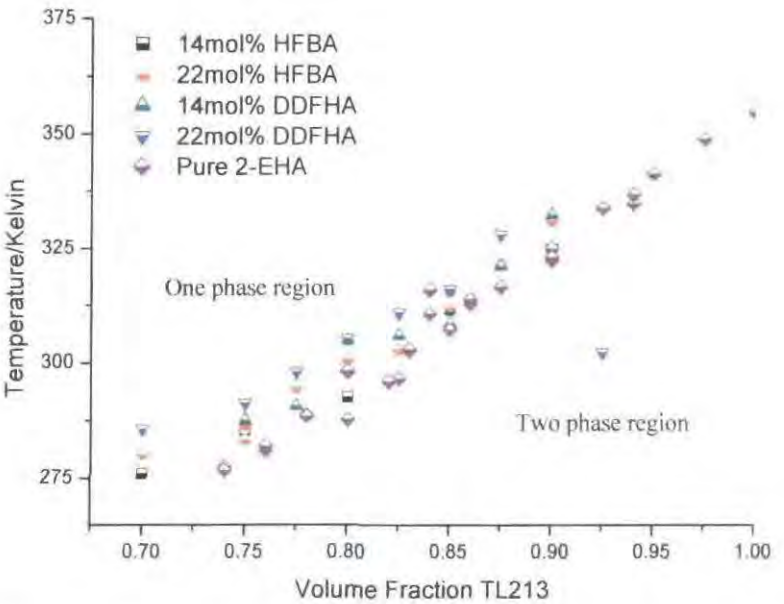

Figure 9 Phase mixing curves for TL213 with 2-ethylhexyl acrylate doped with varying amounts of fluorinated monomer units

Figure 9 shows the unpolymerized phase mixing curves for the systems under test for their electro-optical properties; as the fluorine doping increases the phase curves move higher, although the increase as observed is only slight. As discussed in Section A, it is hard to determine the exact phase mixing temperatures for the undoped TL213:2-ethylhexyl acrylate system due to the proximity of the T_{NI} boundary to the phase mixing temperatures; as such the effect of the doping on the phase properties could be more pronounced than the results suggest. It would seem likely therefore that, while the systems are not in the two phase region at 303 K before polymerisation, it is the case that the degree of polymerisation required to make phase separation favourable is small. It is likely to be the case that for the 14

and 22 mol% dodecafluoroheptyl acrylate doped samples, that phase separation commences before the monomers have had much of a chance to form a polymer network which can act to suppresses phase separation and diffusion. Instead upon initiation of phase separation the monomer has diffused out of the liquid crystal and polymerised in droplets leaving a large sea of liquid crystal as observed under the microscope. This isn't the case for the films cured from monomer solutions doped with 14mol% heptafluorobutyl acrylate and 8mol% dodecafluoroheptyl acrylate, where indistinct droplet morphologies with a small droplet size are formed. It is the belief of the author that in these cases phase separation doesn't occur as quickly as for the higher fluorine doped systems, but that when phase separation does occur network formation is still relatively low. As a result of this two phases are formed; a liquid crystal rich one and a polymer rich one, which then undergoes a subsequent second phase separation at a later point (due to it's continually changing thermodynamic properties). By the point at which this secondary phase separation occurs the monomers have reacted to form a far more developed polymer network, which acts to suppress phase separation, resulting in the observed smaller droplet size. The indistinct morphology observed under the microscope occurs due to the initial phase separation causing localised composition variations.

The improvement seen in the films doped with 8mol% heptafluorobutyl acrylate and 4mol% dodecafluoroheptyl acrylate due to the increase in droplet size will be as a result of the fluorine doping moving the coexistence curve for the unpolymerized system up. This will mean a lower degree of polymerisation is required to initiate phase separation and therefore as discussed in section B the degree of network formation will be lower at the phase separation point, such that it will promote rather than suppress phase separation resulting in a larger morphology droplet size.

These interpretations are supported by the results for the decay times of the films (Figure 10 and Figure 11) as the morphology size increases and the switching fields and rates improve, the decay times become longer. So the decay times for the 8mol% heptafluorobutyl acrylate and the 4mol% dodecafluoroheptyl acrylate films are significantly higher than the undoped films by a similar factor as for the improvements in the switching field and K values. It is also worth noting that the decay times of the 14 and 22mol% films are so high (that they cannot be reasonably shown on the same graph as the lower doped system. This is again likely to be as a result of the film no longer being of a droplet PDLC morphology and instead acting

like polymer droplets in a sea of liquid crystal. As the liquid crystal is not encapsulated in a polymer network, the disordering interface area is significantly reduced compared to the liquid crystal volume, so once the field is removed there is much less of a driving force to cause the liquid crystals to return to their disordered state.

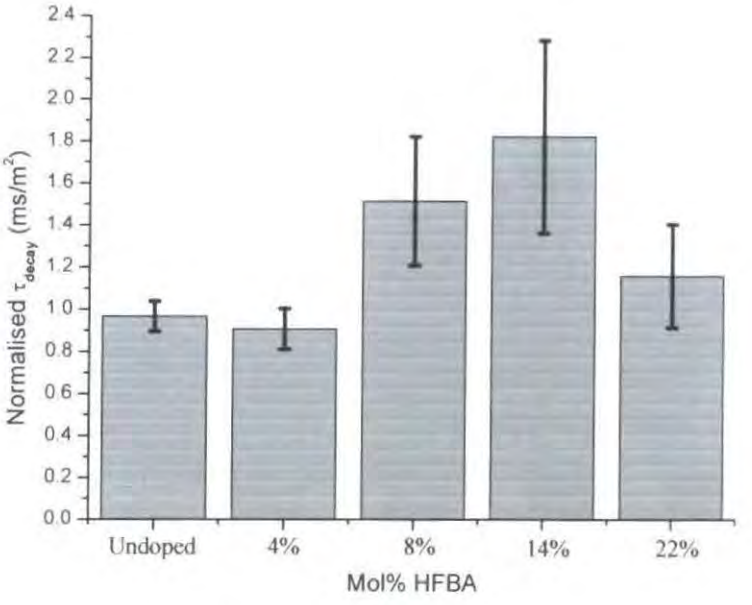

Figure 10 Normalised τ_{decay} for 75:25 TL213:2-ethylhexyl acrylate (15% b/v crosslinker) doped with varying mol% of heptafluorobutyl acrylate, cured at 303 K under 5000 mWm^2 UV (365 nm)

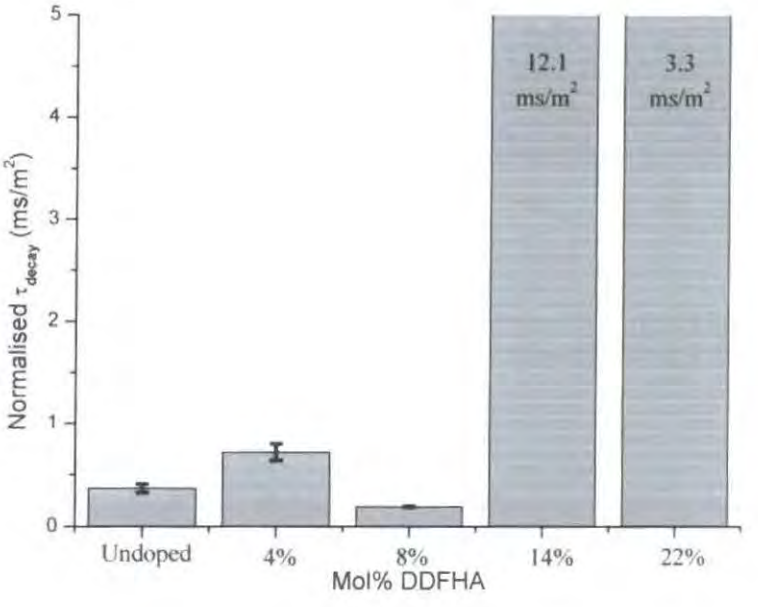

Figure 11 Normalised τ_{decay} for 75:25 TL213:2-ethylhexyl acrylate (15% b/v crosslinker) doped with varying mol% of dodecafluoroheptyl acrylate, cured at 303 K under 5000 mWm^2 UV (365 nm). The results for 14 mol% and 22mol% DDFHA acrylate are much larger than the maximum of the graph refer to discussion for an explanation.

Figure 12 and Figure 13 show the on and off state transmissions and contrast ratios for the films doped with heptafluorobutyl acrylate and dodecafluoroheptyl acrylate. The increasing morphology droplet size with initial fluorine doping results, as would be expected, in an increase in the off state transmission, and therefore a reduction in the contrast ratios. As such the improvements obtained by doping with fluorinated monomers have been at the expense of contrast ratio and off state transmission. It can also be seen that, unsurprisingly, the 14 and 22mol% doped films, which appear to be acting more like liquid crystals, have significant increased off state transmissions and decreased on state transmissions, as there are no longer large areas of polymer/liquid crystal interfaces for light scattering to occur. These films therefore have no potential as the basis for display screen devices.

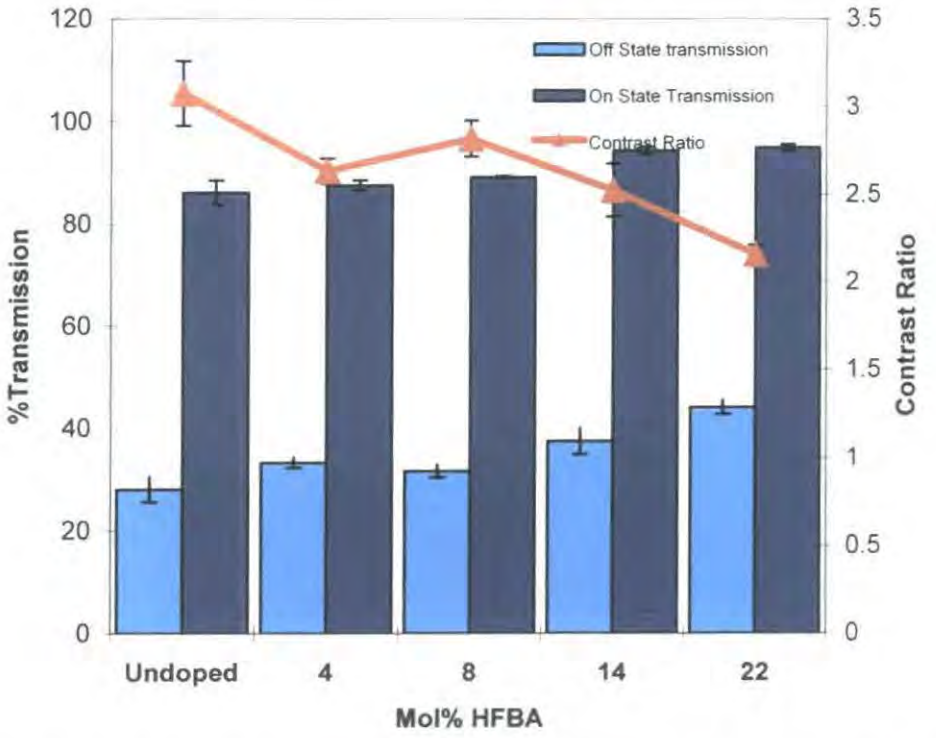

Figure 12 Off and on state %transmissions, and contrast ratios for 75:25 TL213:2-ethylhexyl acrylate (15% b/v crosslinker) doped with varying mol% of heptaflurobutyl acrylate, cured at 303 K under 5000 mWm^{-2} UV (365 nm)

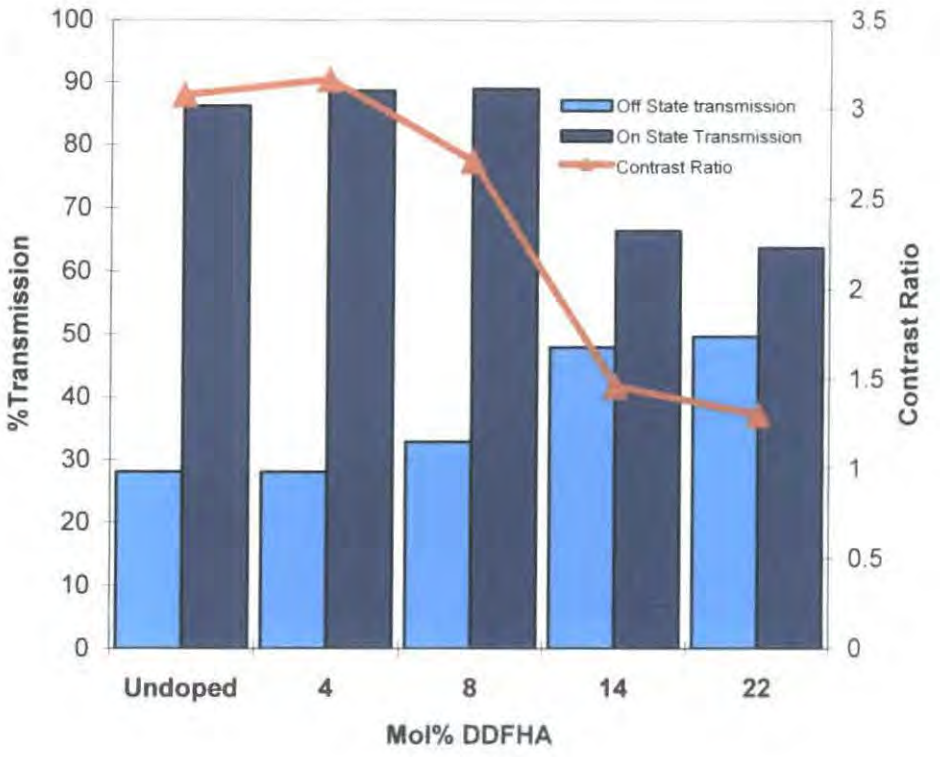

Figure 13 Off and on state %transmissions, and contrast ratios for 75:25 TL213:2-ethylhexyl acrylate (15% b/v crosslinker) doped with varying mol% of dodecafluoroheptyl acrylate, cured at 303 K under 5000 mWm^{-2} UV (365 nm)

One of the aims of the work performed is to determine whether the improvements observed from fluorine doping are as a result of the total amount of fluorine present in the polymer or the number of fluorinated monomer units present in the polymer chains. To this end two different fluorinated monomers were investigated, one which had approximately double the number of fluorine atoms per monomer unit than the other (13 for dodecafluoroheptyl acrylate compared to 7 for heptafluorobutyl acrylate). This means that the 8mol% heptafluorobutyl acrylate and 4mol% dodecafluoroheptyl acrylate films have approximately the same fluorine mol% for the universal system, but the former has approximately twice the number of fluorine doped monomer units.

From Figure 14 which shows the E_{90} switching voltages for the PDLC films made with undoped, 4mol% HFBA, 8mol% HFBA, 4mol% DDFHA and 8mol% polymer component, it can be seen that the effects of doping with 8mol% HFBA and 4mol% DDFHA are approximately the same. As discussed these two films contain approximately the same mol% of fluorine atoms, whereas the results for the films containing approximately the same number fluorinated monomer units (4mol%

HFBA compared to 4mol% DDFHA and 8mol% compared to 8mol% DDFHA) are significantly different.

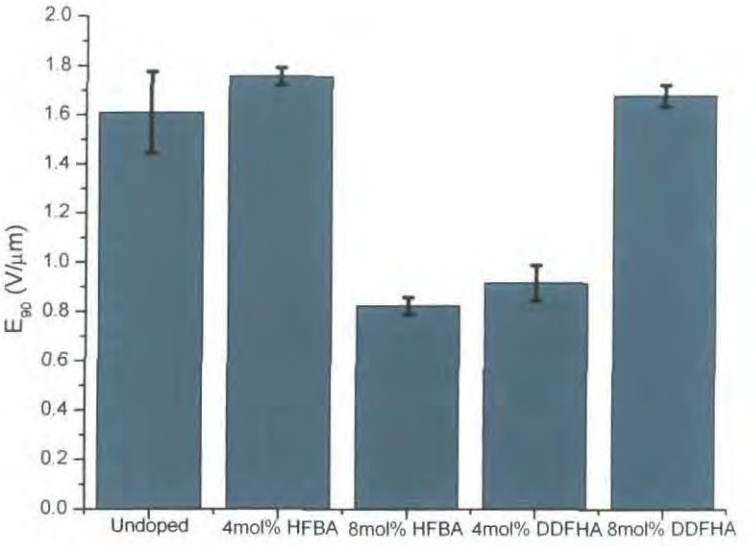

Figure 14 Comparison of the E_{90} *switching fields for* equivalent mol% of heptafluorobutyl acrylate and dodecafluoroheptyl acrylate doped PDLC films

As can be seen in Figure 15 the reason that the 8mol% HFBA and 4mol% DDFHA films produce similar switching field results is due to the fact that they have similar droplet morphology sizes.

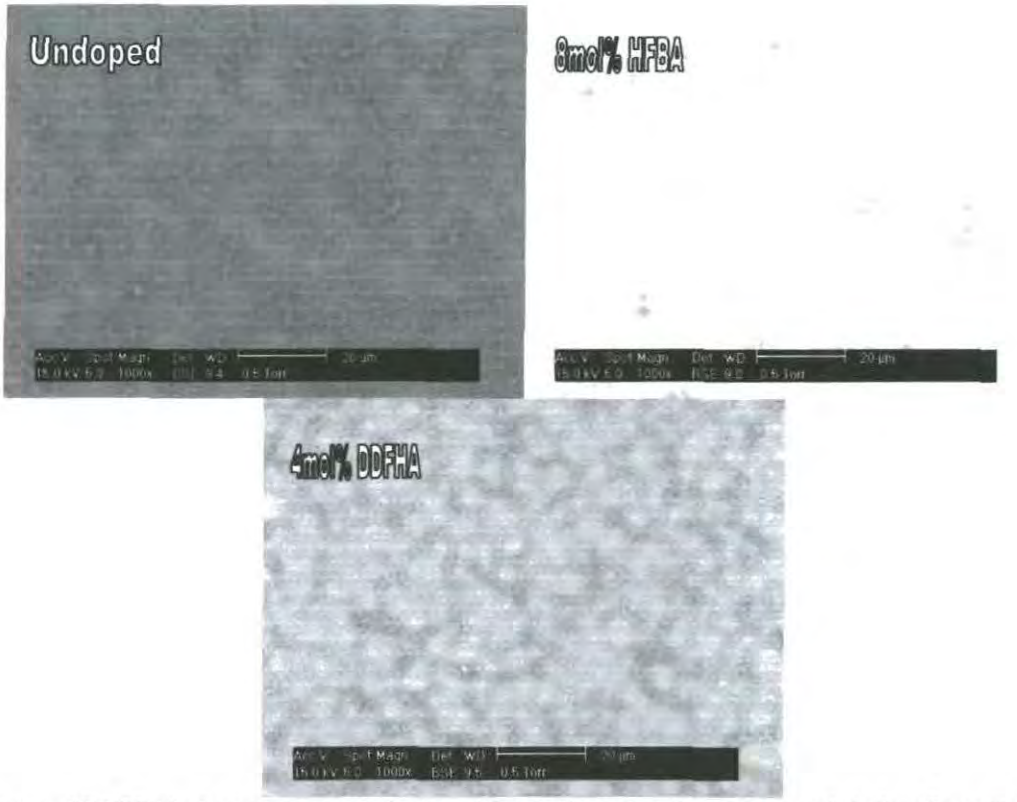

Figure 15 ESEM observed morphologies of heptafluorobutyl acrylate and dodecafluoroheptyl acrylate PDLC films which give similar switching fields (1000x magnification)

Figure 16 shows that the morphologies for the films of approximately the same fluorinated monomer densities, which produce very different E_{90} results, are of very different size and type.

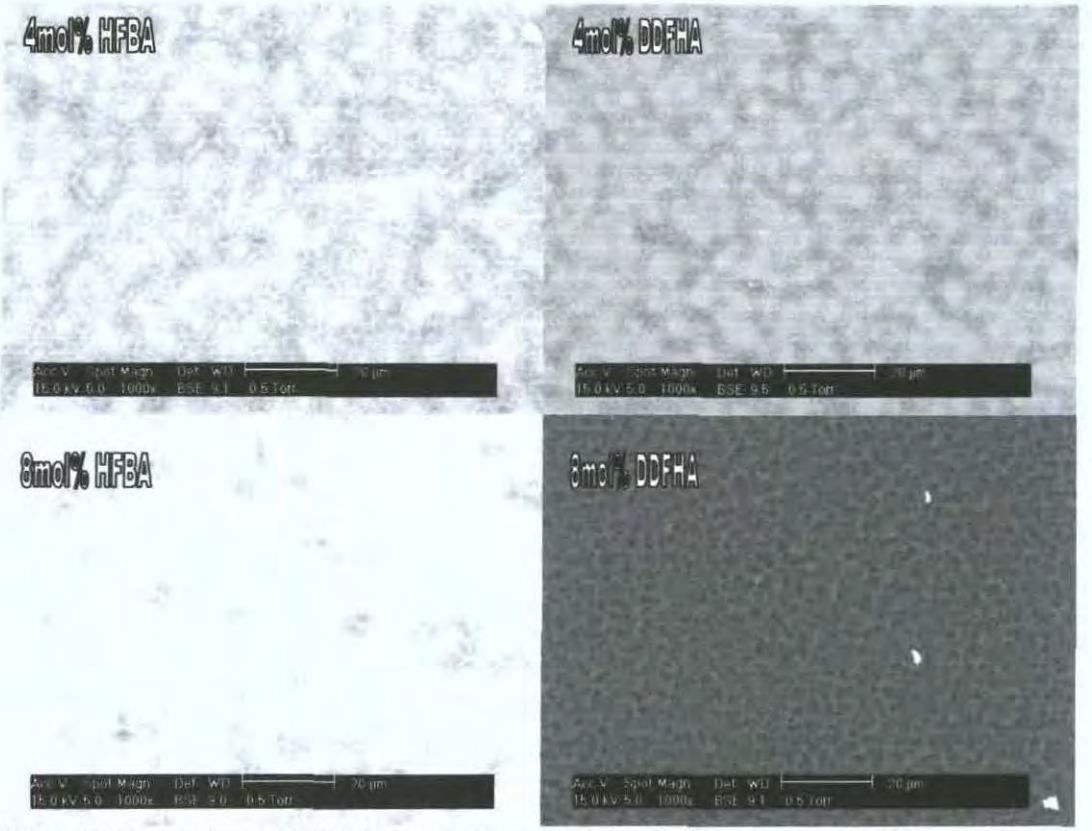

Figure 16 Comparison of ESEM observed morphologies of films prepared with approximately the same fraction of fluorinated monomer units, but with different number of fluorine per monomer unit (1000x magnification)

This would seem to provide good support for the interpretation that the effects of fluorine doping upon the morphology, and as a result the electro-optical properties of the films, are dependent upon the absolute amount of fluorine present and not the number of fluorinated monomer units as a percentage of the total number of monomer units. It can be reasonably assumed therefore that the presence of the fluorinated species have changed the phase properties of the systems by modifying the interaction parameter which has resulted in the different morphologies produced, but not had any noticeable effect upon the properties of the cells at the interface.

5 Contact Angle Measurements

5.1 Aim

The above results have shown that morphology is the most important factor in determining the effect of fluorine doping upon the electro-optical properties; it cannot be proven that there are no anchoring energy effects. For this reason a further

experiment is performed to determine the effect of fluorine doping on the affinity of the liquid crystal blend TL213 to a polymer. Sample films are prepared of 2-ethylhexyl acrylate by spin coating a glass slide (previously washed in methanol and air dried) with monomer solutions containing varying mol% of the heptafluorobutyl acrylate doping species, these slides are then photo-polymerised to form the films. A droplet of the TL213 liquid crystal blend is then pipetted onto the slide and the contact angle measured.

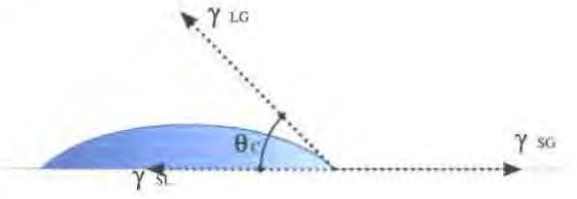

Figure 17 Schematic Diagram of Contact Angle Measurement, where θ_c is the contact angle of the droplet on the surface[8]

Figure 17 is a schematic diagram of how the contact angle is measured, the greater the affinity of the droplet material for the surface material the more it will spread, and the contact angle θ_c will decrease. The thermodynamics of this behaviour is defined by Young's Equation (1.1)

$$\cos\theta_c = \frac{w_{el}}{\gamma_{LG}} - 1 \qquad (1.1)$$

where w_{el} is the adhesion energy, defined by

$$w_{el} = \gamma_{sg} + \gamma_{lg} - \gamma_{sl} \qquad (1.2)$$

and γ_{sg}, γ_{lg}, and γ_{sl} are the surface tensions (interfacial energies) between the solid and gas, the liquid and gas and solid and liquid phases respectively. Therefore the greater the attraction between the droplet and the surface species the greater the adhesion energy and the greater will be $\cos\theta_c$, which as the contact angle is less than 90^o will have the effect of decreasing the contact angle.

It is expected therefore that the fluorine doping should result in repulsion, decreasing the adhesion energy; the droplet will be repelled by the surface and the contact angle will increase.

5.2 Results and Discussion

It had been expected that the TL213 blend containing halogenated (including fluorinated) liquid crystals would be repelled by the doping of the polymer film with the highly electronegative fluorinated monomer units, resulting in an increasing contact angle. In fact Table 1 and Figure 18 show that an increase in fluorine doping of the polymer actually results in a decrease in the contact angle, suggesting that the liquid crystal blend in fact has a greater affinity for the fluorine doped polymer film.

Polymer film	*Contact Angle*
Pure EHA	37.8
EHA Doped with 4mol% HFBA	35.0
EHA Doped with 8mol% HFBA	19.0
EHA Doped with 14mol% HFBA	19.3

Table 1 Contact angle measurements for a droplet of TL213 on polymer films with varying degrees of doping with heptafluorobutyl acrylate

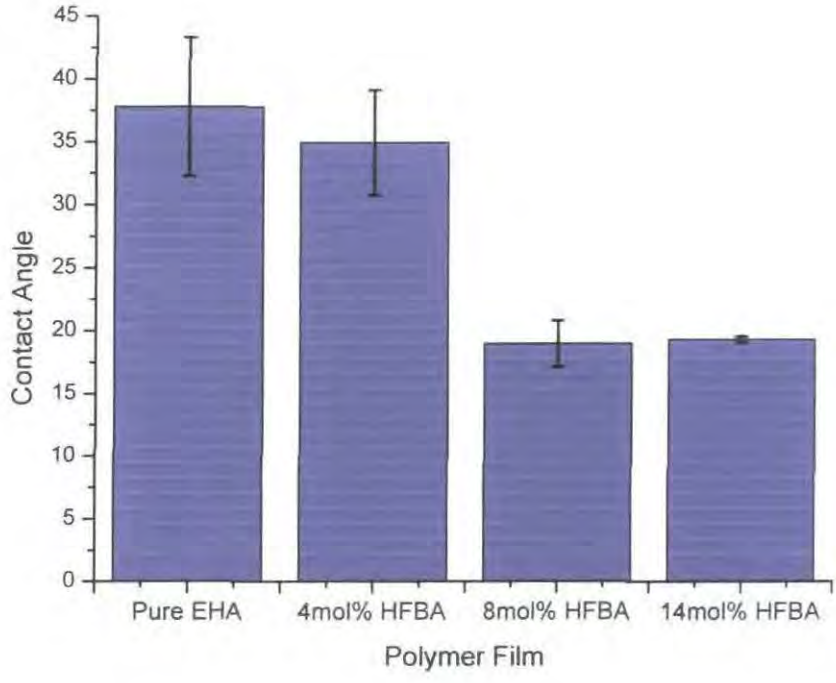

Figure 18 Contact angle measurements for a droplet of TL213 on polymer films with varying degrees of doping with heptafluorobutyl acrylate

The observed reduction in contact angle with increasing concentration of the fluorinated monomer and therefore apparent increase in affinity of the liquid crystal for the polymer film can be explained in one of two ways. Firstly, while there appears no chemical reason why the halogenated terphenyl molecules, which make up TL213, should be attracted more to the fluorinated monomer units than the otherwise chemically similar unfluorinated monomers units this could indeed be the

case. The second possibility could be as a result of the way in which the slides were prepared; it could be the case that as the fluorine concentration increases the repulsion between the monomer solution and the glass slide increases and the monomer is forming into droplets before the cure process is complete. This would result in a surface which only has polymer on it in patches and large areas where only glass is present to the TL213 droplet, as a result at high polymer dopent concentrations (8mol% & 14mol% HFBA) the contact angle being measured is that of the glass slide and not the polymer film. This interpretation is supported by the pure EHA and 4mol% HFBA polymer slides having a similarly high contact angle (~36°), and 8mol% and 14mol% HFBA having a similarly low contact angle (~19°). This would suggest that between 4mol% and 8mol% is a critical doping concentration which causes droplets to form.

The fact that a slight decrease in contact angle is observed even upon doping the polymer film with a low concentration of fluorinated monomer suggests, that there is no significant decrease in affinity of TL213 for the surface with fluorine doping. the fluorine doping should therefore have little effect upon the field required to bring about 90% switching. This would suggest that if there is any electronic interfacial effect on the switching field from the fluorine, it is dwarfed by the effects of the much more significant morphological changes. This supports the view that all the effects observed in the electro-optical results upon fluorine doping are as a result of morphology change.

6 Conclusion

It has been shown by the work presented in this section that fluorine doping has the effect of modifying the phase properties of the monomer/liquid crystal system. Therefore for a given temperature/composition point, the degree of polymerisation required for phase separation to become favourable changes, therefore as discussed in section B, affecting the way in which phase separation occurs and the type of morphologies formed. Initial fluorine doping produces increases in morphology droplet size and reductions in 90% switching fields. Subsequent increases in fluorine doping have the effect of changing the morphology so that it is no longer the droplet morphology desired for display devices.

It has also been shown by contact angle measurements, that the fluorine doping has a limited affect of upon the affinity of the TL213 liquid crystal blend to the polymer.

This suggests therefore that any improvements in electro-optical properties are from morphological changes and not electronic effects. Overall fluorine doping has been shown as a way to improve electro-optical results, but not in any way greater than can be achieved by morphological changes resulting from changes in composition and cure temperature.

Bibliography

1. Amundson, K. *Physical Review E* **1996,** 53, 2412-2422.
2. Amundson, K.; vanBlaaderen, A.; Wiltzius, P. *Physical Review E* **1997,** 55, 1646-1654.
3. LeGrange, J. D.; Carter, S. A.; Fuentes, M.; Boo, J.; Freeny, A. E.; Cleveland, W.; Miller, T. M. *Journal of Applied Physics* **1997,** 81, 5984-5991.
4. Nomura, H.; Suzuki, S.; Atarashi, Y. *Japanese Journal of Applied Physics Part 1-Regular Papers Short Notes & Review Papers* **1990,** 29, 522-528.
5. Heavin, S. C.; Fung, B. M.; Sluss, J. J.; Batchman, T. E. *Molecular Crystals and Liquid Crystals Science and Technology Section a-Molecular Crystals and Liquid Crystals* **1994,** 238, 83-91.
6. Schulte, M. D.; Clarson, S. J.; Natarajan, L. V.; Tomlin, D. W.; Bunning, T. J. *Liquid Crystals* **2000,** 27, 467-475.
7. Schulte, M. D.; Clarson, S. J.; Natarajan, L. V.; Tomlin, D. W.; Bunning, T. J. *Molecular Crystals and Liquid Crystals* **2002,** 373, 155-180.
8. Gillis, J., An illustration of the contact angle between 3 phases (gas, solid, liquid). In Wikipedia: 2006.

Further Work

Presented below are a number of areas of inquiry which if more time had been available would have provided greater support to the conclusions presented, or are ideas which have resulted from the investigations performed and which would provide interesting avenues for future investigations within the field.

1. Modelling of the Flory Lattice Theory for Liquid Crystal Solutions

In Section A it was discussed how the characteristic anisotropic nature of liquid crystals effected their solution thermodynamics, with the number of potential thermodynamic configurations reduced by the excluded volume effects resulting from structural anisotropy. While it is beyond the scope of the work performed for this thesis, it would be of great interest to attempt to model computationally the solution thermodynamics of these systems. In particular it would be desirable to be able to model the Flory liquid crystal lattice theory and produce computational coexistence curves which match the phase properties of the systems under investigation experimentally. This would provide evidence to support the theories about how the structural anisotropy of liquid crystals significantly effect their solvation properties. It should also be theoretically possible to define a Flory-Huggins type interaction parameter, and so quantify the phase properties of the monomer/liquid crystal pair under investigation. Knowing this it should then be possible to make predictions as to how changing the chemistry of the two component species (such as the axial ratio of the liquid crystal species) will effect their phase properties. With such knowledge it would then be possible to make predictions as to the mechanism by which they would phase separate upon polymerisation of the monomer and the type of morphology formed under different conditions. Ultimately it would be hoped that this would help in knowing how to control the morphology formed and as such the electro-optical properties of the films.

2. Investigation of Polymer Reaction Kinetics

In section B it was shown that the extent of polymerisation and network formation at the point of phase separation was the key factor in determining the mechanism of phase separation and therefore the morphology formed. An explanation was

proposed for the observed phase separation morphologies and phase separation times; the basis of which was that the extent of network formation controlled whether phase separation was promoted or suppressed. It would therefore be of great interest to investigate this by tracking the progress of the polymerisation process under different conditions and quantify an extent of polymerisation and network formation. A possible approach to this would be to track the reaction of the acrylate monomer units by the use of IR spectroscopy. The carbon-carbon double bond in the acrylate monomer provides a good stretch to image using IR spectroscopy; the decrease in intensity of this peak should follow the consumption of the monomer and therefore formation of polymer network.

3. Reaction Induced Viscoelastic Phase Separation

As discussed in Section B Tanaka presented work in 1993 demonstrating the viscoelastic phase separation mechanism for a system where phase separation has been initiated by a temperature quench. Much work has been presented on viscoelastic phase separation by temperature quench since. However, very little work is to be found in the literature which discusses or demonstrates phase separation via a viscoelastic mechanism where phase separation is induced by reaction. As it is the belief of the author that, in the absence of a crosslinking species, monomer/liquid crystal solutions undergo reaction induced viscoelastic phase separation, it would be of interest to extend this area of inquiry. In particular to see if this only occurs where a liquid crystalline solvent is present, to provide the energetic gain, from the ordering of the liquid crystal molecules, to overcome the kinetic barrier to nucleation of solvent droplets. Therefore it would be of interest to see if the same results could be achieved with a structurally isotropic solvent molecule such as methanol.

4. PDLCs Formed from Liquid Crystalline Monomers

It was shown in Section C that changing the chemistry of the monomer species by fluorination had the effect of modifying the morphologies formed. However there was no evidence that it had the effect of modifying the anchoring energy at the polymer/liquid crystal interface and thus the desired improvement in switching voltage and switching rate of the film in use as a display screen device. As changing the interface chemistry did not have the desired effect it would be interesting to see if changing the steric properties of the molecules at the interface provides the improved

performance desired. Therefore as a potential line of enquiry, it is proposed to either replace the acrylate monomer species with a liquid crystalline monomer or dope an acrylate monomer with varying amounts of an acrylate based liquid crystalline monomer. The aim being that liquid crystalline pendant groups on the polymer chains at the interface provide an extra ordering effect on the free liquid crystal thus reducing the voltage required to bring about complete switching. This could be further extended by the application of a voltage across the sample during curing to provide an added ordering effect on both free liquid crystal and liquid crystalline monomer.

Appendix A – Morphology Images for Section B Subsection 6

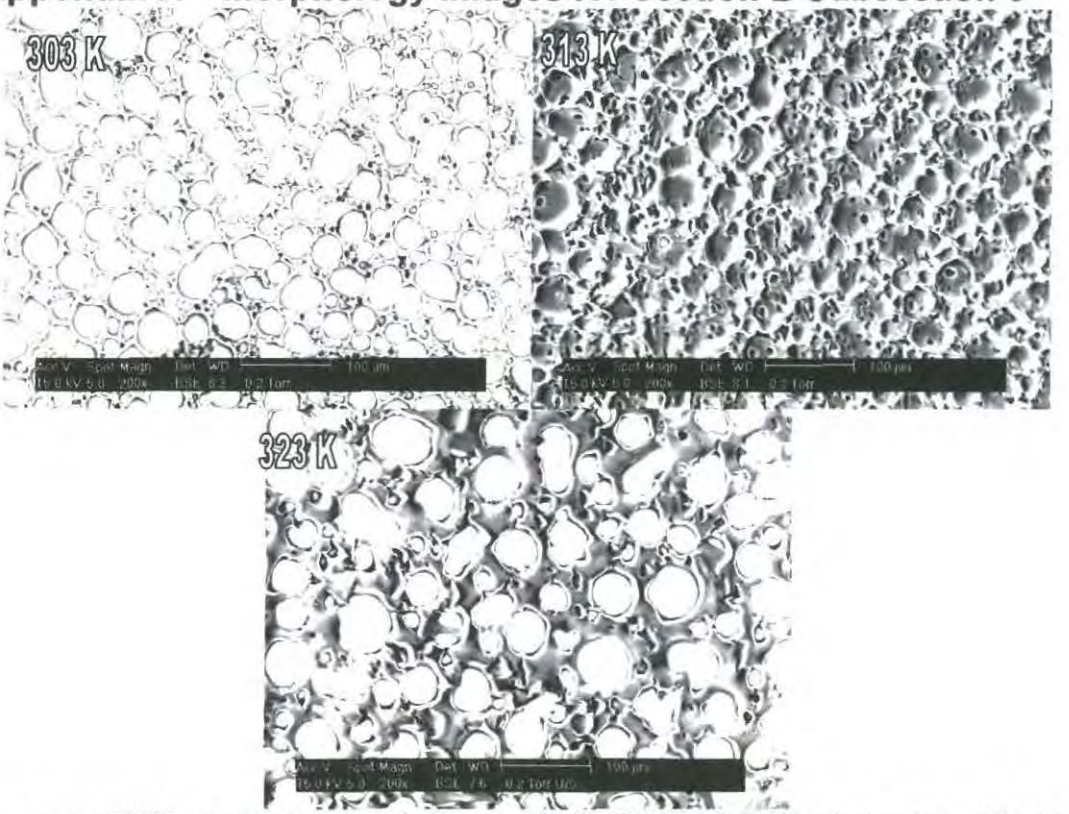

Figure 1 ESEM observed morphologies for 70:30 TL213:2-EthylHexyl Acrylate (2% b/v Crosslinker) polymerized under 2000 mWm^{-2} UV (365 nm) at varying temperatures. All images 200x magnification, measure bar s 100 μm

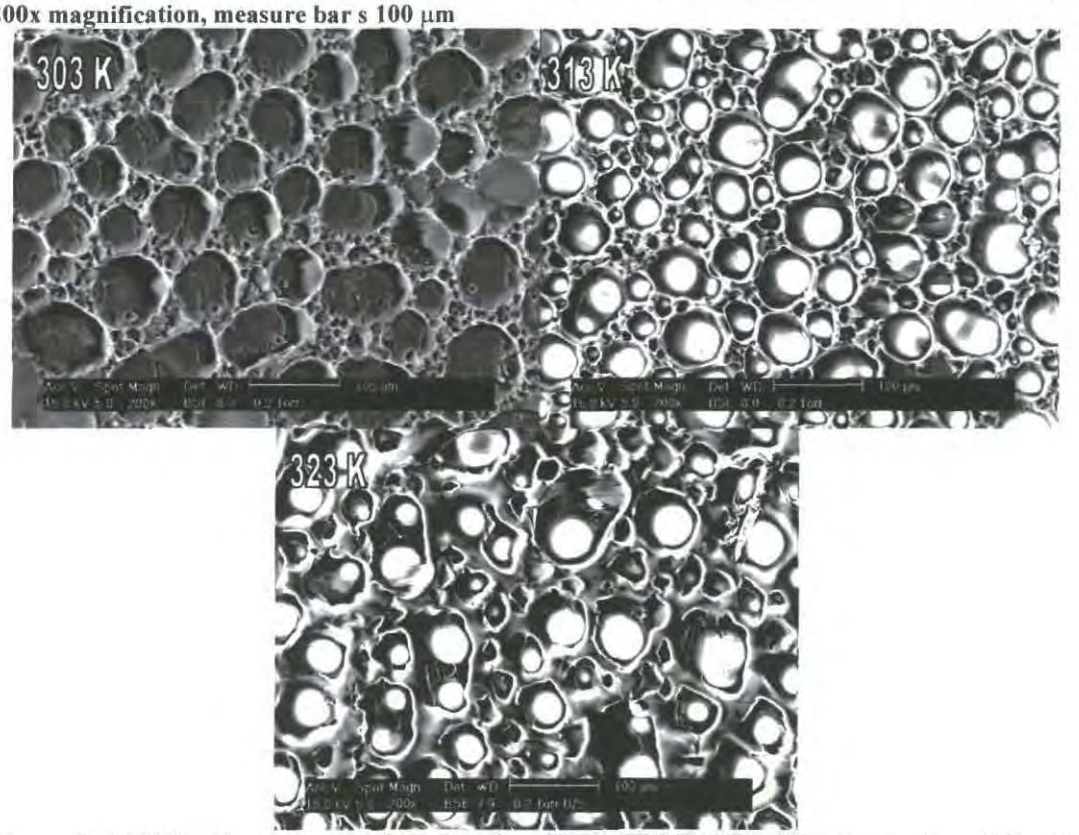

Figure 2 ESEM observed morphologies for 73:27 TL213:2-EthylHexyl Acrylate (2% b/v Crosslinker) polymerized under 2000 mWm^{-2} UV (365 nm) at varying temperatures. All images 200x magnification, measure bar s 100 μm

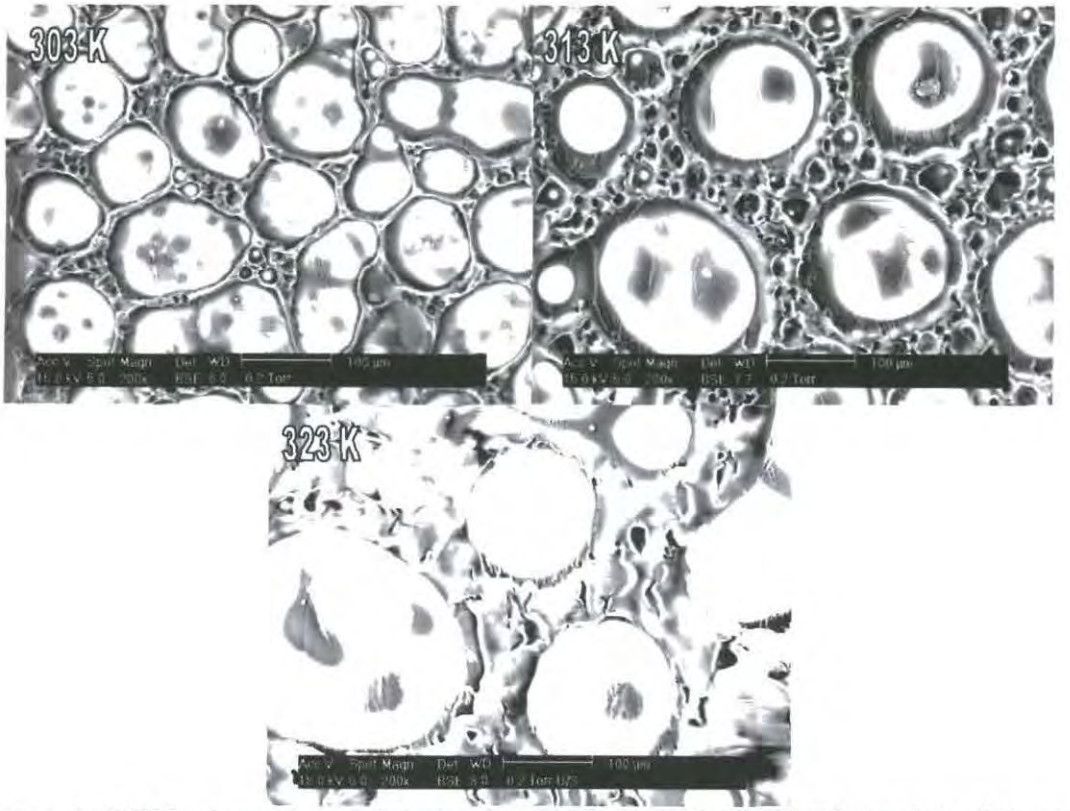

Figure 3 ESEM observed morphologies for 75:25 TL213:2-EthylHexyl Acrylate (2% b/v Crosslinker) polymerized under 2000 mWm^{-2} UV (365 nm) at varying temperatures. All images 200x magnification, measure bar s 100 μm

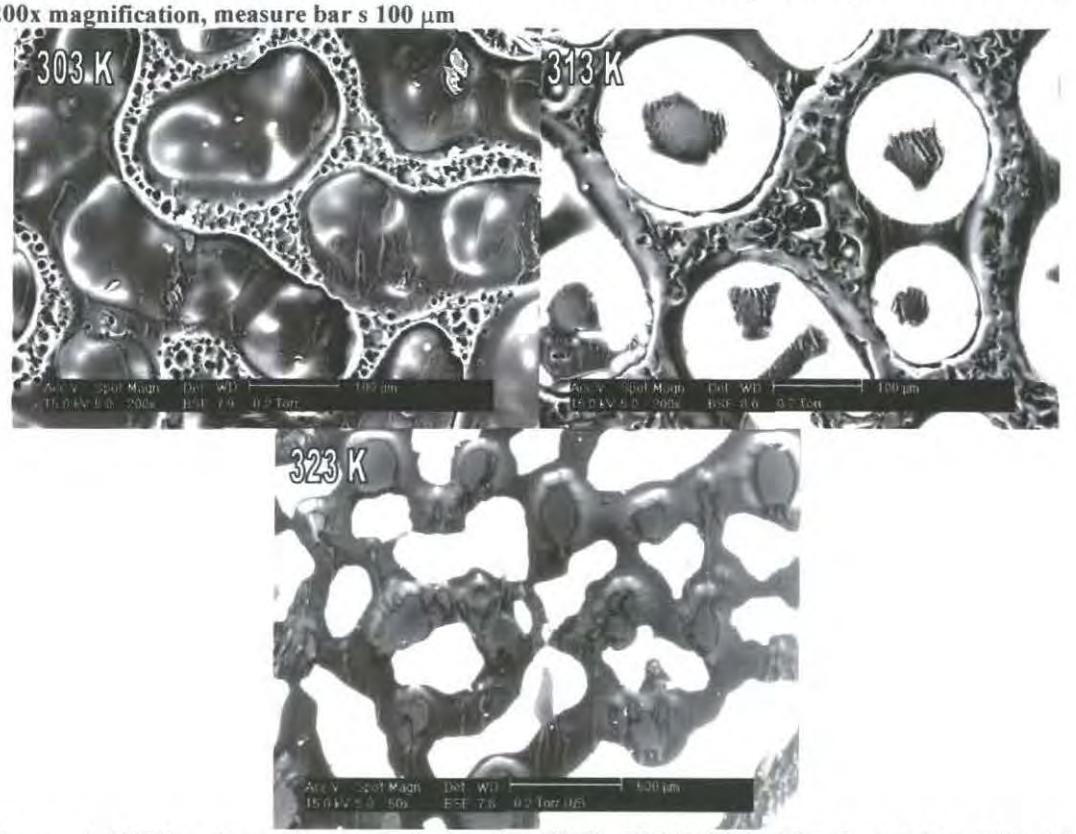

Figure 4 ESEM observed morphologies for 77:23 TL213:2-EthylHexyl Acrylate (2% b/v Crosslinker) polymerized under 2000 mWm^{-2} UV (365 nm) at varying temperatures. 303 K, 313 K images 200x magnification, measure bar s 100 μm, 323 K image 50x magnification, measure bar 0.5 mm

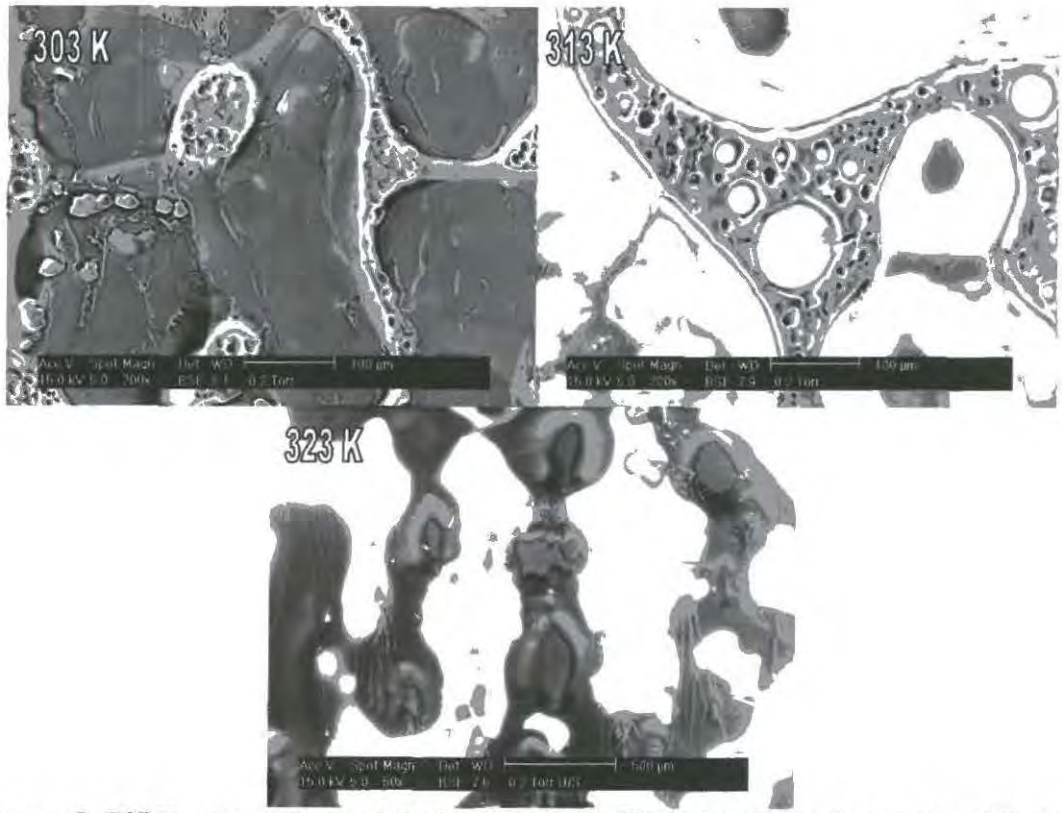

Figure 5 ESEM observed morphologies for 80:20 TL213:2-EthylHexyl Acrylate (2% b/v Crosslinker) polymerized under 2000 mWm^{-2} UV (365 nm) at varying temperatures. 303 K, 313 K images 200x magnification, measure bar s 100 μm, 323 K image 50x magnification, measure bar 0.5 mm

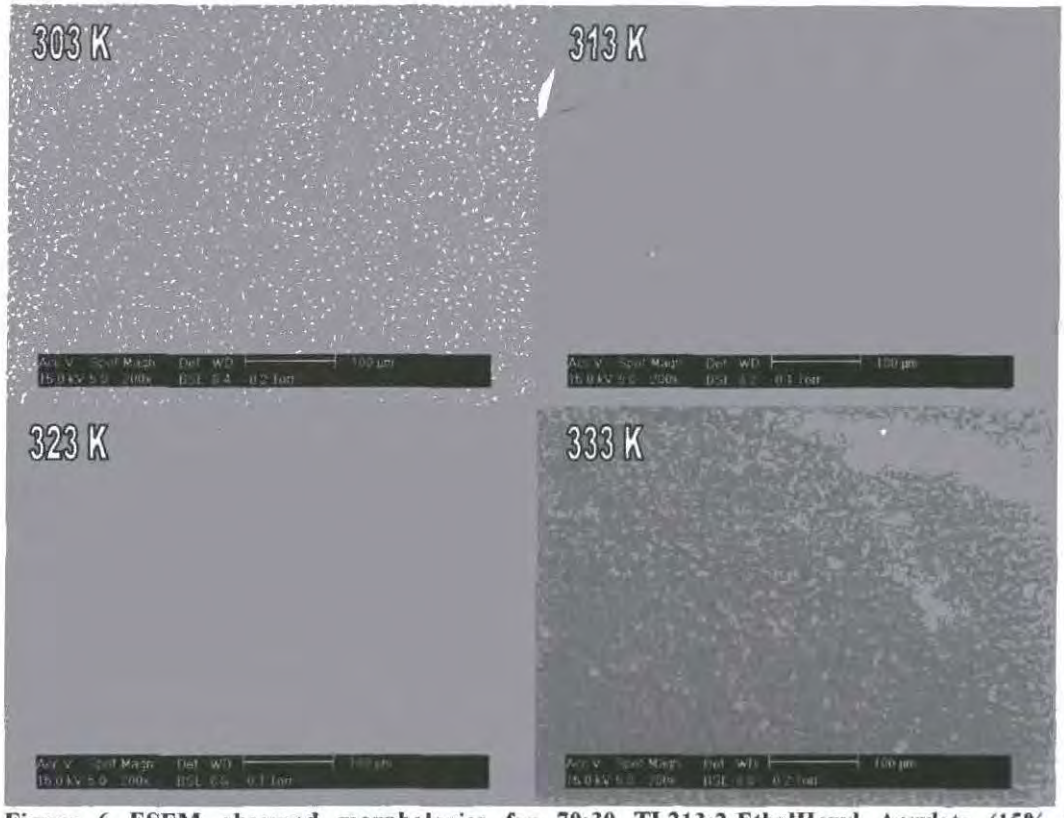

***Figure 6 ESEM observed* morphologies for 70:30 TL213:2-EthylHexyl Acrylate (15% b/v Crosslinker) polymerized under 2000 mWm^{-2} UV (365 nm) at varying temperatures. All images 200x magnification, measure bar is 100 μm**

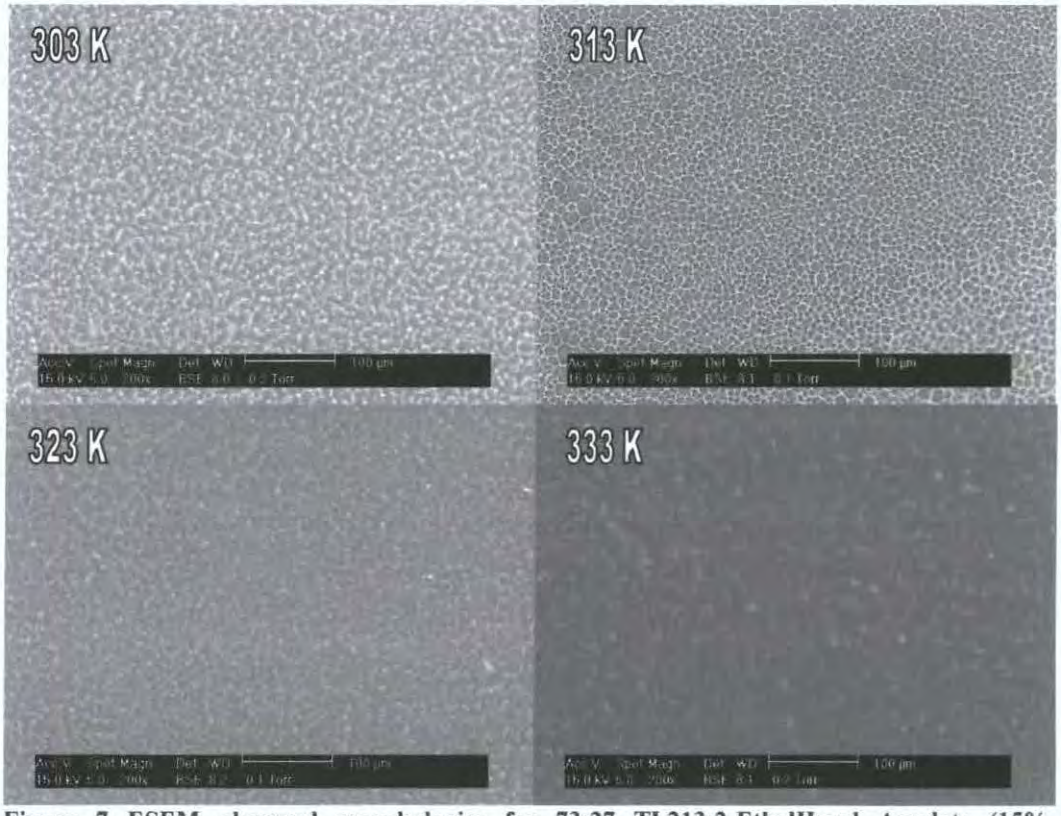

Figure 7 ESEM observed morphologies for 73:27 TL213:2-EthylHexyl Acrylate (15% b/v Crosslinker) polymerized under 2000 mWm^{-2} UV (365 nm) at varying temperatures. All images 200x magnification, measure bar is 100 μm

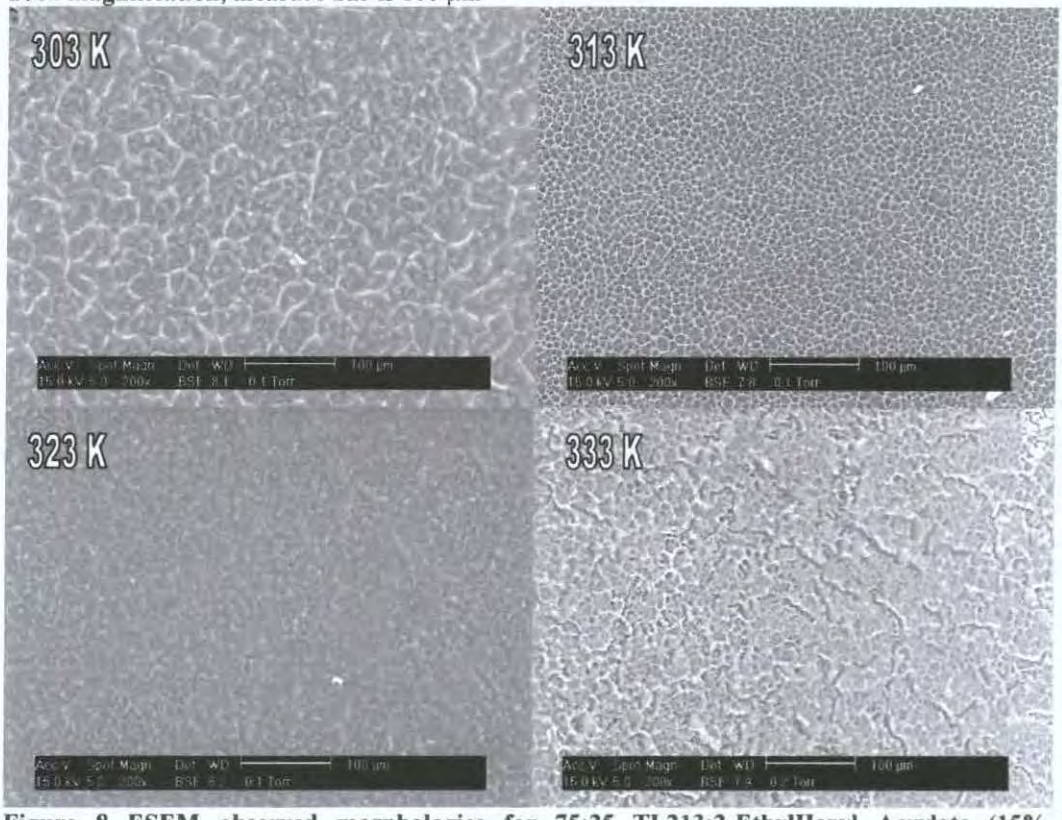

Figure 8 ESEM observed morphologies for 75:25 TL213:2-EthylHexyl Acrylate (15% b/v Crosslinker) polymerized under 2000 mWm^{-2} UV (365 nm) at varying temperatures. All images 200x magnification, measure bar is 100 μm

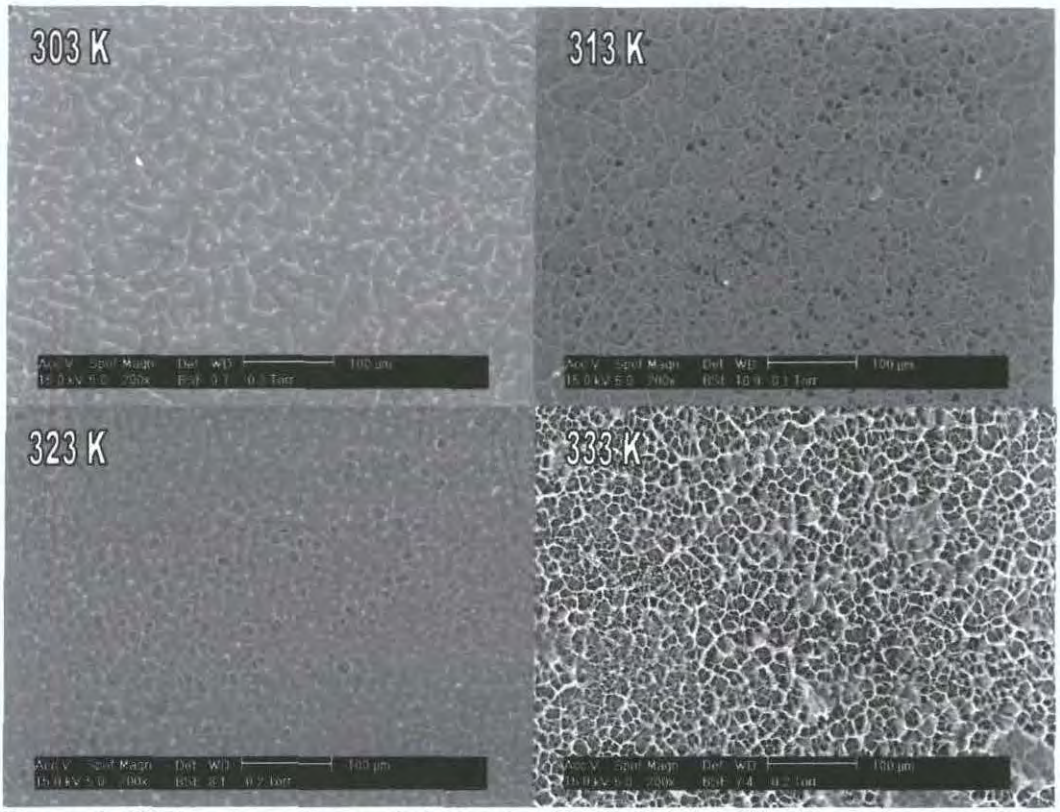

Figure 9 ESEM observed morphologies for 77:23 TL213:2-EthylHexyl Acrylate (15% b/v Crosslinker) polymerized under 2000 mWm^{-2} UV (365 nm) at varying temperatures. All images 200x magnification, measure bar is 100 μm

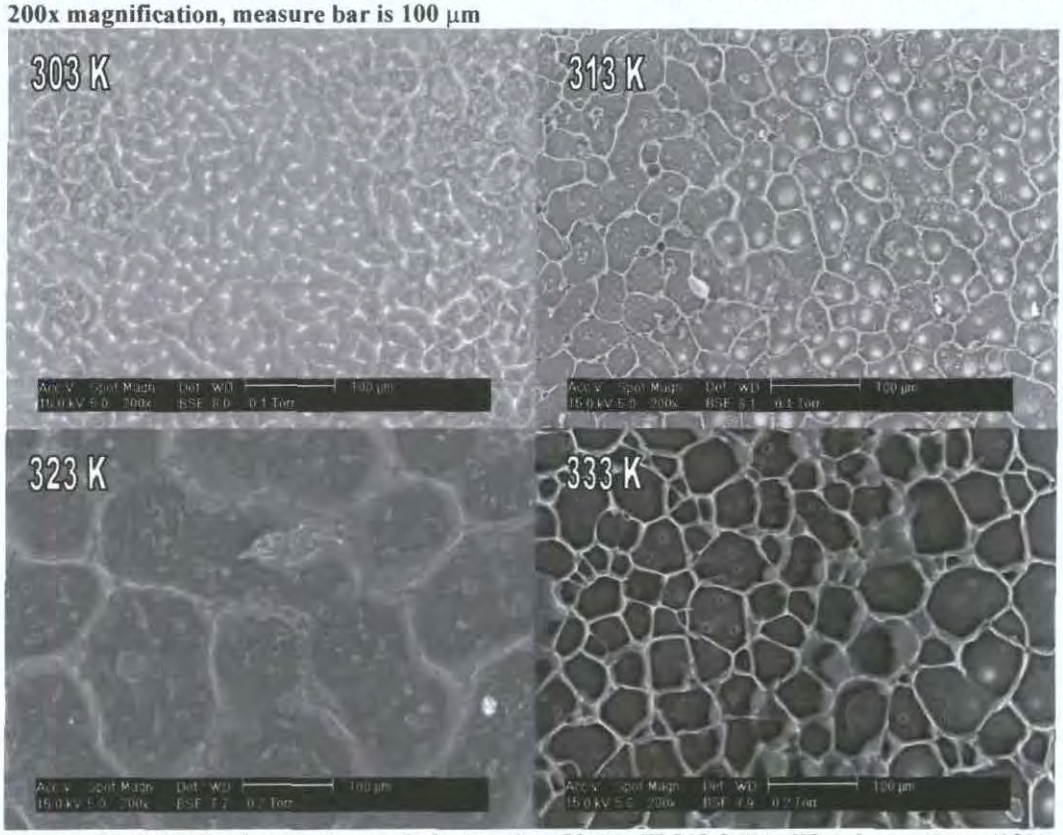

Figure 10 ESEM observed morphologies for 80:20 TL213:2-EthylHexyl Acrylate (15% b/v Crosslinker) polymerized *under 2000* mWm^{-2} UV (365 nm) at varying temperatures. All images 200x magnification, measure bar is 100 μm

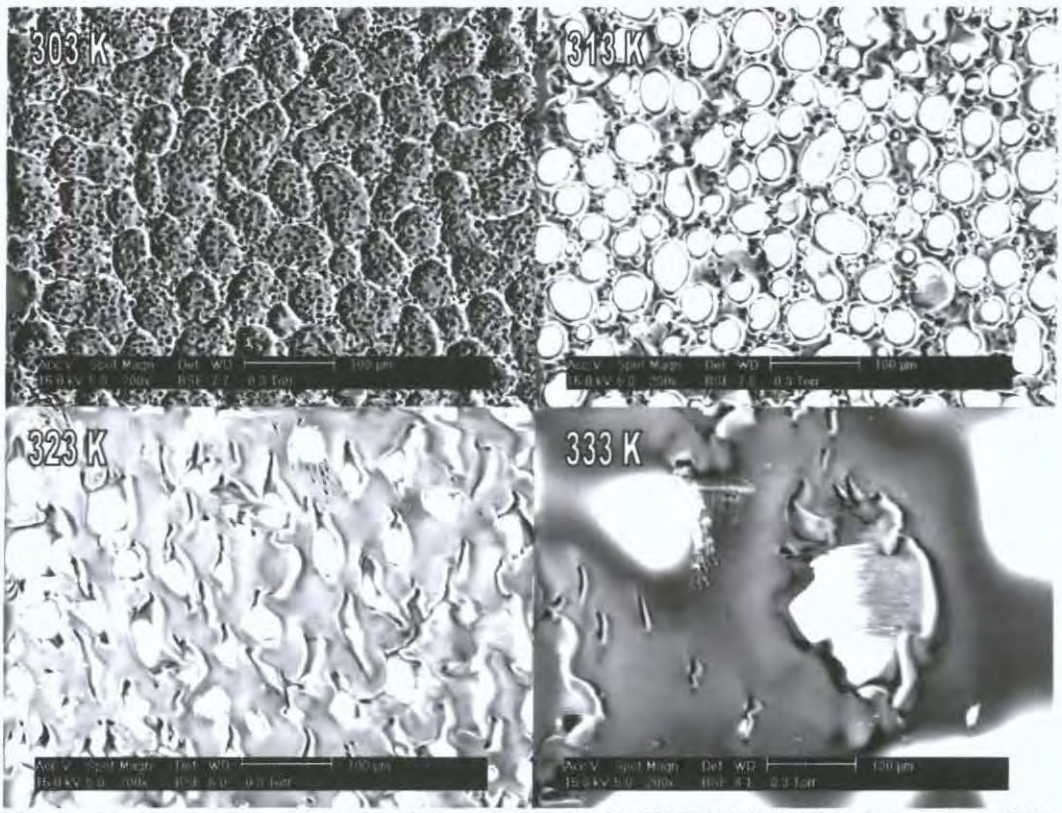

Figure 11 ESEM observed morphologies for 70:30 TL213:2-EthylHexyl Acrylate (2% b/v Crosslinker) polymerized under 5000 mWm^{-2} UV (365 nm) at varying temperatures. All images 200x magnification, measure bar is 100 μm

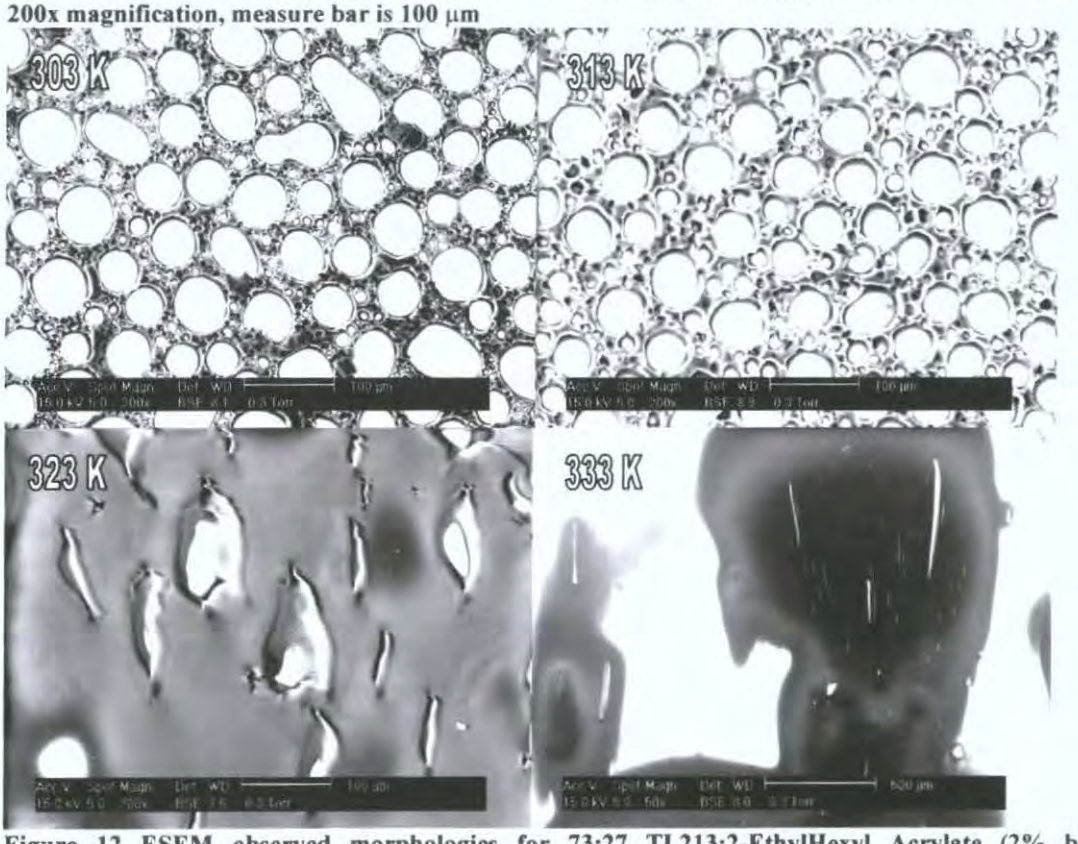

Figure 12 ESEM observed morphologies for 73:27 TL213:2-EthylHexyl Acrylate (2% b/v Crosslinker) polymerized under 5000 mWm^{-2} UV (365 nm) at 303, 313, 323 K images 200x magnification, measure bar is 100 μm 333 K image 50x magnification, measure bar 0.5 mm

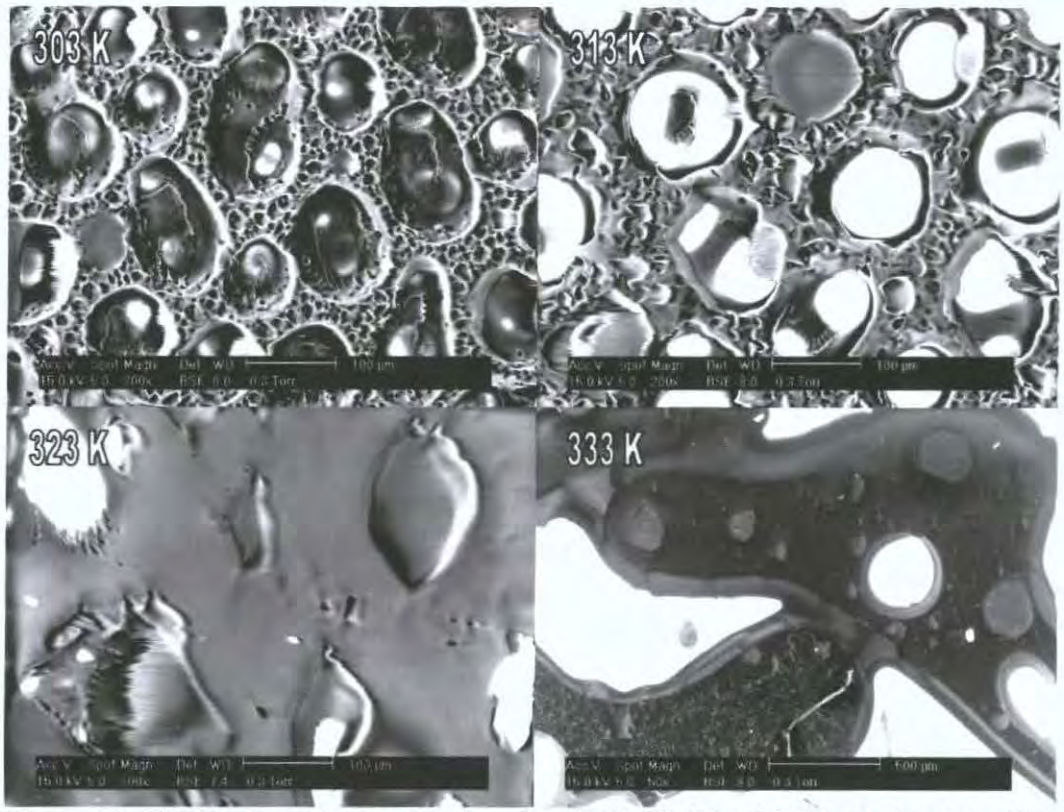

Figure 13 ESEM observed morphologies for 75:25 TL213:2-EthylHexyl Acrylate (2% b/v Crosslinker) polymerized under 5000 mWm^{-2} UV (365 nm) at 303, 313, 323 K images 200x magnification, measure bar is 100 μm. 333 K image 50x magnification, measure bar is 0.5 mm

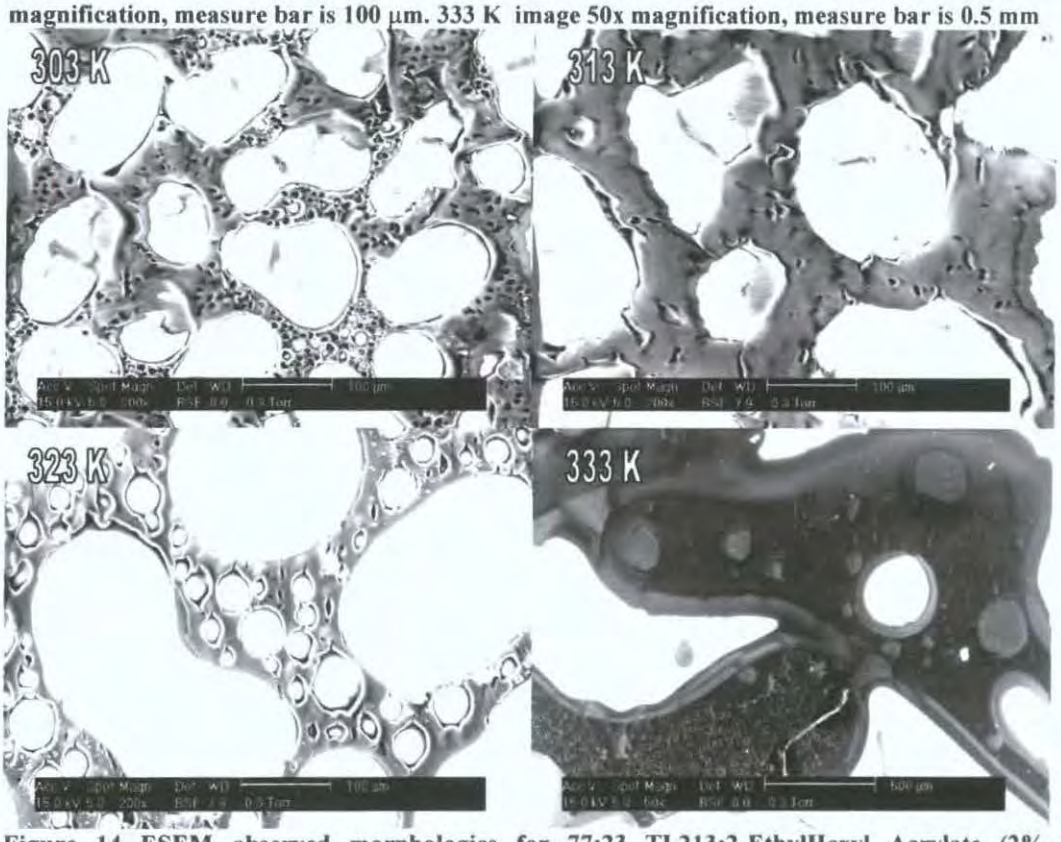

Figure 14 ESEM observed morphologies for 77:23 TL213:2-EthylHexyl Acrylate (2% b/v Crosslinker) polymerized under 5000 mWm^{-2} UV (365 nm) at 303, 313, 323 K images 200x magnification, measure bar is 100 μm. 333 K image 50x magnification, measure bar is 0.5 mm

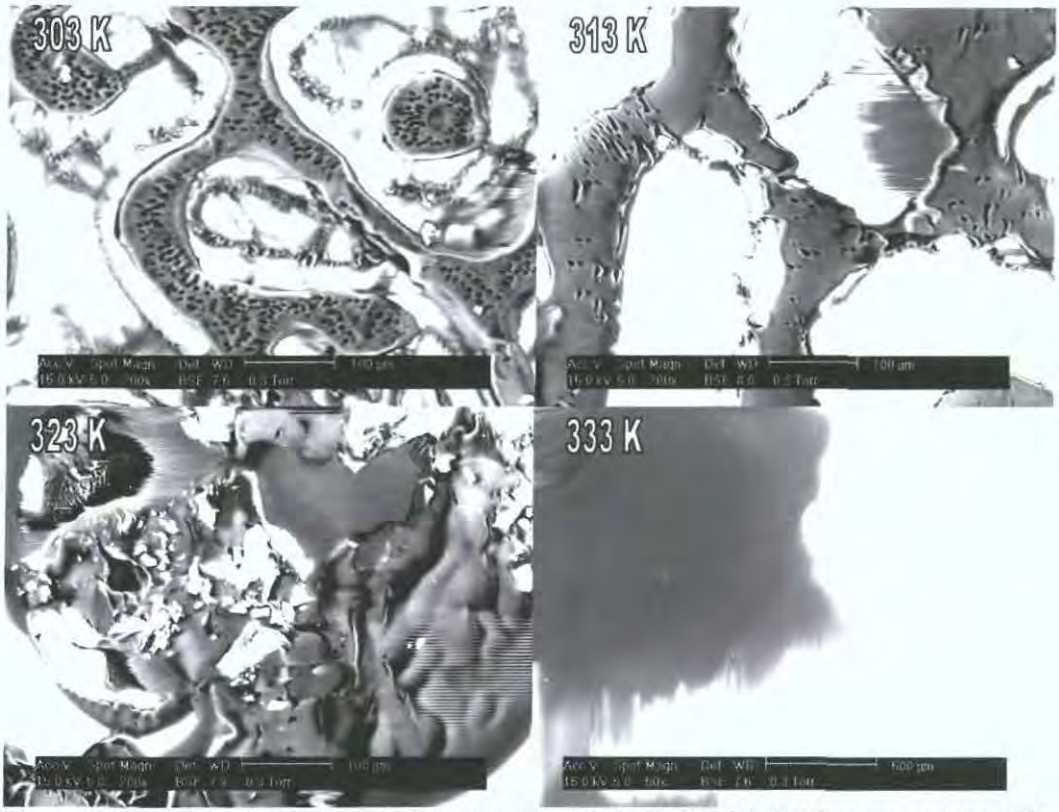

Figure 15 ESEM observed morphologies for 80:20 TL213:2-EthylHexyl Acrylate (2% b/v Crosslinker) polymerized under 5000 mWm^{-2} UV (365 nm) at 303, 313, 323 K images 200x magnification, measure bar is 100 μm. 333 K image 50x magnification, measure bar is 0.5 mm

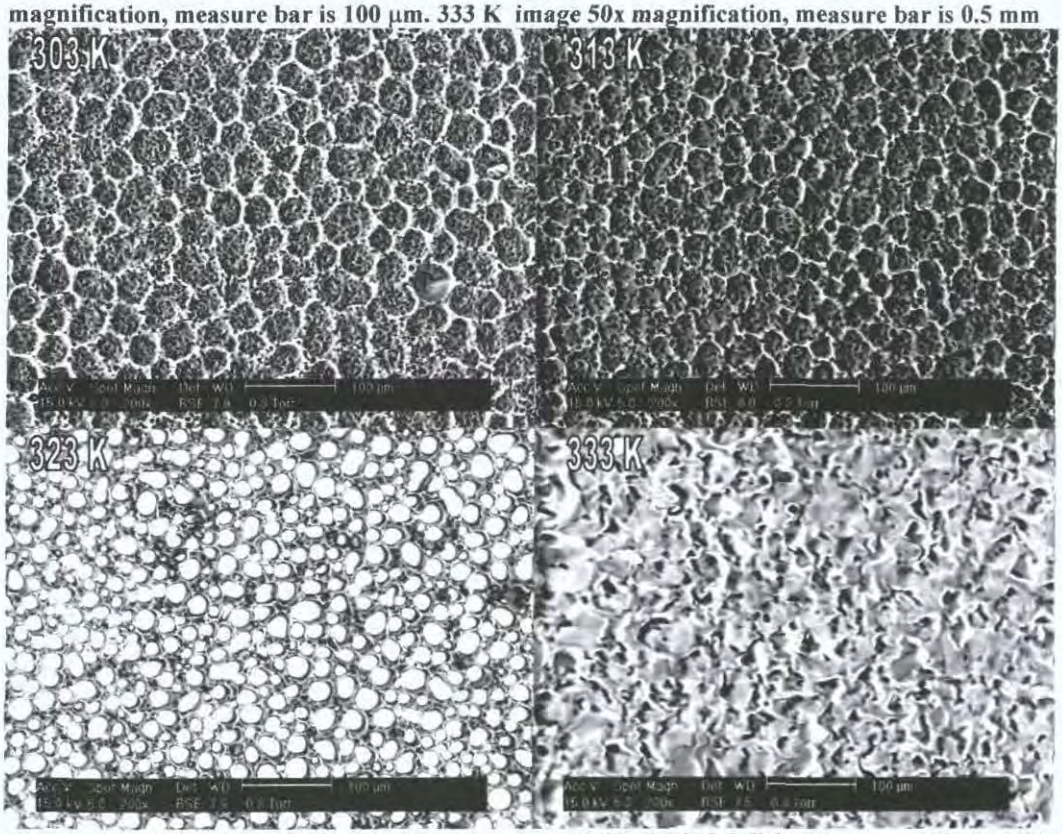

Figure 16 ESEM observed morphologies for 70:30 TL213:2-EthylHexyl Acrylate (5% b/v Crosslinker) polymerized under 5000 mWm^{-2} UV (365 nm) at varying temperatures. All images 200x magnification, measure bar is 100 μm

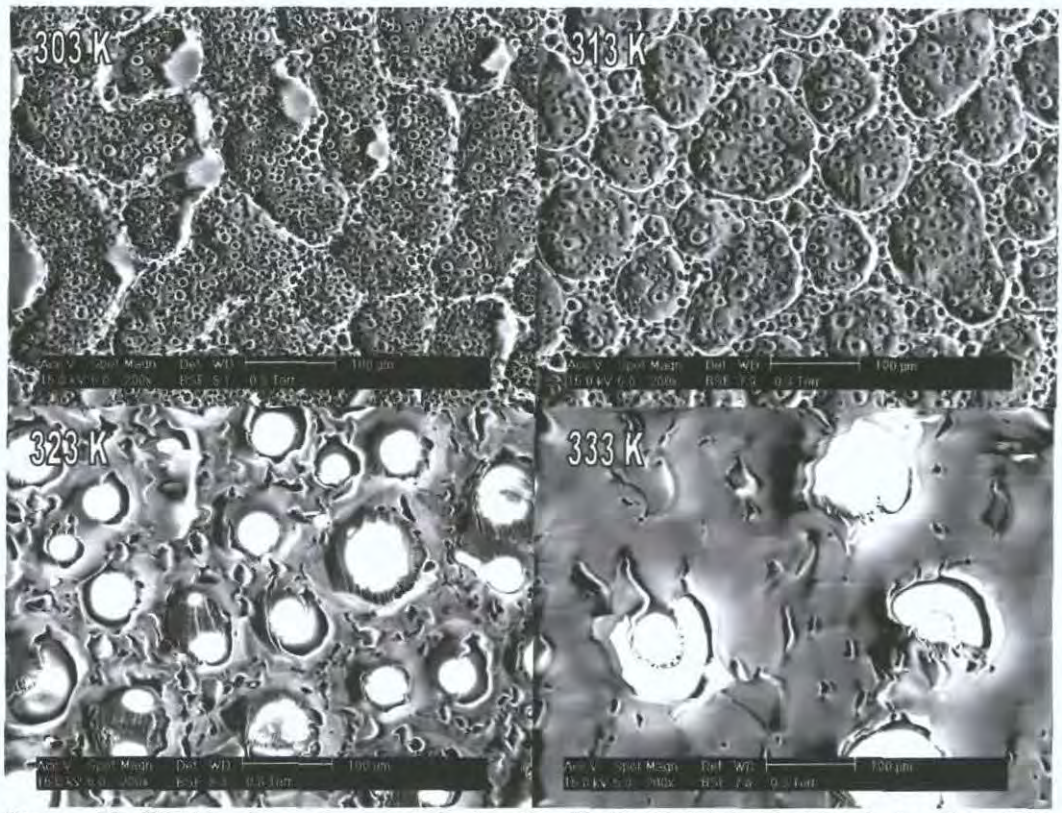

Figure 17 ESEM observed morphologies for 73:27 TL213:2-EthylHexyl Acrylate (5% b/v Crosslinker) polymerized under 5000 mWm^{-2} UV (365 nm) at varying temperatures. All images 200x magnification, measure bar is 100 μm

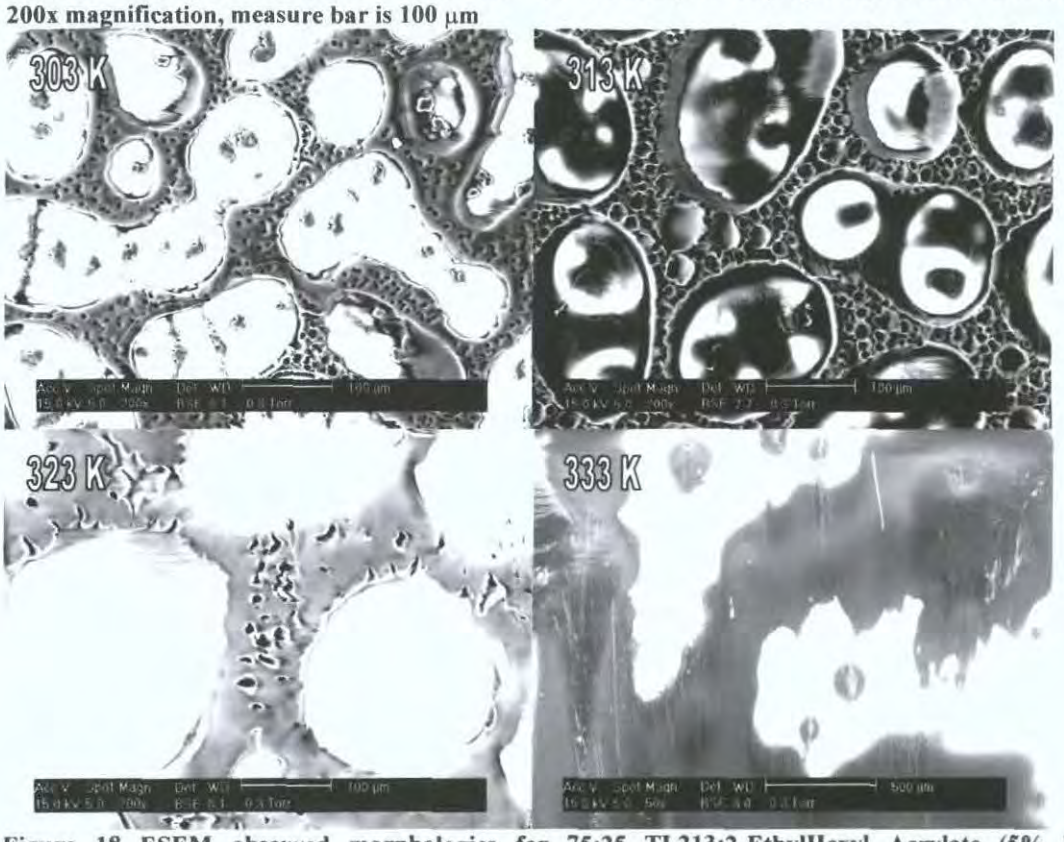

Figure 18 ESEM observed morphologies for 75:25 TL213:2-EthylHexyl Acrylate (5% b/v Crosslinker) polymerized *under 5000 mWm^{-2} UV (365 nm)* at varying temperatures. 303, 313, 323 K images 200x magnification, measure bar is 100 μm. 333 K image 50x magnification, measure bar is 0.5 mm

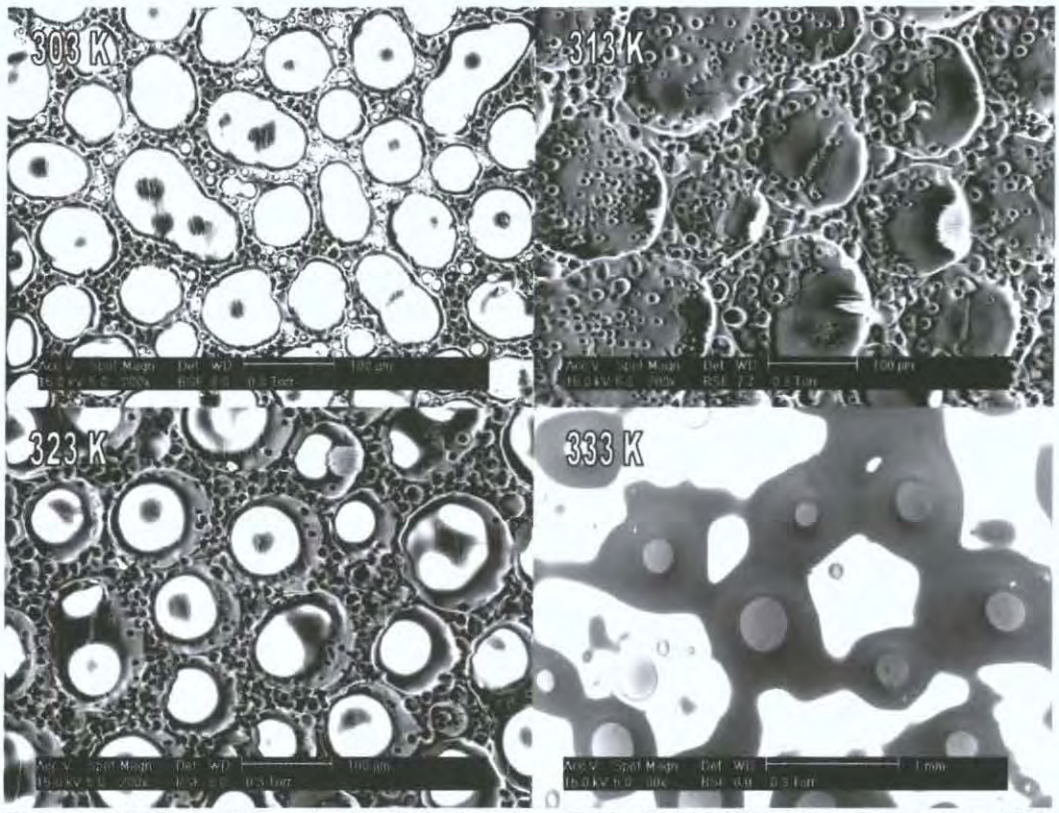

Figure 19ESEM observed morphologies for 77:23 TL213:2-EthylHexyl Acrylate (5% b/v Crosslinker) polymerized under 5000 mWm^{-2} UV (365 nm) at 303, 313, 323 K images 200x magnification, measure bar is 100 μm. 333 K image 30x magnification, measure bar is 0.5 mm

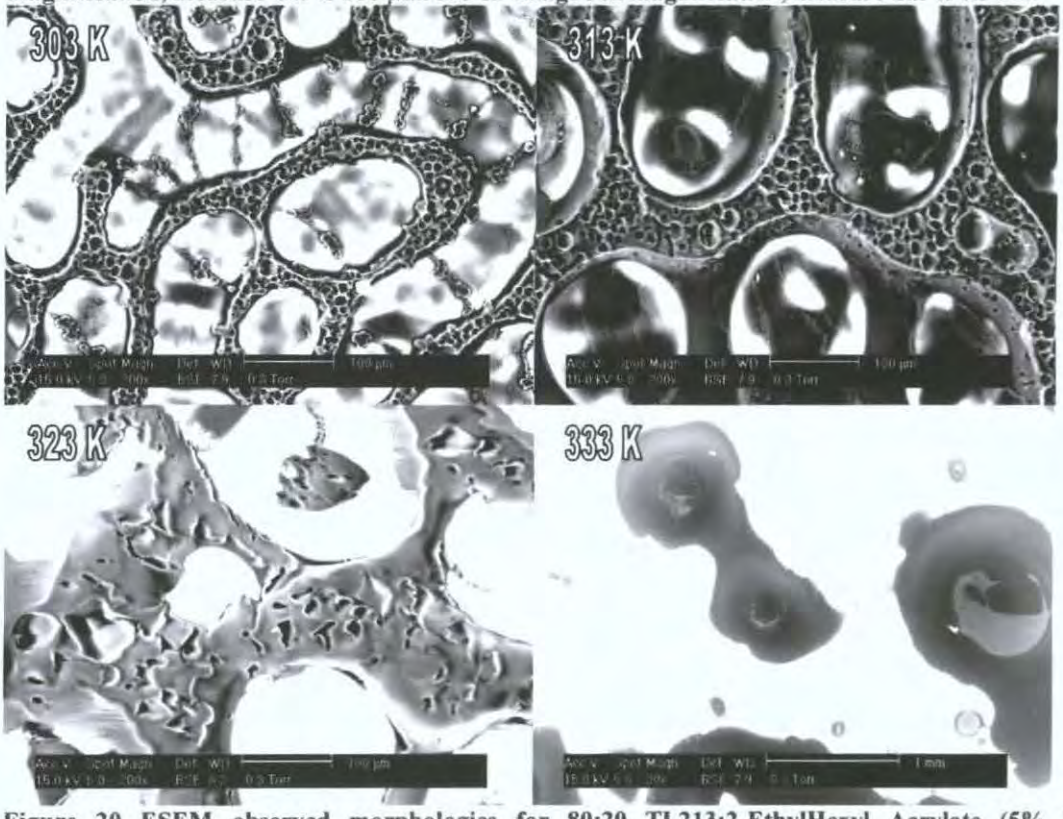

Figure 20 ESEM observed morphologies for 80:20 TL213:2-EthylHexyl Acrylate (5% b/v Crosslinker) polymerized under 5000 mWm^{-2} UV (365 nm) at varying temperatures. 303, 313, 323 K images 200x magnification, measure bar is 100 μm. 333 K image 30x magnification, measure bar is 0.5 mm

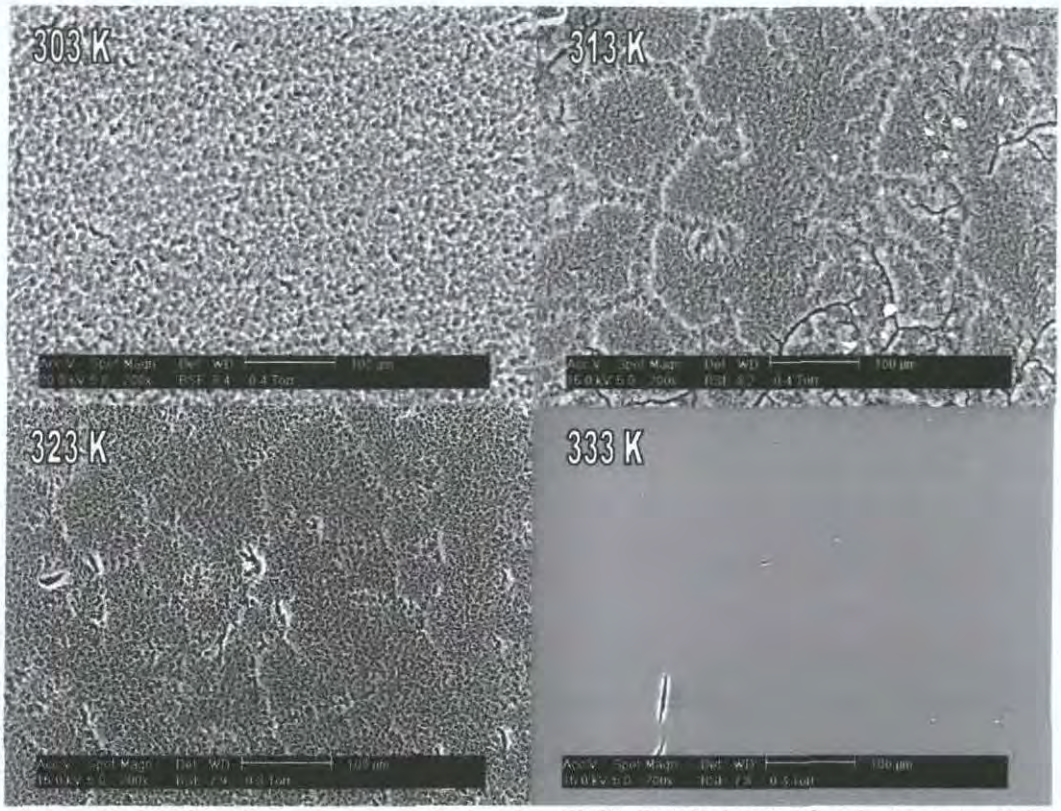

Figure 21 ESEM observed morphologies for 70:30 TL213:2-EthylHexyl Acrylate (15% b/v Crosslinker) polymerized under 5000 mWm^{-2} UV (365 nm) at varying temperatures. All images 200x magnification, measure bar is 100 μm

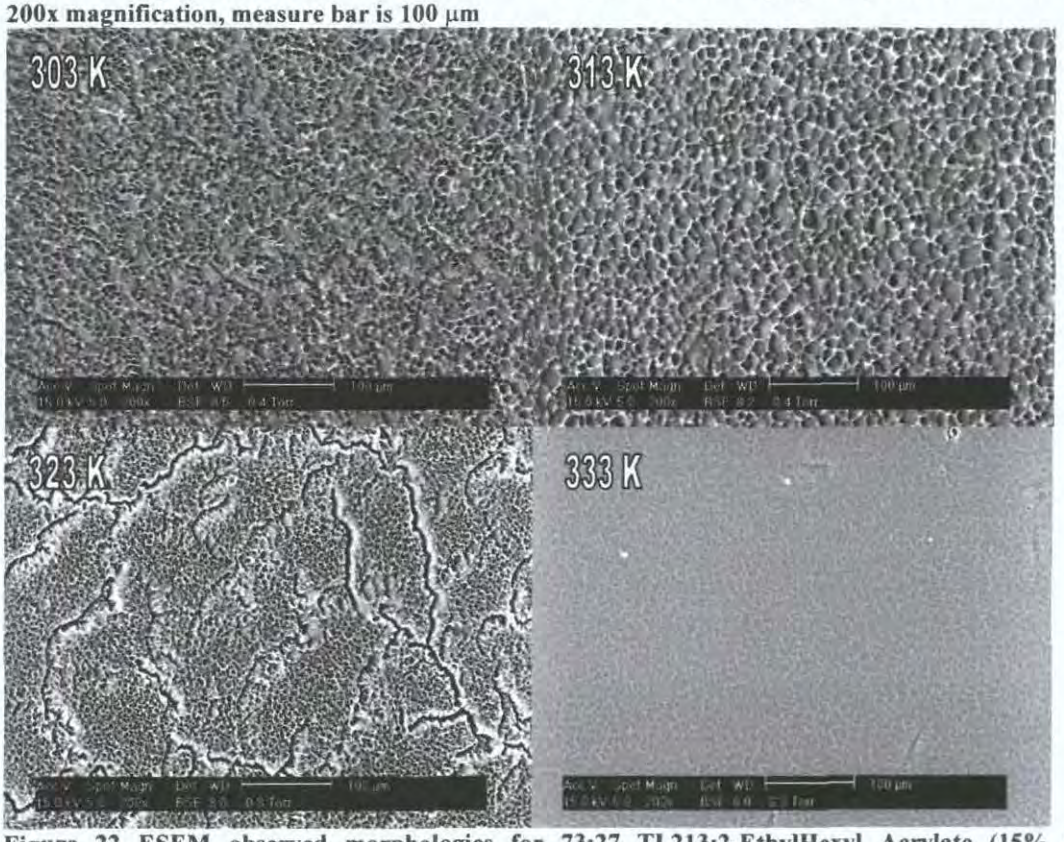

Figure 22 ESEM observed morphologies for 73:27 TL213:2-EthylHexyl Acrylate (15% b/v Crosslinker) polymerized under 5000 mWm^{-2} UV (365 nm) at varying temperatures. All images 200x magnification, measure bar is 100 μm

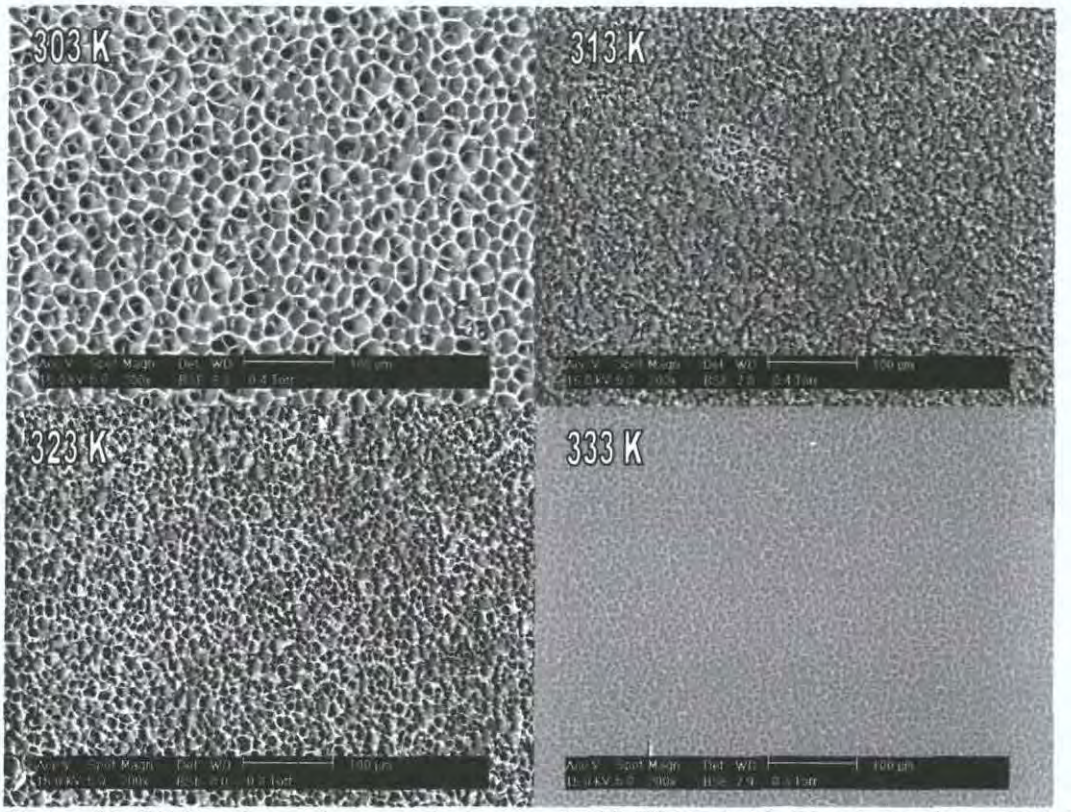

Figure 23 ESEM observed morphologies for 75:25 TL213:2-EthylHexyl Acrylate (15% b/v Crosslinker) polymerized under 5000 mWm^{-2} UV (365 nm) at varying temperatures. All images 200x magnification, measure bar is 100 μm

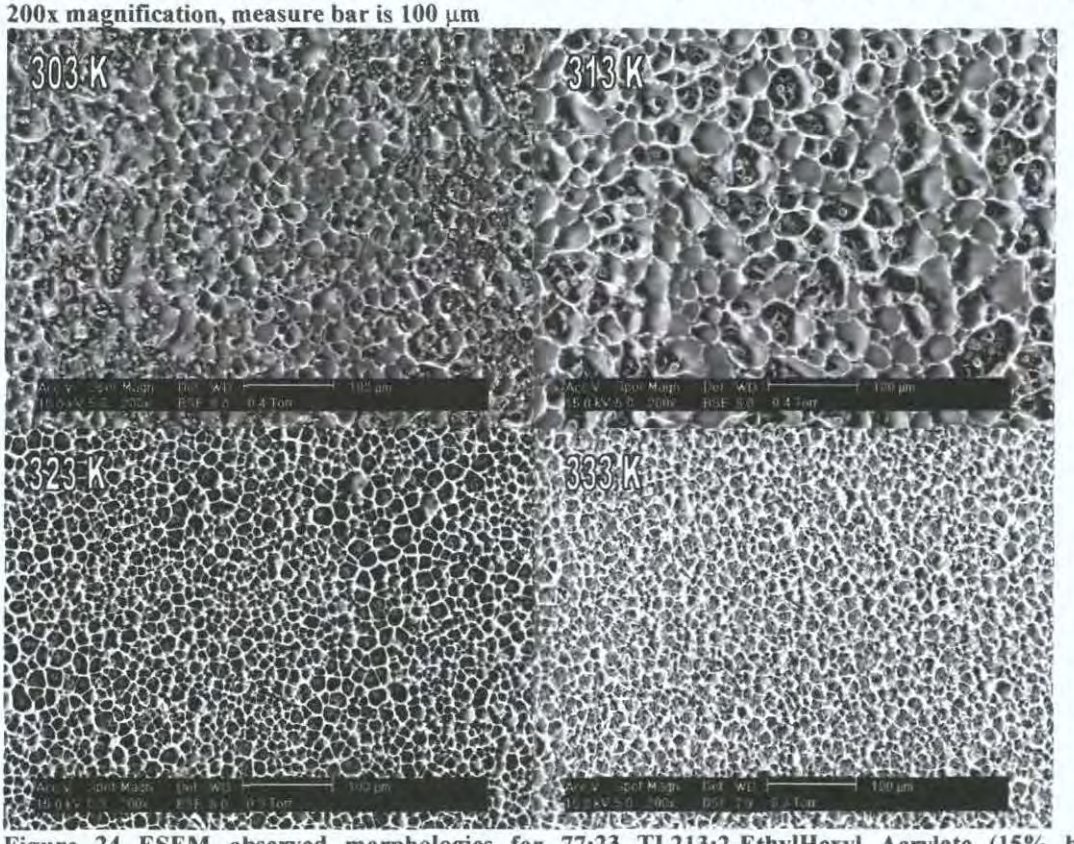

Figure 24 ESEM observed morphologies for 77:23 TL213:2-EthylHexyl Acrylate (15% b/v Crosslinker) polymerized under 5000 mWm^{-2} UV (365 nm) at varying temperatures. All images 200x magnification, measure bar is 100 μm

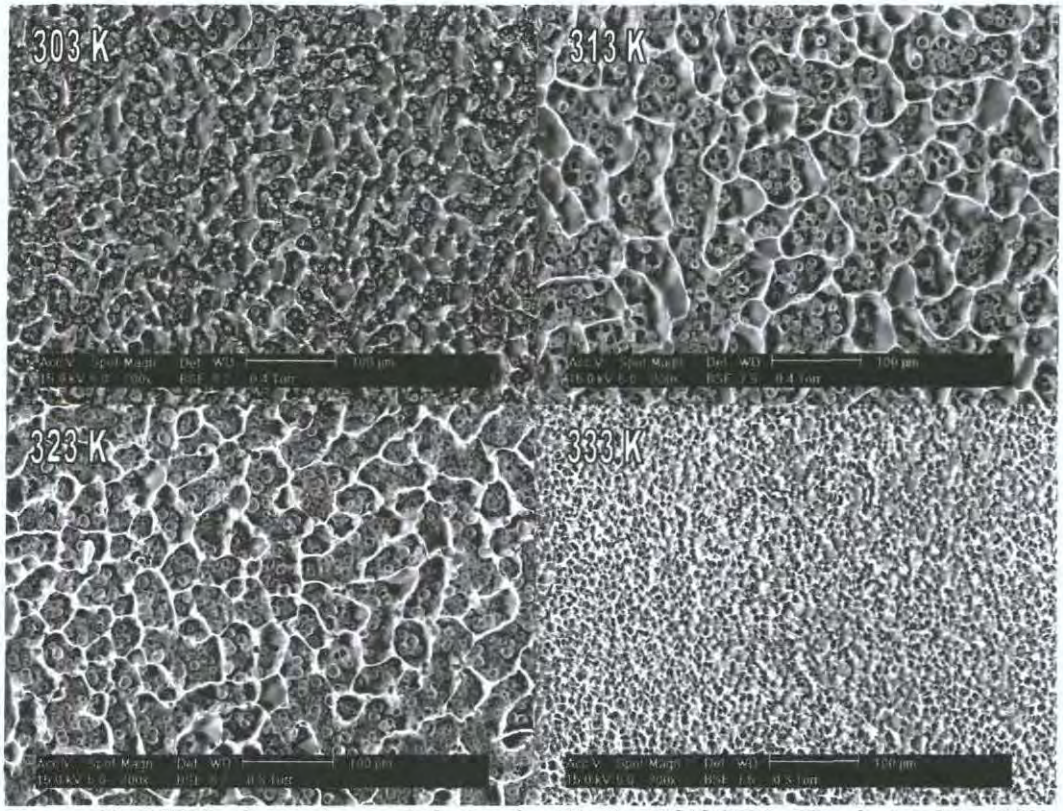

Figure 25 ESEM observed morphologies for 80:20 TL213:2-EthylHexyl Acrylate (15% b/v Crosslinker) polymerized under 5000 mWm^{-2} UV (365 nm) at varying temperatures. All images 200x magnification, measure bar is 100 μm